The Biomechanics of Turning Gait in Children with Cerebral Palsy

Philippe C. Dixon

St Peter's College

University of Oxford

A thesis submitted for the degree of

Doctor of Philosophy

Hilary Term 2015

Contents

1 Introduction **1**

1.1 Rationale . . . 2
1.2 Aims and Hypotheses . . . 2
1.3 Thesis Outline . . . 3

2 Literature Review **4**

2.1 Gait Analysis . . . 5
2.1.1 Historical context . . . 5
2.1.2 Clinical use . . . 5
2.1.3 Technological overview . . . 6
2.1.4 Gait cycle events . . . 7
2.1.5 Anatomical planes . . . 8
2.2 Straight Gait Metrics . . . 9
2.2.1 Spatio-temporal parameters . . . 9
2.2.2 Joint kinematics . . . 11
2.2.3 Joint kinetics . . . 17
2.2.4 Ground reaction forces . . . 21
2.2.5 Free vertical torque . . . 22
2.2.6 Muscular activity . . . 24
2.3 Clinical Tests . . . 26
2.3.1 Muscle strength . . . 26
2.3.2 Joint mobility . . . 27
2.4 Cerebral Palsy . . . 27
2.4.1 Gait patterns . . . 28
2.4.2 Further deviations . . . 30
2.5 Turning Gait . . . 31
2.6 Turning Strategies . . . 31
2.7 Prevalence of Turning . . . 32

2.8 Turning Preference . . . 34
2.9 Anticipation in Turning Gait . . . 35
2.10 Turning Angle . . . 35
2.11 Turning Gait Metrics . . . 36
2.11.1 Spatio-temporal parameters . . . 36
2.11.2 Joint kinematics . . . 38
2.11.3 Joint kinetics . . . 41
2.11.4 Muscular activity . . . 43
2.11.5 Centre of mass kinematics . . . 45
2.11.6 Ground reaction forces . . . 48
2.11.7 Clinical tests . . . 50
2.12 Turning Quality . . . 51
2.12.1 Stability . . . 51
2.12.2 Fluency . . . 52
2.12.3 Kinematic sequencing . . . 52
2.13 Pathological Turning . . . 52
2.14 Conclusion . . . 53

3 Experimental Methods **54**
3.1 Ethical Considerations . . . 55
3.2 Subjects . . . 55
3.3 Experimental Protocol . . . 55
3.3.1 Clinical examination and subject preparation . . . 55
3.3.2 Experimental tasks and set-up . . . 57
3.3.3 Data collection . . . 57
3.4 Data Processing . . . 58
3.4.1 Preparatory steps . . . 59
3.4.2 Event detection . . . 59
3.4.3 Turning strategy identification . . . 60
3.5 Biomechanical Models . . . 61
3.5.1 The Plug-in Gait Model . . . 63
3.5.2 The Oxford Foot Model . . . 68
3.6 Biomechanical Analysis . . . 70
3.6.1 Spatio-temporal parameters . . . 70
3.6.2 Lower-limb joint kinematics . . . 71
3.6.3 Intra-foot and ankle joint kinematics . . . 73

3.6.4 Lower-limb joint kinetics . . . 75
3.6.5 Intra-foot and ankle joint kinetics . . . 79
3.6.6 Implementation . . . 80
3.7 Variability in Gait Curves . . . 80
3.7.1 Standard approaches . . . 80
3.7.2 The Bootstrap approach . . . 82
3.8 Statistical Analysis . . . 85
3.8.1 Representative trial selection . . . 85
3.8.2 Confidence intervals and hypothesis testing . . . 86
3.8.3 Confidence bands and hypothesis testing . . . 87
3.8.4 Limitations . . . 88

4 Turning Gait in Typically Developing Children: Part I Kinematics 90
4.1 Introduction . . . 91
4.2 Methods . . . 91
4.2.1 Ethical considerations . . . 91
4.2.2 Subjects . . . 92
4.2.3 Data collection and processing . . . 92
4.2.4 Statistical analysis . . . 92
4.3 Results . . . 94
4.3.1 Turning frequency . . . 94
4.3.2 Spatio-temporal parameters . . . 95
4.3.3 Joint kinematics . . . 97
4.4 Discussion . . . 99
4.4.1 Turn style preference . . . 99
4.4.2 Spatio-temporal parameters . . . 100
4.4.3 Joint kinematics . . . 100
4.4.4 Clinical applications . . . 101
4.4.5 Limitations and other considerations . . . 102
4.4.6 Conclusions . . . 102

5 Turning Gait in Typically Developing Children: Part II Kinetics 103
5.1 Introduction . . . 104
5.2 Methods . . . 105
5.2.1 Ethical considerations . . . 105
5.2.2 Subjects . . . 105
5.2.3 Data collection . . . 105

5.2.4 Data processing . . . 106
5.2.5 Statistical analysis . . . 107
5.3 Results . . . 108
5.3.1 Ground reaction forces . . . 108
5.3.2 Free vertical torque . . . 108
5.3.3 Ipsilateral joint moments and power . . . 109
5.3.4 Contralateral joint moments and power . . . 111
5.4 Discussion . . . 113
5.4.1 Ground reaction forces . . . 114
5.4.2 Free vertical torque . . . 114
5.4.3 Joint moments . . . 114
5.4.4 Joint power . . . 116
5.4.5 Clinical applications . . . 116
5.4.6 Limitations and other considerations . . . 117
5.4.7 Conclusion . . . 117

6 Turning Gait in Children with Cerebral Palsy: Part I Kinematics 118
6.1 Introduction . . . 119
6.2 Methods . . . 121
6.2.1 Ethical considerations . . . 121
6.2.2 Patient group . . . 122
6.2.3 Control group . . . 124
6.2.4 Data collection . . . 125
6.2.5 Identification and prevalence of turning strategies . . . 125
6.2.6 Spatio-temporal parameters . . . 126
6.2.7 Dynamic stability measures . . . 127
6.2.8 Fluency measures . . . 131
6.2.9 Joint kinematics . . . 131
6.2.10 Normalization of gait metrics . . . 134
6.2.11 Statistical analysis . . . 135
6.3 Results . . . 138
6.3.1 Spatio-temporal parameters . . . 138
6.3.2 Dynamic stability measures . . . 140
6.3.3 Fluency measures . . . 141
6.3.4 Joint kinematics . . . 142
6.4 Discussion . . . 148

6.4.1 Spatio-temporal parameters . . . 148
6.4.2 Dynamic stability . . . 149
6.4.3 Fluency . . . 150
6.4.4 Joint kinematics . . . 151
6.4.5 Clinical applications . . . 152
6.4.6 Limitations and other considerations . . . 153
6.4.7 Conclusion . . . 154

7 Turning Gait in Children with Cerebral Palsy: Part II Kinetics 155
7.1 Introduction . . . 156
7.2 Methods . . . 157
7.2.1 Ethical considerations . . . 157
7.2.2 Patient group . . . 157
7.2.3 Control group . . . 157
7.2.4 Data collection and processing . . . 158
7.2.5 Ground reaction force impulse . . . 159
7.2.6 Free vertical torque . . . 160
7.2.7 Joint kinetics . . . 160
7.2.8 Statistical analysis . . . 162
7.3 Results . . . 162
7.3.1 Ground reaction force impulse . . . 162
7.3.2 Free vertical torque . . . 165
7.3.3 Joint kinetics . . . 165
7.4 Discussion . . . 171
7.4.1 Ground reaction force impulse . . . 171
7.4.2 Free vertical torque . . . 172
7.4.3 Joint kinetics . . . 173
7.4.4 Clinical applications . . . 173
7.4.5 Limitations and other considerations . . . 174
7.4.6 Conclusion . . . 175

8 Musculoskeletal Modelling of Turning Gait 176
8.1 Introduction . . . 177
8.2 Methods . . . 179
8.2.1 Ethical considerations . . . 179
8.2.2 Subjects . . . 179
8.2.3 Data collection and processing . . . 180

8.2.4 Center of mass acceleration during turning . . . 181
8.2.5 Gait2392: a lower-limb musculoskeletal model . . . 182
8.2.6 Development of dynamic simulations . . . 186
8.2.7 Statistical analysis . . . 195
8.3 Validation . . . 197
8.3.1 Subject scaling . . . 198
8.3.2 Inverse kinematics . . . 198
8.3.3 Inverse dynamics . . . 198
8.3.4 Residual reduction . . . 198
8.3.5 Static optimization . . . 199
8.3.6 Induced acceleration analysis . . . 199
8.4 Results . . . 204
8.4.1 Centre of mass acceleration . . . 204
8.4.2 Contributors to centre of mass acceleration . . . 206
8.4.3 Case study . . . 207
8.5 Discussion . . . 208
8.5.1 Control of centre of mass acceleration . . . 209
8.5.2 Clinical applications . . . 210
8.5.3 Limitations and other considerations . . . 211

9 Conclusions 213
9.1 Turning Gait in Typically Developing Children . . . 214
9.2 Turning Gait in Children with Cerebral Palsy . . . 215
9.3 Clinical Recommendations . . . 215
9.4 Future Directions . . . 216

A Derivations and Further Notes 217
A.1 Dynamic Stability . . . 217
A.2 Graphing of a Full Gait Cycle . . . 219

Bibliography 220

List of Figures

2.1 The gait cycle 8
2.2 The anatomical planes 9
2.3 Lower-limb joint kinematics during straight walking 13
2.4 Foot and ankle joint kinematics during straight walking 16
2.5 Lower-limb joint kinetics during straight walking 19
2.6 Ankle joint kinetics during straight walking 20
2.7 Ground reaction forces during straight walking 23
2.8 Free vertical torque during straight walking 23
2.9 Lower-limb muscle activation patterns during straight walking 25
2.10 Diagrammatic representation of step and spin turns (basic) 33

3.1 Graphical representation of experimental set-up 58
3.2 Comparison of gait event detection methods 61
3.3 Identification of turning strategy via pelvis kinematics 62
3.4 Diagrammatic representation of step and spin turns (kinematics) . . . 62
3.5 The Plug-in Gait model 63
3.6 Pelvis local coordinate system 67
3.7 The Oxford Foot Model 68
3.8 Gait curve variability 84
3.9 Statistical analysis of gait curves 88

4.1 Ipsilateral joint kinematics during turning gait 98
4.2 Contralateral joint kinematics during turning gait 98

5.1 Diagrammatic representation of step and spin turns (kinetics) 106
5.2 Ground reaction forces during turning gait 109
5.3 Free vertical torque during turning gait 110
5.4 Ipsilateral joint kinetics during turning gait 111
5.5 Contralateral joint kinetics during turning gait 112

6.1 Demonstration of the gait pattern classification algorithm 124
6.2 Distribution of turn angle by turn style 127
6.3 Inverted-pendulum model of gait 128
6.4 Dynamic stability quantities 131
6.5 Identification of discrete kinematic events during turning gait 133
6.6 Demonstration of subject-level analyses 134
6.7 Statistical process flow chart 137
6.8 Temporal parameters during turning gait 139
6.9 Spatial parameters during turning gait 139
6.10 Dynamic stability measures during turning gait 141
6.11 Center of mass position during turning gait 141
6.12 Fluency measures during turning gait 142
6.13 Discrete kinematic events during turning gait (group-level) 143
6.14 Kinematic Turning Variable Scores (group-level) 144
6.15 Kinematic Turning Profile Score (group-level) 144
6.16 Relative discrete kinematic events during turning gait (subject-level) 146
6.17 Kinematic Turning Variable Scores (subject-level) 147
6.18 Kinematic Turning Profile Score (subject-level) 148

7.1 Identification of discrete kinetic events during turning gait 161
7.2 Contralateral ground reaction force impulse during turning gait . . . 163
7.3 Ipsilateral ground reaction force impulse during turning gait 164
7.4 Free vertical torque during turning gait 166
7.5 Discrete kinetic events during turning gait (group-level) 166
7.6 Kinetic Turning Variable Scores (group-level) 167
7.7 Kinetic Turning Profile Score (group-level) 167
7.8 Relative discrete kinetic events during turning gait (subject-level) . . 169
7.9 Kinetic Turning Variable Scores (subject-level) 170
7.10 Kinetic Turning Profile Score (subject-level) 170

8.1 Diagrammatic representation of spin turns (modelling) 179
8.3 The Gait2392 musculoskeletal model of the human body 183
8.4 Scaling of musculoskeletal model via virtual markers 187
8.5 Identification of major contributors to center of mass acceleration . . 197
8.6 Validation of joint kinematics during straight walking 200
8.7 Validation of ipsilateral joint kinematics during spin turns 200
8.8 Validation of contralateral joint kinematics during spin turns 201

8.9 Validation of joint moments during straight walking 201
8.10 Validation of ipsilateral joint moments during spin turns 202
8.11 Validation of contralateral joint moments during spin turns 202
8.12 Validation of muscle activation patterns during straight walking . . . 203
8.13 Validation of muscle activation patterns during spin turns 203
8.14 Validation of center of mass acceleration during straight walking . . . 204
8.15 Validation of center of mass acceleration during spin turns 204
8.16 Main contributors to centre of mass acceleration 205
8.17 Main contributors to centre of mass acceleration by phase 207
8.18 Diagrammatic representation of muscle contributions to spin turns . . 208

A.1 Construction of gait cycle graphs for straight walking simulations . . 219

List of Tables

2.1 Gait cycle event timings 8
2.2 Spatio-temporal parameters during straight walking 11
2.3 Gait patterns in children with cerebral palsy 29

3.1 List of children in the normative database included in each study . . 56
3.2 Body segment inertial properties 76

4.1 Control group anthropometrics (kinematics) 93
4.2 Frequency distribution of turn style preferences 95
4.3 Spatio-temporal parameters during turning gait 96

5.1 Control group anthropometrics (kinetics) 105

6.1 Patient group anthropometrics and surgical history 123
6.2 Automatic gait classification algorithm 124
6.3 Control and patient group anthropometrics (kinematics) 125
6.4 Frequency distribution of turn style preferences 126
6.5 Frequency distribution of abnormal kinematic discrete events 145
6.6 Frequency distribution of abnormal kinematic scores 146

7.1 Children from patient group included in the kinetic analysis 158
7.2 Control and patient group anthropometrics (kinetics) 159
7.3 Frequency distribution of abnormal discrete kinetic events 168
7.4 Frequency distribution of abnormal kinetic scores 169

8.1 Marker pairs for scaling of body segments 187
8.2 Markers and weightings for inverse kinematics analysis 189
8.3 Muscle groups and associated abbreviations 196
8.4 Top contributors to the center of mass medio-lateral acceleration . . 196

To my parents.

CPC: Concentration, précision, clarté et tu réussis.

—Claudette Archambault

Acknowledgements

This doctoral thesis could not have been achieved without the guidance of my supervisors and strong support from a network of collaborators, friends, family, colleagues, and institutions.

First, I would like to thank my supervisors Julie Stebbins, Tim Theologis, and Amy B. Zavatsky for their encouragement and valuable feedback. They were fully involved throughout my research and were always available to answer my questions and ease my concerns.

I would also like to thank my collaborators Ilse Jonkers and Karen Jansen for their hospitality during my research visit in Leuven and their assistance with the development of my turning gait simulations, the staff at the Oxford Gait Laboratory for their help with the data collection, and all the volunteers and patients who made this research project possible.

In addition, I'm thankful to my colleagues at the Botnar Research Center, especially Richard Franzese and Alpesh Kothari, my friends from Lincoln and St Peter's College, Oded Steinberg and Duncan Paterson, as well as my flatmate Lukasz Stasiak, who helped keep me motivated and whose friendship made my time at Oxford enjoyable (despite the dreary weather).

I also want to express my deepest gratitude to my wife Jenny Maisonneuve. She encouraged me to pursue a doctoral degree, supported me every step of the way, and helped me maintain a sense of balance in my life. I sincerely appreciate her help with the proofreading of this thesis and the personal sacrifices that she has made to allow me to pursue my goals.

Finally, I acknowledge the Natural Sciences and Engineering Research Council of Canada (NSERC), the Fonds de recherche du Québec–Santé (FRSQ), Gustav Born, St Peter's College–Oxford, and the Canadian Centennial Scholarship Fund for their generous financial support.

The Biomechanics of Turning Gait in Children with Cerebral Palsy

Philippe C. Dixon

St Peter's College

University of Oxford

A thesis submitted for the degree of

Doctor of Philosophy

Hilary Term 2015

Turning while walking is a crucial component of locomotion; yet, little is known about how the biomechanics of turning gait differ from those of straight walking. Moreover, it is unclear how populations with restricted gait ability, such as children with cerebral palsy (CP) adapt to turning, compared to their typically developing (TD) peers. Thus, the aims of this thesis were to quantify the biomechanical differences between turning gait and straight walking in TD children and to explore if further, pathology specific, changes present during turning in children with CP. Biomechanical data, including three-dimensional body motion, ground reaction forces, and muscle activity from both groups were collected during straight walking and 90° turning gait using motion capture technology. Experimental data were used to compute joint kinematics (angles) and joint kinetics (moments and power) as well as more novel measures to quantify turning fluency and dynamic stability. These data were also used to derive walking simulations using a musculo-skeletal model of the human body in order to quantify muscle contributions to medio-lateral center of mass (COM) acceleration. The results show that both groups preferred to redirect their body during turning about the inside, rather than the outside, limb (with respect to the turn center). For TD children, substantial biomechanical adaptations occurred during turning, compared to straight walking. Furthermore, turning gait simulations reveal that proximal (hip abductors) and distal (ankle plantarflexors) leg muscles were mainly responsible for the redirection of the COM towards the new walking direction during turning. For children with CP, the results suggest that turning gait may be better able to reveal gait abnormalities than straight walking for a number of kinematic and kinetic gait variables. Potentially, analysis of turning gait could improve the identification and management of gait abnormalities in children with CP.

Chapter 1

Introduction

The biomechanics of walking have been studied extensively; however, relatively little attention has been paid to deviations from the straight-line gait pattern, such as turning while walking (turning gait). This thesis quantifies the biomechanics of turning gait in typically developing (TD) children with a particular focus on the feasibility of implementing such tasks in clinical gait analysis sessions for children with cerebral palsy (CP).

1.1 Rationale

Turning is a crucial component of locomotion accounting for approximately 1 in 5 steps taken daily [199] and up to half the steps taken indoors [87]. Therefore, interventions aiming to improve walking in patients with restricted gait ability should take into account the mechanisms required to successfully redirect the body towards new walking directions.

Many patient groups with gait disabilities may benefit from turning gait analysis; however, this thesis prioritizes assessment in ambulatory children with spastic diplegic CP. This patient group is characterized by a heterogeneity of gait abnormalities and deviations, rendering treatment difficult and, sometimes, of limited benefit. Moreover, as this group represents the dominant proportion of patients seen by the Oxford Gait Laboratory, improvement in their care is of primary importance.

Analysis of real-world tasks, such as turning gait, present opportunities to improve clinical management of gait deviations in children with CP. Furthermore, investigation of turning gait may lead to a better overall understanding of the complexities of the underlying control mechanisms of human locomotion.

1.2 Aims and Hypotheses

The primary aims of this thesis were to characterize the biomechanics of turning in TD children and to explore how analysis of turning gait trials could aid in the management of gait deviations in children with CP. Generally, it was hypothesized that turning gait would induce substantial biomechanical adaptations compared to the straight walking pattern in TD children and that turning gait could more readily identify gait deviations in children with CP than straight walking. Specific aims and hypotheses are presented for each study in this thesis (see Chapters 4–8).

1.3 Thesis Outline

This thesis begins with a review of the literature (Chapter 2) in which the field of gait analysis, including its applications and main metrics, are introduced. Additionally, existing research on turning gait as well as a survey of the main gait deviations in children with CP are presented. In Chapter 3, the main experimental procedures used throughout this thesis are fully described. Procedures limited only to specific investigations are detailed within their respective chapters. The next four chapters summarize the biomechanical adaptations identified experimentally during turning gait in TD children (Chapters 4 and 5) and in children with CP (Chapters 6 and 7). A final study (Chapter 8), based on simulations of turning gait using a musculo-skeletal modelling approach, completes the main body of the thesis. Conclusions, including general guidance for the implementation of turning gait in clinical gait analysis for children with CP, are presented in Chapter 9.

Chapter 2

Literature Review

In this review of the literature, the planned reorientation of the body towards a new direction during walking, known as turning gait, is explored in detail. In line with the aims of this thesis, turning gaits in typically developing (TD) children and children with cerebral palsy (CP) are emphasized; nonetheless, given the paucity of research in this area, the review is augmented by consideration of turning gait research in other populations with restricted mobility. First, however, background on the field of gait analysis, including an overview of common straight-line gait metrics, and typical gait deviations in CP is provided. Additional measures, potentially relevant to turning gait study, are also examined.

2.1 Gait Analysis

2.1.1 Historical context

Human locomotion has been one of the central themes of research in biomechanics for centuries; however, it was not until the nineteenth century that pioneers such as Eduard (1806–1871) and Willhelm (1804–1891) Weber [237], Jules Etienne Marey (1830–1904) [149], and Otto Fischer (1861–1917) [77] made significant contributions to the scientific understanding of gait.

In the early twentieth century, the landmark research of John Saunders (1903–1991), Verne Inman (1905–1980), and Howard Eberhart (1906–1993) describing normal and pathological gait [189], together with the later work of Jacquelin Perry (1914–2013) [173] and David Sutherland (1923–2006) [222], two former students of Saunders, formed the basis of modern gait analysis.

Today, the ubiquitousness of the computer, digital video, and specialized sensors has facilitated numerous investigations into both the biomechanical and neuromuscular mechanisms responsible for human motion.

2.1.2 Clinical use

The use of instrumented clinical gait analysis (CGA) in the treatment and management of gait deviations arising from various pathologies, such as CP, is not yet universal. Many medical centres do not possess dedicated CGA laboratories and still rely on observational visual assessment methods, regardless of their decreased ability to detect gait deviations [187] and decreased reliability and validity [248].

In the 1990s there was a debate in the literature with regard to the use of CGA in the management of gait disability [82, 236], but today, the evidence in favour of its use is building. A recent systematic review by Wren et al. [245] showed that CGA

is effective for the purposes of patient classification and that functional outcomes are superior when treatment decisions are in-line with CGA recommendations. Crucially, a major limitation of the papers reviewed is that no control group was provided. Only in the last few years have truly randomized controlled trial studies provided strong evidence in support of CGA in the case of CP [246, 247].

2.1.3 Technological overview

Generally, CGA relies on three main types of data in order to guide clinical assessments [223]: (1) muscle activation patterns, (2) spatio-temporal parameters (STPs) and joint angles (kinematics), and (3) ground reaction forces (GRFs), joint moments, and joint power (kinetics).

Muscle activity, measured via surface electromyography (sEMG) chronologically preceded kinematic and kinetic estimations [223] and is still used widely today, but alone, provides limited information regarding gait ability. Kinematics allow for a quantification of joint motion and are often computed by tracking the movement of the body using retro-reflective skin mounted markers [223]. The Plug-in Gait (PiG) [128] and Oxford Foot Model (OFM) [213] marker sets are commonly used in children to compute lower-limb joint kinematics and intra-foot movement, respectively. Joint kinetic quantities can be derived by combining GRFs, usually collected by force plates embedded in the walkway, with kinematic and subject-specific anthropometric information via standard Newtonian inverse dynamics analysis approaches [229].

Together, sEMG, kinematics, and kinetics provide a solid foundation for clinical decision making regarding gait abnormalities. Newer methods, such as musculo-skeletal modelling via dynamic simulation, are also beginning to be implemented in the CGA context and show great promise [59, 103, 139, 216].

2.1.4 Gait cycle events

Non-pathological human gait reveals a repeated movement pattern with consistent foot-ground contact and other gait events [173, pp. 9–16]. By convention, a gait cycle is taken to begin with the contact of one foot with the ground (0%) and to end the instant before the next time this same foot strikes the ground (100%) (Fig. 2.1). Thus, during a single cycle, two steps are taken (one stride) and all gait events are observed. The following description of the gait cycle is based on the summary by Perry [173, pp. 4–16], itself reliant on the work of numerous early investigators. The gait cycle comprises two main phases, stance and swing, each further subdivided (Table 2.1). At a comfortable adult walking pace (approximately 1.36 m/s), the stance and swing phases represent 62% and 38% of the gait cycle, respectively.

The stance phase begins with ipsilateral foot-strike and ends at ipsilateral foot-off. The first section of stance is initial contact (0–2%). Shortly thereafter, loading response occurs (2–12%) in which the ipsilateral limb accepts the weight of the body. This first double-limb support period ends when the contralateral foot achieves foot-off. Single-limb support occurs during mid-stance (12–31%) as the body passes over the stationary ipsilateral foot. Terminal stance (31–50%) begins at ipsilateral heel-rise and ends at contralateral foot-strike. Finally, pre-swing (50–62%), the second double-limb support phase in stance, ends the moment before ipsilateral foot-off and completes the stance phase of gait.

Swing begins immediately following stance and comprises three sections: initial swing (62–75%) begins at ipsilateral foot-off and ends when the ipsilateral foot is opposite the contralateral stance foot in the coronal plane, mid-swing (75–87%) continues until the ipsilateral tibia is vertical with respect to the global coordinate system, and swing ends with terminal swing (87–100%) as the tibia advances further and the ipsilateral foot prepares for foot-strike.

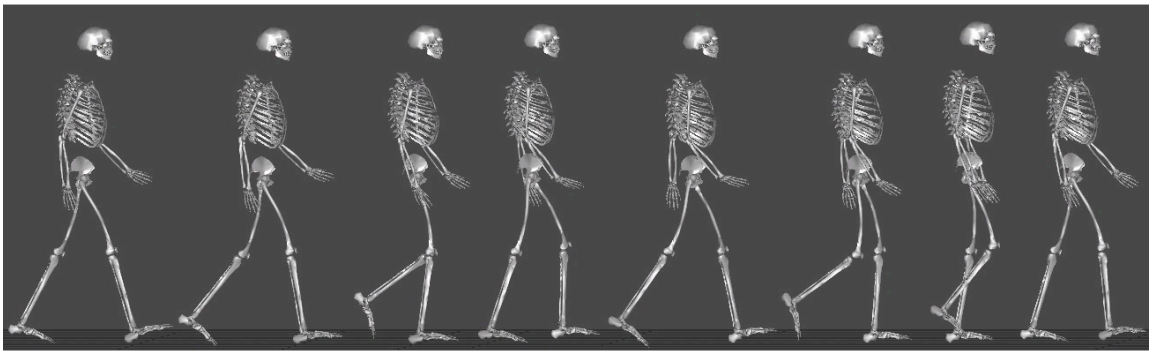

Figure 2.1 – Gait cycle (right leg) based on a representative straight walking trial from the TD child database. The gait cycle begins with a right foot-strike and ends the moment before the next right foot-strike.

Table 2.1 – Normative gait cycle event timings

Event	Gait Cycle Phase	Timing (%)
Initial Contact	Stance	0–2
Loading Response	Stance	2–12
Mid-Stance	Stance	12–31
Terminal Stance	Stance	31–50
Pre-Swing	Stance	50–62
Initial Swing	Swing	62–75
Mid-Swing	Swing	75–87
Terminal Swing	Swing	87–100

Source: [173, pp. 9–16]

2.1.5 Anatomical planes

In analysing human movement, it is convenient to separate the body into three orthogonal planes: the sagittal (side), coronal (frontal), and transverse (horizontal) (Fig. 2.2). These terms are also used to analyse gait; however, for joint kinematic and kinetic quantities it is important to note that the segment planes are not necessarily coplanar with the body planes. The main motion during gait occurs in the sagittal plane, but coronal and transverse plane motions are also of great importance and cannot be neglected, especially in children with CP [173, pp. 345–356].

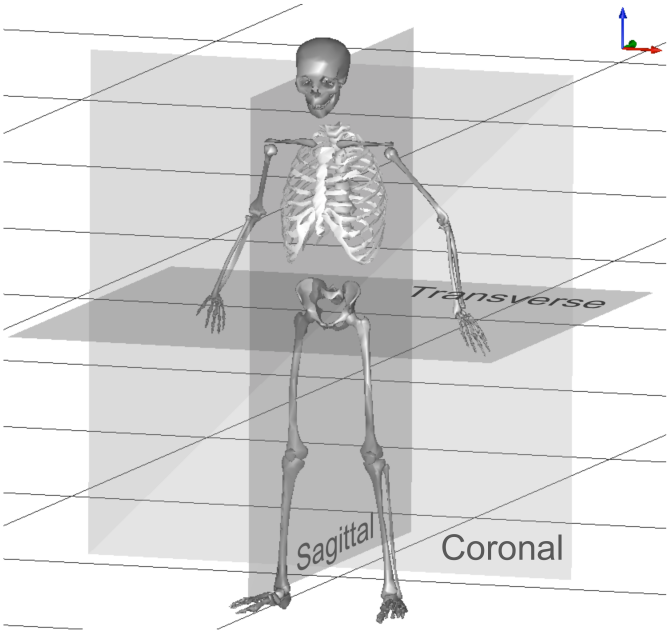

Figure 2.2 – The sagittal, coronal, and transverse anatomical planes.

2.2 Straight Gait Metrics

The main metrics of straight walking analysis (kinematics, kinetics, and muscular activity) (see Section 2.1.3) may be relevant in the study of turning gait and are presented in this section. Normative graphs were generated using the Zoosystem Biomechanical Toolbox [65] in Matlab (v2012b, The Mathworks Inc., Natick, USA).

2.2.1 Spatio-temporal parameters

Distance (spatial) and time (temporal) measurements related to the cyclical patterns of gait are collectively referred to as STPs. Brief definitions of common STPs are provide here, as described by Kaufman and Sutherland [130], Lythgo et al. [146], and many others:

Gait speed Average speed during steady-state walking.

Cadence The number of steps per unit time.

Single Support The time spent on a single limb, i.e. the time from foot-off to foot-strike of the contralateral limb.

Double Support The time spent on two-limbs, i.e. the time from foot-strike of the ipsilateral limb to foot-off of the contralateral limb and the time from foot-strike of the contralateral limb to foot-off of the ipsilateral limb.

Stance Time The total time of Single Support and Double Support.

Step Time The time interval between consecutive steps.

Stride Time The time interval between consecutive steps of the same limb.

Step length The distance, in the direction of progression, between consecutive foot-strike events.

Stride Length The distance, in the direction of progression, between consecutive foot-strike events of the same limb.

Step Width The distance, perpendicular to the direction of progression, between consecutive foot-strike events.

In the early years of childhood, neuromaturation drives changes in STPs, while in later years, differences with respect to adult normative values are mainly due to the reduced stature (specifically leg-length) of children [161, 221]. In children with CP, STPs often show decreased values and increased stride-to-stride variability compared to their TD peers [178], providing a useful assessment of gait pathology.

Normative STP data for TD children and young healthy adults (n=980, age bands of 5, 6, 7, 8, 9, 10, 11, 12–13, and 19 years) during self-selected speed barefoot walking from the research of Lythgo et al. [146, p. 504] show consistent trends across ages with all parameters increasing with age, except for cadence (not shown) (Table 2.2). These data, and other similar sets, can be used to compare STPs across cohorts as

Table 2.2 – Normative spatio-temporal parameter data

Age (years)	Gait Speed (cm/s)	Step Length (cm)	Step Width (cm)	Step Time (ms)
5.7 (0.2)	124.8 (4.6)	48.7 (1.1)	7.1 (0.4)	398 (11)
6.6 (0.3)	127.5 (2.4)	52.2 (0.9)	7.1 (0.3)	415 (8)
7.5 (0.3)	126.1 (2.9)	54.8 (1.0)	7.5 (0.3)	439 (7)
8.5 (0.3)	130.6 (2.7)	57.3 (0.9)	7.5 (0.3)	444 (7)
9.5 (0.3)	127.0 (3.0)	58.7 (1.0)	8.3 (0.3)	468 (7)
10.5 (0.3)	130.3 (3.5)	61.3 (1.2)	8.2 (0.3)	476 (466–484)
11.5 (0.3)	131.7 (2.9)	63.6 (1.1)	8.4 (0.4)	487 (6)
12.6 (0.5)	133.7 (4.4)	67.0 (1.8)	8.2 (0.5)	505 (6)
19.6 (1.6)	141.4 (3.1)	71.8 (1.4)	9.3 (8.3–9.6)	509 (495–514)

Mean (standard deviation) or median (95% confidence interval based on binomial distribution as in [86, pp. 26–31]) by age group during barefoot walking for normally or non-normally distributed datasets, respectively. Source: [146, p. 504].

long as groups are well-matched according to the parameters of the database. Often comparisons of STPs are made between heterogeneous groups. In this case, many authors have implemented normalization approaches to account for STP differences across groups [146, 176, 211]. Through a regression analysis of STPs in TD children, Dixon et al. [64] reported that non-dimensional normalization [110] can render stride length and cadence invariant with respect to anthropometrics; however, after normalization, speed was still found to depend on age. Thus, differences across groups should be assessed via non-normalized speed as long as age is well matched.

2.2.2 Joint kinematics

Joint kinematics describe the motion of the body. In CGA, motion of the hip, knee, and ankle are most often investigated; however, closer exploration of intra-foot joint motion is becoming more common. Although upper-body movements also perform an important role in gait [131, 218], the motion of the lower-limbs is the focus of this thesis and is now described for straight walking. The muscle and external forces

responsible for this motion are described in Sections 2.2.3, 2.2.4, and 2.2.6, while computation details are provided in Section 3.6.2.

Lower-limb kinematics

Lower-limb joint kinematics are often estimated using standard models such as the PiG. The PiG, as implemented in Vicon (Vicon Motion Systems Ltd., Oxford, UK), is based on the work of Davis et al. [54] and Kadaba et al. [128] and has become a popular choice for both research and clinical gait analysis purposes. A repeatability study of the PiG in adults ($n = 40$ with age range 18–40 years) determined that intra-subject variability was good between testing sessions, both within the same day and across visits (one week apart) for the sagittal plane angles only. Although repeatability in the coronal and transverse plane was good within the testing day, upon the second visit, data showed large intra-subject variability compared to the data initially collected (poor reliability), attributed to poor alignment of the markers [129]. A later study, in both TD children and children with CP again showed that sagittal plane data were most reliable; however, substantial differences existed in data for children with CP collected across laboratories [160]. A recent approach using a function calibration method has been found to improve reliability of the PiG [96], but has not become widespread. Instead, many gait laboratories attempt to improve PiG reliability via the use of the Knee Alignment Device (Motion Lab Systems, Inc., Baton Rouge, USA) or optimization approaches [13]. Although the former technique has been used in turning gait studies [61], the latter method, currently preferred by the Oxford Gait Laboratory (OGL), has been implemented in this thesis (see Section 3.5.1).

Normative hip, knee, and ankle joint kinematic data for TD children ($n = 83$ and mean age 10.5 years) walking at a self-selected speed computed via the PiG model are presented based on the work of Schwartz et al. [194] (Fig. 2.3). Hip, knee, and ankle angles represent relative motion between the pelvis and femur, femur and tibia,

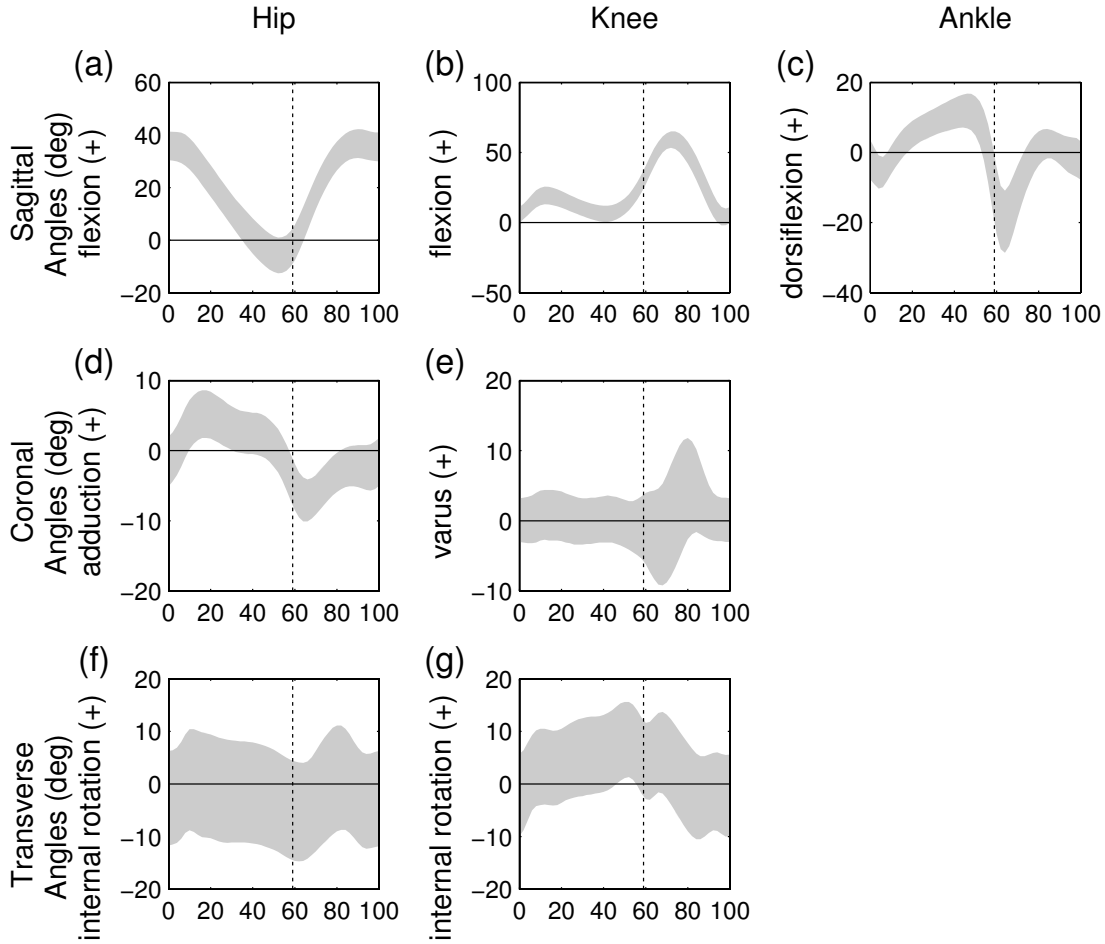

Figure 2.3 – Hip, knee, and ankle joint kinematics in TD children (0–100% of the gait cycle). Grey bands cover ± 1 standard deviation of the mean. Dashed vertical line shows approximate position of foot-off. Source: supplemental data in [194].

and tibia and foot, respectively. Only sagittal motion of the ankle is described for the PiG model, given the limitations of the model (see Section 3.5.1).

Sagittal plane joint displacements generally show the greatest range of motion and are thus easiest to measure accurately [130]. At the hips, reciprocal sinusoidal motions are seen between the two sides. For the ipsilateral hip, maximum flexion occurs at foot-strike. During stance, the flexion angle decreases as the body progresses over the stance limb, placing the hip into extension in terminal stance. Maximum extension is obtained at the start of pre-swing. During swing, the hip then begins to flex in preparation of the next foot-strike (Fig. 2.3 a). The sagittal plane knee angle is

characterized by two flexion peaks: a first during the stance phase as the weight of the body is loaded on the stance limb and a second, larger peak, during swing phase in order to obtain adequate foot clearance [130] (Fig. 2.3 b). The ankle begins in a neutral position at initial contact and quickly goes into slight plantarflexion during loading response. This phase is often referred to as the first rocker. Afterwards as the tibia advances over the stance-limb from mid-stance towards pre-swing (second rocker), the ankle moves into dorsiflexion reaching a maximum near 40%. During the final stage of stance (pre-swing), the dorsiflexion angle decreases and moves the ankle towards plantarflexion (third rocker) in preparation for push-off. In initial swing, the ankle begins to dorsiflex to help with foot clearance and then maintains a neutral posture towards mid-swing in anticipation of ground contact [130] (Fig. 2.3 c).

In the coronal plane, a raise of the ipsilateral pelvis towards the end of loading and a lowering of the pelvis in initial swing contributes to hip adduction and abduction peaks, respectively (Fig. 2.3 d). At the knee, motion is small during the stance phase, but increases first into valgus and then varus during swing (Fig. 2.3 e).

In the transverse plane, the hip rotation profile is quite variable in the child dataset of Schwartz et al. [194], but the mean values shows slight external rotation throughout stance phase and a trend towards internal rotation in mid-swing (Fig. 2.3 f). The knee shows mainly internal rotation with a peak near pre-swing (Fig. 2.3 g).

Foot kinematics

The PiG model provides an accurate description of hip and knee angular motion; however, the assumption of a single segment for the foot may be of limited use given the complex intra-foot motion that occurs during gait [37]. This has led several investigators to advance multi-segment foot models capable of measuring these important movements. In fact, a comprehensive review in 2011 by Deschamps et al. [60] revealed

that fifteen separate models had been proposed in the literature, including the OFM. The OFM has been implemented as a free downloadable plug-in for the Vicon (Vicon Motion Systems Ltd., Oxford, UK) system, spurring its wide spread use in studies of both healthy and pathological gait [60]. Moreover, strong reliability of the model in adult [249] and paediatric [51] populations has further encouraged users to model the foot via the OFM (for derivation, see Section 3.6.3).

The OFM hindfoot with respect to tibia (HF/TB) (combined talocrural and talocalcaneal movement), forefoot with respect to hindfoot (FF/HF), and hallux with respect to forefoot (HLX/FF) angles for TD children ($n = 10$ and age range 7–11 years) walking barefoot at self-selected speed from Stebbins et al. [212] are presented.

In the sagittal plane, both the HF/TB and FF/HF angles show similar patterns to the PiG ankle angles. Thus, coupled motion of dorsiflexion followed by peak plantarflexion after foot-off and a return to a near neutral position in swing is seen in both joints (Fig. 2.4 a and b). The HLX/FF angle shows dorsiflexion at foot-strike, but quickly moves to a near neutral position throughout the rest of stance. As the forefoot is loaded and the pre-swing phase commences, the HLX/FF angle shows dorsiflexion with a peak nearly coincident with foot-off (Fig. 2.4 c).

In the coronal plane, the small medio-lateral deformations of the foot during loading can be distinguished. At foot-strike, as the heel is loaded, the HF/TB moves from a slightly inverted position to an everted posture. Slight eversion is maintained during mid-stance, but the ankle then begins to invert as the weight of the body moves over the metatarsal region reaching a peak at foot-off (Fig. 2.4 d). In the coronal plane, the FF/HF angle remains mostly suppinated (Fig. 2.4 e). The HLX/FF internal/external rotation angle cannot be computed as the hallux segment is only modelled as a vector [213].

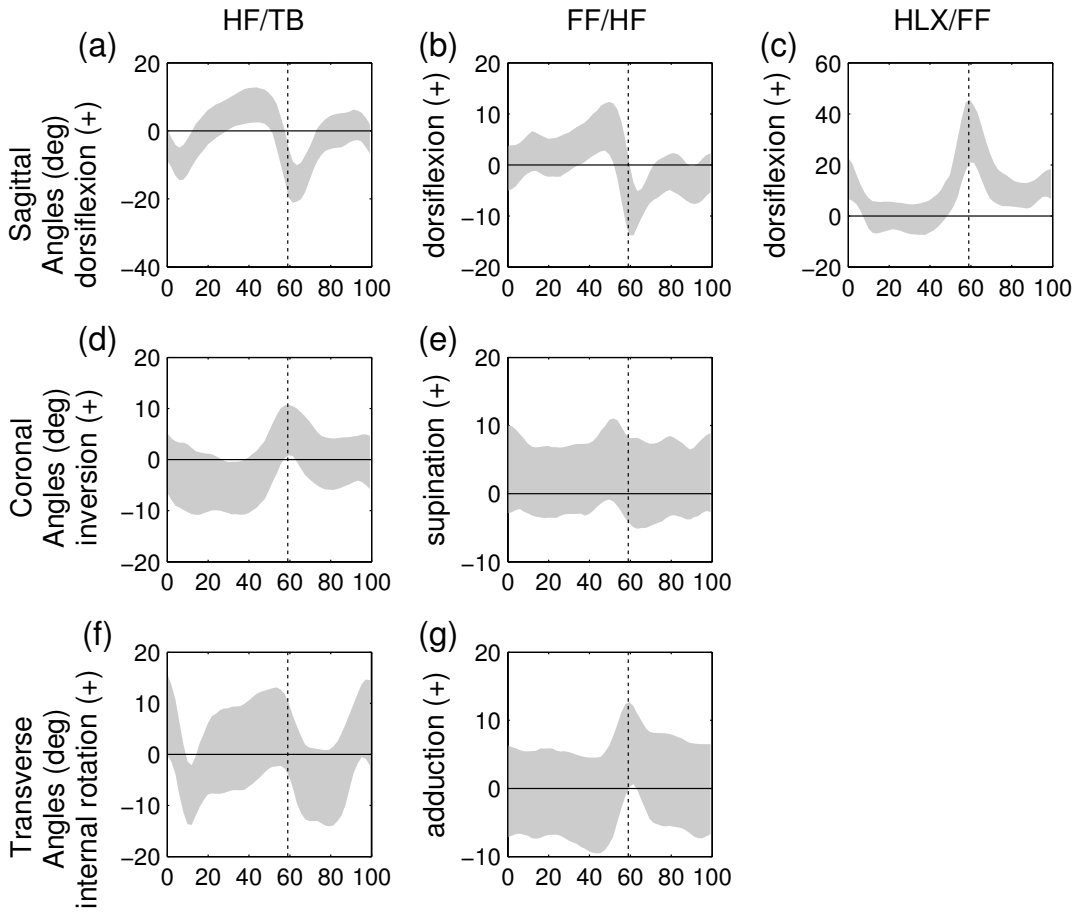

Figure 2.4 – Hindfoot/Tibia (HF/TB), forefoot/hindfoot (FF/HF), and hallux/forefoot (HLX/FF) angles in TD children (0–100% of the gait cycle). Grey bands cover ± 1 standard deviation of the mean. Dashed vertical line shows approximate position of foot-off. Source: graphs (digitized) in [212].

In the transverse plane, the internally rotated HF/TB at initial contact quickly externally rotates during loading, and then return towards internal rotation for the rest of the stance phase. Initial and mid-swing, see a return to external rotation and finally the HF/TB internally rotates in preparation for the next foot-strike (Fig. 2.4 f). The FF/HF is near neutral in stance, but shows an adduction peak towards foot-off before a return to a neutral position in swing (Fig. 2.4 g). The transverse plane HLX/FF angles were not reported by Stebbins et al. [213], but can be analysed to measure valgus/varus alignment (for example, see [215]).

2.2.3 Joint kinetics

The joint kinematics described in Section 2.2.2 are driven by muscles, ligaments, passive structures, and external forces that act by exerting moments across the joints of the body. The net internal joint moments represent the sum of all these forces acting at various distances (moment arms), while power describes the rate of work done. Normative net internal joint kinetic data for the hip, knee, and ankle are presented from the TD dataset of Schwartz et al. [194], except for the hip and knee transverse plane quantities, described by Schache et al. [192] for a group of adult males ($n = 9$). The refined net internal ankle kinetic quantities, based on the OFM for TD children ($n = 10$, mean age 14 years) reported by Dixon et al. [63], are also discussed and presented.

Lower-limb kinetics

For the sagittal hip moment, three peaks are observed. First, from foot-strike to mid-stance, an extensor moment pulls the centre of mass (COM) forward and upwards by rotating the hip towards an extended position. This action is also reflected by hip power generation during the same period. Next, near the start of pre-swing, peak hip flexor moment and power absorption occur as the hip flexor muscles are elongated under the action of gravity. Near toe-off, a flexor moment and power generation burst help initiate swing limb advancement. This moment also aids in producing swing knee flexion [175]. Finally, in terminal swing, a hip extensor moment helps slow the progression of the swing limb in preparation for foot-strike [53] (Fig. 2.5 a and f).

At the knee, an extensor moment and associated power absorption during loading aid in stabilizing the knee and controlling flexion. The knee extensor moment continues to grow and power generation is seen; consistent with a now extending knee until approximately 25% of the gait cycle. In terminal stance, a knee flexor moment is

seen in preparation for the swing phase. Near foot-off, an extensor moment and power absorption control the flexion rate. Flexion continues during initial swing under the influence of both ankle and hip moments. In mid-swing, momentum passively extends the knee. This extension is finally controlled in terminal swing by a flexor moment (and power absorption) [53] (Fig. 2.5 b and h).

At initial contact, the ankle begins to plantarflex under the action of a GRF vector posterior to the ankle joint. This plantarflexion is controlled by a dorsiflexor moment. Shortly thereafter, during loading response, a plantarflexor moment begins. At first this moment controls dorsiflexion of the ankle caused by the advancing tibia, as evident from the ankle absorption from loading to approximately 40% of the gait cycle. Finally, this continued plantarflexor moment begins to plantarflex the ankle reaching a maximum power generation and moment around the start of pre-swing. This large power generation burst helps initiate swing (along with the hip flexor moment already discussed) [53] (Fig. 2.5 c and i).

In the coronal plane, the hip and knee show similar patterns. At the hip, an abductor moment controls pelvic obliquity throughout stance. This moment balances the torque produced by the pull of gravity on the COM [53] (Fig. 2.5 d). The torque generated by gravity must also be controlled at the knee. Without a valgus moment, the knee would be pulled into varus alignment under this action [53] (Fig. 2.5 e). Coronal ankle kinetics are usually not reported in the PiG, given the model limitations.

In the transverse plane, hip and knee moments are not normally assessed in CGA. Nonetheless, they reveal repeatable patterns, albeit dependent on the reference frame in which they are expressed [192]. These quantities may be especially relevant in the description of turning gait and are therefore presented (expressed in the anatomical frame of the distal segment). For the hip, an internal rotator peak dominates the loading phase, while an external rotator moment is seen in terminal stance as the

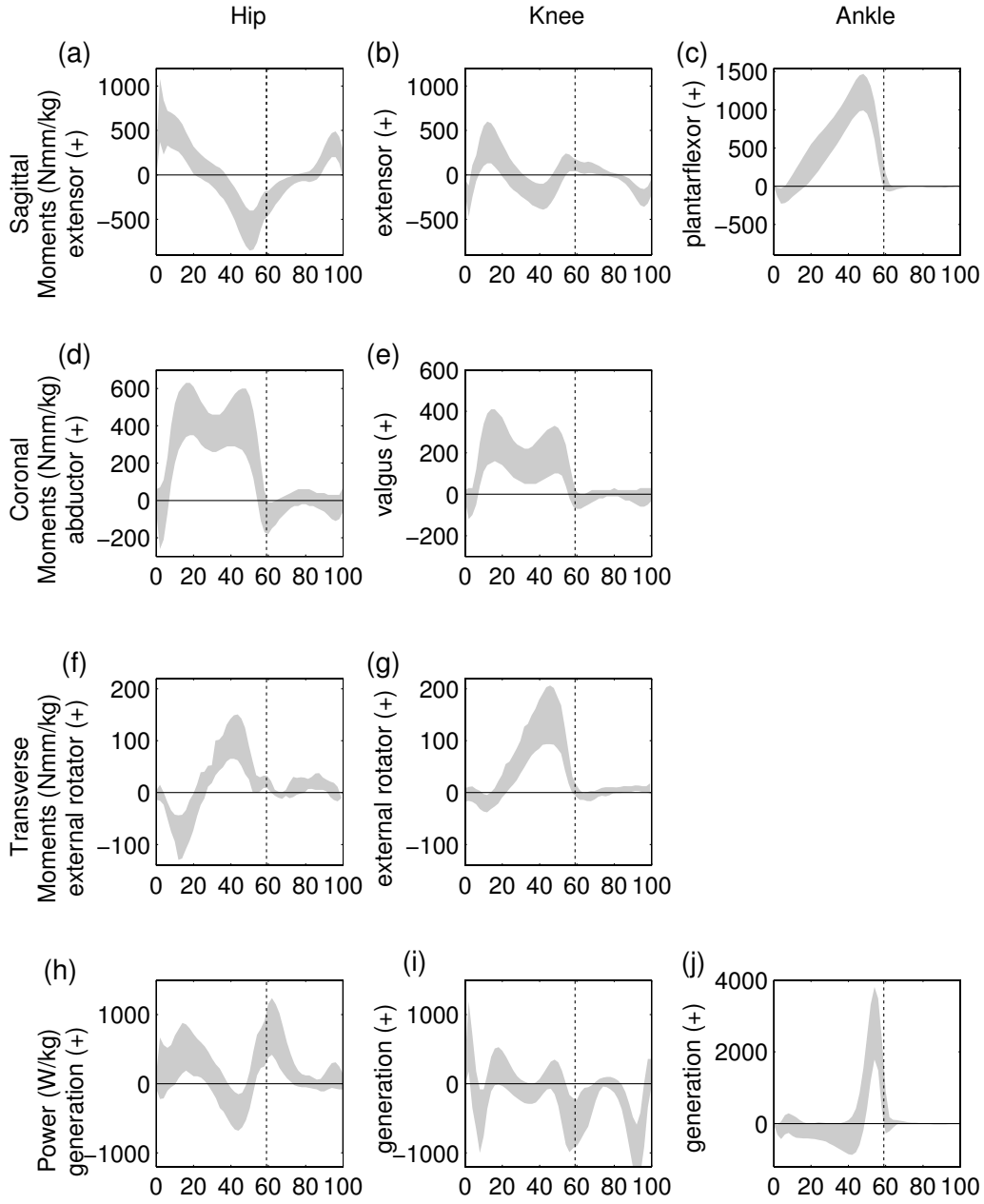

Figure 2.5 – Hip, knee, and ankle kinetics (0–100% of the gait cycle). Grey bands cover ± 1 standard deviation of the mean. Dashed vertical line shows approximate position of foot-off. Source: hip and knee transverse plane moment graphs (digitized) in [192]. All other parameters from supplemental data in [194].

pelvis is rotated externally (Fig. 2.5 f). The knee moment shows a single external rotator moment, coincident with the hip, in terminal stance (Fig. 2.5 g). As in the coronal plane, transverse ankle moments are not reported.

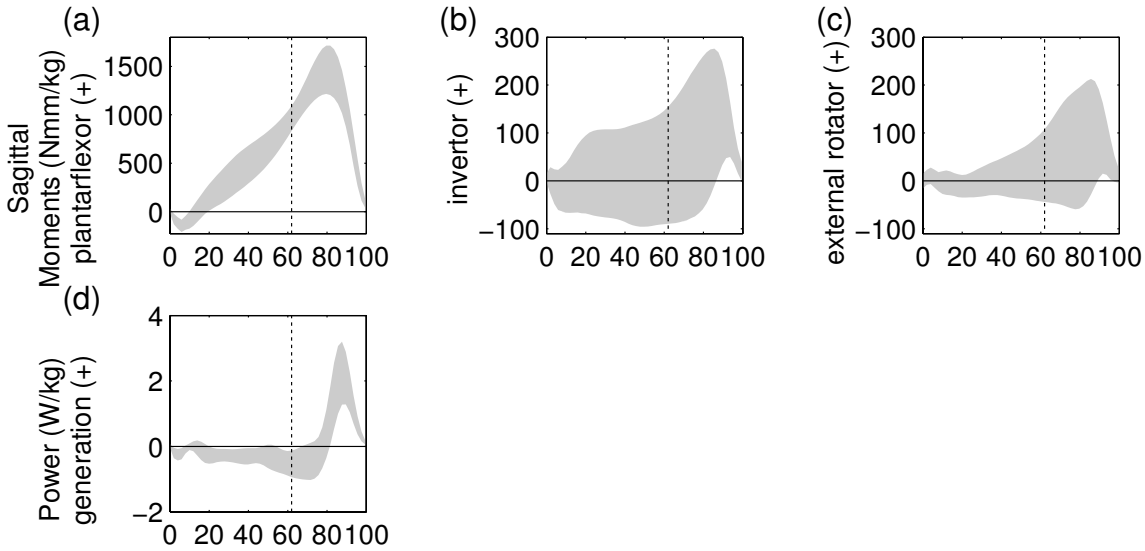

Figure 2.6 – Hindfoot/tibia kinetics in TD children (0–100% of the stance phase). Grey bands cover ± 1 standard deviation of the mean. Dashed vertical line shows approximate position of foot-off. Source: original data in [63].

Foot kinetics

The PiG ankle kinetics suffer from the same limitation as the PiG ankle kinematics, i.e. they are derived via an assumption of a single foot segment and are unable to appropriately represent non-sagittal plane quantities. A number of investigators have reported multi-segment foot kinetics in order to address these limitations [28, 63, 147, 197, 198]; however, only Dixon et al. [63] did so using the OFM.

The OFM ankle moments in the sagittal plane are similar to quantities computed via the PiG model (Fig. 2.6 a). Quantities in the coronal and transverse plane, although variable, show peak invertor and external rotator moments, respectively, in pre-swing (Fig. 2.6 b and c).

OFM ankle power reveals a similar pattern to the PiG version; however, the power generation peak is decreased (Fig. 2.6 d), due to changes in estimates of segment angular velocities across models [63].

2.2.4 Ground reaction forces

The net forces exerted on the body by the ground are estimated by the GRFs. In gait analysis, these forces are not usually directly considered, but rather they are collected in order to estimate joint kinetic quantities (see Section 2.2.3). Nonetheless, an understanding of typical GRF patterns is important as gait pathology is also reflected in this metric. For example, see White et al. [238] for a comparison of the variability in GRF components between TD children and children with CP. The three-dimensional GRFs can be separated into vertical and horizontal shear (antero-posterior and medio-lateral) components that are best understood with respect to the movement of the body's COM. The COM accelerates and decelerates regularly, driven by forces, producing an oscillatory pattern throughout the gait cycle [53].

Normative GRF data for TD children were only available for the vertical and antero-posterior components in the work of Schwartz et al. [194]. Thus, considering the importance of medio-lateral GRF during turning gait, normative data in all three planes from healthy young adults ($n = 10$ and mean age 22.6 years) are reproduced here based on the study by Dixon et al. [66].

The vertical GRF component makes up the majority of the total GRF vector. During straight walking, it displays a "double-bump" pattern with two peaks above body weight separated by a trough below. In the loading phase, the mass of the body is transferred to the leading stance limb and the vertical GRF begins to increase. During mid-stance, the COM is accelerated upwards reaching a maximum positive acceleration coincident with the first peak in vertical GRF (20% of the stance phase). A decreasing upwards acceleration continues until approximately 40% when the COM reaches its highest point. At this time, the COM accelerates downwards reaching a maximum negative acceleration in the trough (50%). This negative acceleration is gradually reduced, reverses polarity, and reaches a maximum positive acceleration at

the end of terminal stance, coincident with contralateral foot-strike. In pre-swing, the body's mass is transferred to the contralateral limb in preparation for a new gait cycle and the vertical GRF of the now trailing limb decreases [53] (Fig. 2.7 c).

The antero-posterior shear GRF is related to the acceleration and deceleration of the COM in the direction of progression. At the start of the gait cycle, the heel of the advancing stance foot strikes the ground with a forward velocity and an equal and opposite (posterior) GRF allows the foot to remain stationary (avoid slipping). This posterior force gradually reaches a peak at the end of loading before gradually reducing in mid-stance as the COM is positioned above the stance limb. In terminal stance, the body begins to re-accelerate the COM and an anterior GRF, reaching a peak near the start of pre-swing, is seen in response to the muscle action required for push-off [53] (Fig. 2.7 b).

The medio-lateral GRF is a consequence of walking with a non-zero step width. During the first part of the loading phase, a short-lived laterally directed GRF is observed, but generally throughout the rest of the gait cycle a medial GRF helps keep the body balanced in the coronal plane: the vertical GRF and the body weight create a force couple tending to rotate the body towards the swing limb, while a laterally directed inertial force, generated from the trailing swing-limb and the medial GRF act to rotate the body in the opposite direction [53].

2.2.5 Free vertical torque

The torque developed as a reaction to the horizontal GRF couple exerted on the foot is referred to as the free vertical torque (T_Z) [6] (see Section 3.6.4 for calculation details). The T_Z profile can be used to discern straight walking from turning [104] and to identify pathology in runners [155]. Therefore, T_Z is potentially an important metric

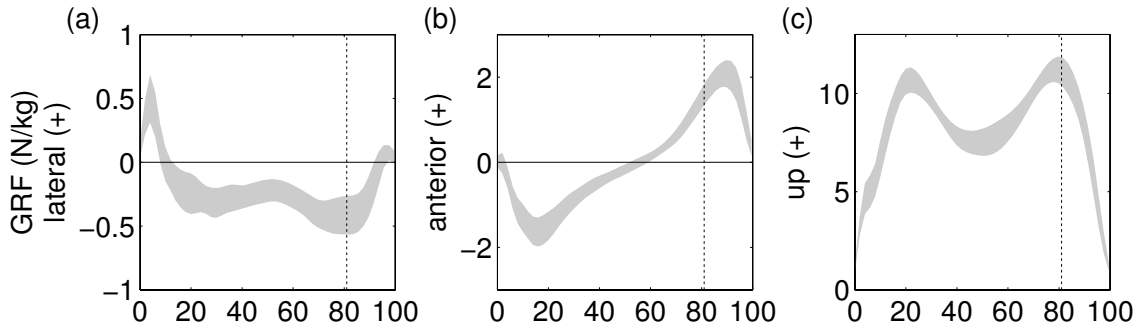

Figure 2.7 – Ground reaction force (GRF) (0–100% of the stance phase) in the (a) medio-lateral, (b) antero-posterior, and (c) vertical direction for healthy young adults. Grey bands cover ± 1 standard deviations of the mean. Dashed vertical line shows approximate position of contralateral foot-strike. Source: original data in [66].

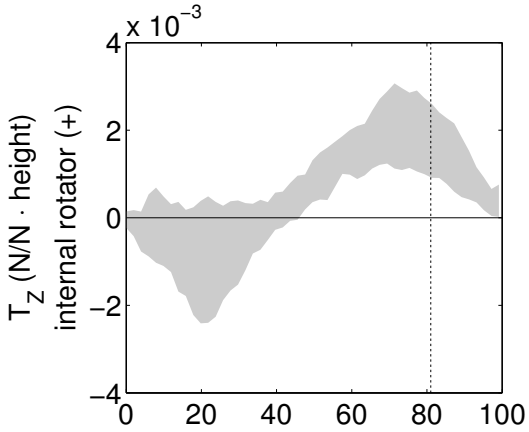

Figure 2.8 – Ground reaction free vertical torque (T_Z) (0–100% of the stance phase) for healthy young adults. Grey bands cover ± 1 standard deviations of the mean. Dashed vertical line shows approximate position of contralateral foot-strike. Source: graph (digitized) in [6].

in the analysis of turning gait in children with CP. Normative T_Z data are presented based on the work of Almosnino et al. [6] in healthy young adults ($n = 11$).

The T_Z profile is a sinusoidal waveform with a small external rotator moment reaching a peak near 20% of stance and a larger internal rotator moment peak in terminal stance (70% stance) (Fig. 2.8).

2.2.6 Muscular activity

Walking is achieved via the contraction of different muscle groups during specific phases of the gait cycle. The metabolically efficient gait seen in TD children and healthy adults is produced mainly via eccentric or isometric muscle contraction and through passive mechanisms. The reliance on energy inefficient concentric contractions is minimized, but nonetheless important to advance the body and complete certain tasks [21]. In this section, the activation timings with respect to the gait cycle of the main muscle groups are described.

Normative muscle activity data in TD children ($n = 87$, age 3–18) walking at a comfortable walking speed were digitized from graphs of Chang et al. [40]. Data from Schwartz et al. [194] were not used as only a limited number of muscles activation patterns were presented. In the description below, gluteus medius and gluteus maximus represent hip abductors and extensors, respectively (Fig. 2.9 a and b). Rectus femoris and vastii (medial and lateral) are shown to represent knee extensor activity (Fig. 2.9 c–e), while hamstrings (medial and lateral) approximate behaviour of the knee flexors (Fig. 2.9 g and h). Finally, tibialis anterior and gastrocnemius represent ankle dorsiflexor and plantarflexor activity, respectively (Fig. 2.9 f and i).

Starting at initial contact, co-contraction of the knee flexors and extensors helps to stabilize the knee, while eccentric activity of the ankle dorsiflexors slows the placement of the foot on the floor (avoids "foot slap"). Contraction of the hip extensors also contributes to knee extension [21]. During loading, the knee extensors resist knee flexion (eccentric contraction and power absorption) and begin to extend the knee (concentric contraction and power generation). Assistance in knee extension is provided from eccentric ankle plantarflexor activity which moves the point of GRF application anteriorly towards the forefoot and thus reduces the external knee flexion moment. Furthermore, contraction of the hip abductors (mainly isometric gluteus

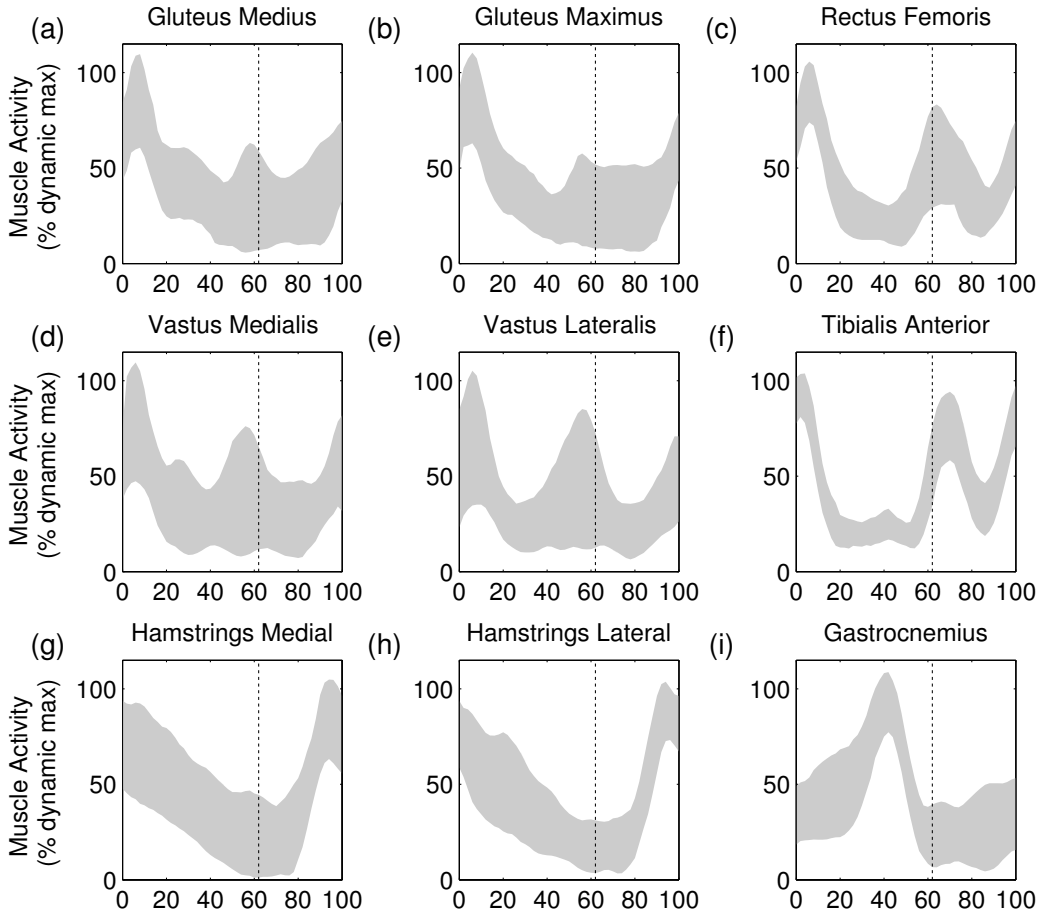

Figure 2.9 – Muscular activity of the major lower-limb muscles in TD children (0–100% of the gait cycle). Grey bands cover ± 1 standard deviation of the mean. Dashed vertical line shows approximate position of foot-off. Source: graphs (digitized) in [40].

medius activity) prevents excessive drop of the contralateral pelvis by producing an internal hip abductor moment [21]. During mid-stance, continued plantarflexor activity allows the leg to remain relatively straight and passively moves the body COM forward (falling inverted pendulum) [21]. In terminal stance, concentric activity of the ankle plantarflexors, having halted ankle dorsiflexion, begins to plantarflex the ankle and provides push-off power to re-accelerate the body COM [21].

Towards the end of stance, preparation for swing-limb advancement begins. Pre-swing sees a short burst of concentric contraction of the hip flexors which aid in lifting the stance limb off the ground during the swing phase [21]. The large thigh

muscles remain relatively inactive during initial and mid-swing as the limb passively moves forward (as in a swinging pendulum); however, the ankle dorsiflexors produce concentric contractions to lift the foot and thus provide foot clearance. Finally, during terminal swing, the knee flexors eccentrically contract to control knee extension (and hip flexion), while near isometric contraction of the ankle dorsiflexors maintains the ankle in a neutral position in preparation for the next foot-strike [21].

2.3 Clinical Tests

In addition to the gait metrics derived from CGA, it is common to also collect muscle strength and joint mobility information, collectively known as clinical gait tests. An investigation by Desloovere et al. [61] in a large sample of children with CP ($n = 200$) found poor correlation between gait analysis metrics and clinical tests prompting the authors to conclude that both datasets provide different, yet relevant, information for the management of gait disability. A short summary of common tests is presented from Adams and Perry [2].

2.3.1 Muscle strength

Manual muscular strength testing (MMT) is conducted for the major muscle groups of the lower-limbs (see Section 2.2.6). MMT is rated on a scale from 0–5 with values ranging from no muscle contraction (0) to normal strength (5). Intermediate values of 2, 3, or 4 represent poor, fair, and good muscle strength, respectively [2]. Given the subjective nature of MMT, some devices have been developed and successfully used to gauge muscle strength in children with CP [11, 239]. Nonetheless, many laboratories, including the OGL, successfully use MMT.

2.3.2 Joint mobility

Manual joint mobility tests measure the passive range of motion (ROM) available at each joint. In children with CP, limited ROM due to joint contractures is often identified. It is important to note that the dynamic ROM used during gait might be both larger than measured during manual assessment in children with CP as elastic contractures can "yield" under the greater forces exerted on the joints during walking [2] or smaller due to velocity-dependent spasticity effects.

2.4 Cerebral Palsy

CP refers to a group of disorders characterized by an injury to the central control system of the brain and has a prevalence of between 1.3 and 3 per 1000 live births in Europe for the birth cohort of 1980 to 1986 [152]. CP predominantly affects the legs (diplelgia), one side of the body (hemiplegia), or all extremities (quadriplegia), making gait difficult or impossible [95]. There are four main types of movement disorders associated with CP: spastic, dyskinetic, ataxic, and mixed [95]. Across Europe, the spastic subcategory represents 53.9% (diplegic) and 31.0% (hemiplegic) of children with CP born between 1980 and 1996 [152]. These children present with spastic muscles, i.e. muscles that contract involuntarily under rapid stretching. From a motor-control perspective, walking can be thought of as a reflex-driven task in which the main role of the brain is to control reflex activity [173, pp. 345–356]. Without the brain's inhibitory role on reflex-response, the smooth gait patterns seen in TD children and healthy adults, cannot be achieved. Moreover, poor motor control, decreased balanced, joint contractures, and muscle weakness are known to contribute to the development of abnormal walking patterns [173, pp. 345–356]. These gait deviations can be precisely analysed through CGA protocols. The use of CGA in the planning of treatment interventions in populations with gait disabilities is quickly

becoming standard practice and has been shown to improve post-operative gait parameters [76]. Surprisingly, CGA usually assesses the aforementioned parameters solely during straight walking regardless of the prevalence of non-linear gait tasks such as turning in everyday locomotion.

2.4.1 Gait patterns

Children with spastic CP can also be classified by gait style with Sutherland and Davids [224] suggesting four main patterns: jump, crouch, stiff knee, and recurvatum knee. In jump gait, walking is characterized by increased knee and hip flexion at initial contact as well as ankle equinus. Increased hip flexion is a secondary problem arising from spasticity of the hip flexors (primarily iliopsoas) that also interferes with the normal hip extension seen in non-pathological gait and leads to decreased step length. The crouch gait movement pattern also exhibits increased flexion of the knee and hip during stance, but here flexion remains persistent throughout the stance phase. Moreover, the ankle may remain dorsiflexed (calcaneus) [173, pp. 345–356]. A calcaneus deformity often results from surgical procedures in which only the achilles tendon is lengthened (single event surgery). Multi-level surgery avoids the development of such iatrogenic problems [173, pp. 345–356]. In stiff knee gait, the knee is unable to flex adequately during the swing phase, usually due to over-active knee extensors. This gait pattern makes foot clearance during swing difficult and therefore compensatory behaviours at proximal joints and segments are often needed [173, pp. 345–356]. The recurvatum knee pattern is distinguishable by a noted knee hyperextension during stance. It is the least common of the four gait patterns described by Sutherland and Davids [224] and often arises due to plantarflexor spasticity or joint contractures. Perry notes that surgical over-lengthening of the hamstring tendon can also lead to the recurvatum knee pattern [173, pp. 345–356].

Table 2.3 – Primary gait patterns in children with cerebral palsy

Pattern	Pelvis	Hip	Knee	Ankle
True Equinus	Typical/ Anterior	Typical	Typical/ Recurvatum	Equinus
Jump	Typical/ Anterior	Flexed	Flexed	Equinus
Apparent Equinus	Typical/ Anterior	Flexed	Flexed	Normal
Crouch	Typical/ Anterior/ Posterior	Flexed	Flexed	Calcaneus
Asymmetrical	Different patterns for left and right legs			
Mild	Within 1 standard deviation of typical patterns			

Patterns based on sagittal plane kinematics. Source: Table 1 (modified) in [184].

Rodda et al. [184] have suggested the removal of recurvatum knee as a stand-alone pattern and introduced true equinus, apparent equinus, asymmetrical, and mild gait as additional gait pattern categories (Table 2.3). The true equinus gait pattern mostly involves an ankle which remains in equinus during the gait cycle. An equinus ankle arises from a spastic gastrocnemius muscle which manifests as persistent ankle plantarflexion throughout the gait cycle [173, pp. 345–356]. Additionally, the knee may hyper-extend (recurvatum). In true equinus, the pelvis can exhibit excessive anterior tilt, but generally the more proximal joints present more typical patterns [184]. Children with an apparent equinus gait pattern, as the name implies, appear to walk with a plantarflexed ankle as a result of excessive knee and hip flexion. The pelvis may show some abnormalities [184]. Finally, Rodda et al. [184] defined asymmetric gait as a pattern in which the two limbs are classified differently using the above criteria, while mild gait identifies children whose gait kinematics are within one standard deviation of their TD peers.

Identification of these patterns based on kinematic curve and video analysis has shown good intra and inter-rater repeatability [184] and, more recently, Sangeux et al. [188] have proposed an automatic algorithm to identify these gait patterns based on ankle and knee kinematics alone. The algorithm was tested on 200 legs and correctly classified 196 patterns (the four limbs incorrectly classified showed very mild deviations compared to normative data). Other gait pattern categories have been proposed in the literature [16] and automatic classifiers abound [5, 36, 162, 257]. Nonetheless, the Sangeux algorithm was implemented in this thesis (see Section 6.2.2) as it is a valid tool that can be easily run to identify gait patterns without the intervention of experienced gait analysis personnel.

2.4.2 Further deviations

In addition to the deviations described in Section 2.4.1, the hip and foot may show further abnormalities, especially in the non-sagittal planes.

At the hip, increased adduction and femoral anteversion are common. Increased hip adduction arises not only from spasticity, but also from weakness of the hip abductors, such as gluteus medius [173, pp. 345–356]. In healthy children, the loading of the femur experienced during walking in early childhood allows for femoral derotation to occur naturally; however, in children with CP, restricted gait does not permit such action. The internally rotated hip not only makes walking difficult, but may lead to increased external tibia rotation and disturbed foot posture producing an "in-toeing" gait pattern and knee instability [173, pp. 345–356].

At the foot, varus and valgus deformations are known to occur. Varus deformity is common in children with spastic hemiplegia, whereas valgus is prevalent in diplegia. Varus usually arises from over-active tibialis posterior or tibialis anterior tending to pull on the medial aspect of the foot. A valgus deformity is often associated with

increased femoral anteversion and external tibia rotation. Both deviations may lead to stance phase instability [173, pp. 345–356].

2.5 Turning Gait

Hase and Stein [105] describe turning gait as a transient process in which (1) the forward momentum of the body COM is reduced, (2) the body is rotated, and (3) a step out to the new direction is performed. In healthy subjects, the process is smooth and flows from one stage to the next [171]. This process requires anticipatory postural adjustments [250] and may be more challenging from a stability perspective than straight-line walking [201].

It is often convenient to separate turning gait into approach (initiation), turn (apex), and depart (termination) steps (turning cycle) for analysis [88, 219]. Since turning gait is a continuous process, especially in normal populations, each step in the turning cycle may contain more than one of the three phases described above.

2.6 Turning Strategies

Given the nature of bipedalism, turning gait can be performed using predominantly either the outside or inside leg, first described in the walking literature by Hase and Stein [105] as the “step” and “spin” turn technique, respectively (Fig. 2.10).

From a balance perspective, step turns appear to be more stable than spin turns. For step turns, the COM remains within the base of support throughout the turning manoeuvre, while for the spin technique, the COM moves towards the lateral side of the stance limb [105, 172, 226]. Moreover, the minimum distance between the feet is larger during step turns, implying a reduced risk of tripping [226]. From an energetics point of view, the step turn may also be advantageous as peak moments and

powers are generally greater for spin turns suggesting greater muscular demand [226, 251]. Furthermore, Patla et al. [172] proposed that spin turns might also be more demanding based on characteristics of the medio-lateral GRF profile.

A pilot study ($n = 9$) investigating turning gait in TD children confirmed that both step and spin turn strategies were implemented during a 90° turning task [154]. In an investigation of young adult gait ($n = 10$, mean age 22.8 years), Taylor [225] and Taylor et al. [226] reported division of spin turns into pivot ($n = 4$) and cross-over ($n = 6$) subcategories. Note, although both the doctoral thesis of Taylor [225] and the manuscript by Taylor et al. [226] examine the same dataset, only the former performs statistical analysis between conditions. Therefore, the thesis work is referenced when describing statistical claims of difference between conditions, otherwise the manuscript is referenced for ease of access for the reader. In pivot turns, rotation of the forefoot occurs with respect to the walking surface, while for the cross-over a rooted foot (foot flat) turning strategy is employed [226]. These sub-techniques have not been reported by other investigators during 90° turning gait and evidence that they represent two distinct biomechanical techniques is lacking.

2.7 Prevalence of Turning

An early study by Bracha et al. [24], tracking turning behaviour in adults ($n = 135$, mean age 33 years) using a portable belt-mounted device, reported an incidence of approximately 73 full turns (360°) during a 7–8 hour period. Their experimental protocol did not allow the recording of the overall frequency of turning steps compared to straight steps, leaving this task for later investigators.

In a task analysis of turning frequency in older adults ($n = 4$, mean age 76 years), Sedgman et al. [199] found via standard video recording that between 1.3 (collecting mail) and 2.4 (answering the telephone) turning steps per 10 steps were required

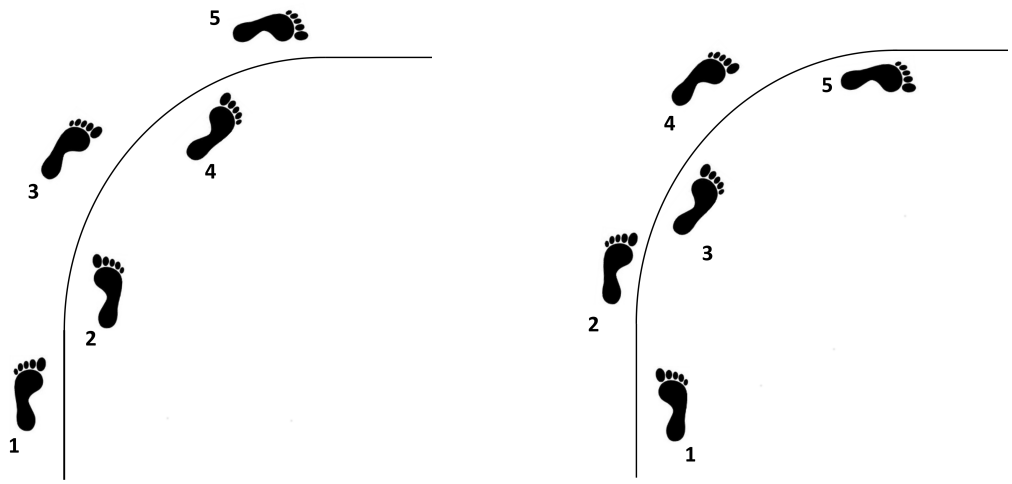

Figure 2.10 – Diagrammatic representation of (a) a 90° step turn to the right and (b) a 90° spin turn to the right. For the step turn, the ipsilateral limb is left (outside at step 3), while for the spin turn, the right leg (inside at step 3) is taken to be ipsilateral.

to successfully complete tasks. In this study, turns were defined as "a rotary motion in which the body changes direction, occurring whilst in upright stance on two legs" [199]. Thus, the actual number of turning gait steps might be lower than the numbers quoted above as some steps might have been static [199].

A later study by Glaister et al. [87], also using video recording, quantified the number of turning steps in daily activities outside the home in healthy young adults ($n = 11$, mean age 31 years). The subjects in this investigation completed on average 0.8, 3.5, 4.5, and 5.0 turning steps for every 10 steps as they walked through an office, a parking lot, a cafeteria, and a convenience store, respectively [87].

Newer foot-worn sensor technologies have also been used to measure straight and turning gait parameters in both TD children and children with CP [27]. To date, a full task analysis has not been attempted using this technology.

Overall, these studies reveal that turning is a crucial component of locomotion that should not be overlooked, prompting some authors to recommend the assessment of turning in clinical gait analysis [61, 87, 199].

2.8 Turning Preference

The study of Bracha et al. [24], while measuring total numbers of turns, had as its main purpose the establishment of a relationship between brain hemispheric dominance and turning behaviour in men and women. They found that, in general, women completed more turns than men during the study period [24]. Moreover, left hemisphere dominant men preferred to turn right, while left-hemisphere dominant women tended to turn left [24]. Later work ($n = 93$, age range 21–59), showed specifically that handedness predicts turning behaviour with right handers preferring left-side turns and left-handers preferring right-side turns [156]. Although asymmetrical turning behaviour in animals (rats [92] and cats [93]) is linked to hemispheric dopamine asymmetries, no attempt to measure dopamine was made in human studies.

The neuro-chemical basis for turning preference remains unclear; however, the choice of turning style, at least, might be predicted from mechanical factors. Patla et al. [172] suggested that:"the preferred change in direction of locomotion is therefore guided by stability and parsimony in modulation of locomotor patterns to achieve a safe and economical adaptation of gait". Patla et al. [172] were referring specifically to the change in magnitude and direction of the medio-lateral GRF during spin turns and suggested that step turns, which simply amplify the straight pattern, would be preferred. In a later study, Akram et al. [3] reported the turning preferences of older adults ($n = 19$, mean age 66 years) in the completion of 45 and 90° turns at slow, comfortable and fast speeds. The step turn technique was only favoured for high-speed 90° turns, suggesting that balance and energetics may not be strong predictors of turn selection, even in older adults.

Overall, step turns most closely resemble straight-line gait [226]; yet, this strategy does not appear to be the universally preferred turning strategy across populations.

The work of Hase and Stein [105] suggests this might be the case for unplanned turns, but it remains unclear if the same is true for planned turning manoeuvres.

2.9 Anticipation in Turning Gait

Turns can be either planned or unplanned. In the latter case, an individual may need to quickly reorient his or her body towards a new direction in response to an unexpected perturbation. In the former situation, ample time is provided to the central nervous system to make decisions. Early work has shown that when a cue to turn is given after the COM has passed anterior to the leading limb (unplanned), subjects tended to use the step turn strategy [105]. Moreover, different control strategies are implemented based on planning time. When the turn is planned, subjects can implement a foot strategy, in which the foot placement is changed, while during unplanned tasks, the hip initiates increased pelvic obliquity [171]. The foot strategy was found to be implemented by TD children during 90° turning gait [154].

Although unplanned turns may cause significant challenges to children with CP, planned turns are likely to be more frequent and should be understood first before moving to more complex situations involving late cueing.

2.10 Turning Angle

Turns can rotate the body through any desired number of degrees in order to accomplish a given task; however, in order to assess the biomechanics of turning gait, investigators have typically measured specific angular rotations between 20–360° [172] or even circular walking [47, 165, 200]. Steady-state turning tasks, such as circular walking, are blind to the important transition steps between straight walking and turning and therefore are not investigated further in this literature review.

In Parkinson's disease, studies of large angle turns (180–360°) are popular [207, 208, 210, 233] as freezing behaviour often arises during large angular rotations [190]. In elderly adults, the 180° turn is often investigated as it is a component of the timed "Up and Go" test (TUG), a common clinical test of mobility in this population [177]; however, Paquette et al. [168] recommend the use of smaller turn angles in this population to reduce the physical demands on the subjects.

In the task analysis study of Sedgman et al. [199], the majority of turn angles resulted in a reorientation of 76–120° with respect to the original walking direction. Presumably, the preference for angular rotations in this range is related to the ubiquity of 90° turns in the built environment and has led many investigators to focus on the 90° turn [1, 3, 4, 19, 61, 88, 94, 121, 137, 138, 150, 154, 186, 209, 219, 225, 250]. These studies are a strong motivation for the use of 90° angles in turning gait studies. Thus, Section 2.11 focuses on the adaptations to gait metrics during 90° turning.

2.11 Turning Gait Metrics

Turning gait requires biomechanical adaptations in order to ensure successful completion of the task. In general, past research has focused on the main gait metrics used in the analysis of straight walking: STPs, joint kinematics, joint kinetics, and muscular activity. Furthermore, investigation of centre of pressure (COP) progression, GRF profiles, and COM kinematics has also been conducted. Both these categories of variables are now described. Clinical tests involving turning tasks are also explored.

2.11.1 Spatio-temporal parameters

The very nature of turning requires modification of STPs; yet, few studies have investigated differences in these metrics compared to straight walking or between turning

styles. To date, research has focused on cadence, stride and step length, stride and step width, and stance time. For a discussion of gait speed, see Section 2.11.5.

Starting with cadence, the pilot work of Milandri [154] found this metric to be similar across tasks (turning gait vs straight walking) in TD children, in agreement with the work of Hase and Stein [105] where the "underlying walking rhythm" was found to be unaffected in most subjects.

Stride length was also investigated by Milandri [154]. This study found that in TD children stride length was reduced near the apex of the turn. In older adults, a trend towards decreased step length was reported [19]. Of note, both of these studies failed to separate step and spin strategies for analysis. In the study of Taylor [225] looking across turning styles, only the cross-over strategy showed a significant decrease in step length, compared to straight-line gait. In disagreement with Taylor [225], another investigation found that step length (and stride length) was reduced during step turns, with the greatest reduction during the turn phase [219]. Although, stride (and step) length differences might not be present in all studies, possibly due to differences in experimental protocols, it appears that a decrease could be related to lower-limb adaptations intending to slow the forward progression of the COM [105]. A recent study involving 180° turning gait in TD children and children with CP reported a reduction in stride length in both groups [27].

Another important STP of turning gait is step width. Using the toe-to-toe distance as a surrogate measure for step width, Taylor [226] found that step turns resulted in the largest step width. Both spin techniques reduced step width, with the cross-over sub-technique showing the greatest reduction [225]. In a step turn study, the turn phase had the maximum step width [219].

Stance time, in healthy adults, was found to increase only during the ipsi-pivot sub-technique of spin turns [225]. In step turns, the work of Strike et al. [219] revealed

an increase (significant only for the right limb) during the turn phase compared to straight-line gait. Returning to the work of Brégou-Bourgeois et al. [27], a significant increase in stance time was only noted for the CP group during turning, indicative of an increased need for stability in this population.

Overall, the STP adaptations of turning gait are consistent with the requirements of the task. STP analysis provides a good overall picture of gait and is a direct outcome of the neuro-muscular control strategies employed. STP analysis of 90° turning gait in children with CP could provide further information about the adaptations required to successfully complete this relevant turning task.

It is important to note that the formulae for calculating straight STPs must be modified in the case of curvilinear motion [120]. In fact, the formulae proposed by Huxham et al. [120] are more general and can be used for both gait patterns. Furthermore, Huxham et al. [120] suggested that in the case of turning, the term stride width should be used in place of the standard step width, as the width in question is related to the stride (see Section 3.6.1 for more details).

2.11.2 Joint kinematics

The lower-limb joint kinematics of the turning limb (inside limb for spin and outside limb for step) during 90° turning gait in adults reveal substantial differences between turn strategies and compared to straight walking. The majority of findings presented here are from the work of Taylor et al. [225] and Taylor [226].

Starting at the ankle, both turning strategies reveal decreased dorsiflexion in mid-stance compared to straight walking [225]. In the coronal plane, increased eversion was found in terminal stance for step turns, while cross-overs showed increased inversion, compared to straight-line gait [225]. In the transverse plane, the only noted

difference was large external rotation for step turns compared to slight internal rotation for straight gait towards terminal stance [225]. Importantly, the exact motion of the ankle is difficult to interpret via the single-segment foot PiG model. The use of multi-segment foot models allow for improved three-dimensional motion at the ankle [37, 213]. From this perspective, and in disagreement with Taylor [225], Jenkyn et al. [125] reported similar dorsiflexion at the ankle (talo-crural joint) between 45° step turns and straight-line gait ($n = 12$, mean age 27 years). It remains unclear if this disagreement arises from the different tasks (45 vs 90°) or models (single vs four segment foot) investigated. In the coronal plane, the general trend of inversion to eversion (subtalar joint) was also observed in the multi-segment foot study, prompting the authors to suggest that in the event of an uncontrolled turn, inversion would continue and may lead to ligamentous damage [125]. The other reported intra-foot motions were similar between tasks [125].

At the knee, peak knee flexion angle in stance decreased for the step and cross-over spin turns [226], possibly revealing decreased loading, but no significant difference was reported [225]. During terminal stance, the decrease in flexion for step turns compared to straight walking [226] was significantly different [225]. Range of motion in the coronal plane appeared increased for all turning strategies with the spin techniques showing abduction and step revealing adduction, throughout most of the stance phase [226]. In the transverse plane, the step turn led to external rotation, while the spin conditions produced internal rotation [226]; however, differences were not significant [225], possibly due to large variability. Again, the non-sagittal plane knee angles of Taylor et al. [226] and Taylor [225] might be erroneous. It is well known that in the PiG model cross-talk between the reported angles can occur if the flexion-extension axis of the knee is poorly defined from a misaligned thigh wand marker [13]. A number of methods exist to remedy this problem [191] (see Section 3.5.1 for the solution of Baker et al. [13] used in this thesis), none of which were implemented by

the referenced studies [225, 226]. A more recent study investigating numerous tasks, including 90° step and spin turns, in which the knee axis was aligned using the Knee Alignment Device (Motion Lab Systems, Inc, Baton Rouge, USA), may provide more accurate angular values. In the sagittal and coronal planes, there were no significant differences between tasks [61]. In the transverse plane, the spin turn revealed increased maximal internal rotation, while the step turn showed increased maximal external rotation and range of motion, compared to straight walking [61].

Finally, at the hip, no significant differences were found in the sagittal plane [225], although trends were apparent [226]. Both the step and cross-over techniques showed reduced flexion during loading response, while towards the end of stance phase, it was the spin conditions that presented decreased extension (neutral to slight flexion), compared to straight-line gait [226]. These adaptations may have allowed for the reduced stride length reported elsewhere [219]. In the coronal plane, although the spin conditions showed slight increases in peak adduction (non significant), the greatest difference was for step turns where the hip became abducted throughout stance as the limb steps out in the opposite direction to the turn [225, 226]. Both the step and pivot spin trials showed large external rotation from mid-stance onwards, while the cross-over technique most resembled straight-line gait—save for increased external rotation in early stance [226]. Again, a misaligned thigh wand marker may have led to errors in the aforementioned hip joint kinematics [13].

Although the work of Taylor [225] and Taylor et al. [226] represent the most complete analysis of 90° turning gait lower-limb joint kinematics, their non-sagittal plane angles are difficult to interpret in light of the PiG model limitations and the small number of subjects investigated. Future work in this area using multi-segment foot models is warranted, especially in children, as it is unknown if they show similar adaptations to adults due to neuromaturation effects and anthropometric differences.

2.11.3 Joint kinetics

Joint moment and power adaptations during 90° turning gait are drivers of kinematic changes and warrant investigation. In addition to the studies of Taylor [225], Taylor et al. [226], and Jenkyn et al. [125], further work by Xu et al. [251] ($n = 5$, mean age 21.0 years) and Glaister et al. [90] ($n = 10$, age range 24–27 years) has analysed the lower-limb joint moments during 90° turning gait and are included in this review.

Beginning in the sagittal plane for the ankle, turning gait showed an early rise in ankle internal plantarflexor moment during loading response [226, 251], with the greatest increase seen in the cross-over technique [225]. Statistical analysis revealed that differences occurred between all turn styles and straight walking [225]. Also, the maximum plantarflexor moment peak appeared reduced for cross-over spins [226] and spin turns in general [251]. This reduction for the cross-over was found to be significant [225]. Using a multi-segment foot model, these adaptations were found to be non-significant by Jenkyn et al. [125]. Nonetheless, this strategy appears to be related to an attempt at braking, through eccentric contraction of the plantarflexors, to slow the forward progression of the COM [251]. In the coronal plane, for the step turn, Taylor [225] found a clear increased peak invertor moment towards terminal stance, while Xu et al. [251] found reduced evertor moments. As these quantities were computed via the PiG, they are difficult to interpret. The multi-segment foot findings of Jenkyn et al. [125] show subtalar joint internal evertor moment throughout stance that arrests the subtalar inversion seen in the first half of stance. For the spin turn, Xu et al. [251] reported invertor moments, while Taylor et al. [226] showed an evertor moment for cross-over (significant [225]) and near-zero moment for the pivot technique towards terminal stance [226]. Unfortunately, no spin data are available from Jenkyn et al. [125]. Transverse plane moments of the ankle for spin turns are inconsistent between studies with Taylor et al. [226] showing increased external

rotator moments and Xu et al. [251], increased internal rotator moments. For step turns, Glaister et al. [90] found significantly decreased external rotator moments (only a trend in Taylor et al. [226]). Multi-segment foot analysis did not reveal any changes in this plane [125]. The behaviour of the ankle during turning gait remains unclear. Future research using larger cohorts and a multi-segment foot model in both 90° step and spin turns needs to be conducted.

At the knee, internal knee extension moment during loading is significantly reduced for the cross-over spin [225], despite similar kinematics to straight-line gait [226]. This reduction was also noted for spin turns in general, possibly in response to the greater role of the ankle in the braking process [251]. Towards terminal stance, a trend of decreased extensor moment was seen for cross-over spins [226], spin turns in general, and step turns [251]. These changes may be related to the reduced need to re-accelerate the COM in the forward direction during turning [251]. Knee coronal plane moments during terminal stance reveal significantly decreased valgus moment for the step turn compared to straight walking [225]. Trends of increased valgus moment for the spin turns were also apparent [226, 251]. In the transverse plane, external rotator moments were increased for pivot spin turns according to Taylor et al. [226]. This is in contrast to Xu et al. [251] who found a trend of increased internal rotator moment for spin turns and external rotator moments for step.

For the hip, sagittal plane moments were not greatly affected by turning gait [226, 251]. In the coronal plane, only the step turn showed a trend for decrease in abduction moment in terminal stance [226, 251], while only Xu et al. [251] found that spin turns trended towards increased abduction moment. Finally, in the transverse plane, step turns appear to reveal near-zero moments [226, 251]. For spin turns in general, increased internal rotator moments was suggested [251], while for the pivot spin, external rotator moment was significantly increased compared to straight-line

gait [225]. Unfortunately, hip moments have only been reported in the stance phase. Possibly, changes may occur in swing as the limb is prepositioned in anticipation of the requirements of the turning task.

With both main works reporting three-dimensional moments from the PiG model [225, 226, 251], having small cohorts, and not presenting inferential statistics (only in Taylor thesis [225]) or standard deviation bands, interpretation is limited. Further, as Jenkyn et al. [125] only reported step turn foot data, joint kinetic quantities are still largely unexplored and demand further investigation.

Net power profiles have also revealed some differences between turning gait and straight walking. At the ankle, both step [90] and cross-over spin [225] turns showed significantly decreased peak power generation, possibly due to the decreased need for forward propulsion [251] as the stance limb is mainly used for support [90]. At the knee and hip, small differences were also seen in pre-swing with all turn styles showing decreased absorption and generation, respectively [225, 226].

By separating the power into planar contributions using the method of Eng and Winter [74], Taylor [225] found that the main contributions to net power changes were sagittal ankle power as well as coronal plane knee and hip power. This separation of power into planar components is unusual in gait analysis and also difficult to interpret given the known weaknesses of the PiG model.

Power contribution of the contralateral side has not been investigated. It might be expected that, for spin turns at least, ankle (pre-swing) and hip (initial swing) power generation might increase in order to prepare the body for rotation [105].

2.11.4 Muscular activity

Research to date has not focused on the measurement of muscular activity during 90° turning; however, similar protocols that may reveal the motor control strategies used

during turning gait have been investigated. In the study by Hase and Stein [105], sEMG was used to measure the muscular activity of numerous lower-limb muscles for the ipsilateral side during 180° turning gait.

For the spin turn, after a cue during contralateral foot-strike, the ipsilateral limb prepares for swing, as in straight-line gait, with a concentric burst of tibialis anterior activity [105]. In initial swing, bicep femoris shows a larger, earlier sEMG burst, compared to straight gait, via eccentric contraction, possibly to initiate early foot-strike [105]. This sEMG activity may also explain the decreased stride length during 90° cross-over turns [225]. Bicep femoris may also contribute to hip external rotation and leg prepositioning for turning [105], though this is not its major role. In terminal swing, both vastus lateralis and soleus concentrically contract, possibly to extend the knee and plantarflex the ankle [105]. This kinematic strategy is not observed during 90° turning gait [226] and may only occur in 180° turns or when subjects make initial floor contact with the forefoot [105]. During loading response, the gluteus medius is also activated [105], possibly in an effort to stabilize the hip [105] and maintain a similar hip adduction profile as in straight walking [226]. The erector spinae and bicep femoris show prolonged activation during the turning phase, consistent with an increased stabilizing role as the body spins about the foot [105]. Although sEMG were only placed on the ipsilateral side, Hase and Stein [105] have hypothesized the activity of the contralateral limb. They suggest that in the ipsilateral stance phase, the contralateral soleus should produce a push-off force to initiate turning, while contralateral hip flexor activity may generate power to aid in body rotation [105].

For the 180° step turn, soleus and bicep femoris activity during the approach step help decelerate the COM [105]. Presumed further deceleration, or rather lack of acceleration, during the propulsion phase occurs due to reduced soleus and increased tibialis anterior activity [105]. The movement of the COM towards the turn is also facilitated

by the inversion action of the tibialis anterior, while pelvic stability is maintained by the gluteus medius [105]. A further braking force is hypothesized for the muscles of the contralateral stance-phase limb. Afterwards, the ipsilateral limb steps towards the new direction and resembles the straight walking pattern [105].

Some of the muscular adaptations in turning gait are similar to those found in rapid stopping [105]. Hase and Stein [105] suggest that comparison of these tasks may help determine turning specific activity. Specifically, an erector spinae and second gluteus medius sEMG burst in the turn stance phase may help control COM position.

2.11.5 Centre of mass kinematics

Many studies have focused on COM kinematics given the importance of maintaining stability as the COM is slowed, redirected, and re-accelerating during turning [105, 171]. Position, velocity, and acceleration of COM are explored in this section.

Position

The position of the COM during turning gait may provide insight on balance and stability strategies. In a study of pre-planned turns (20–60°) in healthy adults ($n = 6$, mean age 22.5 years), foot placement, was found to be the main strategy by which to achieve redirection of the COM, given ample planning time [171]. Patla et al. [171] suggested that in a spin turn the ipsilateral foot is prepositioned towards the body mid-line (away from the turn) during swing to facilitate movement of the COM towards the new walking direction.

The actual path of the COM during turning gait can also reveal differences in technique. For example, a recent conference abstract comparing both 90 and 180° turning gait in TD children ($n = 13$, mean age 14.8 years) and children with diplegic CP ($n = 13$, mean age 14.3 years) revealed that children with CP increase the turning

path length and time taken to complete the turn compared to their TD peers [186]. Although, these adaptations alone may reflect compensations for balance and motor deficits, the simultaneous analysis of the point of force application (COP) at the foot-ground interface can provide additional information.

In the study of Romkes [186], this interaction with the ground was simply measured using markers placed on the lateral aspect of each heel. She showed that during 90° turning gait most children with CP (9 out of 14) did not allow the COM to drift laterally outside the border of the foot. These findings provide further evidence of compensatory behaviour during turning gait of children with CP [186]. Unfortunately, in this study, turn style was not assessed. In healthy adults (n = 8, mean age 21 years), the relationship between the COM and COP has been investigated for both step and spin turns [250]. Xu et al. [250] found that the COM movement was modified in both the antero-posterior and medio-lateral directions. At foot-off, the angle between the COM and COP in the sagittal plane during the approach step of a 90° turn was increased compared to straight walking [250]. This indicates that the subjects did not lean as far forward, even under constraints of constant stride length, but with no differences between step and spin turns [250]. In the medio-lateral direction, there were large differences between styles with the COM moving laterally with respect to the stance foot (COP position) during spin turns [250]. For step turns, the COM overlapped with the COP position in the approach step, but was medial to the turn step COP [250]. These changes are consistent with assessments that spin turns are more challenging to balance than step turns [105, 226].

Investigation of the COM-COP relationship may provide clues about the dynamic stability requirements of turning gait; however, Bruijn et al. [30] highlighted that this measure has not been validated. The use of the extrapolated COM concept of Hof [112] may be more appropriate (see Section 2.12.1).

Velocity

The magnitude of the tangential velocity (speed) of the COM is often measured in gait analysis and is known to decrease with decreasing turning radius in a predictable manner [232]. During turning gait, an easily quantifiable steady state pattern does not emerge, making prediction more difficult.

Pilot work in children by Milandri [154] and a study in older adults by Bhatt [19] revealed a reduction in the magnitude of tangential COM velocity during 90° turning gait compared to straight-line walking; however, these studies did not investigate possible strategy-dependent changes. This approach was undertaken by Taylor [225] and revealed that only 90° step turns and the pivot spin sub-strategy led to reductions in gait velocity, compared to straight walking [225]. Unfortunately, the results of Taylor [225], did not differentiate across phases of the turning cycle. Returning to the study in TD children, a local minimum in tangential velocity was found towards the apex of the turn [154] suggesting that the decrease in speed is not uniform across the turning phases. In fact, a study of step turns in adults reported differences in the COM tangential velocity throughout the three phases of the turn [219]; however, the spin strategy was not analysed. A complete study in which speed is investigated across turn styles and phases is needed to better understand turning gait.

Acceleration

As turning gait is not a steady state pattern, the direct investigation of acceleration might also be of benefit. The study of Milandri [154] computed radial acceleration in order to quantify stability using the centre of balance. This method provides interesting findings, but has not been repeated elsewhere. Rather, studies have focused on identifying the muscles contributing to COM acceleration via dynamic simulation

approaches [124, 144, 145, 167] (see Chapter 8 for review of literature on simulation of gait and analysis of turning using this approach).

2.11.6 Ground reaction forces

Early investigations into turning gait explored GRF profiles and found differences between the GRF components of turning gait compared to straight walking [104, 172, 226, 250]. Regrettably, these studies reported GRF components in the force plate coordinate system (FCS). During straight walking, it is assumed that the FCS is coincident with the body-based coordinate system (BCS) representing the medio-lateral (X), antero-posterior (Y), and vertical (Z) anatomical planes of the body. This approximation holds true as long as normal foot progression angle is maintained [203]. As the body (and foot) rotates about the force plate, the GRF components in the FCS are no longer aligned with the BCS. For example, the Y–component of the GRF may represent the antero-posterior braking force in the early part of the turn, but would contain cross-talk from the medio-lateral direction in late stance. Thus, in order to correctly interpret turning gait GRF profiles, the components should be reported relative to a BCS. This approach was undertaken by Glaister et al. [89]. They investigated applying rotation transformation matrices to the GRF components based on COM and pelvis based BCS. The authors recommended the use of either BCS frames as they provided similar results (for sampling rates greater than 60 Hz) [89]. Since then, other researchers have also reported GRFs using similar BCS methods [88, 200, 219, 230]. A foot based reference frame has been proposed [203], but has not been taken up in the turning literature. Likely, larger foot progression angle variability would make this approach less desirable than the COM and pelvis methods.

Starting with the step turn, GRF profiles showed increased posterior braking force in the early part of stance, in line with the need to slow the forward momentum

of the COM before the turn [88, 172, 219, 226]. As the body re-accelerates the COM during the depart phase, an increased anterior propulsion force is exerted on the body [88, 219]. Note that the increased propulsion GRF was not observed in the work of Patla et al. [172] and Taylor et al. [226], highlighting the importance of rotating GRF components into a BCS before interpreting the profiles. In the medio-lateral direction, GRF must be increased compared to straight walking, given the task requirements [88, 172, 219, 226].

For spin turns, the GRF adaptations have not been studied extensively. In the work of Patla et al. [172] (60° turns), a single subject opted for the spin strategy and showed increased braking and decreased propulsion forces in the antero-posterior direction [171]. The former result appears reasonable (BCS aligned with FCS in early stance), but the latter finding may have underestimated the propulsion GRF, as in the case of step turns in this same study [171]. In the work of Taylor et al. [226], similar results to those seen by Patla et al. [172] are reported for 90° pivot and cross-over spin turn sub-strategies. In the medio-lateral direction, results appear reasonable with GRF pointing in the direction of the turn (opposite to the straight and step turn medio-lateral GRF) [225].

The vertical GRF of step and spin turns exhibit small changes compared to straight walking. Looking at the vertical ground reaction impulse (GRI) in step turns, Strike et al. [219] discovered a significantly increased value compared to straight walking. They attributed this change to a larger GRF during mid-stance caused by a reduction in velocity [219]. A larger vertical GRF in mid-stance was indeed found in two earlier studies [172, 226]. Additionally, Taylor et al. [226] reported that the greatest decrease in vertical GRF occurred in the cross-over strategy [225].

Further investigation of rotated GRF profiles, especially in spin turns, might allow for a better understanding of the net forces exerted on the body during turning gait.

2.11.7 Clinical tests

There are a number of clinical tests that contain turning type tasks; however, some standard balance tests, such as the Berg Balance Scale (BBS) [18] and the Performance Oriented Mobility Assessment [228] simply measure 360° static turns and therefore might be of limited use in the assessment of turning gait.

More promising are the TUG (see Section 2.10), Dite test, and Emory Functional Ambulation Profile (EFAP). In the TUG test, subjects are instructed to rise from a seated position, walk 3 metres, turn around, return to the chair and sit down [177]. The task is timed and is said to reflect the ability of an individual to walk safely outdoors [177]. Dite and Temple [62] defined a set of nine criteria by which to judge the turning portion of the TUG (The Dite test). This scale attempts to quantify turn characteristics such as fluency and steadiness and distinguishes between fallers and non-fallers [62]. To date, this scoring scheme has only been reported in Parkinsonian patients [80], but the approach could be implemented to analyse turning gait in children with CP. The EFAP test contains a turning gait component in which a large obstacle must be avoided [243]. A weakness common to the TUG, Dite, and EFAP tests is that turn direction is not controlled for with subjects being able to turn to their preferred side during the assessment.

A study by Lam et al. [137] investigating 45, 90, and 180° turns found that patients with stroke (n = 13, median age 63 years) took more steps and took longer to turn than age matched controls (n = 10, median age 71 years) for all turning gait tasks [137]. Although the relationships were stronger for the 180° turn, correlations were found between the 90° turning time and results from TUG and BBS, as well as affected (paretic) side number of steps to the TUG [137].

Of the aforementioned tests, the BBS and TUG have been validated for use in children with CP [83] and could potentially be used to measure turning ability.

2.12 Turning Quality

Although it is important to measure the ability of children with CP to perform a task, the assessment of performance quality is also crucial [23]. In the context of this thesis, quality of turning is especially relevant as all children with CP matching the inclusion criteria (see Section 3.2 for criteria) are expected to be able to manage the 90° turning gait task. Thus, quantification of stability, fluency, and level of kinematic sequencing might be of value.

2.12.1 Stability

In quiet standing, stability is maintained as long as the COM remains within the base of support (BOS). During walking, the position of the COM alone cannot predict unstable gait. For example, at the start of single-limb support, the COM is behind the BOS, but momentum will safely carry the body over the stance limb.

Stability measures can be divided into those arising from dynamic systems theory and those derived from biomechanical principles [30]. Most often, the former, including maximum Lyapunov exponent and Floquet multipliers, require numerous gait cycle samples [30]. The maximum Lyapunov exponent has been analysed during circular walking [200, 201], but would be difficult to implement in a transient turning gait scenario. Of the latter, the extrapolated COM (xCOM) of Hof et al. [112] might be applicable to turning gait. Based on the inverted pendulum-model of gait, the xCOM incorporates the velocity of the COM into consideration of stability. Returning to the example of gait at the start of single-limb support, the system would be considered stable as the velocity vector would "push" the xCOM into the BOS. The xCOM possesses good construct validity [30], unlike basic COM-COP measures, and may be a good measure to assess stability during turning. More details about the xCOM measure are presented in Chapter 6.

2.12.2 Fluency

The quality of movement might be quantified using measures of fluency [133]. In a manuscript exploring a sit-to-walk task, Kerr et al. [133] argue that fluency comprises three elements: level of hesitation, coordination, and smoothness of movement. Hesitation was calculated as the maximum difference in forward velocity of the COM, coordination attempted to quantify the coupling behaviour of the hip and knee in the sagittal plane, and smoothness measured the number of inflexion points in the COM jerk curve [133]. Of these, hesitation could be easily implemented in the analysis of turning and may be able to distinguish quality of movement. More details about hesitation in the context of turning gait are presented in Chapter 6.

2.12.3 Kinematic sequencing

During a turning task, a smooth top-down kinematic sequence is expected. The eyes and head should guide the body into the turn. In adults ($n = 6$, mean age 33 years), this behaviour was confirmed during 90° turning gait [94]. The authors suggested that this mechanism was part of a feed-forward control system to anticipate the motor control requirements of the task [94]. The pilot investigation of 90° turning in children found some evidence of kinematic sequencing with the head rotating into the turn ahead of the rest of the body [154]. Although kinematic sequencing may be important from a motor control perspective, the requirement of using a full-body marker set may limit the applicability of this approach.

2.13 Pathological Turning

As mentioned in Section 2.10, turning gait research is popular in the study of Parkinson's disease [19, 98, 190, 207, 208, 210, 233] and the elderly [4, 19, 33, 50, 81, 98,

119, 137, 138, 168, 206] as the former may freeze [190] and the latter may fall and injure themselves [50] during turning. Research in turning gait is also found in patients suffering hemispheric gait deviations such as stroke survivors [43, 113, 137, 138], single-limb amputees [200, 202, 225, 230], and patients with unilateral total knee replacement [45]. In the sport science literature, cutting (quick turning manoeuvres during jogging or running) has also been assessed mainly in patients suffering from anterior-cruciate ligament (ACL) damage [114, 115, 235].

A recent study focusing on rehabilitation in stroke patients found that the experimental group having received training on a turning treadmill (circular walking) had improved muscle strength, straight walking ability, and balance compared to a control group having received conventional rehabilitation only [43].

Turning gait in children with diplegic CP, the group of interest in this thesis, has been seldom investigated [186], even though their decreased motor control, impaired balance, muscular weakness and contractures [173, pp. 345-358] might make this common locomotor task increasingly difficult compared to straight-line gait.

2.14 Conclusion

Turning gait has the potential to be an effective assessment tool in clinical management of gait deviations in children with CP [61]. To date, it remains unclear how turning gait affects a number of gait metrics and quality measures in both TD children and children with CP. Based on the measures considered in this review, the remainder of the thesis focuses on STP, joint kinematic, and joint kinetic adaptations during 90° turning gait. Stability measures as well as advanced methods using dynamic simulations of gait are also presented in the hope of improving the diagnosis, treatment, and management of gait deviations in children with CP.

Chapter 3

Experimental Methods

This chapter outlines the main methodological procedures used to collect, process, and analyse data throughout this thesis. Methods limited to specific investigations are described within their respective chapters.

3.1 Ethical Considerations

Ethical approval for the collection of turning gait data in typically developing (TD) children and children with cerebral palsy (CP) was obtained prior to the start of the study (Ethics reference 09/H1102/88, approved by National Research Ethics Services, London–South East committee). All children provided written assent/consent before participating in this study.

3.2 Subjects

Fifty-four TD children and twenty-two children with CP between the ages of five and eighteen were recruited into this study. The exclusion criteria for the TD control group were any history of gait or musculo-skeletal abnormality. For the CP group, inclusion criteria were confirmed diagnosis of spastic diplegic CP, a classification of 1 or 2 on the Gross Motor Classification Scale (GMFCS) [166], and the ability to perform straight and 90° turning gait trials independently without walking aids. As not all desired gait metrics were available for each subject, each investigation relies on a subset of children for analyses (Table 3.1). Thus, specific anthropometric and subject information is summarized within each relevant chapter.

3.3 Experimental Protocol

3.3.1 Clinical examination and subject preparation

Oxford Gait Laboratory (OGL) protocols for the preparation and collection of clinical gait data were followed. In preparation for gait analysis, body-mass, height, leg-length, hip-width, knee-width, and ankle-width were obtained [231]. For the CP group, additional data related to gait ability, such as joint range of motion, posture,

Table 3.1 – List of children in the normative database included in each study

Subject	TD Kinematics (Chapter 4)	TD Kinetics (Chapter 5)	CP Kinematics (Chapter 6)	CP Kinetics (Chapter 7)	Modelling (Chapter 8)
DH047A	✓	✓	✓	✓	
EB053A	✓	✓	✓	✓	
HC002D	✓	✓	✓	✓	
HC003B	✓	✓	✓	✓	✓
HC004B	✓		✓		
HC013A	✓	✓	✓	✓	
HC014A	✓		✓		
HC015A	✓	✓	✓	✓	
HC016A	✓		✓		
HC019A	✓	✓	✓	✓	
HC020A	✓	✓			✓
HC021A	✓	✓	✓		
HC022A	✓	✓	✓		
HC023A	✓	✓	✓	✓	
HC025A	✓	✓	✓	✓	
HC026A	✓	✓	✓	✓	
HC028A	✓	✓	✓	✓	
HC030A	✓	✓	✓	✓	✓
HC031A	✓	✓	✓	✓	
HC032A	✓	✓	✓	✓	
HC033A	✓	✓	✓	✓	✓
HC034A	✓		✓		
HC036A		✓		✓	✓
HC037A		✓			
HC038A	✓	✓	✓	✓	
HC039A	✓	✓	✓	✓	
HC040A	✓	✓			
HC041A	✓	✓		✓	
HC042A	✓	✓	✓	✓	
HC043A	✓	✓	✓	✓	
HC044A	✓	✓	✓	✓	
HC045A	✓	✓	✓	✓	
HC046A	✓	✓	✓	✓	
HC047A	✓	✓	✓		
HC050A	✓	✓	✓	✓	
HC054A		✓			
HC055A	✓	✓	✓	✓	
HC057A	✓	✓	✓	✓	
HC059A	✓	✓	✓	✓	
HC060A	✓	✓	✓	✓	
HC128A	✓	✓	✓	✓	✓
HC129A	✓	✓	✓	✓	✓
HC135A	✓	✓	✓	✓	✓
HC136A		✓		✓	
HC137A	✓	✓	✓	✓	
HC138A	✓	✓	✓	✓	✓
HC139A	✓	✓	✓	✓	✓
HC140A	✓	✓	✓	✓	
HC141A	✓	✓	✓	✓	
HC142A		✓		✓	✓
IL052A	✓	✓	✓	✓	
JB054A	✓	✓	✓	✓	
n	47	48	44	41	11

All TD children analysed in this thesis. Sample size (n) for each study also shown.

muscle strength, and spasticity were also recorded. Afterwards, subjects were fit with skin mounted retro-reflective markers in accordance with the Oxford Foot Model (OFM) [213] and either the lower-limb or full-body Plug-in Gait (PiG) [128] marker sets. For a subset of children (TD group $n = 47$ and CP group $n = 12$), muscle activity of the rectus femoris, hamstrings, medial gastrocnemius, tibialis anterior, and gluteus medius (TD group only $n = 4$) were recorded via surface electromyographic (sEMG) electrodes. Considerations for choice of marker set and inclusion of sEMG, either unilaterally or bilaterally, were based on time constraints and, in the case of the CP group, clinical requirements.

3.3.2 Experimental tasks and set-up

Participants completed all straight walking trials before performing 90° turning gait trials to the left and right. This order was followed as the straight walking trials for the CP group, to be used for clinical gait assessment, were prioritized. Only if time permitted were turning tasks completed. All trials were performed barefoot along a 10.0 m walkway within the OGL. With regard to turning, subjects were instructed to walk around a small object near the center of the walkway and then to walk toward a reference point on a wall, on a path perpendicular to the starting line of progression (Fig. 3.1). Subjects freely chose their walking speed, starting foot, foot placement strategy, and turning radius. Start position was varied as needed to ensure subjects walked over force plates embedded in the gait walkway.

3.3.3 Data collection

Clinical data measured by a trained physiotherapist from the OGL were manually recorded by an assistant (OGL engineer or present author). In the case of the CP group, the additional clinical data were recorded in an electronic database.

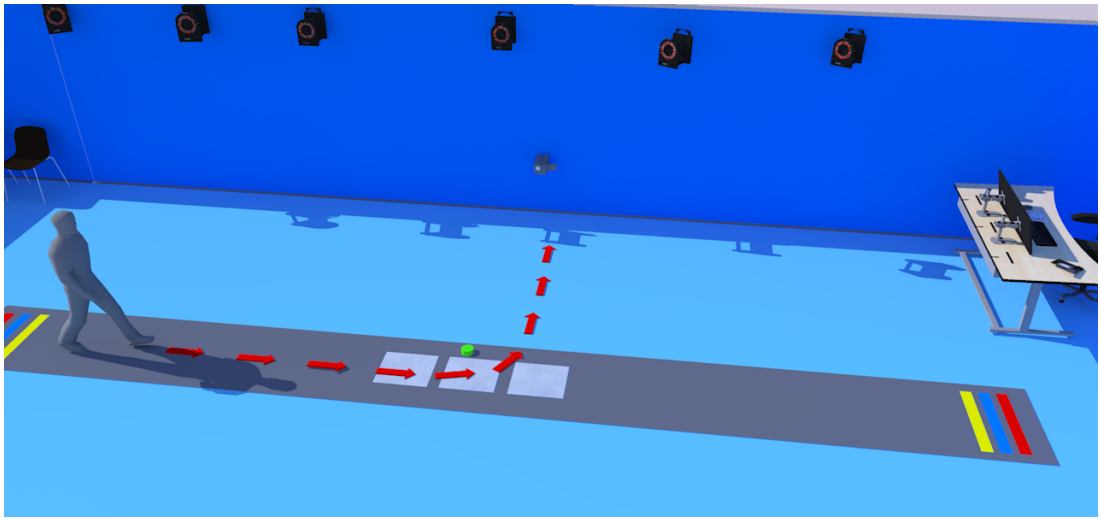

Figure 3.1 – Graphical representation of experimental set-up within the Oxford Gait Laboratory. Subjects were instructed to walk around a small green object near the centre of the space and turn towards a digital camera positioned perpendicular to their original direction of progression. No marks were made on the floor, but subjects generally followed the path shown by the red arrows. Figure created in SketchUp (v.14 Trimble Navigation, Ltd., Sunnyvale, USA) and rendered via Kerkythea (Solid Iris Technologies, Haidari, Greece).

Positions in space of the markers were collected at 100 Hz using a Vicon (Vicon Motion Systems Ltd., Oxford, UK) motion capture system, while force plates (Advanced Mechanical Technology Inc., Watertown, USA) embedded within the gait walkway were used to record ground reaction forces (GRFs) at 1000 Hz. The system originally comprised twelve MX40 cameras and two force plates (model OR-6), but was upgraded for later data collection sessions. An additional OR-6 force plate was installed in July 2013 and the original cameras were replaced by sixteen T40 cameras in November 2014. Muscle activity were recorded via sEMG electrodes at 1000 Hz using a 12-channel wireless system (Wave, Cometa Srl., Milan, Italy).

3.4 Data Processing

Three main data processing steps were followed to prepare data for analyses. The preparatory steps are common operations performed by motion capture software,

while the steps of event detection and turn identification are customized and more focused on gait and turning, respectively. The initial data processing steps were run within the Vicon Nexus software environment (v1.8.4, Vicon Motion Systems Ltd., Oxford, UK), while the latter two were conducted in Matlab (v2012b, The Mathworks Inc., Natick, USA). The Zoosystem Toolbox [65] was used as a framework for analysis, batch processing, and visualization of data. Graphs and diagrams were produced using Zoosystem tools and GIMP (v2.8.4) image editing software, respectively.

3.4.1 Preparatory steps

First, automatic identification of markers was manually verified and gaps in marker position information filled via cubic spline interpolation. The limb (left or right) associated with each force plate contact was also manually identified. Force plates with missing or partial foot contact data (foot crossing edge of plate) were labelled as invalid. Data were then filtered using the Woltring algorithm [244]. Trials in which subjects tripped or misunderstood instructions were not processed further.

Next, for the straight walking trials, the PiG model was run to provide an initial measure of knee varus/valgus angle. In an iterative process, the orientation of the knee flexion/extension axis was optimized to minimize this quantity [13] (see Section 3.5.1). The PiG and OFM models were then run on all trials in order to compute joint kinematic and kinetic quantities. A summary of computational models and methods used to estimate joint dynamics is presented in Sections 3.5 and 3.6. Finally, all trial information was exported to c3d file format for further analyses.

3.4.2 Event detection

Walking is characterized by a repeating pattern of foot-strike (FS) and foot-off (FO) events [173, pp. 3–6]. Accurate estimation of these events allows gait data to be

divided into stance and swing phases and also permits comparison across subjects via time normalization of these phases. Gait event timings estimated via GRFs are considered to be most accurate [163], but can be difficult to obtain, especially during turning gait. Therefore, a number of marker-based algorithms have been suggested [58, 116, 163, 256]. Of these, the coordinate-based algorithm of Zeni [256] is simple to implement and performs well in populations with cerebral palsy (CP) [29]. This method estimates gait events by computing the relative position of the heel (HEE) and toe (TOE) markers with respect to the sacral (SACR) marker along the global antero-posterior axis of the laboratory. The relative positions of the HEE and TOE markers form sinusoidal curves in which the timings of the peaks and troughs represent FS and FO, respectively [256]. For turning gait, the distance in the horizontal plane of the HEE and TOE markers from the SACR marker was computed to take into account the changing direction of progression. As in the straight walking case, peaks and troughs of the resulting waveforms were used to determine the FS and FO events, respectively. Comparison of event timing via this modified Zeni method shows good agreement with GRF data (first and last frames with vertical GRF $\geqslant$ 10 N); however, FS was slightly anticipated (Fig. 3.2). The modified Zeni method was used to identify all gait events for which GRF data were unavailable. Otherwise, first and last frames with vertical GRF $\geqslant$ 10 N were assigned as FS and FO events, respectively.)

3.4.3 Turning strategy identification

As described in the literature review (Section 2.6), 90° turns are commonly classified as step or spin based on the role of each limb in the task execution [105]. Although most investigators have instructed subjects on which turn style to perform [1, 61, 88, 90, 150, 219, 250], unprescribed turning [3, 226] may be advantageous as subjects' freely chosen strategy can be assessed, albeit in a post-hoc fashion. While Taylor et al. [226] relied on visual assessment, only Akram et al. [3] implemented an algorithmic

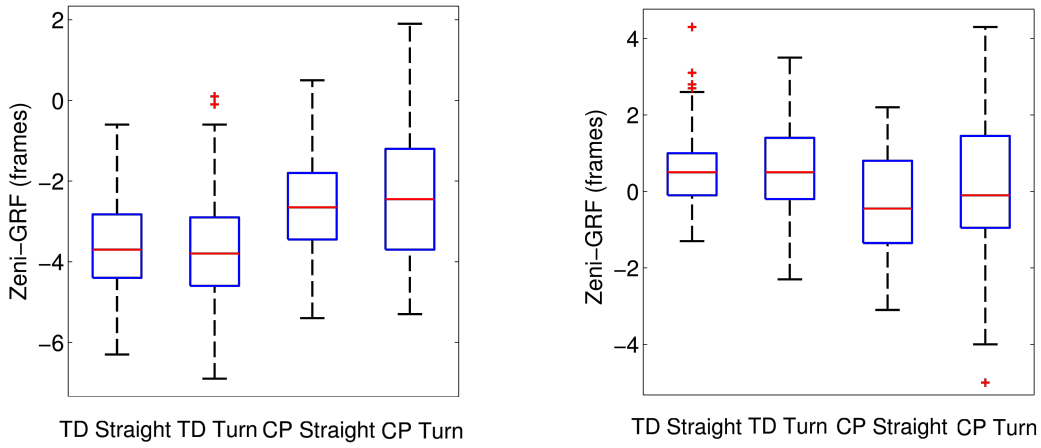

Figure 3.2 – Event timing via modified Zeni method and the vertical ground reaction force (GRF) for the TD and CP groups. (a) Foot-strike and (b) foot-off. Boxplot center and edges show median as well as 25 and 75th percentiles. Outliers (∗) also shown.

approach. This method is based on the medio-lateral displacement of each foot and represents an improvement over visual-assessment; however, it may not be robust against pathological foot progression angle profiles common in children with CP. Thus, a novel method based on pelvic movement was implemented herein. Trials were categorized as either step or spin based on the single-limb support phase in which the greatest amount of horizontal pelvic rotation, relative to the global coordinate system (GCS), occurred. If the identified limb was opposite to the turning direction, the turn was classified as step; otherwise the turn was labelled spin. The method is illustrated diagrammatically for a representative step and spin turn (Fig. 3.3). The turn was then divided into the three phases. The main phase identified using the pelvic rotation is described as the turn phase, while the previous and subsequent steps are referred to as the approach and depart phases, respectively (Fig. 3.4).

3.5 Biomechanical Models

The PiG [128] was used to compute hip and knee joint kinematics and kinetics, while the OFM [213] estimated foot kinematics, ankle kinematics, and ankle kinetics.

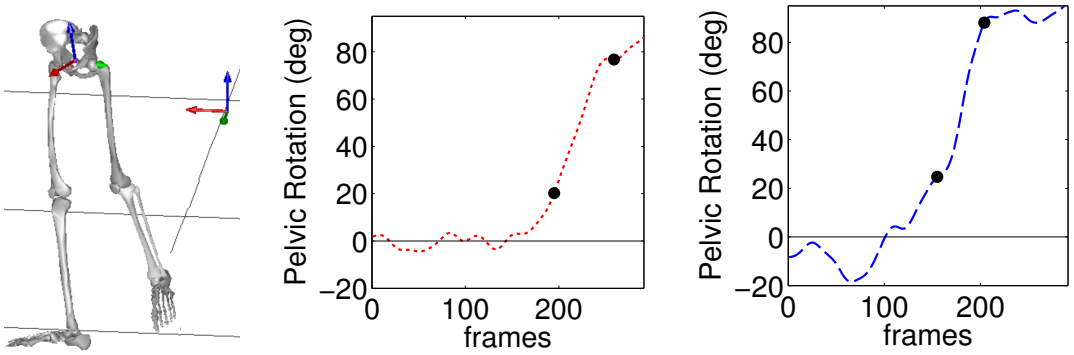

(a) (b) (c)

Figure 3.3 – Turn style identification via (a) the transverse plane movement of the pelvis which, for the representative trials shown here, rotates (b) 56.5° (step turn) and (c) 63.4° (spin turn) during single-limb support (black dots show start and end).

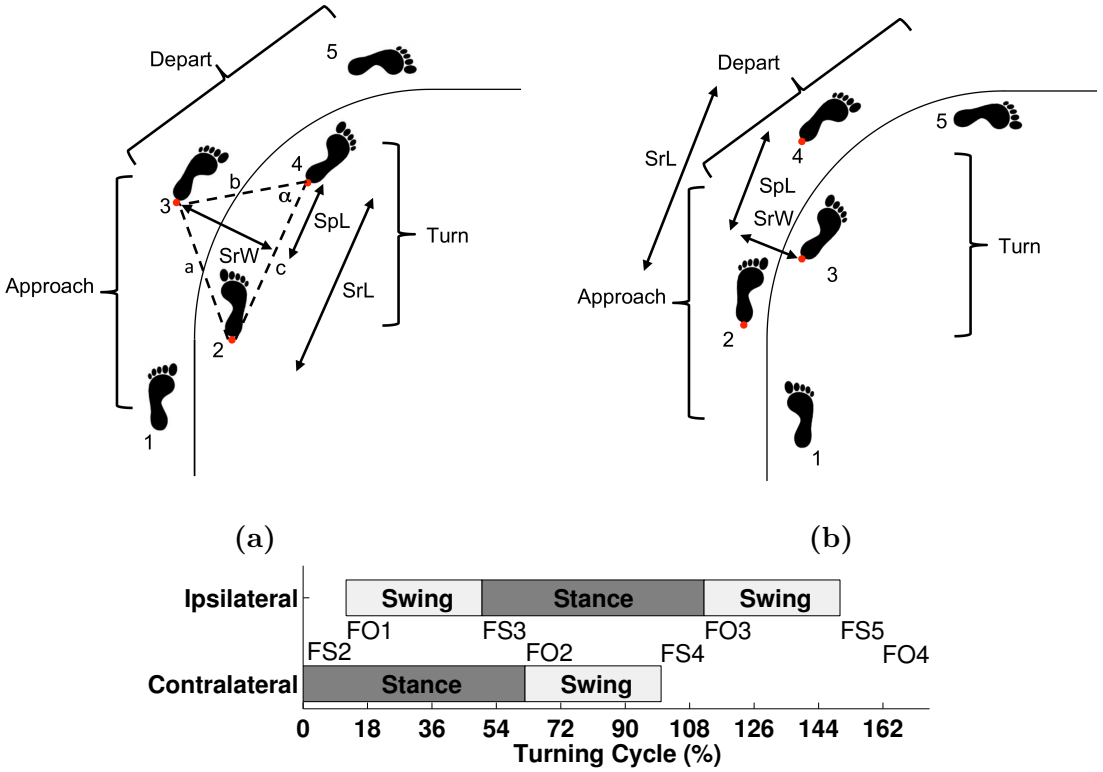

(a) (b) (c)

Figure 3.4 – Diagrammatic representation of the three phases (approach, turn, and depart) of (a) a 90° step turn to the right and (b) a 90° spin turn to the right. For the step turn the left leg, or turning limb, is taken to be the ipsilateral limb, while for the spin turn the ipsilateral limb is the right leg. The turn phase step length (SpL), stride length (SrL), and stride width (SrW) are shown (see Section 3.6.1 for formulae). (c) Foot-strike (FS) and foot-off (FO) events as a percentage of the turning cycle (162% of the gait cycle) (FS2 to FO4).

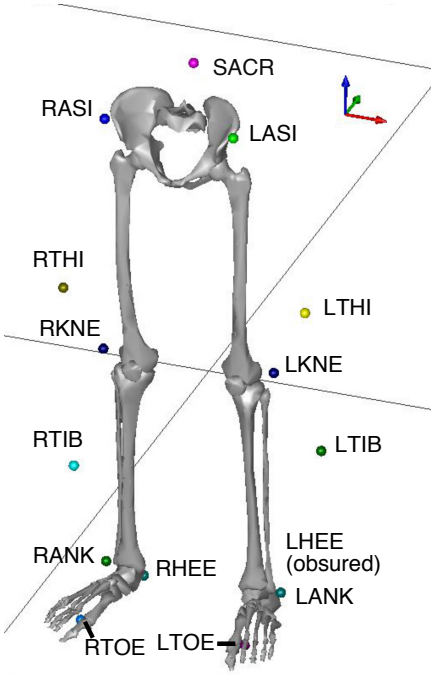

Figure 3.5 – Model of a subject from the TD child database with Plug-in Gait marker positions shown. Note that RTHI, LTHI, RTIB, and LTIB markers are attached to rigid rods (wands) secured firmly to a skin-mounted base.

Justification for use of these particular models is provided in Section 2.2.2. Only the computation of ankle kinetics required custom code [63], the other operations were performed within the Vicon Nexus software environment (v1.8.4, Vicon Motion Systems Ltd., Oxford, UK).

3.5.1 The Plug-in Gait Model

The PiG lower-limb model comprises fifteen retro-reflective skin mounted markers placed at key anatomical positions with the aim of defining pelvis, thigh (femur), shank (tibia), and foot segments (Fig. 3.5). For the pelvis, the orientation is defined relative to the GCS axes with X perpendicular to the gait walkway, Y pointing along the walkway, and Z oriented upwards. For the hip, knee, and ankle, motion is defined as the movement of the distal segment relative to the proximal segment [128].

Subject Anthropometry

Subject-specific anthropometric quantities measured during the subject preparation phase support the PiG modeller and are defined below:

Inter-ASIS Distance (IA) The distance between the left and right anterior superior iliac spines (measured directly or via the RASI and LASI markers).

Leg-length (LL) The distance from the anterior-superior iliac spine to the medial malleolus, via the medial femoral condyle.

Knee Width (KW) The width of the knee about the estimated flexion axis.

Ankle Width (AW) The distance between the medial and lateral ankle malleoli.

Joint Centres

The hip (HJC), knee (KJC), and ankle (AJC) joint centres can be computed from marker data and subject-specific anthropometrics.

Starting at the hip, Kadaba et al. [128] suggested using equations derived from pelvic radiograph data to estimate the HJC (based on personal communication between said authors and J. Gage and S. Tashman, 1985); however, a method later described by Davis et al. [54] is implemented in the PiG model.

First, the distance between the anterior-superior iliac spine and the greater trochanter is estimated as:

$$AT = 0.1288(LL) \tag{3.1}$$

Next, a constant C is derived from the average leg-length ($\overline{LL}$):

$$C = 0.115(\overline{LL}) - 15.3 \tag{3.2}$$

Finally, the X, Y, and Z coordinates of the HJC can be computed as:

$$HJC_X = C\cos\theta\sin\beta - (AT + r_m)\cos\beta \tag{3.3}$$

$$HJC_Y = -C\sin(\theta) + AT/2 \tag{3.4}$$

$$HJC_Z = -C\cos\theta\cos\beta - (AT + r_m)\sin\beta \tag{3.5}$$

where r_m is the radius of the retro-reflective markers

$\theta = 0.500$ radians

$\beta = 0.314$ radians

Note for $LHJC_Y$ the Y–offset, $AT/2$, is negated.

For the knee, the joint centre is defined using the previously computed HJC, the measured KW, and the KNEE and THI markers. The KJC is assumed to lie a distance $KW/2$ medially from KNE and in the plane formed by the HJC, THI, and KNE positions, such that HJC-KJC and KNE-KJC are perpendicular. Therefore, the orientation of the THI wand marker is crucial and must be carefully positioned. The mathematical method described by Baker et al. [13], not in the original PiG implementation, was used to adjust the orientation of the THI wand marker, and thus the KJC, in a post-hoc process. This action minimizes cross-talk between the varus/valgus and flexion/extension angles through iterative changes in the orientation angle of the THI wand marker position and improves kinematic estimations.

At the ankle, the joint centre is determined using the original knee method, except via the computed KJC as well as the TIB and ANK markers.

Segment-Embedded Axes

Each segment is defined by a set of three orthogonal unit vectors forming an xyz local coordinate system (LCS). In the equations below, normalization of unit vectors to unit length is assumed, but not strictly necessary.

The pelvis LCS can be defined using the RASI, LASI, and SACR marker positions (treated as vectors) (Fig. 3.6). First, $\hat{\mathbf{j}}_{\boldsymbol{pel}}$ pointing from the RASI to the LASI marker is defined as:

$$\hat{\mathbf{j}}_{pel} = \mathbf{LASI} - \mathbf{RASI} \tag{3.6}$$

Next, a temporary x–axis is created from the SACR and RASI markers:

$$\boldsymbol{x}_{temp} = \mathbf{RASI} - \mathbf{SACR} \tag{3.7}$$

By the cross-product, $\hat{\mathbf{k}}_{\boldsymbol{pel}}$, mutually perpendicular to $\hat{\mathbf{j}}_{\boldsymbol{pel}}$ and $\boldsymbol{x}_{\boldsymbol{temp}}$ and pointing proximally, is obtained:

$$\hat{\mathbf{k}}_{pel} = \boldsymbol{x}_{temp} \times \hat{\mathbf{j}}_{pel} \tag{3.8}$$

Finally, the true x–axis, $\hat{\mathbf{i}}_{\boldsymbol{pel}}$, pointing anteriorly, is created as:

$$\hat{\mathbf{i}}_{pel} = \hat{\mathbf{j}}_{pel} \times \hat{\mathbf{k}}_{pel} \tag{3.9}$$

The pelvis LCS origin is located at **PELO**:

$$\mathbf{PELO} = (\mathbf{RASI} + \mathbf{LASI})/2 \tag{3.10}$$

The thigh (femur) segment LCS is determined from the HJC, KJC, and adjusted THI markers (Fig. 3.6). First, the primary long axis of the thigh, pointing from the KJC to the HJC, is determined:

$$\hat{\mathbf{k}}_{thi} = \mathbf{HJC} - \mathbf{KJC} \tag{3.11}$$

Next, $\hat{\mathbf{j}}_{thi}$ is computed:

$$\hat{\mathbf{j}}_{thi} = \mathbf{KNE} - \mathbf{KJC} \tag{3.12}$$

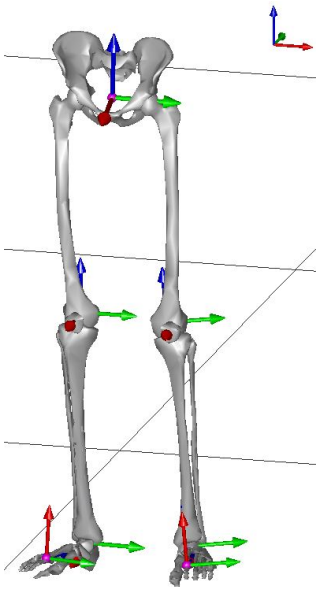

Figure 3.6 – Model of a subject from the TD child database showing the position of the LCS for the pelvis, thigh, shank, and foot segments. Red, green, and blue colours represent anterior, lateral, and proximal vectors, respectively.

Finally, the anterior vector $\hat{\mathbf{i}}_{thi}$ is made orthogonal to $\hat{\mathbf{j}}_{thi}$ and $\hat{\mathbf{i}}_{thi}$:

$$\hat{\mathbf{i}}_{thi} = \hat{\mathbf{j}}_{thi} \times \hat{\mathbf{k}}_{thi} \tag{3.13}$$

The origin of the thigh LCS, **FEO**, is coincident with the KJC position.

In a similar fashion, the LCS of the shank (with origin **TIO** coincident with the AJC position) is formed as:

$$\hat{\mathbf{k}}_{shank} = \mathbf{KJC} - \mathbf{AJC} \tag{3.14}$$

$$\hat{\mathbf{j}}_{shank} = \mathbf{ANK} - \mathbf{AJC} \tag{3.15}$$

$$\hat{\mathbf{i}}_{shank} = \hat{\mathbf{j}}_{shank} \times \hat{\mathbf{k}}_{shank} \tag{3.16}$$

For the foot, the LCS origin **FOO** is positioned at the TOE marker and the primary long axis is determined from HEE and TOE markers:

$$\hat{\mathbf{k}}_{foot} = \mathbf{TOE} - \mathbf{HEE} \tag{3.17}$$

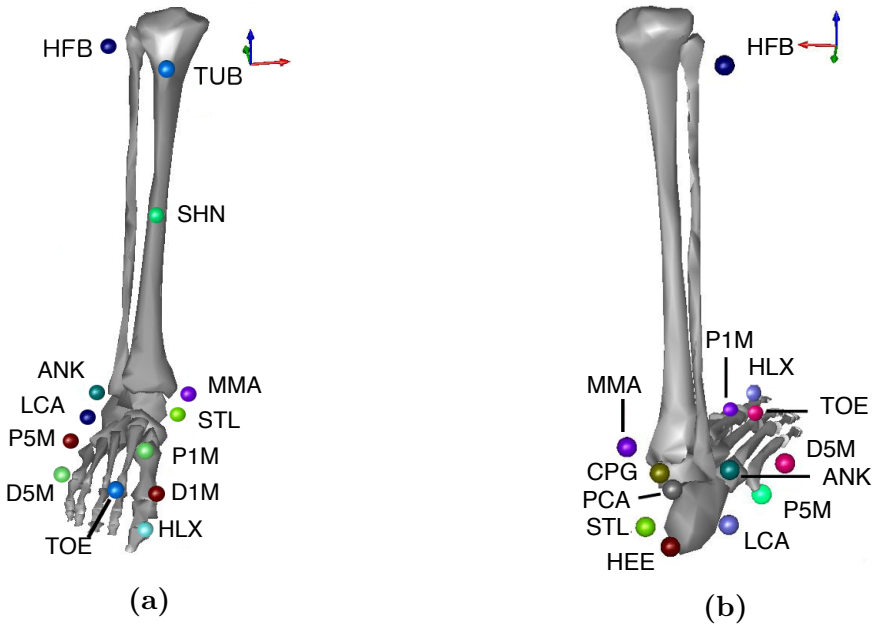

Figure 3.7 – Model of a subject from the TD child database with Oxford Foot Model markers positions shown (a) anterior and (b) posterior view.

3.5.2 The Oxford Foot Model

The OFM was first developed by Carson et al. [37] and further refined for use in children by Stebbins et al. [213]. The OFM is made up of the tibia, hindfoot, forefoot, and hallux segments defined by 30 markers (Fig. 3.7). These segments allow for the estimation of angular quantities for the foot and ankle.

Segment-embedded axes

As with the PiG, the OFM LCS for each segment is constructed from a set of three orthogonal $\hat{\mathbf{i}}\hat{\mathbf{j}}\hat{\mathbf{k}}$ unit vectors.

For the shank (tibia), the long axis $\hat{\mathbf{k}}_{shankofm}$ is constructed as in the PiG model via Eq. 3.14; however the AJC, and segment origin, is defined as the midpoint between the ANK and MMA markers and does not rely on the position of the TIB wand marker. The transmalleolar axis $\hat{\mathbf{j}}_{shankofm}$ and anterior axis $\hat{\mathbf{i}}_{shankofm}$ can then be

constructed using Eqs. 3.15 and 3.16, respectively. The origin of the shank LCS is positioned at the AJC.

For the hindfoot, the origin is the HEE marker, while the HEE, PCA, STL, and LCA markers are used to construct the anterior axis $\hat{\mathbf{i}}_{hf}$. It is located in the plane defined by HEE and PCA passing through the midpoint of the STL and LCA and parallel to the GCS XY–plane, i.e. the floor. Adjustment to $\hat{\mathbf{i}}_{hf}$ can be made for subjects unable to achieve "foot-flat" during static standing. This was not required in the present study. The $\hat{\mathbf{j}}_{hf}$ vector is perpendicular to the previously defined plane and $\hat{\mathbf{k}}_{hf}$ is mutually perpendicular to the other axes and points proximally:

$$\hat{\mathbf{k}}_{hf} = \hat{\mathbf{j}}_{hf} \times \hat{\mathbf{i}}_{hf} \tag{3.18}$$

For the forefoot, the origin of the segment is created from the P5M and P1M markers. The origin of the forefoot can be thought of as the position of a theoretical midfoot joint centre (MFJC):

$$\mathbf{MFJC} = (\mathbf{P5M} + \mathbf{P1M})/2 \tag{3.19}$$

Next, a temporary axis is created:

$$\boldsymbol{x}_{temp} = \mathbf{TOE} - \mathbf{MFJC} \tag{3.20}$$

This vector is then projected into the plane formed by markers P5M, D5M, and D1M to form the primary axis $\hat{\mathbf{i}}_{ff}$. As with the hindfoot $\hat{\mathbf{k}}_{ff}$ is perpendicular to this plane and $\hat{\mathbf{j}}_{ff}$ is mutually perpendicular to $\hat{\mathbf{i}}_{ff}$ and $\hat{\mathbf{k}}_{ff}$.

Finally, the hallux segment is defined by a single vector $\hat{\mathbf{i}}_{hlx}$:

$$\hat{\mathbf{i}}_{hlx} = \mathbf{D1M} - \mathbf{HLX} \tag{3.21}$$

3.6 Biomechanical Analysis

3.6.1 Spatio-temporal parameters

A number of spatio-temporal parameters (STPs) defined in Section 2.2.1 were retained for the analysis of straight and turning gait trials. Formulae used to compute these STPs are now described. Stance time was obtained by multiplying the number of frames between FS and FO by the time for a single frame Δt (1/100sec). Velocity (gait speed) was estimated by numerically differentiating and then averaging the position of the SACR marker over n frames of a complete gait cycle:

$$\text{velocity} = \frac{1}{n}\sum_{i=1}^{n-1}\frac{\boldsymbol{SACR_{i+1}} - \boldsymbol{SACR_i}}{\Delta t} \tag{3.22}$$

Spatial parameters of turning gait can be computed by considering the triangle formed by steps 2, 3, and 4 in Fig. 3.4 and as described by Huxham [120]. The locations of the vertices of this triangle were defined using the position of the left and right heel markers (LHEE and RHEE from the PiG, respectively) at the time of each respective FS. The Euclidean distances, in the horizontal plane, between the vertices, sides a, b, and c were then computed. Then, by the cosine rule and law of cosines, the length SpL representing the step length was computed:

$$\text{SpL} = b\cos\alpha = \frac{b^2 + c^2 - a^2}{2c} \tag{3.23}$$

The stride width SrW can then be calculated via the Pythagorean theorem:

$$\text{SrW} = \sqrt{b^2 - (SpL)^2} \tag{3.24}$$

Finally, side c represents the stride-length (SrL). These formulae, unlike traditional ones, can be universally applied to any non-linear walking condition [120].

3.6.2 Lower-limb joint kinematics

The angular position of PiG body segments are obtained by comparing the orientation of the distal segment axes to the orientation of the proximal segment axes.

If $\hat{\mathbf{i}}_{\boldsymbol{p}}$, $\hat{\mathbf{j}}_{\boldsymbol{p}}$, and $\hat{\mathbf{k}}_{\boldsymbol{p}}$ represent the anterior, lateral, and proximal unit vectors of the proximal segment, respectively, a matrix of proximal vectors can be defined:

$$T_P = \begin{bmatrix} \hat{\mathbf{i}}_{px} & \hat{\mathbf{i}}_{py} & \hat{\mathbf{i}}_{pz} \\ \hat{\mathbf{j}}_{px} & \hat{\mathbf{j}}_{py} & \hat{\mathbf{j}}_{pz} \\ \hat{\mathbf{k}}_{px} & \hat{\mathbf{k}}_{py} & \hat{\mathbf{k}}_{pz} \end{bmatrix} \tag{3.25}$$

Similarly, a matrix can be used to define the distal segment:

$$T_D = \begin{bmatrix} \hat{\mathbf{i}}_{dx} & \hat{\mathbf{i}}_{dy} & \hat{\mathbf{i}}_{dz} \\ \hat{\mathbf{j}}_{dx} & \hat{\mathbf{j}}_{dy} & \hat{\mathbf{j}}_{dz} \\ \hat{\mathbf{k}}_{dx} & \hat{\mathbf{k}}_{dy} & \hat{\mathbf{k}}_{dz} \end{bmatrix} \tag{3.26}$$

A transformation matrix describes the relationship between T_D and T_P:

$$[T_R] = [T_D] \cdot [T_P]^T \tag{3.27}$$

Or expressed via the unit vectors:

$$T_R = \begin{bmatrix} \hat{\mathbf{i}}_d \cdot \hat{\mathbf{i}}_p & \hat{\mathbf{i}}_d \cdot \hat{\mathbf{j}}_p & \hat{\mathbf{i}}_d \cdot \hat{\mathbf{k}}_p \\ \hat{\mathbf{j}}_d \cdot \hat{\mathbf{i}}_p & \hat{\mathbf{j}}_d \cdot \hat{\mathbf{j}}_p & \hat{\mathbf{j}}_d \cdot \hat{\mathbf{k}}_p \\ \hat{\mathbf{k}}_d \cdot \hat{\mathbf{i}}_p & \hat{\mathbf{k}}_d \cdot \hat{\mathbf{j}}_p & \hat{\mathbf{k}}_d \cdot \hat{\mathbf{k}}_p \end{bmatrix} \tag{3.28}$$

The matrix in Eq. 3.28 can be used to find the three (Euler) angles which define the orientation of the proximal and distal segment coordinate systems. In the PiG model, the solution for the pelvis, hip, and knee joints is obtained using Euler angles in a Cardanian "YXZ" sequence to build a rotation matrix R. For the ankle, knee, and hip joints, angles are referenced relative to anatomically meaningful positions known as the orthopaedic angles [142], while for the pelvis angles are referenced to the GCS XYZ–axes [128]:

$$[R] = [R_Z] \cdot [R_X] \cdot [R_Y] \tag{3.29}$$

The first rotation matrix represents a tilt (pelvis) or flexion/extension (hip and knee) movement of angle θ about the y–axis:

$$R_Y = \begin{bmatrix} \cos\theta & 0 & -\sin\theta \\ 0 & 1 & 0 \\ \sin\theta & 0 & \cos\theta \end{bmatrix} \tag{3.30}$$

The second rotation matrix represents the obliquity (pelvis) or abduction/adduction (hip and knee) movement of angle ϕ about a new or "floating" axis denoted x':

$$R_X = \begin{bmatrix} 1 & 0 & 0 \\ 0 & \cos\phi & \sin\phi \\ 0 & -\sin\phi & \cos\phi \end{bmatrix} \tag{3.31}$$

Finally, a third rotation matrix represents the internal/external rotation motion of angle ψ about the twice rotated z–axis, denoted z'':

$$R_Z = \begin{bmatrix} \cos\psi & \sin\psi & 0 \\ -\sin\psi & \cos\psi & 0 \\ 0 & 0 & 1 \end{bmatrix} \tag{3.32}$$

Applying matrix multiplication to Eq. 3.29 using the terms built in Eqs. 3.30, 3.31, and 3.32:

$$R = \begin{bmatrix} C\theta C\psi + S\theta S\phi S\psi & C\phi S\psi & -S\theta C\psi + C\theta S\phi S\psi \\ -C\theta S\psi + S\theta S\phi C\psi & C\phi C\psi & S\theta S\psi + C\theta S\phi C\psi \\ S\theta C\phi & -S\phi & C\theta C\phi \end{bmatrix} \tag{3.33}$$

where C is the cosine function

S is the sine function

Finally, the angles θ, ϕ, and ψ can be obtained by equating the appropriate terms in matrices T_R and R. From T_{R32} and R_{32}:

$$-\sin\phi = \hat{\mathbf{k}}_{\boldsymbol{d}} \cdot \hat{\mathbf{j}}_{\boldsymbol{p}} \tag{3.34}$$

Thus solving for ϕ:

$$\phi = \arcsin(-\hat{\mathbf{k}}_{\boldsymbol{d}} \cdot \hat{\mathbf{j}}_{\boldsymbol{p}}) \tag{3.35}$$

Similarly for θ, using the terms for the third row and first column of T_R and R along with Eq. 3.35:

$$\theta = \arcsin[(\hat{\mathbf{k}}_{\boldsymbol{d}} \cdot \hat{\mathbf{i}}_{\boldsymbol{p}})/\cos\phi\ ] \tag{3.36}$$

and finally for ψ:

$$\psi = \arcsin[(\hat{\mathbf{i}}_{\boldsymbol{d}} \cdot \hat{\mathbf{j}}_{\boldsymbol{p}})/\cos\phi] \tag{3.37}$$

For the foot, only θ and ψ are considered, representing the plantar/dorsiflexion and internal/external rotation of the ankle joint, respectively. Thus, the rotational matrix R_F is built only with rotations about the Y and Z–axes:

$$[R_F] = [R_Z] \cdot [R_Y] \tag{3.38}$$

$$R_F = \begin{bmatrix} C\theta C\psi & S\psi & -S\theta C\psi \\ -C\theta S\psi & C\psi & S\theta s\psi \\ S\theta & 0 & C\theta \end{bmatrix} \tag{3.39}$$

Therefore Eq. 3.38 can be used to solve for two angles:

$$\psi_{foot} = \arcsin(-\hat{\mathbf{i}}_{\boldsymbol{d}} \cdot \hat{\mathbf{j}}_{\boldsymbol{p}}) \tag{3.40}$$

$$\theta_{foot} = \arcsin(\hat{\mathbf{k}}_{\boldsymbol{d}} \cdot \hat{\mathbf{i}}_{\boldsymbol{p}}) \tag{3.41}$$

Note that the Vicon implementation of the conventional gait model sometimes modifies the axes used to compute the pelvis angles in order to control for the direction of progression (either global X or Y–direction) [231, p. 27]. Thus, in the case of turning, reliance on the PiG pelvic angle ψ can sometimes leads to angles offset by $\pm 90°$ that must be corrected.

3.6.3 Intra-foot and ankle joint kinematics

The OFM allows the estimation of a number of inter-segmental joint angles. Starting proximally, the ankle joint motion is defined as the relative movement of the hindfoot

with respect to tibia (HF/TB) and represents the combined motion of the talo-crural and talo-calcaneal (subtalar) joints. The movement of the forefoot with respect to the hindfoot (FF/HF) combines numerous joints and can be thought of as the rotation of these segments about a theoretical midfoot joint. Finally, the movement of the hallux with respect to the forefoot (HLX/FF) is representative of the motion about the first metatarsal-phalangeal joint [213].

The OFM angles are computed by the Grood and Suntay [97] joint coordinate system (JCS) [37]. The JCS has the advantage of being order independent, i.e. the rotational sequence does not have to be predefined as with the Eulerian/Cardanian methods [97]; however, the JCS is equivalent to the YXZ Cardanian sequence [41].

In the JCS, rotation between a proximal and distal segment is defined by two body fixed axes $\mathbf{e}$ and a single floating axis $\mathbf{f}$. Each segment holds a single body fixed axis, $\mathbf{e_p}$ and $\mathbf{e_d}$ for the proximal and distal segments, respectively, while $\mathbf{f}$ is perpendicular to both $\mathbf{e_p}$ and $\mathbf{e_d}$:

$$\mathbf{f} = \mathbf{e_d} \times \mathbf{e_p} \tag{3.42}$$

A sagittal plane flexion/extension movement θ is computed using $\mathbf{e_p}$ (or another proximal segment vector for convenience—depending on the joint) and $\mathbf{f}$:

$$\theta = \arccos(\mathbf{f} \cdot \mathbf{e_p}) \tag{3.43}$$

Abduction/adduction motion ϕ is computed using the two body fixed axes (or a combination of convenient proximal and distal vectors):

$$\phi = \arccos(\mathbf{e_p} \cdot \mathbf{e_d}) \tag{3.44}$$

An internal/external rotation movement ψ can be computed using $\mathbf{e_d}$ (or again another distal vector) and $\mathbf{f}$:

$$\psi = \arccos(\mathbf{f} \cdot \mathbf{e_d}) \tag{3.45}$$

The choice of body fixed axes depends on the segment and motion of interest. Generally, axes are chosen to avoid a situation where the angle between vectors moves across the 180° threshold, since the dot product would always return the lesser angle. With θ, ϕ, and ψ representing plantar/dorsiflexion, inversion/eversion, and internal/external rotation, respectively, one obtains motion for each joint.

For motion of the HF/TB:

$$\theta = -\arccos(\mathbf{f} \cdot \hat{\mathbf{k}}_{shankofm}) + 90^\circ \tag{3.46}$$

$$\phi = \arccos(\hat{\mathbf{j}}_{shankofm} \cdot \hat{\mathbf{i}}_{hf}) - 90^\circ \tag{3.47}$$

$$\psi = \arccos(\mathbf{f} \cdot \hat{\mathbf{j}}_{hf}) - 90^\circ \tag{3.48}$$

For motion of the FF/HF:

$$\theta = -\arccos(\mathbf{f} \cdot \hat{\mathbf{i}}_{hf}) + 90^\circ \tag{3.49}$$

$$\phi = -\arccos(\hat{\mathbf{j}}_{hf} \cdot \hat{\mathbf{i}}_{ff}) + 90^\circ \tag{3.50}$$

$$\psi = \arccos(\mathbf{f} \cdot \hat{\mathbf{j}}_{hf}) - 90^\circ \tag{3.51}$$

For motion the HLX/FF:

$$\theta = -\arccos(\mathbf{f} \cdot \hat{\mathbf{i}}_{hf}) + 90^\circ \tag{3.52}$$

$$\phi = -\arccos(\hat{\mathbf{j}}_{hf} \cdot \hat{\mathbf{i}}_{ff}) + 90^\circ \tag{3.53}$$

Above relations are only valid for the right HF/TB, FF/HF, and HLX/FF angles. Left limb angles are obtained by changing sign and offset.

3.6.4 Lower-limb joint kinetics

Required quantities

Lower-limb joint kinetics are obtained from the PiG modeller within the Vicon Nexus software environment (v1.8.4, Vicon Motion Systems Ltd., Oxford, UK). The PiG

Table 3.2 – Body segment inertial properties

	Mass	COM	ROG
Pelvis	0.1420	0.895	0.310
Thigh	0.1000	0.567	0.323
Shank	0.0465	0.567	0.302
Foot	0.0145	0.500	0.475

Mass as proportion of body mass, centre of mass (COM) distance relative to segment length from the distal end, and radius of gyration (ROG) about the COM along the x or y–axes. ROG about long axis assumed negligible. Source: [231, p.60].

modeller implements approximations of segment mass, centre of mass (COM), and radius of gyration (ROG) as summarized by Winter [240, ch.3] (Table 3.2).

Moreover, the segmental angular velocities ω_s can be computed with respect to the body axes. Recalling the Cardanian YXZ rotation sequence:

$$\omega_s = [R_Z(\psi)] \cdot [R_X(\phi)] \cdot \begin{bmatrix} 0 \\ \dot{\theta} \\ 0 \end{bmatrix} + [R_Z(\psi)] \cdot \begin{bmatrix} \dot{\phi} \\ 0 \\ 0 \end{bmatrix} + \begin{bmatrix} 0 \\ 0 \\ \dot{\psi} \end{bmatrix} \tag{3.54}$$

Inserting the matrix elements of R_Z and R_X into Eq. 3.54:

$$\omega_s = \begin{bmatrix} \dot{\theta} C\phi S\psi + \dot{\phi} C\psi \\ \dot{\theta} C\phi C\psi - \dot{\phi} S\psi \\ -\dot{\theta} S\phi + \dot{\psi} \end{bmatrix} \tag{3.55}$$

Differentiation of ω_s leads to an expression for the segmental angular velocity:

$$\alpha_s = \begin{bmatrix} \ddot{\theta} C\phi S\psi - \dot{\theta}\dot{\phi} S\phi S\psi + \dot{\theta}\dot{\psi} C\phi C\psi + \ddot{\phi} C\psi - \dot{\phi} S\psi \\ \ddot{\theta} C\phi C\psi - \dot{\theta}\dot{\phi} S\phi C\phi - \dot{\theta}\dot{\psi} C\phi C\psi - \ddot{\phi} S\phi - \dot{\psi}\dot{\phi} C\psi \\ -\ddot{\theta} S\phi - \dot{\theta}\dot{\phi} C\phi + \ddot{\psi} \end{bmatrix} \tag{3.56}$$

Joint kinetics can be obtained by combining subject anthropometry, segment parameters, and external forces via a process known as inverse dynamics analysis (IDA). There are several approaches, but the standard Newtonian IDA method [229] is applied in the PiG model. Starting at the foot, the forces and moments at the proximal joint for each segment are computed before moving to the next joint.

First, the moment of inertia, which represents a segment's capacity to resist rotation, can be determined for each segment s from the segment parameters (Table 3.2) according to [240, Eq.3.9]:

$$\mathbf{I_s} = m_s(\mathbf{ROG_s})^2 \tag{3.57}$$

It is convenient to then define the rate of change of angular momentum with respect to $\mathbf{I_s}$ and $\boldsymbol{\omega_s}$ [229, Eqs.B.82–B.84]:

$$\dot{\mathbf{L}}_{sx} = \mathbf{I_{sz}} \cdot \dot{\boldsymbol{\omega}}_{\boldsymbol{sx}} + (\mathbf{I_{sx}} - \mathbf{I_{sy}})\boldsymbol{\omega}_{\boldsymbol{sy}} \cdot \boldsymbol{\omega}_{\boldsymbol{sz}} \tag{3.58}$$

$$\dot{\mathbf{L}}_{sy} = \mathbf{I_{sy}} \cdot \dot{\boldsymbol{\omega}}_{\boldsymbol{sy}} + (\mathbf{I_{sz}} - \mathbf{I_{sx}})\boldsymbol{\omega}_{\boldsymbol{sx}} \cdot \boldsymbol{\omega}_{\boldsymbol{sz}} \tag{3.59}$$

$$\dot{\mathbf{L}}_{sz} = \mathbf{I_{sx}} \cdot \dot{\boldsymbol{\omega}}_{\boldsymbol{sz}} + (\mathbf{I_{sy}} - \mathbf{I_{sz}})\boldsymbol{\omega}_{\boldsymbol{sx}} \cdot \boldsymbol{\omega}_{\boldsymbol{sy}} \tag{3.60}$$

Note, the PiG assumes that $\mathbf{I_{sz}}$ is negligible and that $\mathbf{I_{sx}}$ and $\mathbf{I_{sy}}$ are equal [231].

Joint forces and moments

Starting at the foot, the components of the force at the ankle $\boldsymbol{F_{ank}}$ in the GCS can be obtained via Newton's second law by substituting the value of the acceleration of the foot COM ($\boldsymbol{a_{foot}}$) and the measured GRF:

$$\boldsymbol{F_{ank}} = m_{foot} \cdot \boldsymbol{a_{foot}} - \mathbf{GRF} \tag{3.61}$$

Note, $\boldsymbol{a_{foot}}$ and all other segment COM accelerations are obtained by twice differentiating the COM position estimates from Table 3.2.

Next, the moment $\boldsymbol{\mu}$ due to the forces acting on the foot is computed:

$$\boldsymbol{\mu_{foot}} = \boldsymbol{F_{ank}} \times \boldsymbol{p_{foot}} + \mathbf{GRF} \times \boldsymbol{d_{foot}} + \mathbf{T_Z} \tag{3.62}$$

where $\boldsymbol{p_{foot}}$ is the distance from the foot COM to the AJC

$\boldsymbol{d_{foot}}$ is the distance from the foot COM to the centre of pressure

$\mathbf{T_Z}$ is the torque applied on the force plate by the foot

Note that $\mathbf{T_Z}$ only has a component in the vertical global Z–axis and is known as the free vertical torque, possibly to distinguish it from the moment channel output by the force plate. Specifically, $\mathbf{T_Z}$ can be obtained as [136, Centre of Pressure]:

$$\mathbf{T_Z} = \mathbf{M_z} - (x - x_0)\mathbf{F_y} + (y - y_0)\mathbf{F_x} \tag{3.63}$$

where $\mathbf{M_z}$ is the moment about the vertical axis of the force plate

x, y are the horizontal components of the COP

x_0, y_0 are the horizontal components of the force plate true origin

$\mathbf{F_x}, \mathbf{F_y}$ are the horizontal components of the GRF

The net moment acting on the ankle $\boldsymbol{M_{ank}}$ can then be obtained using Newton's second law in angular form (Euler's second law):

$$\boldsymbol{M_{ank}} = \dot{\boldsymbol{L}}_{\boldsymbol{foot}} - \boldsymbol{\mu_{foot}} \tag{3.64}$$

For the knee joint, $\boldsymbol{F_{knee}}$ and $\boldsymbol{M_{knee}}$ are obtained from Eqs. 3.61 and 3.64 with $\boldsymbol{F_{ank}}$ replacing $\mathbf{GRF}$, the omission of $\mathbf{T_Z}$, and the appropriate masses and accelerations for the shank segment:

$$\boldsymbol{F_{knee}} = m_{shank} \cdot \boldsymbol{a_{shank}} - \boldsymbol{F_{ank}} \tag{3.65}$$

$$\boldsymbol{M_{knee}} = \dot{\boldsymbol{L}}_{\boldsymbol{shank}} - \boldsymbol{\mu_{shank}} \tag{3.66}$$

Similarly for the hip joint:

$$\boldsymbol{F_{hip}} = m_{hip} \cdot \boldsymbol{a_{thigh}} - \boldsymbol{F_{knee}} \tag{3.67}$$

$$\boldsymbol{M_{hip}} = \dot{\boldsymbol{L}}_{\boldsymbol{thigh}} - \boldsymbol{\mu_{thigh}} \tag{3.68}$$

Joint power

The power developed at each joint can be determined by evaluating the contributions of distal and proximal muscles to segment power [136, Joint Energetics].

Starting with the ankle, the power from the shank and foot can be obtained from M_{ank} and the corresponding $\boldsymbol{\omega_s}$:

$$P_{shank} = \mathbf{M}_{ank} \cdot \boldsymbol{\omega_{shank}} \tag{3.69}$$

$$P_{foot} = -\mathbf{M}_{ank} \cdot \boldsymbol{\omega_{foot}} \tag{3.70}$$

The power at the ankle joint is then:

$$P_{ankle} = P_{shank} + P_{foot} \tag{3.71}$$

$$P_{ankle} = \mathbf{M}_{ank}(\boldsymbol{\omega_{shank}} - \boldsymbol{\omega_{foot}}) \tag{3.72}$$

Similarly, for the knee and hip:

$$P_{knee} = \mathbf{M}_{knee}(\boldsymbol{\omega_{thigh}} - \boldsymbol{\omega_{shank}}) \tag{3.73}$$

$$P_{hip} = \mathbf{M}_{hip}(\boldsymbol{\omega_{pelvis}} - \boldsymbol{\omega_{thigh}}) \tag{3.74}$$

3.6.5 Intra-foot and ankle joint kinetics

Although the OFM outputs in Vicon (Vicon Motion Systems Ltd., Oxford, UK) do not include kinetic quantities, they can be obtained by applying the standard Newtonian IDA approach described in Section 3.6.4 to the segments of the foot (with only the forefoot and hindfoot considered) as demonstrated by Dixon et al. [63].

Starting at the FF, the force $\boldsymbol{F_{mf}}$ and moment $\boldsymbol{M_{mf}}$ at the theoretical midfoot (mf) joint between the forefoot and hindfoot segments are computed as:

$$\boldsymbol{F_{mf}} = m_{\boldsymbol{ff}} \cdot \boldsymbol{a_{ff}} - \mathbf{GRF} \tag{3.75}$$

$$\boldsymbol{M_{mf}} = \dot{\boldsymbol{L}}_{\boldsymbol{ff}} - \boldsymbol{\mu_{ff}} \tag{3.76}$$

Similarly, for the ankle, joint forces and moments can be obtained:

$$\boldsymbol{F_{ank}} = m_{hf} \cdot \boldsymbol{a_{hf}} - \boldsymbol{F_{mf}} \tag{3.77}$$

$$\boldsymbol{M_{ank}} = \dot{\boldsymbol{L}}_{\boldsymbol{hf}} - \boldsymbol{\mu_{hf}} \tag{3.78}$$

Finally, power at the midfoot and ankle joint can also be estimated:

$$P_{mf} = \mathbf{M}_{mf}(\boldsymbol{\omega_{hf}} - \boldsymbol{\omega_{ff}}) \tag{3.79}$$

$$P_{ankleofm} = \mathbf{M}_{ankleofm}(\boldsymbol{\omega_{shankofm}} - \boldsymbol{\omega_{hf}}) \tag{3.80}$$

It has been demonstrated that the PiG overestimates the ankle power due to an overestimation of relative motion between the shank and the single foot segment [63]. Moreover, non-sagittal ankle moments computed by the PiG are thought to be a less valid representation of the true ankle moments. Therefore, throughout this thesis ankle (HF/TB) quantities are derived from the OFM as described here. Mid-foot kinetic quantities are not reported.

3.6.6 Implementation

The PiG joint kinematics and kinetics as well as the OFM kinematics presented in this thesis were computed by standard pipelines within the Vicon Nexus software environment (v1.8.4, Vicon Motion Systems Ltd., Oxford, UK). Only OFM ankle moments and power were directly computed from Eqs. 3.78 and 3.80, respectively.

3.7 Variability in Gait Curves

The estimation of variability in gait curves is of great importance in research and clinical applications [195]. In this section, standard approaches, and their shortcomings, are presented before expounding on an improved method that was selected for analysis of time-dependant gait metrics throughout this thesis.

3.7.1 Standard approaches

In many fields of biomechanics, including gait, a variable of interest is often recorded over a given time period resulting in a one-dimensional (1D) curve. During subsequent

analyses, a collection of such curves is often summarized as a mean signal surrounded by a variability cloud. Curve variability itself is most often expressed using the sample standard deviation s over the time interval t of interest:

$$s(t) = \sqrt{\frac{\sum_{i=1}^{n}[x_i(t) - \overline{x}(t)]^2}{n-1}} \tag{3.81}$$

where n is the sample size

$x_i(t)$ is the ith curve in the sample

$\overline{x}(t)$ is the mean (arithmetic) curve of the sample

This measure of variability reveals little regarding the distribution of the sample at hand. As eloquently stated by Todd C. Pataky: "While error clouds objectively quantify trajectory variability, experimental design complexities conspire to dissolve the connection between variability and probability" [170]. A more appropriate metric to quantify variability is the confidence interval (CI). A CI surrounding $\overline{x}$ provides a range of plausible values within which the true population mean μ may lie. Formally, at a given probability level α, in $(1-\alpha)\%$ of the cases, the CI contains μ. Thus, the corresponding expression can be formulated as [134, pp. 50–51]:

$$CI = \overline{x} \pm c_\alpha \cdot \frac{s}{\sqrt{n}} \tag{3.82}$$

where c_α is the test statistic

In parametric statistics, the value of c_α depends on properties of the underlying population, n, and the α significance level. Larger samples ($n \geqslant 60$) usually follow a Gaussian distribution, while for smaller samples the Student's t-distribution should be applied. Regardless of sample size, it is common for studies to report CIs using $c_\alpha = 1.96$ (Based on the z–score value at $\alpha = 0.05$) [134, pp. 54–55].

In the case of 1D curves, the creation of a confidence band (CB) via the point-by-point application of Eq. 3.82 implies the use of multiple statistical tests (one for each data

point along the curve) and leads to an increased family-wise error rate (increased risk of Type I error). This is certainly of concern in gait applications where curves are often presented over 101 points (0–100% of a complete gait cycle) [141].

A basic method to deal with the multiple comparison problem encountered when constructing CBs is the Bonferroni corrected α significance level:

$$\alpha_{BON} = \frac{\alpha}{n} \tag{3.83}$$

Returning to the example for gait curves, starting with the standard $\alpha = 0.05$ significance level and $n = 101$ data points, Eq. 3.83 returns $\alpha_{BON} \approx 0.0005$. Thus, assuming a normal distribution, c_α from Eq. 3.82 would take on a value of 3.48, leading to exaggeratedly large bands, compared to the standard 1.96 value.

There are a number of methods that can be used to adjust the width of a CB that represent a substantial improvement over the Bonferroni approach, such as simultaneous confidence intervals [73], functional data analysis [180], statistical parameter mapping [169], and Bootstrapping [72]. Of these, the Bootstrap approach has been most popular in the field of gait analysis [12, 42, 71, 141, 164, 174], is relatively straightforward to conceptualize, and can be quickly implemented in higher level programming languages such as Matlab (The Mathworks Inc., Natick, USA). This approach is used throughout this thesis and is described in detail in Section 3.7.2.

3.7.2 The Bootstrap approach

The Bootstrap procedure was introduced by Bradley Efron in 1979 [72]. Bootstrapping involves randomly re-sampling with replacement B times from a given dataset in order to estimate a summary statistic. In the parametric approach, summary statistics are computed by making assumptions about the distribution of the underlying

population. The Bootstrap approach frees the user from relying on parametric assumptions and uses the sample at hand as a pseudo-population, from which it collects numerous Bootstrap samples [205]. In other words, the sample itself is treated as the population from which it is then possible to extract numerous sample sets. It has been shown that as $B \to \infty$ the set of B summary statistics follows the same distribution as their traditionally computed analogues [20, 204]. In general, $1000 \leqslant B \leqslant 2000$ provides sufficient accuracy for most applications [35] and is not computationally expensive on modern computing platforms. Therefore, it is argued that Bootstrapping the parameters from Eq. 3.82 allows for a reasonable approximation of the CI width without undue complexity. The width of the Bootstrap CB is generally larger than one constructed by successive point-by-point CI computations, but appreciably smaller than a Bonferonni corrected CI [170].

The creation of Bootstrap CBs is demonstrated for $B = 1000$ iterations of a sample of straight walking sagittal plane knee angle curves from $n = 27$ children in the TD dataset (Fig. 3.8), with both the standard error (SE) ($s/\sqrt{n}$) and c_α estimated using the Bootstrap procedure. First, the Bootstrap SE (SE_B) is estimated by taking the standard deviation of the B mean curves. As expected, SE_B is similar to the traditional SE computed from the sample at hand (Fig. 3.8 c). Next, from the inverse of the Student's t cumulative distribution function with degrees of freedom ($n - 1 = 26$) and $\alpha = 0.05$, the c_α parameter results in a value of 2.06. Via the Bootstrap approach, B t-statistics are computed from:

$$t_b = \frac{max_t\{|\overline{x}_b(t) - \overline{x}(t)|\}}{SE_B} \tag{3.84}$$

Note that Eq. 3.84 is similar to the parametric t-statistic except that:

1. Parameters μ and $\overline{x}$ are replaced by $\overline{x}$ and $\overline{x}_b$, respectively, in keeping with the Bootstrap concept.

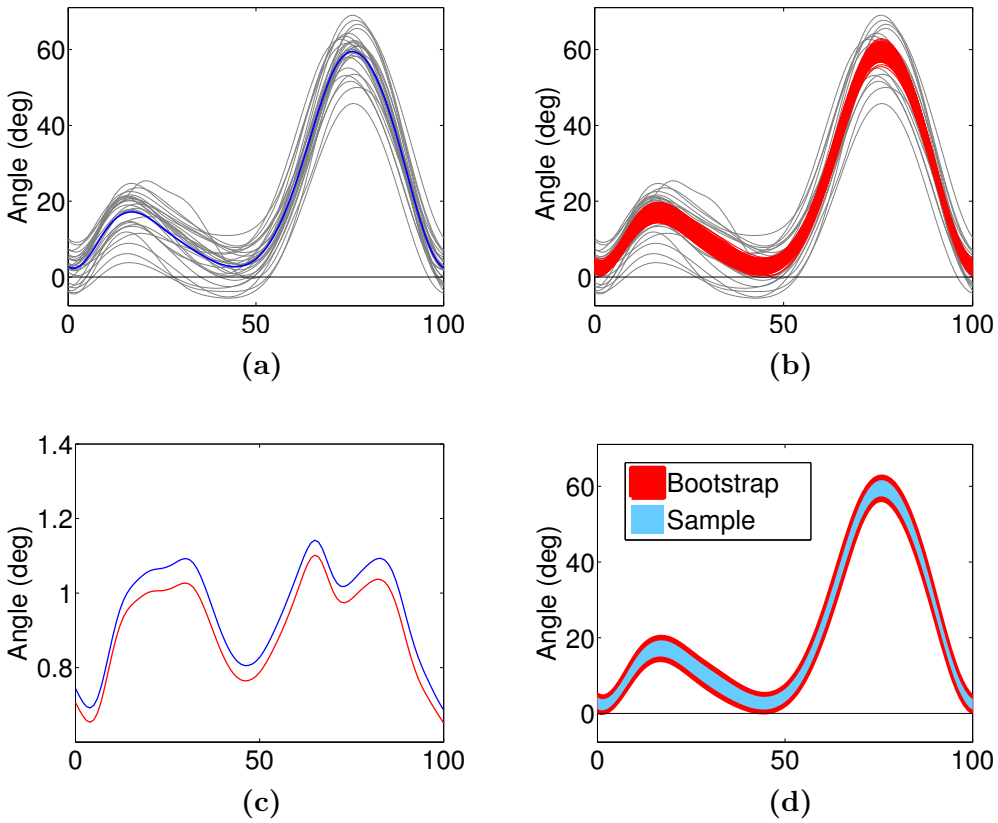

Figure 3.8 – Summary of steps for the creation of a Bootstrap confidence band (CB) using $n = 27$ sample kinematic curves (0–100% of the gait cycle). (a) Individual subject (grey) and mean (blue) curves, (b) Individual subject and $B = 1000$ Bootstrap mean (red) curves, (c) Standard error estimates via the parametric (blue) and Bootstrap approaches, (d) Mean curve from sample and Bootstrap pseudo-samples.

2. The maximum difference over the entire time interval t is computed to ensure that the appropriate CI coverage, $(1 - \alpha)\%$, is maintained [141].

The set of t-statistics $t_b = \{t_1,\ t_2,\ \ldots,\ t_B\}$ is sorted and the value corresponding to the $1 - \alpha/2$ percentile is retained. This approach provides the same result as the method proposed by Lenhoff et al. [141], but avoids their iterative procedure in which the CB width is increased until $(1 - \alpha)\%$ of the B mean curves fit within the CB. The CBs can now be constructed and compared across methods. As expected, Bootstrapping produces a wider band than the parametric approach (Fig. 3.8 d).

The Bootstrap approach improves the estimation of variability in gait curves; however, it is important to stress that Bootstrapping cannot overcome the limitations of a small

sample. Bootstrap pseudo-samples constructed from very small samples ($n < 20$) may not adequately represent the original sample distribution [35].

3.8 Statistical Analysis

During inferential statistical analysis of gait data, the goal is usually to determine if there are differences in a particular metric across groups or conditions. A gamut of statistical tests can be performed depending on the experimental design parameters, especially for univariate data (e.g. step width or gait speed). In this section, the use of a CI comparison technique for 1D curve data, is illustrated. Specific analyses for univariate data are presented in their respective chapters.

3.8.1 Representative trial selection

Prior to all statistical analysis procedures, a representative trial was identified for analysis. Often, a mean curve is used as a representative trial; however, this approach may lead to the loss of important curve features, such as peaks and troughs through a "washing out" effect [42]. Although more complex methods have been proposed [42, 196] to avoid the averaging effect, here, for each child, condition, and channel, the root mean squared (RMS) difference between each curve and the mean curve was computed over the time interval t of interest:

$$RMS = \sqrt{\frac{1}{n} \cdot \sum_{t=1}^{n} \left(x_{ij}(t) - \overline{x}_i(t)\right)^2} \tag{3.85}$$

where x_{ij} is the ith channel curve for the jth trial

$\overline{x}_i$ is the ith channel mean curve

The RMS values were gathered in an $i \times j$ matrix and averaged across the channel dimension i, resulting in a vector made up of each trial's average RMS value ($\overline{r_j}$).

The trial with the minimum $\overline{r}$ was selected as the representative trial:

$$Rep\ \ Trial = min\{[\overline{r}_1, \overline{r}_2, \ldots, \overline{r}_j]\} \tag{3.86}$$

3.8.2 Confidence intervals and hypothesis testing

Considering two groups with sample means $\overline{x}_1$ and $\overline{x}_2$, it is possible to test whether they likely arise from different populations by setting up a hypothesis test :

$$H_0 : \mu_1 = \mu_2 \tag{3.87}$$

$$H_1 : \mu_1 \neq \mu_2 \tag{3.88}$$

If the CIs are known, it is convenient to rewrite the null hypothesis as:

$$H_0 : \mu_1 - \mu_2 = 0 \tag{3.89}$$

H_0 can be rejected if the CI difference interval does not contain zero [134, p. 76].

As the CI (and thus the p-values) depend on the sample size n, effect size which informs about the magnitude or size of the difference and therefore may be more clinically relevant, should also be reported [220]. Standardized effect size in which the magnitude of differences between groups is divided by a standard deviation term is useful for comparisons across studies. In cases where equality of variance across groups can be assumed, Cohen's d (d) can be computed. First, a simplified pooled standard deviation (s_p) is computed [46, p.67]:

$$s_p = \sqrt{\frac{s_1^2 - s_2^2}{2}} \tag{3.90}$$

Next, Cohen's d is obtained:

$$d = \frac{\overline{x}_1 - \overline{x}_2}{s_p} \tag{3.91}$$

Otherwise, Glass's delta (Δ) can be used in which the s_p term in Eq. 3.91 is replaced by the control group's standard deviation (s_c) [91, p. 29]:

$$\Delta = \frac{\overline{x}_1 - \overline{x}_2}{s_c} \tag{3.92}$$

The s_c term was computed based on the TD data for all group comparisons. For comparisons within the TD group, the straight walking data were used.

3.8.3 Confidence bands and hypothesis testing

The approach of Section 3.8.2 can also be extended to gait curve analysis to assess statistical differences at any point along the curve [141]:

$$H_0(t) : \mu_1(t) - \mu_2(t) = 0 \tag{3.93}$$

$$H_1(t) : \mu_1(t) - \mu_2(t) \neq 0 \tag{3.94}$$

The process is demonstrated using sagittal knee joint kinematics during straight (X_1) and spin turn (X_2) trials from the TD child database ($n = 27$). In this example, all subjects performed both walking conditions (Fig. 3.9 a):

$$X_1 = \{x_{11}(t),\ x_{12}(t),\ \ldots,\ x_{1n}(t)\} \tag{3.95}$$

$$X_2 = \{x_{21}(t),\ x_{22}(t),\ \ldots,\ x_{2n}(t)\} \tag{3.96}$$

where x_{1n} is the straight walking curve of the nth subject

x_{2n} is the spin turn curve of the nth subject

First, a set of difference curves is computed:

$$X_D = X_2 - X_1 = \{x_{21}(t) - x_{11}(t),\ x_{22}(t) - x_{12}(t),\ \ldots,\ x_{2n}(t) - x_{1n}(t)\} \tag{3.97}$$

Next, the mean value and Bootstrap 95% CB are computed for X_D. From Fig. 3.9 b, statistical differences between the groups can be easily assessed: any frames for

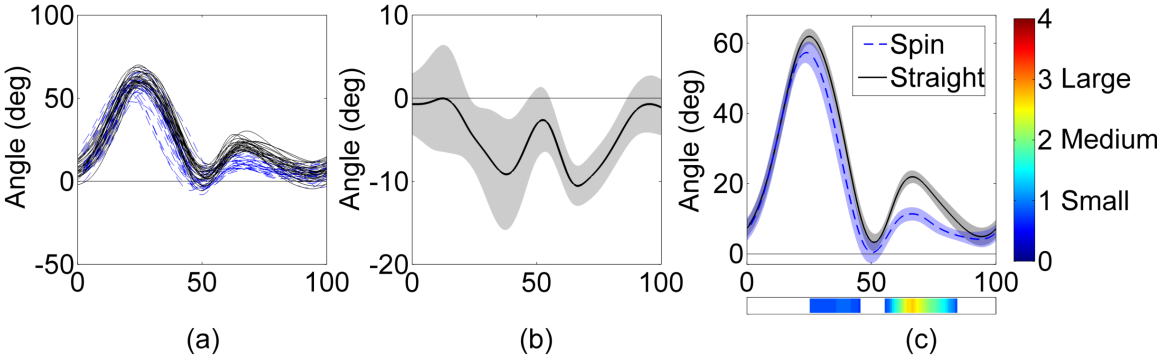

Figure 3.9 – Summary of steps for for statistical analysis of group difference via Bootstrap confidence bands (CBs) using two groups of kinematic curves over 100% of the gait cycle: (a) individual curves for each group, (b) mean difference curve with Bootstrap CB, (c) mean curves with Bootstrap CBs and colour scale representing effect size. Select curves from database chosen for illustrative purposes.

which the CB does not cross the zero-line is a frame at which significant differences with $p < 0.05$ exist between the groups [134, p. 76]. P-values could also be extracted at every point along the line. Analogous to the CI case, a standardized effect size, across time can be computed in conjunction with the Bootstrap CB:

$$d(t) = \frac{\overline{X}_1(t) - \overline{X}_2(t)}{s_p(t)} \tag{3.98}$$

A colour bar graphically illustrates changes in $d(t)$ across the gait cycle. An arbitrary reference scale with 1, 2, and 3 representing small, medium, and strong effect size, respectively, is shown for demonstration purposes (Fig. 3.9 c). Note that $d(t)$, has not been computed (or corrected) by the Bootstrap procedure.

In the case of unequal sample size, a stratified Bootstrap approach is followed. Instead of Bootstrapping X_D to obtain B mean difference estimates, the data for each group are averaged separately B times and their difference is computed (B times) [44].

3.8.4 Limitations

The use of Bootstrap CBs result in the maintenance of the theoretical coverage over the entire curve (for example, 95%), whereas point by-point CIs produce narrow

bands leading to increased Type I error rates [71, 141, 195]. Nonetheless, analysis of CB differences for curve data has a number of limitations.

First, the procedure may become overly conservative over a large number of time points (CB width increases with number of frames). Based on previous gait studies using Bootstrap CBs [141, 174], a number of frames of the order of 100 allows for reasonably wide CBs able to detect relevant differences across groups/conditions. Also, it is not possible to separate group or condition variability from variability arising from covariates [185]. Functional data analysis [180] can overcome this limitation, but is itself fraught with numerous issues, such as the legitimacy of time-warping and requiring user-selected parameter values as inputs. Non-linear model fitting [157] and statistical parameter mapping [169] may also be advantageous, but the current method was chosen as it addresses the weaknesses of point-by point analysis and is relatively easy to implement and interpret. Variability was reduced by testing children during a single session, without removing markers between conditions, and by optimizing kinematic data [13]. Finally, the number of paired comparisons from which CBs are created should be limited. A Bonferroni correction could be implemented to control for increased Type I error; however, as only three conditions are investigated in this thesis (straight walking, spin turns, and step turns), the width of the difference CBs were not further modified. When conducting statistical analysis using discrete points, specific curve features that are often not reproducible or have a different temporal component between trials/individuals must be correctly identified. This difficulty is avoided with the Bootstrap CBs; however, the approach is sensitive to loss of information from ensemble averaging. Overall, analysis of Bootstrap CBs represents a clear improvement over standard approaches and has been shown to produce similar results to more complex corrections [170].

Chapter 4

Turning Gait in Typically Developing Children

Part I Kinematics

Quantities related to foot-strike (FS) and foot-off (FO) timings and three-dimensional motion of the lower-limbs are standard measures used to characterize gait during straight walking. This chapter focuses on presenting the adaptations to these metrics required to successfully complete turning tasks. As these changes are hitherto unknown in typically developing (TD) children, these data provide a normative database from which to compare adaptations in other populations, such as children with cerebral palsy (CP). This chapter presents an updated version of the manuscript published in *Gait and Posture* in 2013 [68]. Here, the use of a stratified Bootstrap procedure [44, pp. 67–71] and the recruitment of additional children has allowed for a larger sample of TD children to be analysed. Also, statistical corrections of post-hoc tests were made less conservative by considering only planned comparisons. These changes have not resulted in altered conclusions.

4.1 Introduction

Turning in adults requires modification of biomechanical variables from those of straight walking, such as spatio-temporal parameters (STPs) [219] and joint kinematics (frontal and transverse planes) [226]. Little is known about the adaptations required for TD children to turn; however, data from the Master's thesis of Milandri [154] indicate that decreased velocity and maintenance of cadence characterize turning in this population.

Thus, the aims of this study were to investigate the STP and lower-limb joint kinematic adaptations required for TD children to navigate 90° step and spin turns. It was hypothesized that for the step turn, velocity and stride length would decrease while stance time and stride width would increase compared to straight walking [219]. Similar changes were expected in velocity, stride length and stance time for the spin turn, but a decreased stride width (based on the increased ipsilateral hip adduction reported in adults [226]). Finally, it was hypothesized that the majority of kinematic changes would occur in the coronal and transverse planes [226].

A comprehensive study of turning in TD children may yield greater insight into the biomechanical requirements of this common task and may lead to the development of improved diagnostics, rehabilitation, and surgical outcomes for populations with restricted gait ability, such as children with CP.

4.2 Methods

4.2.1 Ethical considerations

All procedures were approved by the local ethics committee and all children provided informed assent/consent for inclusion in the study (see Section 3.1).

4.2.2 Subjects

Fifty-four TD children from the database were considered for this study. Turning strategy was determined for each, but seven were excluded from the rest of the analyses due to marker occlusions within the turning cycle. All remaining subjects ($n = 47$) performing straight walking and at least a single turning trial were compared across groups (Table 4.1). See Table 3.1 for a list of the subjects analysed.

4.2.3 Data collection and processing

The data collection and processing steps are fully described in Sections 3.3.3 and 3.4, respectively. See Fig. 3.4 for diagrammatic representation of turn styles and important turn cycle events. Of note, the hallux marker was prone to falling off leading to the possible rejection of additional children in the database due to missing data. Thus, in order to maximize the number of subjects analysed the hallux with respect to forefoot angular changes, which were few in the original study [68], are not reported here. Kinematic data for the hip, knee, hindfoot with respect to tibia (HF/TB), and forefoot with respect to hindfoot (FF/HF) were retained.

4.2.4 Statistical analysis

Spatio-temporal parameters

For the STPs, each of the three strides (approach, turn, and depart) of the two turning conditions (step and spin), along with a single stride from the straight walking condition were analysed using a one-way within-subject ANOVA (1×7) design. No attempt was made to control experiment-wise error rates, i.e. the increased chance of committing a Type I error due to the evaluation of multiple ANOVAs. Feise [75] has argued that defining a "family" in this context is fairly arbitrary and that considering each ANOVA independently, without correction, allows for clearer interpretation of

Table 4.1 – Summary of subject anthropometric data by condition

Condition	n	Age (years)	Weight (kg)	Height (cm)	Sex
Straight	47	10.7 (2.8)	39.8 (14.0)	147.5 (16.3)	23F, 24M
Spin	46	10.8 (2.8)	39.9 (14.1)	147.8 (16.4)	22F, 24M
Step	22	11.5 (2.6)	41.3 (12.3)	151.1 (15.6)	12F, 10M

Mean (standard deviation) of anthropometrics by condition. All subjects performed straight walking trials. Sample size (n) and sex (female (F) and male (M)) also shown.

the data. Thus, the raw ANOVA main effect p-values are reported here. However, in the case of a significant main effect test, $n = 15$ planned post-hoc comparisons (straight vs all phases of step and spin (6), across phases within each turn style (6), and across styles for each phase (3)) were assessed using a Bonferroni correction (see Section 3.7.1). Raw p-values were multiplied by the n planned comparisons instead of adjusting the α level. Normality was not assessed before performing the main effect tests given the robustness of ANOVA against this possible deviation [134, p.83]. The assumption of homogeneity of variance across conditions (Sphericity) was verified using Mauchley's test, resulting in the reporting of the Greenhouse-Geisser corrected p-values for stride velocity and stride width.

For the post-hoc planned comparisons, normality for each member of the pair and each paired difference was assessed via visualization of the Q-Q plots, supplemented by a conservative Lilliefors test in cases of doubt ($\alpha_{LIL} = 0.01$), while equality of error variance was measured via Levene's test. Non-normally distributed differences were found for the following pairs: step depart vs straight, spin turn vs spin depart, and step approach vs step turn for stance time as well as step turn vs straight for stride length. Unequal variance across pairs was suspected for all phases of the spin as well as the turn phase of the step technique, compared to straight walking for the stride width parameter. Departures from any of the parametric assumptions led to

the use of the Wilcoxon signed-rank test, otherwise, paired t-tests were implemented. Cohen's d (d) was reported if parametric assumptions held, otherwise Glass's delta (Δ) approach was implemented (see Section 3.8.2). ANOVAs were performed in SPSS (v21, IBM Corp., Armonk, USA), while post-hoc tests were implemented in Matlab (v2012b, The Mathworks Inc., Natick, USA). The significance level was set at $\alpha = 0.05$ unless otherwise stated.

Joint kinematics

For the kinematics, statistical analyses were conducted over the entire turning cycle by investigating the mean difference 95% confidence band (CB) between pairs of conditions [141]. Here (unlike in the manuscript version [68]), given the unequal sample sizes, the stratified Bootstrap approach was invoked: in lieu of Bootstrapping a single set of differences to obtain n mean Bootstrap difference estimates, data from each group were averaged and their difference computed n times [44, pp. 67–71] (see Section 3.7.2). Data from each side (ipsilateral and contralateral) were compared only across turning strategies. Effect sizes (without Bootstrap adjustment) were calculated for each comparison over the length of the curve using Cohen's d [46]. A graphical representation of Cohen's d via colour coded bars illustrates strength of the differences with values of 1, 3, and 5 representing, small, medium, and large effect sizes, respectively (see Section 3.8.3). Zones of significant difference less than 5% of maximum CB width are not shown within graphs.

4.3 Results

4.3.1 Turning frequency

The children in the complete TD dataset ($n = 54$) favoured turning using the spin technique (Table 4.2). The minimal reliance on step turns was noticed mid-way

Table 4.2 – Frequency distribution of turn style preferences

Group	Step and Spin	Spin only	Step only
TD-O	17/33	15/33	1/33
TD-N	13/21	8/21	0/21
TD-C	30/54	23/54	1/54

TD children original (TD-O), new (TD-N) and complete (TD-C) datasets.

through the original data collection process ($n = 33$). Later, as more subject data were collected ($n = 21$), step turns were encouraged without alerting the subjects via changes in start position (see Fig. 3.1). This did not lead to more subjects selecting step turns. Overall, 43% of subjects only performed spin turns, 56% performed both step and spin, and only a single subject chose to solely perform step turns.

4.3.2 Spatio-temporal parameters

All STPs showed a significant main effect difference ($p < 0.001$) resulting in post-hoc analyses for all cases (Table 4.3).

Stride velocity was reduced for all turning phases compared to the straight condition ($p < 0.001$ and $d = [0.94, 2.68]$). For both turn types, the turn and depart phases were slower than the approach ($p < 0.001$ and $d = [0.80, 1.66]$) and the depart phase was slower than the turn ($p \leqslant 0.014$ with $d = 0.56$ and $d = 0.27$ for the step and spin conditions, respectively). The step depart phase was the slowest (0.89 m/s).

Stance time for all turn conditions, except the approach to the spin turn, were longer than for straight ($p \leqslant 0.020$) with effect-sizes for spin turn ($d = 0.57$), spin depart ($d = 0.27$), step approach ($d = 0.47$), step turn ($d = 0.57$), and step depart ($\Delta = 0.60$) small. For the spin condition, the turn phase was longer than the approach and depart phases ($p < 0.001$ with $d = 0.45$ and $\Delta = 0.28$, respectively). The approach phase for step turn was longer than for spin ($p = 0.023$ and $d = 0.33$).

Table 4.3 – Spatio-temporal parameters during straight and turning conditions

Condition	Stride Velocity (m/s)	Stance Time (s)	Stride Length	Stride Width
Straight	1.33 [1.28, 1.38]	0.60 [0.58, 0.63]	1.59 [1.55, 1.64]	0.11 [0.10, 0.12]
Spin (A)	1.18 [1.14, 1.23]*	0.61 [0.58, 0.64]	1.45 [1.40, 1.50]*	0.20 [0.18, 0.20]*
Spin (T)	1.06 [1.01, 1.10]*^{a}	0.65 [0.62, 0.68]*^{a}	1.42 [1.36, 1.47]*	0.15 [0.13, 0.18]
Spin (D)	1.01 [0.96, 1.06]*^{at}	0.63 [0.60, 0.65]*^{t}	1.37 [1.31, 1.42]*^{at}	0.28 [0.26, 0.30]*^{at}
Step (A)	1.17 [1.09, 1.25]*	0.66 [0.62, 0.70]*^{s}	1.47 [1.39, 1.54]*	0.08 [0.05, 0.10]^{s}
Step (T)	0.98 [0.91, 1.05]*^{sa}	0.67 [0.63, 0.72]*	1.15 [1.08, 1.22]*^{sa}	0.38 [0.35, 0.41]*^{sa}
Step (D)	0.89 [0.82, 0.96]*^{sat}	0.67 [0.63, 0.71]*	1.40 [1.30, 1.48]*^{t}	0.07 [0.05, 0.09]st

Mean [95% confidence interval] for straight walking along with the approach (A), turn (T), and depart (D) phase of step and spin turns. Statistically significant difference from straight (∗), approach stride same turn condition (a), turn stride same condition (t), and between conditions for the same phase (s) also shown.

Stride length was shorter for all step and spin condition turning strides compared to straight walking ($p < 0.001$). Effect-sizes for all turn condition comparisons to straight walking were small ($d = [0.84, 1.37]$) except for step depart ($\Delta = 3.04$). The step condition turn stride was shorter than the spin turn stride as well as the step approach and step depart strides ($p < 0.001$ and $d = [1.52, 1.97]$). Also, the spin depart stride was shorter than the spin approach ($p = 0.001$ and $d = 0.45$) and spin turn ($p = 0.035$ and $d = 0.27$) strides.

Finally, stride width for the spin approach ($p < 0.001$ and $\Delta = 2.28$) and depart ($p < 0.001$ and $\Delta = 4.48$) as well as the step turn ($p < 0.001$ and $\Delta = 6.35$) phase were strongly increased compared to straight walking. The turn stride of the step condition was wider than for the spin turn ($p < 0.001$ and $d = 2.79$); however, both the approach ($p < 0.001$ and $d = 1.69$) and depart ($p < 0.001$ and $d = 4.00$) strides of the step turn were narrower than their spin counterparts. For the step condition, the turn stride (0.38) was wider than both the approach ($p < 0.001$ and $d = 4.87$) and depart strides ($p < 0.001$ and $d = 5.33$) while for spin, depart was wider than approach ($p < 0.001$ and $d = 1.12$) and the turn ($p < 0.001$ and $d = 1.72$) phase.

4.3.3 Joint kinematics

The average variation of the Bootstrap CBs for all kinematic parameters was approximately 1.5 times larger than the point-by-point Gaussian confidence interval width (2.94 vs 1.96). Overall, effect sizes were generally small (Figs. 4.1 and 4.2).

In the sagittal plane, few differences were observed at the hip, knee, HF/TB, and FF/HF of the ipsilateral (Fig. 4.1 a–d) and contralateral (Fig. 4.2 a–d) sides.

Numerous significant differences occurred in the coronal plane, most notably for the ipsilateral limb (medium effect size). At the hip, the step condition involved an abduction angle, while the spin and straight conditions showed adduction resulting in a difference of up to 10° near 80% of the turning cycle. For the knee, differences ranging from 2–7° were detected near 50 and 100% of the turning cycle. For the HF/TB, differences of up to 16° were identified during the stance phase of FS3 arising from large inversion for the step condition and increased eversion for the spin compared to straight. Increased supination for the FF/HF of the step condition occurred in comparison to spin and straight (Fig. 4.1 e–h). For the contralateral side, significant differences at the hip were expressed as increased adduction for the step and decreased adduction for the spin compared to straight. At the knee, both turning styles showed out of phase increased peak angles compared to straight walking. For the HF/TB, spin presented consistently greater inversion (2–11°) compared to both step and straight. For the FF/HF, consistent increased supination (2–7°) was seen for the spin condition compared to step (Fig. 4.2 e–h).

In the transverse plane, differences were found for both limbs. For the ipsilateral side, the hip had external rotation centred about FS4 for the step condition, while internal rotation was present for the spin and straight conditions (10–13° differences). The knee revealed an out-of-phase angular pattern throughout the middle of the turning cycle between conditions. Similarly, the HF/TB presented oppositely directed angles

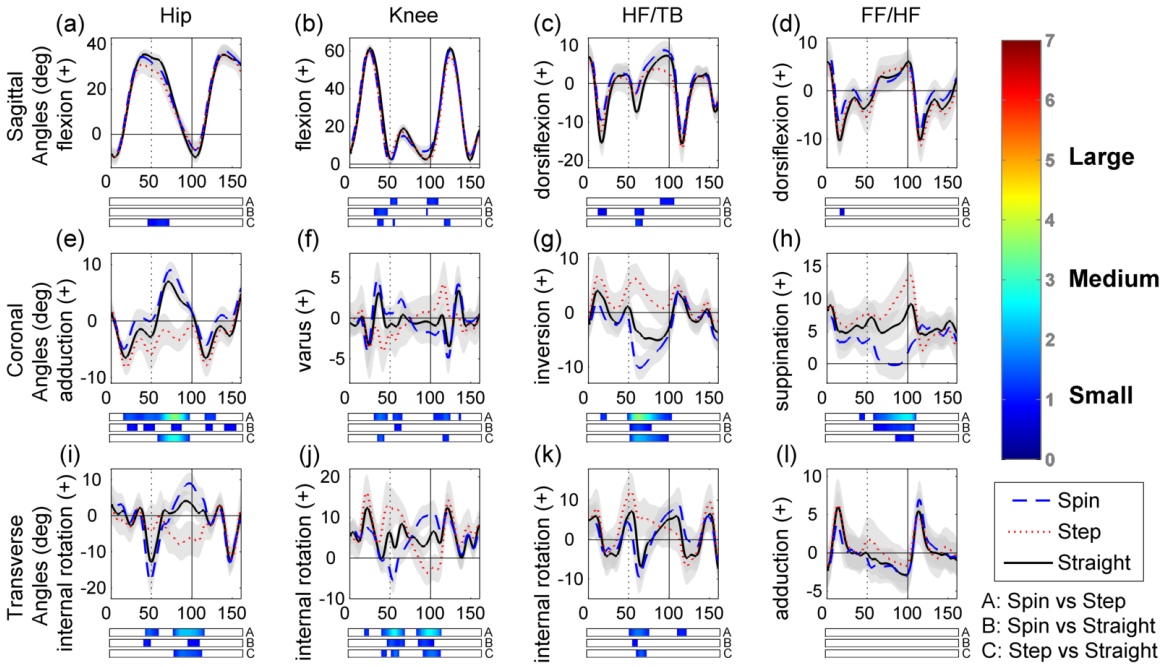

Figure 4.1 – Ipsilateral hip, knee, hindfoot/tibia (HF/TB), and forefoot/hindfoot (FF/HF) joint kinematics for step, spin, and straight conditions with corresponding Bootstrap confidence bands (CBs) over the turning cycle (FS2 to FO4). Dotted vertical lines at ipsilateral foot-strike (FS3 at 50%) and solid vertical lines at contralateral foot-strike (FS4 at 100%). Colourbars show where mean difference CBs reveal significant differences with intensity representing effect size from small (blue) to large (red).

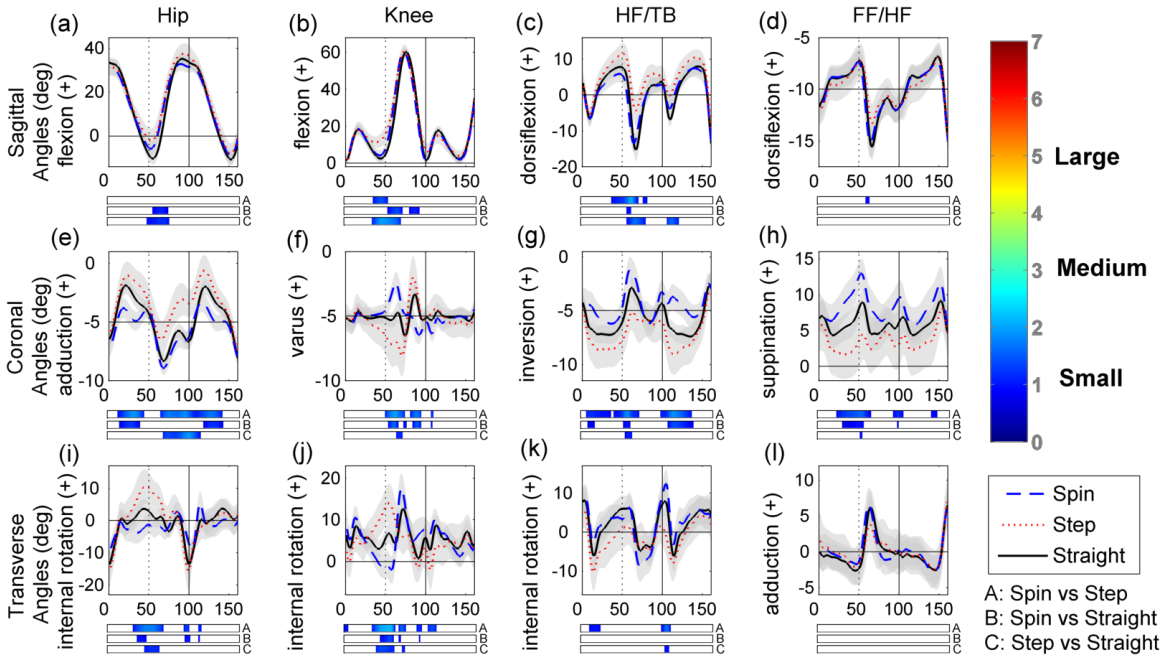

Figure 4.2 – Contralateral hip, knee, hindfoot/tibia (HF/TB), and forefoot/hindfoot (FF/HF) joint kinematics for step, spin, and straight conditions over the turning cycle (FS2 to FO4). See Fig. 4.1 for explanation of colourbar and line annotations.

between turning conditions (8–16° differences) during the stance phase of FS3 and FS4 (Fig. 4.1 i–k). On the contralateral side, differences were mainly apparent at the hip and knee. For the hip, all conditions differed from each other with the greatest changes occurring about FS3 between the step and spin. At the knee, differences were again centred about FS3 with the spin condition near external rotation and the step presenting increased internal rotation compared to straight. Finally, at the HF/TB, increased internal rotation was noted for the spin turn compared to step at FS4. The step condition also showed less internal rotation than straight (Fig. 4.2 i–k). All differences noted above were significantly different with $p < 0.05$.

4.4 Discussion

This study investigated the STPs and lower-limb kinematics of TD children during 90° step and spin turns and compared the results to straight walking. The kinematic analysis procedure implemented represents a rarely used, yet effective, conservative statistical approach that succinctly summarized differences throughout the turning cycle. This is the first study to describe the kinematics of turning in TD children, the STPs for the 90° spin turn, and the kinematics based on the multi-segment Oxford Foot Model for both turning strategies in any population. In general, this investigation has demonstrated that turning gait requires numerous lower-limb biomechanical adaptations and may be challenging for children with CP.

4.4.1 Turn style preference

The present cohort predominantly chose to perform turns using the spin strategy regardless of a possible increased risk of tripping [226]. This finding is in agreement with the work of Akram et al. [3] in which healthy older adults also preferred spin turns. Their cohort only switched to a step turn dominant strategy during the fastest

walking condition [3]. Clearly, the current protocol did not pose a significant threat to balance in this cohort. Possibly, decreased stride velocity and stride length as well as increased stance time and stride width aided the maintenance of a stable base of support minimizing the risk of falling and subsequent injury during turning, allowing subjects to chose the spin turn without risk.

4.4.2 Spatio-temporal parameters

The results for straight walking are in agreement with previous data [146]. With regard to the turning conditions, as hypothesized, stride length and stride velocity were found to decrease compared to straight walking in agreement with step turn data presented by Strike and Taylor [219], while stance time generally increased. Moreover, also in agreement with Strike and Taylor [219], increased stride width was found during the turn phase of the step condition. Contrary to the STP hypothesis, no significant changes in stride width were observed for the turn phase of the spin turn, while the approach and depart phases revealed increased stride width compared to straight walking. This phenomenon may have occurred due the positioning of the approach (FS2) and depart (FS4) steps in an attempt to maintain balance through widening of the base of support. These assertions may be supported by the decreased hip adduction seen for the contralateral limb.

4.4.3 Joint kinematics

Joint kinematics for straight walking are in agreement with previous work [194, 213]. As hypothesized, coronal and transverse plane angles showed important differences from straight walking. These results are similar to those found by Taylor et al. [225]; however, caution must be exercised when making comparisons between the two studies as populations sampled, protocols implemented, and biomechanical models computed

differ. A major disparity between this study and the research of Taylor et al. [226] is that here, a single spin turn strategy was identified. In a group of healthy adults ($n = 10$), Taylor et al. [226] divided the spin technique into two sub-categories: the ipsilateral pivot ($n = 4$) where the foot rotates with respect to the surface during the turning stance phase and the ipsilateral cross-over ($n = 6$), where the turning foot is rooted as the contralateral limb is swung into the new direction. This subdivision of spin turns has not been confirmed by other authors [105]. It is likely that the emergence of the ipsilateral pivot is dependent on increased gait velocity. The approach speed from the Taylor et al. [226] study was 1.38 m/s, while here, children approached the spin turn with a mean velocity of 1.18 m/s. Alternatively, although the present cohort seem to possess a mature straight walking pattern, it is possible that the increased demands of turning might expose remaining gait immaturity leading to a fusion of the more complex turning sub-strategies identified in adults. A further point to make is that here the knee kinematics were optimized [13], whereas Taylor et al. [226] presented data that may be subject to error due to misaligned thigh wand markers. Finally, as Taylor et al. [226] only investigated a portion of the turning cycle for the ipsilateral limb, important information over the entire turn and the role of the contralateral limb are not available for comparison.

4.4.4 Clinical applications

Children with CP often present with impaired balance, weak hip abductors, in-toeing, and ankle contractures [173, pp.345–356], making the aforementioned turning gait adaptations difficult. The inclusion of turning tasks in clinical gait analysis might help improve the assessment, diagnosis, treatment, and mobility outcomes for children with CP. In particular, assessing turning gait in the presence of pathology could help reveal deviations and problems that may not be obvious, or as pronounced, during straight walking tasks.

4.4.5 Limitations and other considerations

For the kinematic data, Bootstrap CBs were used to represent the variability and conduct statistical analyses. Despite the limitations of this approach (see Section 3.8.4), the Bootstrap remains a robust option for the representation of variability, especially when used to build a normative database, and to provide statistical analysis in continuous gait data. Also, analysis of turning gait focused on pre-planned manoeuvres over a change in direction of 90°. Thus, the effect of anticipation or other angular changes in direction were not investigated. Unanticipated turns do not allow for pre-planning, possibly leading to different kinematic patterns and increased injury risk [125].

4.4.6 Conclusions

Overall, the changes presented reveal that turning may be biomechanically distinct from straight walking. In straight gait, motion of the COM in the plane of progression is passively controlled by momentum and inertia [84]. During turning, forward progression of the COM must be quickly halted and redirected over a relatively stable base of support, possibly requiring greater active control from the central nervous system. Each turning strategy may represent a different solution to the redirection problem with step turns being more stable and spin turns possibly more economical [226]. An investigation of turning gait kinetics in TD children may provide greater information regarding these control strategies and complete the picture of the normative changes occurring in this population.

Chapter 5

Turning gait in typically developing children

Part II Kinetics

The results of Chapter 4 reveal numerous spatio-temporal and joint kinematic changes during turning gait compared to straight walking in typically developing (TD) children. Here, the influence of joint kinetics on these adaptations are explored. The results of this chapter have been published in manuscript format by the *Journal of Biomechanics* in 2014 [69].

5.1 Introduction

In adults, previous research has shown that kinematic changes occur during 90° turning gait compared to straight walking. The results presented in Chapter 4 demonstrate that similar kinematic adaptations occur during 90° turning gait in TD children, despite their immature locomotor systems. To date, the forces and moments responsible for these changes still require investigation. Presumably, these adaptations are driven by altered muscular patterns required to redirect the body centre of mass (COM) towards the new direction, as demonstrated by changes in ground reaction forces (GRFs), ground reaction free vertical torque (T_Z), and lower-limb joint moments and powers [88, 104, 219, 226, 251].

Therefore, the aims of this study were to compare GRFs, T_Z, lower-limb joint moments, and lower-limb joint power during 90° turning gait (step and spin) and during straight walking in TD children. It was hypothesized that (1) the medio-lateral GRF would increase for turning compared to straight walking given the required direction change [88, 200], (2) T_Z would increase during spin turns as the foot rotates about the ground [104], (3) joint moments at the hip, knee, and ankle (coronal and transverse planes) would be modified to control kinematics [226, 251], and (4) peak ankle power generation would decrease for turning compared to straight walking due to a decreased need for forward acceleration [226].

Taken in combination with the kinematic findings of Chapter 4, this investigation may lead to a broader understanding of turning biomechanics in TD children and could be used to assess turning gait adaptations in children with cerebral palsy (CP).

5.2 Methods

5.2.1 Ethical considerations

All procedures were approved by the local ethics committee and all children provided informed assent/consent for inclusion in the study (see Section 3.1).

5.2.2 Subjects

Fifty-four TD children from the database were considered for this study. Of these, six were excluded due to marker occlusions or missing force plate data. All subjects performing straight walking trials and at least a single turning trial with a clean force plate hit during the approach or turn phase were retained ($n = 48$) (Table 5.1). See Table 3.1 for a list of the subjects analysed.

Table 5.1 – Summary of subject anthropometric data by condition

Condition	n	Age (years)	Weight (kg)	Height (cm)	Sex
Straight	48	10.6 (2.9)	39.6 (14.3)	147.1 (17.3)	22F, 26M
Spin (A)	39	10.9 (2.9)	40.5 (14.9)	148.4 (17.1)	18F, 21M
Spin (T)	37	10.5 (2.9)	39.1 (14.4)	146.2 (16.8)	15F, 22M
Step (A)	21	11.6 (3.0)	43.7 (13.2)	155.0 (17.2)	9F, 12M
Step (T)	16	11.3 (2.9)	42.3 (14.7)	149.8 (17.6)	8F, 8M

Mean (standard deviation) of anthropometrics for straight walking along with the approach (A) and turn (T) phase of step and spin turns. All subjects performed straight walking trials. Sample size (n) and sex (female (F) and male (M)) also shown.

5.2.3 Data collection

The data collection protocol of Section 3.3.3 was followed. Diagrammatic representation of turn styles and gait events are shown in Fig. 5.1 and 3.4, respectively.

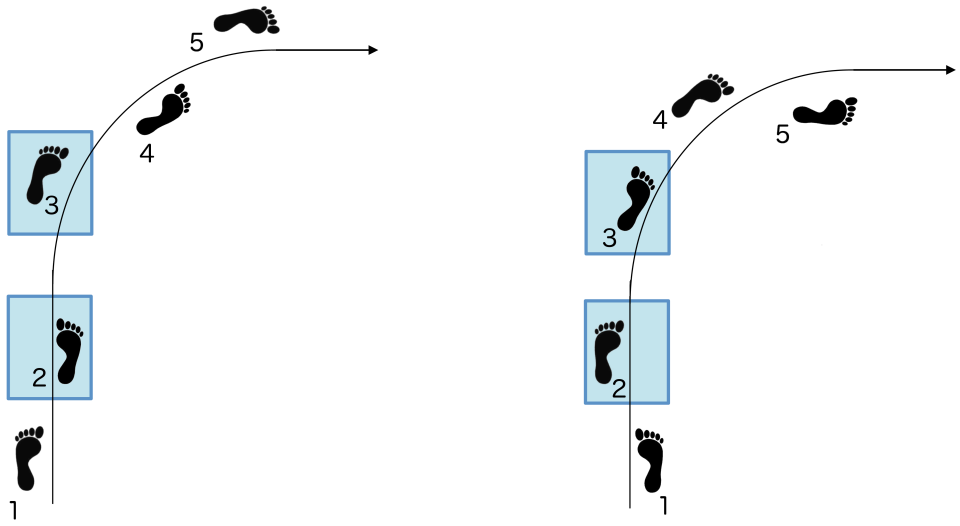

(a) (b)

Figure 5.1 – Diagrammatic representation of (a) a 90° step turn to the right and (b) a 90° spin turn to the right with shaded rectangles representing force plates.

5.2.4 Data processing

In preparation for inverse dynamic analysis, the raw GRF, centre of pressure (COP), and T_Z data were filtered using a fourth order zero-lag Butterworth filter with an 18 Hz cut-off frequency and down-sampled to match the kinematic data. These data, along with anthropometric quantities, were input into standard inverse dynamics equations applied to the Oxford Foot Model (OFM) to compute ankle (hindfoot with respect to tibia) three-dimensional net internal joint moments and power (see Section 3.6.5 for associated formulae). In contrast to Dixon et al. [63], who reported ankle moments when only the OFM forefoot segment made ground contact, ankle moments were calculated for the entire gait cycle. Finally, joint kinetic data were filtered using a fourth order zero-lag Butterworth filter (10 Hz cut-off frequency). Filter cut-off frequencies were determined via a frequency spectrum analysis.

To allow for anatomically meaningful analysis of GRFs, components were aligned with the turning direction [89] estimated via the horizontal projection of the anterior

pelvic vector into the global coordinate system. The polarity of the medio-lateral component of the GRF (F_{ML}) and T_Z were reversed for trials where the left foot made contact with the force plate to maintain a common right foot reference system. Data for the left and right turns were pooled.

Kinematic changes during turning gait have been previously identified between the second foot-strike (FS2) and the fourth foot-off (FO4) (see Chapter 4), representing approximately 162% of a gait cycle (Fig. 3.4 c). To capture the majority of this cycle for kinetics, data for the ipsilateral limb were partitioned from FO1 to FS3, from FS3 to FO3, and from FO3 to FS5, while data for the contralateral side were partitioned from FS2 to FO2 and from FO2 to FS4. Thus, force plate data were obtained for the approach (2nd) and turn (3rd) steps only (Fig. 5.1).

Events during force plate contact (FS2, FO2, FS3, and FO3) were identified using a 20 N cut-off, while the others (FO1, FS4, FO4, and FS5) were estimated using the marker coordinate algorithm of Zeni et al. [256]. After time normalization, the ipsilateral and contralateral sides represented approximately 12–150% and 0–100% of the turning cycle, respectively. All quantities were normalized to body mass.

Identification of turn styles and representative trials, as well as the estimation of variability using the 95% Bootstrap confidence bands were obtained as described in Sections. 3.4.3, 3.8.1, and 3.7.2, respectively.

5.2.5 Statistical analysis

Differences between dependent variables were analysed via the mean difference 95% Bootstrap confidence band (stratified Bootstrap approach) [44, pp. 67–71]. Effect size was calculated, without Bootstrap adjustment, for each comparison along the entire curve via Cohen's d [46] with the values of 1, 3, and 5 chosen to represent, small,

medium, and large effect sizes, respectively (see Section 3.8.3). Zones of significant difference less than 5% of maximum CB width are not shown within graphs.

5.3 Results

5.3.1 Ground reaction forces

Statistical analysis of the GRF data revealed significant differences between conditions and across limbs (Fig. 5.2). For the ipsilateral limb, the medially directed F_{ML} was significantly increased for step turns compared to straight walking and also to spin turns which showed lateral F_{ML}. For the antero-posterior force (F_{AP}), spin turns resulted in increased braking (posterior) force compared to step turns. Increased propulsive (anterior) force was observed for step turns compared to straight walking. Small changes were found in the vertical force (F_V) with spin turns showing a shallower mid-stance trough compared to straight walking (Fig. 5.2 a–c). For the contralateral F_{ML}, it was spin turns that showed increased medial force, while step turns were laterally directed. For F_{AP}, braking was increased and propulsion decreased during turning compared to straight walking. Finally, for F_V, the mid-stance trough was shallower and the second peak smallest for step turns, mostly compared to straight walking (Fig. 5.2 d–f).

5.3.2 Free vertical torque

For the ipsilateral T_Z, differences were seen between all paired comparisons with the step and spin tasks showing decreased and increased magnitudes, respectively, compared to straight walking, reaching maximum differences near opposite ground contact (FS4) (Fig. 5.3 a). For the contralateral limb, the trend was reversed with step turns increasing and spin turns decreasing T_Z (Fig. 5.3 b).

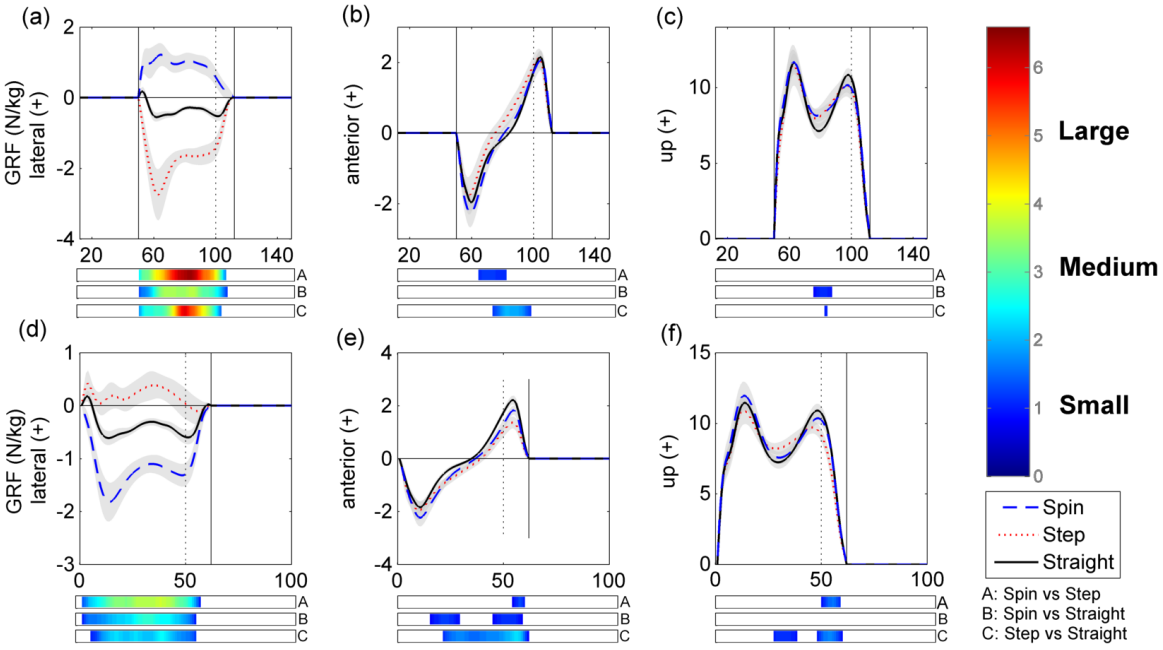

Figure 5.2 – Ground reaction forces (GRFs) for step, spin, and straight conditions with Bootstrap confidence bands (CBs) over the stance phase for the ipsilateral (a–c) (50–112%) (turn phase) and the contralateral limb (d–f) (0–62%) (approach phase). Dotted vertical lines indicate opposite foot-strike (FS4 at 100% and FS3 at 50% for the ipsilateral and contralateral sides, respectively) and solid vertical lines, transitions between swing and stance. Colourbars show where mean difference CBs reveal significant differences with intensity representing effect size from small (blue) to large (red).

5.3.3 Ipsilateral joint moments and power

Significant differences were found in most ipsilateral joints (Fig. 5.4). In the sagittal plane, only a few adaptations were seen: at the hip, a decreased peak flexor moment was observed for the turning conditions, while at the knee increased flexor moment was noted for the step condition compared to spin and straight, both during opposite ground contact (Fig. 5.4 a and b). In the coronal plane, differences were noted for all joints. For the hip, main changes were found in swing: abductor moments for spin and adductor moments for step. At the knee, during the approach and depart swing phases, spin turns showed valgus moments, while step turns revealed varus moments. Furthermore, decreased valgus moment, followed by increased varus moment was observed in pre-swing for step turns compared to the straight and spin trials. At the

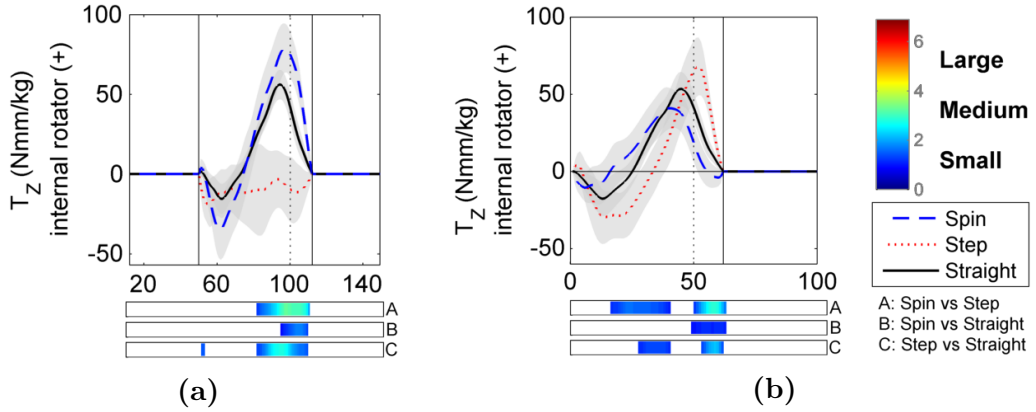

Figure 5.3 – Free vertical torque (T_Z) for step, spin, and straight conditions with corresponding Bootstrap confidence bands (CBs) over the stance phase for the ipsilateral (a) (50-112%) (turn phase) and the contralateral limb (b) (0–62%) (approach phase). Dotted vertical lines indicate opposite foot-strike (FS4 at 100% and FS3 at 50% for the ipsilateral and contralateral sides, respectively) and solid vertical lines, transitions between swing and stance. Colourbars show where mean difference CBs reveal significant differences with intensity representing effect size from small (blue) to large (red).

ankle, the step trials revealed an invertor moment, while spin trials lead to evertor moments throughout most of stance (Fig. 5.4 d–f). For the transverse plane, the hip showed increased external rotator moments for spin turns and decreased external rotator moments for step turns, compared to straight walking near terminal stance with larger changes occurring in swing with step and spin turns revealing external and internal rotator moments, respectively. The knee mainly showed increased external rotator moments for spin turns and decreased external rotator moments for step turns, compared to straight walking near terminal stance. For the ankle, the step turn showed an external rotator moment at the ankle during the loading response, while the spin turn required an internal rotator moment (Fig. 5.4 g–i).

At the knee, step turns showed power generation while absorption was found for spin and straight in pre-swing. At the ankle, a very narrow zone of decreased generation was seen for step turns compared to spin and straight walking (Fig. 5.4 k and l).

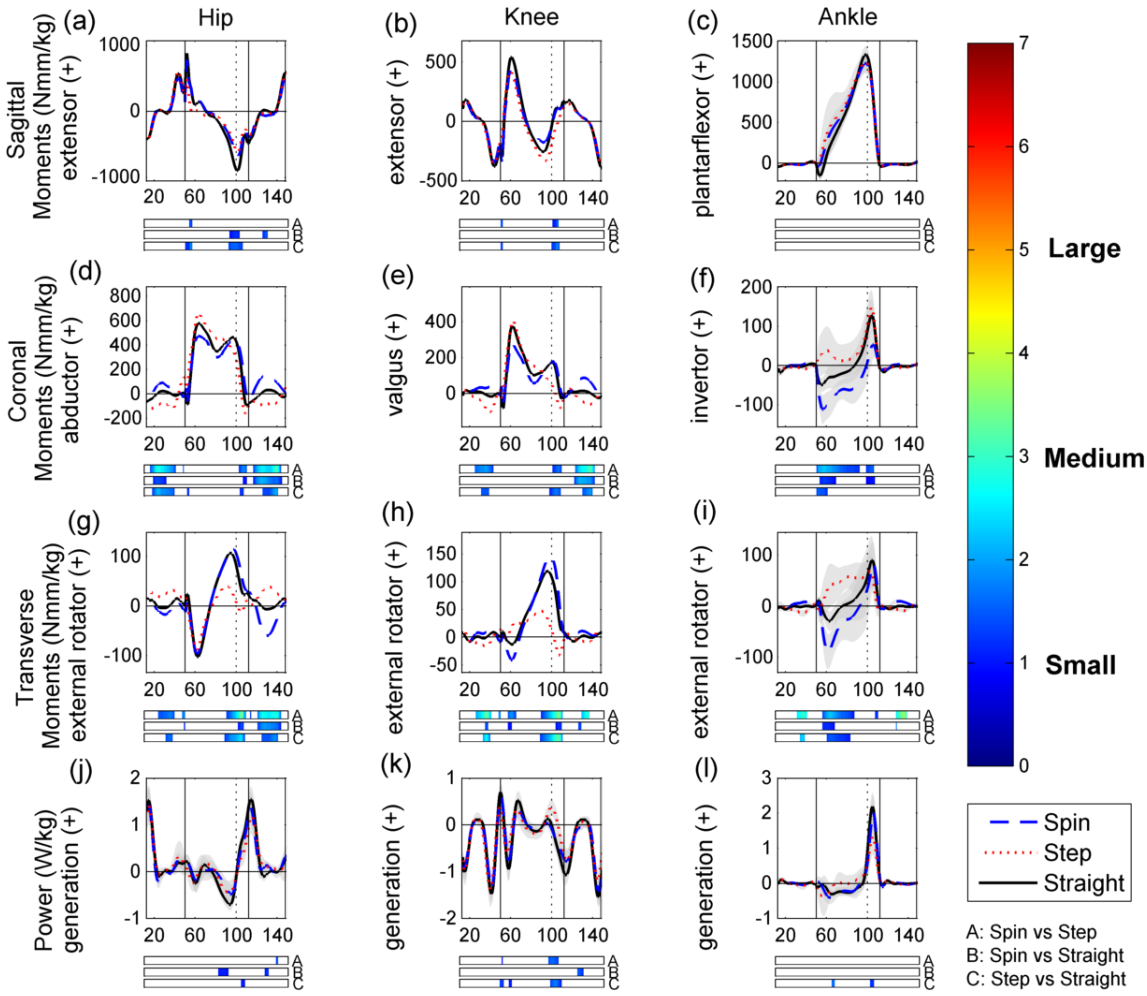

Figure 5.4 – Ipsilateral hip, knee, and ankle joint moments and power for step, spin, and straight conditions with corresponding Bootstrap confidence bands (CBs) from 12–150% of the turning cycle. Dotted vertical lines indicate opposite foot-strike (FS4 at 100%) and solid vertical lines, transitions between swing and stance (FS3 and FO3). Colourbars show where mean difference CBs reveal significant differences with intensity representing effect size from small (blue) to large (red).

5.3.4 Contralateral joint moments and power

Significant differences with larger effect sizes were found for the contralateral limb (Fig. 5.5). In the sagittal plane, at the hip, step turns presented decreased flexor moments starting in pre-swing and continuing during swing, compared to straight walking. At the knee, step turns showed reduced flexor moments compared to spin turns and straight walking. For the ankle, step turns showed decreased peak plan-

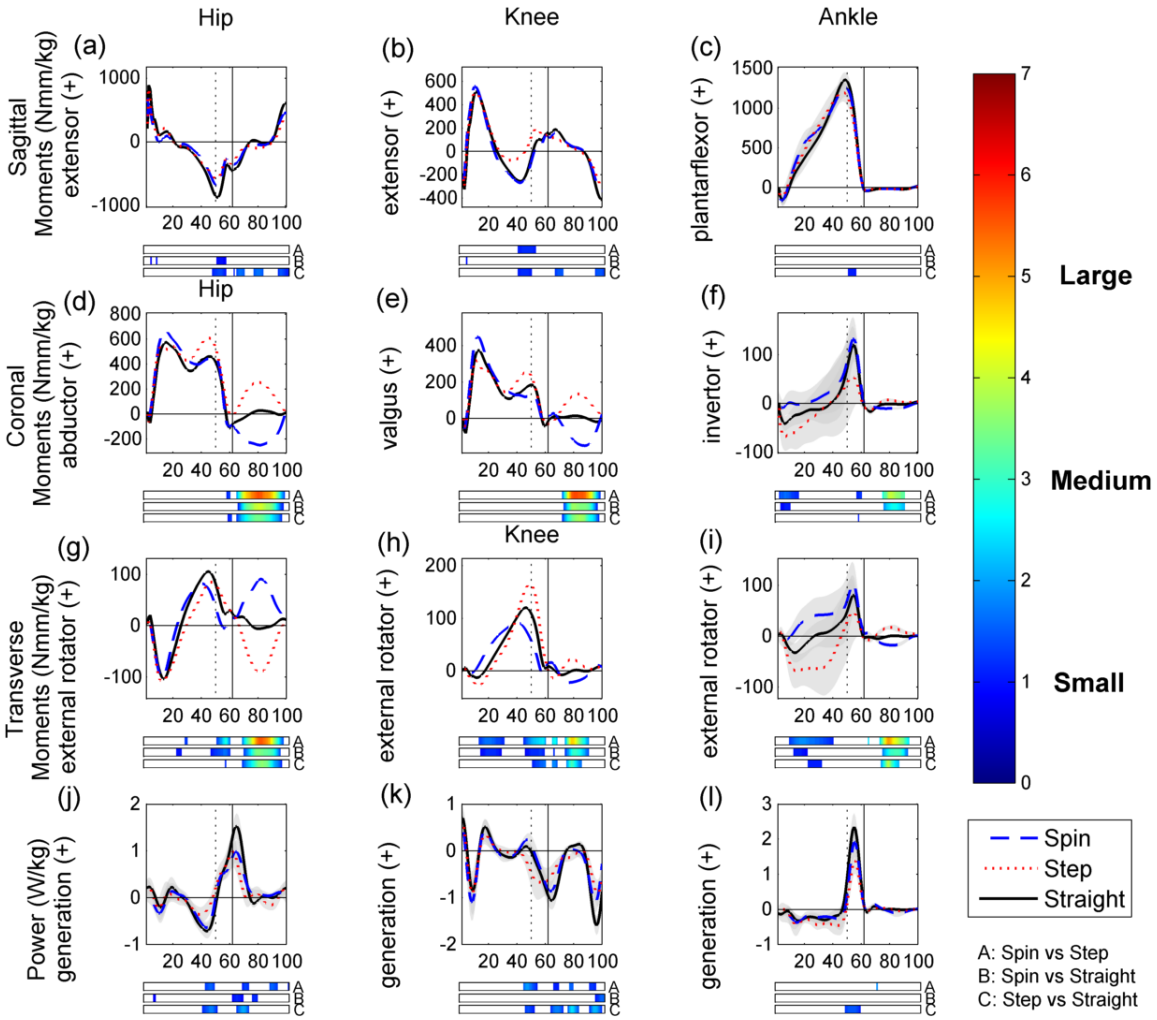

Figure 5.5 – Contralateral hip, knee, and ankle net internal joint moments and power for step, spin, and straight conditions with corresponding Bootstrap confidence bands (CBs) from 0–100% of the turning cycle. Dotted vertical lines indicate opposite foot-strike (FS3 at 50%) and solid vertical lines, transitions between swing and stance (FO2). Colourbars show where mean difference CBs reveal significant differences with intensity representing effect size from small (blue) to large (red).

tarflexor moment compared to straight walking (Fig. 5.5 a–c). Important changes were seen in the coronal plane. At the hip, step turns revealed large swing abductor moments, while spin turns showed large adductor moments. Similarly, for the knee, changes were found in swing with the step and spin turn showing valgus and varus moments, respectively. For the ankle, step turns increased evertor moments compared to spin, while spin turns decreased evertor moments compared to straight walking during loading (Fig. 5.5 d–f). The transverse plane of the hip showed major changes

in swing with step and spin turns producing internal and external rotator torques, respectively. For the knee, changes occurred near 50% of the turning cycle with step and spin turns producing increased and decreased external rotator moments, respectively, compared to straight walking. In swing, step turns required external rotator moments, while spin turns relied on internal rotator torques. The ankle showed differences during stance and swing between turning styles. Step turns started with an internal rotator moment (stance) followed by an external rotator moment (swing), while the trend was reversed for spin (Fig. 5.5 g–i).

Power differences were seen in all joints. At the hip, both turning styles decreased peak power generation. At the knee, zones of decreased power absorption were seen from FS4 onwards for the step turn, while spin showed reduced power absorption in terminal swing compared to straight walking. For the ankle, peak power generation was decreased for step turns compared to straight walking (Fig. 5.5 j–l).

5.4 Discussion

This study compared the kinetics of 90° turning gait and straight walking in TD children. Turning was found to require kinetic adaptations compared to straight walking, presumably to control kinematic changes previously observed with the goal of redirecting the COM towards the new walking direction. More specifically, it appears that TD children preposition their lower-limbs mainly via modification of swing limb non-sagittal moments. These changes modify joint kinematics, resulting in altered medio-lateral GRF and T_Z profiles. This study is the first to analyse kinetic changes for step and spin strategies for both limbs over the approach and turn steps. Moreover, this investigation provides the first reference database of turning gait kinetics in TD children.

5.4.1 Ground reaction forces

As hypothesized, F_{ML} was increased during turning. For step turns, F_{ML} was similar to values from Glaister et al. [88] for both the approach and turn steps. Results for the inside (contralateral step and ipsilateral spin) and outside (ipsilateral step and contralateral spin) limbs are similar to those of Segal et al. [200], but show a greater magnitude during the turn step, due to the more dynamic nature of 90° turning gait compared to circular walking. Changes in step turn F_{AP} are also in agreement with Glaister et al. [88]. Modulation in F_V were minimal, but might be related to decreases in velocity observed in Chapter 4. Thus, it appears that GRF adaptations during turning are strategy, rather than population (children vs adults), dependent.

5.4.2 Free vertical torque

As hypothesized, spin turns showed increased T_Z. A large T_Z does not appear to be the result of action by the stance limb or the contralateral trailing limb plantarflexors, but likely from contralateral hip activity, as suggested by large changes seen in hip kinetics during swing and electromyographic data from Hase and Stein [105]. T_Z also increased, but with a lesser magnitude for step turns (approach phase), suggesting that a small spin type manoeuvre is performed by the inside limb at this time.

5.4.3 Joint moments

In line with the third hypothesis, joint kinetics were mainly modified in the coronal and transverse planes. Previous investigations only analysed stance phase moments and thus it is not possible to compare the current findings for swing. Moreover, the spin turn results of Taylor et al. [226] are difficult to compare to the present findings as they divided spin turns into two-subcategories: the ipsilateral pivot and cross-over. There has been no such noticeable differentiation in children thus far. For the ankle

coronal plane, disagreements with previous work are likely due to the use herein of a more biomechanically accurate foot model (multi-segment OFM used here vs single segment foot Plug-in Gait implemented by Taylor et al. [226] and Xu et al. [251]). The noted changes in ankle moment are consistent with the kinematics from Chapter 4. Stance phase kinetics at the knee and hip are in general agreement with both Taylor et al. [226] and Xu et al. [251] and may be associated with the control of the COM during turning. In contrast, previous studies revealed increased hip abductor moments for spin turns in late stance of the turn step [226, 251], while here a trend towards a decreased moment was noted. This disagreement might be related to differences in COM position and/or pelvis orientation across populations during turning. Thus, although children and adults show similarities during turning, this study has highlighted areas where they may differ, possibly related to gait maturity.

The main joint kinetic changes during turning were found in swing phase and reveal the important role of the hip musculature. For spin turns, the inside limb is first moved away from the body's midline via a hip abductor moment during the first swing phase (Fig. 5.4 i) in preparation for the turn stance phase. During the turn stance phase, the outside limb must resist abduction caused by inertial forces and be brought back towards the body's midline via an adductor moment (Fig. 5.5 i), while preventing over-rotation of the limb through an external rotator moment (Fig. 5.5 l). Further inside limb hip abductor and internal rotator moments provide control and enable correct foot placement for exiting the turn during the second swing phase (Fig. 5.4 i and l). For step turns, seemingly opposite action is taken; however, a common motor control strategy becomes clear from the viewpoint of the inside or outside limb (rather than turn type). The outside limb is brought towards the turning direction via an adductor moment during the first swing phase (Fig. 5.4 i). During the turn stance phase, the external rotator moment of the outside limb hip is reduced (Fig. 5.4 l) as the pelvis is rotating in the same direction towards the new walking

direction, possibly driven by the abducting moment of the inside hip (Fig. 5.5 i). Then during the second swing phase, the outside limb is brought back towards the body midline via an adductor moment (Fig. 5.4 i) while an external rotator moment further controls pre-positioning and over-rotation for the next stance phase (Fig. 5.4 l). Future studies using musculo-skeletal modelling could confirm the role of joint kinetics in modulating COM and lower-limb joint kinematics during turning gait.

5.4.4 Joint power

For straight walking, ankle power generation patterns are consistent with findings from previous multi-segment foot model studies [63, 147]. For turning, it was expected that peak ankle power generation would decrease. Only limited evidence for this was found for step turns, possibly revealing a passive "falling" strategy with a decreased need to propel the body forward [226]. For spin turns, although the ankle power was similar to the straight condition, it appears to have been used to assist turning and propel the body towards the new walking direction.

5.4.5 Clinical applications

Turning analysis is relevant in the clinical management of gait in children with CP, as these children often present with lower-limb joint instability, weakness, and contractures. Differences in COM path have already been identified in children with CP during turning [186] and further research could expose underlying problems that are attenuated during straight walking. Investigation of turning gait could also help improve classification in terms of severity of involvement, plan surgical interventions, and quantify rehabilitative outcomes.

5.4.6 Limitations and other considerations

The limitations of the Bootstrap method are described in Section 3.8.4; however, two points should be highlighted. First, the approach may become overly conservative over a large number of frames. For example, pilot work in which only the stance phase was analysed showed significant differences during that time [67] that, here, failed to meet the significance threshold as the variability band was further increased. Second, given the small sample for the step condition turn phase ($n < 20$), the Bootstrap sample may not have adequately represented its shape and spread.

In the current analysis, it was only possible to collect force plate data for the approach and turn steps. Future work should aim to acquire data over the entire turning cycle for each trial in order to better represent the entire turning task. Also, although seldom analysed in a clinical setting, transverse plane moments were presented given their relevance to turning gait. These moments were no more variable than their sagittal and coronal counterparts, but are more sensitive to computation methods [192]. Finally, analysis of trunk and upper limb biomechanics may also provide relevant insight, especially in clinical populations, but were not analysed herein.

5.4.7 Conclusion

Investigation of turning gait kinetics in TD children revealed the forces and moments responsible for the altered kinematics of Chapter 4; however, how muscle activation patterns are modified to induce body reorientation via changes in net joint torques remains unclear. Although it is difficult to acquire muscle activation data for the numerous muscles crossing the lower-limb joints, simulation approaches using dynamic musculo-skeletal models show considerable promise [56]. Moreover, it is unknown how children with CP alter both kinematic and kinetic patterns to successfully turn. These aspects of turning gait warrant further investigation.

Chapter 6

Turning Gait in Children with Cerebral Palsy

Part I Kinematics

Investigation of standard measures during turning gait in typically developing (TD) children in Chapters 4 and 5 suggests that 90° turns while walking induce substantial kinematic and kinetic adaptations compared to straight walking. It remains unclear if children with cerebral palsy (CP) show similar adaptations. This chapter explores kinematic measures that may be useful in the analysis of turning gait for both clinical and research purposes. Kinematic measures are compared and contrasted across conditions and groups in order to understand the interaction between turning tasks and the complex gait deviations present in children with CP.

6.1 Introduction

Turning gait requires adaptations compared to straight walking in many populations [68, 81, 200, 207, 226] and is a crucial component of activities of daily living [87, 199]. Unfortunately, little is known about how children with CP adapt to the biomechanical requirements of this complex locomotor task [27, 186].

It has been suggested that children with CP modify spatio-temporal parameters (STPs) of gait during turning in an attempt to increase stability [27]. In fact, recent studies have shown that children with CP take a longer path and time to complete 90° turning manoeuvres [186] and that they also require an increased stance time to complete 180° turning tasks, compared to their TD peers [27]; however, in these studies, stability was not assessed directly. In children with CP, reduced stability during straight walking has been noted in work by Hsue et al. [117, 118] via centre of mass (COM) and centre of pressure (COP) quantities (position, velocity, and acceleration). Unfortunately, these measures have not been validated for use as stability metrics during walking. More recently, Bruijn et al. [31] showed that children with CP walk with reduced dynamic stability as measured via the Foot Placement Estimator. This method, based on conservation of angular momentum, has been validated, but requires the use of a full body marker set [30]. A review of stability measures suggested that the extrapolated COM (xCOM) concept of Hof [111], which takes into account the velocity of the COM to determine a margin of stability (MOS) during dynamic situations, represents a worthy alternative to more complex measures, such as the Foot Placement Estimator [30]. This approach has been validated and has the advantage of not explicitly requiring a full body marker set or an instrumented force plate, making it popular in dynamic stability studies [17, 32, 99, 153].

Pathological motion can often be distinguished from healthy movement patterns by a lack of fluency. Qualitative assessment of fluency is often made in rehabilitation con-

texts [193], but quantitative reports are more rare. Recent work by Kerr et al. [133] explored three metrics believed to quantify fluency. During a sit-to-walk task, hesitation, co-ordination, and smoothness were able to distinguish between young and older adults. Of these measures, hesitation, defined as the drop in the forward velocity during the movement [148] might be adaptable to the turning situation. It is plausible that a larger velocity drop (V_{DROP}) might be associated with poor, or less fluent turning ability. Similarly, a competent turner might rotate the body towards the new direction of walking using a minimum number of steps. Measurement of body rotation during each turn step (θ_{TURN}) might therefore also provide insight.

Finally, standard lower-limb joint kinematic measures are often assessed in children with CP in order to guide clinical gait management choices. In gait interpretation sessions, clinicians often focus their attention on key discrete events, such as knee flexion at foot-strike (FS) or maximum dorsiflexion in stance [214]. It is then possible to determine if a given event falls within the expected range for TD children and if not, how far away from the normative average the event may lie. Although the discrete analysis approach has strong merits in this context, it has been argued in this thesis that analysis of the entire gait cycle provides richer information about gait adaptations. Of late, this approach has also become popular for the interpretation of clinical gait data via composite scores such as the Gait Variable Score (GVS) and Gait Profile Score (GPS) of Baker et al. [14]. These scores take into account the entire gait cycle, yet provide clinicians with a single number from which to draw conclusions about potential gait deviations. The original GPS of Baker et al. [14] is based on lower-limb parameters relevant to common gait pathologies exhibited by children with CP during straight walking, but others have expanded the concept to study, for example, trunk movement in children with CP [109]. GVS and GPS analogues for turning may be useful in summarizing data for interpretation and research purposes, but none have been proposed to date.

The majority of the metrics proposed above successfully identify pathology in children with CP during straight walking analysis. Therefore, changes to these same measures across groups would need to be different or disproportionately larger during turning gait, compared to straight walking, to warrant implementation in clinical practice. Consequently, the overall aim of this part of the thesis was to determine if STPs, MOS, fluency measures, and lower-limb joint kinematics could better identify gait deviations during turning gait compared to straight walking. Specifically, it was hypothesized that the following adaptations from normative data occur in an amplified or different manner during turning gait for children with CP, compared to straight walking: (1) for STPs, decreased stride velocity and stride length, as well as increased stance time and stride width [27, 186], (2) changes in MOS as in transtibial amputees [17], (3) for fluency measures, increased V_{DROP} based on similar adaptations in older adults during the sit-to-walk movement [133] and decreased θ_{TURN}, (4) for joint kinematic measures, greater deviations in both discrete and continuous measures.

Knowledge of turning gait adaptations represents an important step in the understanding of gait deviations in children with CP and can provide further insight into their real-world mobility difficulties. Importantly, the possibility that turning gait may amplify underlying deficiencies not revealed by straight walking analysis would strengthen the case for the use of this novel task during gait assessment of children with CP for both treatment planning and assessing outcomes.

6.2 Methods

6.2.1 Ethical considerations

All procedures were approved by the local ethics committee and all children provided informed assent/consent for inclusion in the study (see Section 3.1).

6.2.2 Patient group

Twenty-two ambulatory children with spastic diplegic CP, classified as levels 1 or 2 by the Gross Motor Function Classification System (GMFCS) [166], were recruited into this study and asked to perform turning gait tasks following their clinical gait analysis session at the Oxford Gait Laboratory (Table 6.1). Subject specific anthropometric data and clinical information were collected before the gait analysis session. Medical records were reviewed and history of gait interventions recorded.

The automatic algorithm of Sangeux et al. [188] was used to classify children in the CP group by gait pattern (details regarding gait patterns in children with CP can be found in Section 2.4.1). This algorithm assesses how different a given child's sagittal plane knee and ankle kinematics are compared to TD controls. Here, normative TD data were extracted from the dataset available in Schwartz et al. [194]. The index (I) quantifies the distance (in standard deviations) that a given child's kinematic curve is from the normative kinematic curve during 20–50% of the gait cycle.

$$I = \frac{1}{50 - 20 + 1} \sum_{t=20}^{50} \frac{k_i(t) - \overline{K}(t)}{\sigma(t)} \tag{6.1}$$

where t is the time as a percentage of gait cycle

k_i is the kinematic curve for the ith child

$\overline{K}$ is the mean of the normative kinematic curve

σ is the standard deviation of the normative kinematic curve

Once indices are obtained for the knee and ankle, the gait pattern can be classified (Table 6.2). Moreover, as suggested by Rodda et al. [184], if limbs show two different patterns, a child's gait is described as asymmetrical.

The results of the algorithm are demonstrated for a child from the CP group in Fig. 6.1. Overall, most children were classified as having an asymmetrical gait (17/22).

Table 6.1 – Anthropometrics and surgical history of all children in CP group

Subject	Sex	Age (years)	Mass (kg)	Height (cm)	Leg-length (cm)	GMFCS	Gait Pattern Left	Gait Pattern Right	Last Intervention (years)	Intervention details
C0635E	M	14	70.0	175.0	91.0	2	Mild	Mild	4.3	L gast lengthening
C0701E	F	12	44.0	145.0	78.0	2	Mild	N/C	-	-
C0716D	M	14	45.0	168.0	94.0	2	Jump	Mild	-	-
C0831D	M	16	72.0	178.5	95.3	1	Mild	Mild	1.0	R femoral de-rotation osteotomy R distal tibia osteotomy R+L hams and R+L gast lengthening
C0842E	M	16	58.0	118.0	60.0	2	Crouch	App Eq	0.5	R+L hams and R+L gast botox
C0850G	F	11	37.0	150.0	77.8	2	Jump	App Eq	2.5	R+L femoral de-rotation osteotomy R+L rectus femoris transfer R+L hams and L gast lengthening
C1090C	F	8	33.0	130.0	71.0	2	Jump	Mild	2.5	R gast lengthening
C1171B	M	9	26.0	135.5	71.0	2	Jump	N/C	2.5	R+L plantarflexor lengthening
C1215B	F	8	23.0	118.0	60.0	1	True Eq	Mild	0.7	L serial casting
C1268A	M	15	53.0	171.0	88.8	2	N/C	True Eq	-	-
C1270A	M	12	32.0	141.0	77.5	2	N/C	Mild	-	-
C1313A	F	10	32.0	150.0	83.0	2	Mild	Mild	-	-
C1314A	M	12	34.0	140.0	74.0	1	N/C	True Eq	unknown	R+L hams and gast botox
C1318A	M	9	28.0	134.0	68.0	1	Mild	True Eq	-	-
C1320A	F	18	50.0	148.0	77.0	2	True Eq	True Eq	8	R+L gast botox
C1393A	F	10	31.0	142.5	73.0	1	Jump	True Eq	$\leqslant 2$	R+L serial casting
C1423A	F	14	44.0	157.0	82.3	1	N/C	True Eq	1.8	R gast botox
C1424A	M	12	33.0	143.0	75.5	1	Mild	App Eq	1.0	R+L hams and gast botox
C1495A	M	11	32.0	146.0	77.0	2	Mild	True Eq	-	-
C1499A	M	16	59.5	174.0	92.5	1	Crouch	N/C	-	-
C1500A	M	14	44.8	171.0	86.8	1	N/C	Jump	-	-
N0258B	M	12	40.0	157.0	84.0	1	Mild	Mild	-	-

Anthropometric and clinical information for female (F) and male (M) children with CP. Main interventions: lengthening of right (R) and (L) hamstrings (hams) and gastronemius (gast) or Botulinum Toxin injections (botox). Gait patterns: true and apparent (App) Equinus (Eq), jump, crouch, mild, and non-classified (N/C). Gross Motor Classification System (GMFCS) level also shown.

Table 6.2 – Automatic gait classification algorithm

Index (I)	Ankle < -1	$-1 \leqslant$ Ankle $\leqslant 1$	Ankle > 1
Knee > 1	Jump	Apparent Equinus	Crouch
$-1 \leqslant$ Knee $\leqslant 1$	True Equinus	Mild	Not classified
Knee < -1	True Equinus	Not classified	Not classified

Source: Table 1 in [188].

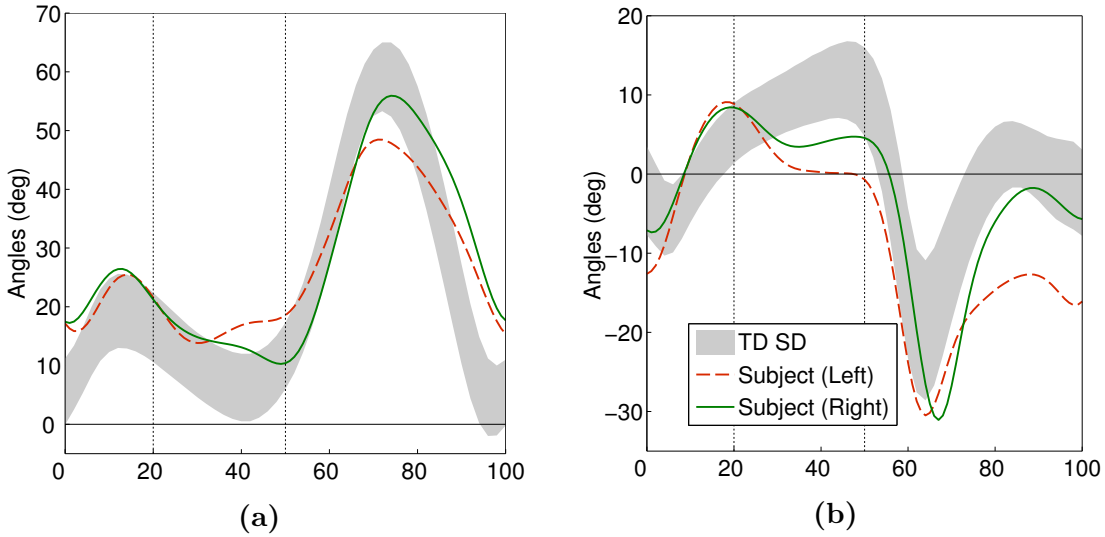

Figure 6.1 – Demonstration of the gait pattern classification algorithm [188] via (a) knee and (b) ankle kinematics over 100% of the gait cycle. For the left side, indices of 1.1 (knee) and -1.5 (ankle), results in a classification of "jump". The right is classified as "mild" given indices of 0.8 (knee) and -0.9 (ankle). Vertical dotted lines (20 and 50%) delimit the zone used to determine gait pattern. Grey bands represent ±1 standard deviation (SD) of the normative data for TD children from Schwartz et al. [194].

From the perspective of limbs, the algorithm revealed mild (16), true equinus (9), jump (6), apparent equinus (3), crouch (2) and non-classified (8) gait patterns.

6.2.3 Control group

Fifty-four TD children from the database were considered for this study. As in Chapter 4, turn style was analysed for each. For the remaining analyses, seven were excluded due to marker occlusions in the turning cycle and a further child with no spin data was removed. This group ($n = 46$) was significantly younger than the CP group

Table 6.3 – Summary of subject anthropometric data

Group	n	Age (years)	Weight (kg)	Height (cm)	Leg-length (cm)	Sex
TD-U	46	10.8 (2.8)*	39.9 (14.1)	147.8 (16.6)	78.0 (9.3)	22F, 24M
TD-M	44	11.0 (10.2–11.8)	40.7 (13.9)	149.1 (15.5)	78.8 (8.8)	21F, 23M
CP	22	12.4 (2.8)	41.9 (13.7)	149.7 (17.7)	79.0 (9.9)	8F, 14M

Mean (standard deviation) or median (95% confidence interval based on binomial distribution [86, pp. 26–31]) for normally or non-normally distributed anthropometrics, respectively, in the unmatched (TD-U), matched (TD-M), and CP groups. Sample size (n), sex (female (F) or male (M)), and significant difference from CP group ($*$) shown.

($p = 0.021$, unpaired t-test). Exclusion of children younger than seven years formed a control group ($n = 44$) matched for age ($p = 0.056$, Wilcoxon rank-sum test), mass ($p = 0.744$), height ($p = 0.889$), and leg-length ($p = 0.945$) (Table 6.3). See Table 3.1 for a list of the subjects analysed. The matched TD group was not normally distributed for age. Given the limited effect of maturation on gait in children older than six [221], no action was taken to remedy the skewness of the distribution.

6.2.4 Data collection

All subjects performed 90° step and spin turns to the left and right. The data collection protocol described in Section 3.3.3 was followed, except here for the CP group, the upper-body markers from the Plug-in Gait marker set were not used, in line with the clinical gait analysis procedures set by the Oxford Gait Laboratory.

6.2.5 Identification and prevalence of turning strategies

Turn style (step or spin) was identified as described in Section 3.4.3, but few children chose to perform step turns (Table 6.4). In the complete TD group, 43% of subjects only performed spin turns, 56% performed both step and spin, and only a single subject chose to solely perform step turns. The TD group performed 350 spin and 70

Table 6.4 – Frequency distribution of turn style preferences

Group	Step and Step	Spin only	Step only
TD-C	30/54	23/54	1/54
CP	12/22	10/22	0/22

Complete TD (TD-C) and CP group datasets.

step turns. For the CP group, a greater reliance on step turns was expected, but no child chose to solely perform step turns. The group performed 142 spin and 30 step turns with most (55%) subjects choosing both strategies and the remaining 45% only performing spin turns. These results are in agreement with work in older adults in which step turns only dominate under the fastest walking conditions [3]. It remains unclear if factors, such as speed, disability, or age, dictate the choice of strategy.

Although step and spin turns have been analysed as two distinct strategies herein and elsewhere [3, 105, 226, 251], it is likely that the two methods represent part of a continuum for a single turning paradigm. For the majority of spin turns and some step turns, the turn step is responsible for more than 45° of rotation. In other cases, this proportion is greatly reduced, i.e. the turn step is less dominant, making the categorization as either spin or step based on very small angular differences. This phenomenon occurs in both the TD and CP groups (Fig. 6.2). Nonetheless, as spin turns were identified as the main strategy used by both groups to perform unanticipated 90° turns, the step turn strategy is not analysed further in this chapter.

6.2.6 Spatio-temporal parameters

Stride velocity, stance time, stride length, and stride width, as described in Section 3.6.1 were used to define the temporal and spatial characteristics of gait during straight walking and the spin approach, turn, and depart phases.

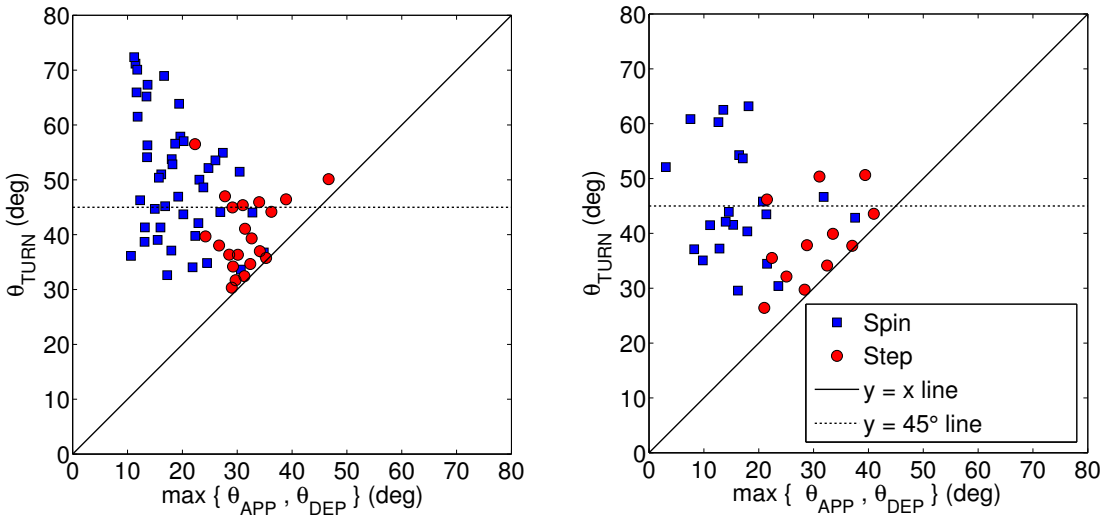

(a) (b)

Figure 6.2 – Distribution of turn angle by style for the (a) TD and (b) CP group. The y-axis shows rotation during the turn phase (θ_{TURN}), while the x-axis presents the larger of the approach (θ_{APP}) or the depart (θ_{DEP}) angle.

6.2.7 Dynamic stability measures

Theoretical considerations

As demonstrated in the review of Bruijn [30], the xCOM concept of Hof [112] is a valid measure for assessing dynamic stability in short range walking trials in which a full-body marker set is not available. A derivation of key quantities related to the xCOM is shown for the sagittal plane, but results can be extended to the medio-lateral orientation. First, Euler's second law of motion is applied to the inverted pendulum model of gait (Fig. 6.3) [112]:

$$\sum \tau = I\alpha \tag{6.2}$$

The torques on the left side of Eq. 6.2 are created by weight (mg) applied at a distance x and ground reaction force (R) at p_x:

$$Rp_x - mgx = I\alpha \tag{6.3}$$

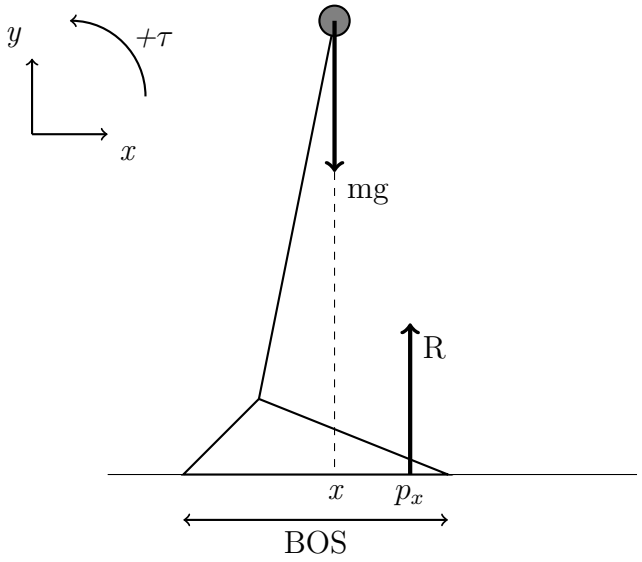

Figure 6.3 – Free body diagram of the inverted-pendulum model of gait. Weight (mg) and ground reaction force (R) vectors, as well as margins of the base of support (BOS), position of centre of pressure (p_x), and x-coordinate of mg vector shown.

For small movements, the linear acceleration along the x–axis can be approximated from α [241] for an inverted pendulum of length l_v as:

$$\alpha = \frac{-\ddot{x}}{l_v} \tag{6.4}$$

In Eq. 6.4, the negative sign arises from the differentiation operations.

In humans, the parameter l_v can be estimated from body height h using the regression equations from Hensiger [107]:

$$l_v = 0.557h + 0.014 \tag{6.5}$$

Using the equation for the moment of inertia of a point mass m at the end of the massless rod of length l_v [100, pp. 295–300], the value of α from Eq. 6.4, and the approximation that the magnitudes of R and mg are equal in the inverted pendulum model, Eq. 6.3 can be rewritten as:

$$p_x - x = -\frac{l_v \ddot{x}}{g} \tag{6.6}$$

Introducing the parameter $\omega_0 = \sqrt{g/l_v}$, representing the eigenfrequency of a regular pendulum [112], Eq. 6.6 can be re-expressed as:

$$p_x - x = -\frac{\ddot{x}}{\omega_0^2} \tag{6.7}$$

The solution to the second order linear differential equation in Eq. 6.7 for initial position x_0 and initial velocity v_{0x} can be solved under the assumption of constant p_x (see Appendix A.2 for a full derivation):

$$x(t) = p_x + (x_0 - p_x)\cosh(\omega_0 t) + \frac{v_{0x}}{\omega_0}\sinh(\omega_0 t) \tag{6.8}$$

With the COM restricted to stay within the base of support (BOS) for all t, then $x(t) \leqslant p_x$ and:

$$(x_0 - p_x)\cosh(\omega_0 t) + \frac{v_{0x}}{\omega_0}\sinh(\omega_0 t) \leqslant 0 \tag{6.9}$$

$$(p_x - x_0) \geq \frac{v_{0x}}{\omega_0}\tanh(\omega_0 t) \tag{6.10}$$

For a positive t, tanh $\leqslant 1$, so Eq. 6.10 leads to:

$$x_0 + \frac{v_{0x}}{\omega_0} \leqslant p_x \tag{6.11}$$

The quantity on the left side of Eq. 6.11 is what is referred to by Hof [112] as the xCOM. As long as p_x can be altered via muscular activity in response to a perturbation, the condition for dynamic stability in Eq. 6.11 can be maintained. Otherwise, xCOM exceeds the rocker base and the inverted pendulum topples over. Of course falling can be avoided by taking a new step. For dynamic stability in the medio-lateral direction, the y-components of initial position (y_0), initial velocity (v_{0y}), and the COP (p_y) replace the quantities in Eq. 6.11:

$$y_0 + \frac{v_{0y}}{\omega_0} \leqslant p_y \tag{6.12}$$

Implementation

The position of the COM was estimated by the sacral marker since the COM position computed by the Plug-in Gait model is only available when the full marker set is implemented (CP children data collected with lower-limb model only). Regardless, the two estimates are similar (Fig. 6.4 a). Moreover, in practice, it is difficult to obtain the coordinates of p_x and p_y without a force plate. In lieu, foot markers can be used to define the extreme edge of the BOS [17, 85]. Here, the lateral edge of the BOS was defined by the distal fifth metatarsal (D5M) and lateral calcaneus (LCA) markers (Fig. 6.4 b). The medio-lateral MOS is defined from the medio-lateral xCOM of Eq. 6.12 and the markers of the BOS [112, Eq.A.2]:

$$MOS = \frac{(x_2 - x_1)(y_0 - y_1) - (y_2 - y_1)(x_0 - x_1)}{\sqrt{(x_2 - x_1)^2 + (y_2 - y_1)^2}} \tag{6.13}$$

where x_1 and y_1 are the horizontal coordinates of the D5M marker

x_2 and y_2 are the horizontal coordinates of the LCA marker

x_0 and y_0 are the horizontal coordinates of the xCOM

The distance between a point and a line is found by adding the absolute value to the numerator of Eq. 6.13; however, here the sign remains to differentiate between a medial and a lateral MOS, with respect to the BOS line. For the left foot, positive and negative values of MOS coincide with a medially and laterally positioned xCOM, respectively. Changing the sign of MOS values from Eq. 6.13 results in the same convention for the right foot. MOS minimum (MOS_{MIN}) and average (MOS_{AV}) during the single-limb support phase of straight walking as well as the approach, turn, and depart phase of the spin turn were evaluated. To aid interpretation of the MOS data, the medio-lateral distance between the COM and the BOS line was computed by plugging in the coordinates of the COM into x_0 and y_0 of Eq. 6.13. Minimum (COM_{MIN}) and average (COM_{MIN}) values were then evaluated.

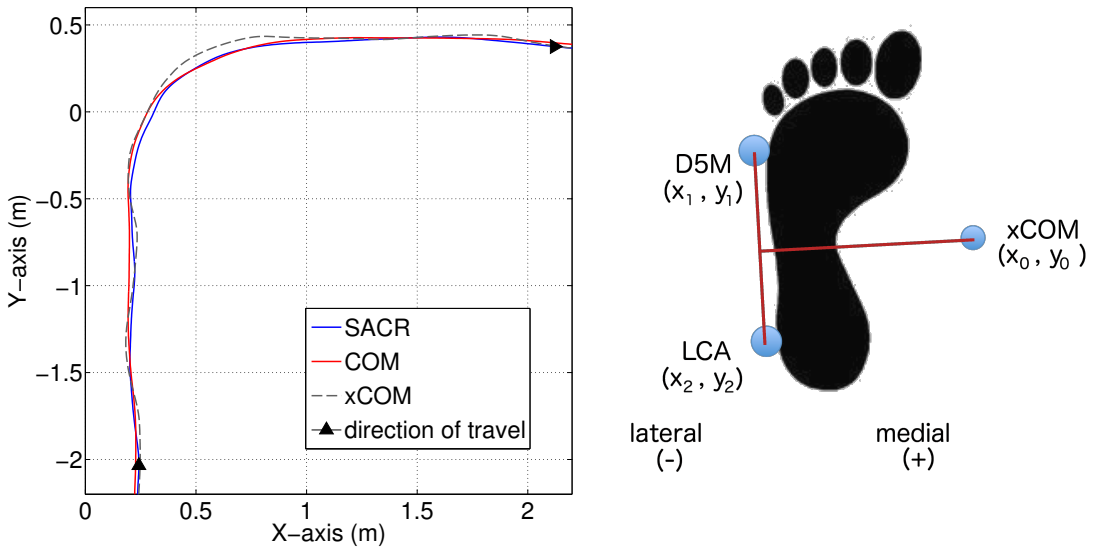

Figure 6.4 – Dynamic stability quantities: (a) sacrum (SACR), centre of mass (COM), and extrapolated COM (xCOM) position during a representative trial and (b) diagrammatic representation of medio-lateral margin of stability (MOS) defined as the distance between the D5M to LCA line and the xCOM.

6.2.8 Fluency measures

Fluency was explored via an assessment of two parameters. The estimate for V_{DROP} was derived from the magnitude of the tangential velocity of the sacral marker (in all three planes) during the stance phase:

$$V_{DROP} = max\{V\} - min\{V\} \tag{6.14}$$

The θ_{TURN} computation is the same used to determine turn style of Section 3.4.3. Both quantities were measured during the approach, turn, and depart phases of the turning gait trials. No equivalent measure was computed for straight walking.

6.2.9 Joint kinematics

The investigation of joint kinematics focused on the ipsilateral (turning) limb using two methods: a discrete approach in which specific points of interest in the gait cycle were identified and a continuous method reliant on curve analysis.

First, a discrete approach was implemented in which eight events (e) were identified starting at FS of the second step (turn step) in the turning cycle (Fig. 6.5): knee (KneeFS) and hindfoot with respect to tibia (HF/TB) (AnkleFS) angles as well as minimum knee flexion in terminal stance (KneeTS) and maximum HF/TB dorsiflexion (AnkleDF) were identified as variables of interest based on clinical relevance [214], while maximum hip adduction (HipAdd) and internal rotation (HipIntRot), HF/TB maximum eversion (AnkleEve), and forefoot with respect to hindfoot(FF/HF) maximum supination (FFootSup) were extracted based on known turning gait adaptations in TD children (see Chapter 4). As the directionality of changes in kinematics with respect to normative data may differ due to individual pathology (e.g. a child with crouch gait and a child with true equinus gait might show more and less dorsiflexion at the ankle, respectively compared to their TD peers), relative events (δe) were also computed as the absolute difference between each child's event value and the mean event value from the TD group for each condition:

$$\delta e = |e_i - \overline{E}| \tag{6.15}$$

where e_i is the event for the ith child

$\overline{E}$ is the mean normative event

Second, for the continuous analysis, the entire stance phase of the turning step (ipsilateral limb) was considered in an attempt to represent general turning adaptations (see Fig. 3.4). As in the evaluation of the GVS from Baker et al. [14], the root mean square (RMS) difference between a specific subject's joint kinematic curve and the mean normative curve was computed. The curves corresponding to the discrete events previously identified (Fig. 6.5) were selected for analysis, i.e. hip (coronal and transverse plane), knee (sagittal plane), HF/TB (sagittal and coronal plane), and FF/HF (coronal plane) angles.

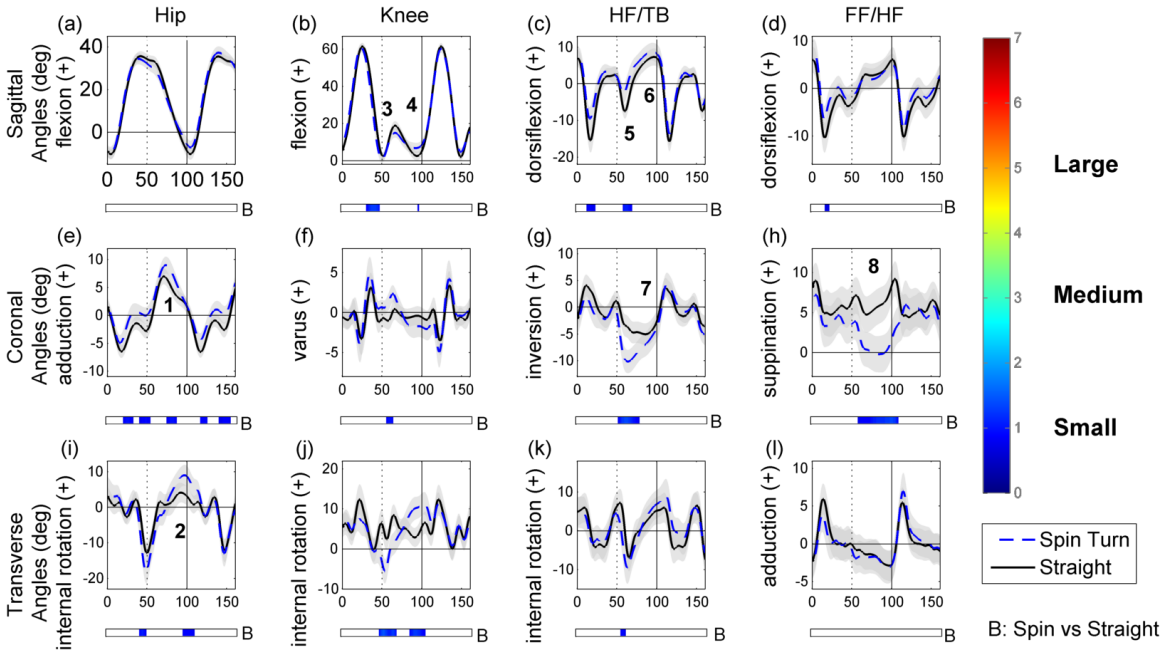

Figure 6.5 – Ipsilateral hip, knee, hindfoot with respect to tibia (HF/TB), and forefoot with respect to hindfoot (FF/HF) kinematics from the TD group for straight and spin conditions. Location of events: HipAdd (1), HipIntRot (2), KneeFS (3), KneeTS (4), AnkleFS (5), AnkleDF (6), AnkleEve (7), and FFootSup (8) also shown.

Each curve was used to define a Turning Variable Score (TVS) (TVS HipAdd, TVS HipRot, TVS KneeFlx, TVS AnkleDF, TVS AnkleEve, and TVS FFootSup):

$$TVS = \sqrt{\frac{\sum_{t=1}^{100}\left[k_i(t) - \overline{K}(t)\right]^2}{t}} \tag{6.16}$$

where t, k, and $\overline{K}$are as defined in Section 6.2.2, Eq. 6.1

Similar to the GPS of Baker et al. [14], the RMS average of all six TVS values was computed to form a single Turning Profile Score (TPS):

$$TPS = \sqrt{\frac{\sum_{s=1}^{6}(TVS_s)^2}{6}} \tag{6.17}$$

The TPS can be used to quantify turning gait adaptations in children with CP using a single overall measure of turning ability.

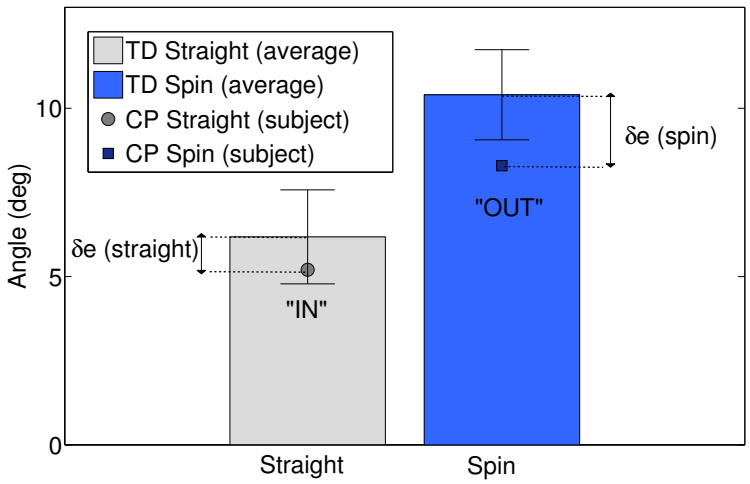

Figure 6.6 – Demonstration of subject-level analysis for a kinematic event variable. In this example, based on the normative confidence interval range, the subject is identified as having an abnormal kinematic pattern only during turning ("OUT"). Also, the difference between the subject data and the normative data increased during turning, compared to straight walking: δe (spin) $> \delta e$ (straight).

In addition to a statistical analysis of overall group adaptations to turning (see Section 6.2.11), results for joint kinematics (e, δe, TVS, and TPS) are presented for individual subjects. Again, this approach was deemed necessary as adaptations could differ based on specific pathology. For each e, the number of children with CP outside the 95% confidence interval range of the TD group was counted for each condition. These children were considered to exhibit abnormal kinematic patterns for the corresponding condition. Also, the number of children with CP with δe larger for spin turns, i.e. data relatively further from the TD group for turning, was tabulated. These two analyses are demonstrated in Fig. 6.6 for a single subject. The same methods were used for the analysis of TVS and TPS measures.

6.2.10 Normalization of gait metrics

Stride velocity and stance time were analysed using non-dimensionally normalized units as normalization has not shown to be beneficial in temporal parameters [64]. Other quantities (MOS_{MIN}, MOS_{AV}, COM_{MIN}, COM_{AV}, V_{DROP}, and θ_{TURN}) were

also analysed in non-normalized form in order to facilitate comparison to existing literature. Only stride length (SL) and stride width (SW) were non-dimensionally normalized using leg-length (LL) in accordance with Hof [110]:

$$||SL|| = \frac{SL}{LL} \tag{6.18}$$

$$||SW|| = \frac{SW}{LL} \tag{6.19}$$

6.2.11 Statistical analysis

Main statistical tests

For all dependent variables, an analysis of variance (ANOVA) was implemented to test for differences across the study factors (independent variables). For the STP and stability measures (stride velocity, stance time, stride length, stride width, MOS_{MIN}, MOS_{AV}, COM_{MIN}, and COM_{AV}), the model included the between-subject factor group (two levels: CP and TD) and within-subject factor condition (four levels: straight, spin approach, spin turn, and spin depart). Thus, a 2×4 mixed ANOVA was performed. For fluency (θ_{TURN} and V_{DROP}), 2×3 mixed ANOVAs were run since these metrics do not have straight walking analogues. Finally, for the kinematic measures (e, δe, TVS, and TPS), two conditions were explored (straight and turn phase of spin), thus 2×2 ANOVAs were run.

Analysis began with the interpretation of the group $\times$ condition interaction, based on the procedure described by Maxwell and Delany [151, pp.325–335] (Fig. 6.7). In the case of a significant two-way interaction, simple main effect tests for group, i.e. testing for differences at each level of condition across groups (e.g. CP Spin Approach vs TD Spin Approach), were performed. In the case of a non-significant two-way interaction, the main effect for group, i.e. differences across groups with all conditions pooled, was investigated. For the condition factor, main (comparison of conditions with groups

pooled) and simple main (comparison of conditions within a group) effects were not explored as those tests did not directly answer hypotheses relevant to this study.

Assumptions and other considerations

Prior to performing statistical analyses, a number of parametric assumptions were assessed in order to guide the choice of appropriate procedures.

For the main two-way ANOVAs with more than two within-subject variables, Sphericity, i.e. homogeneity of variance in population differences across within-subject factors, was estimated using Mauchley's test prior to interpretation of the interaction effect. If heterogeneity was suspected, the Greenhouse-Geisser corrected p-value was reported, otherwise, the uncorrected p-value was used. Deviations from normality were not tested during the ANOVAs as the design is robust against departures from normality [134, p.83].

For the simple main effect tests, normality and homogeneity of error variance across data pairs were assessed. Normality was tested via Q-Q plot visualization and supported by a conservative Lilliefors test (set at $\alpha_{LIL} = 0.01$ to guard against Type I error), while homogeneity of error variance was verified using Levene's test. Any paired grouping having failed Levene's test or in which at least one of the two groups showed deviations from normality were analysed using the Wilcoxon rank-sum test, otherwise unpaired t-tests were performed [134, p.345].

Standardized effect size, Cohen's d (d) under parametric assumptions and Glass's delta (Δ) otherwise (see Section 3.8.2), were computed for pairwise comparisons of groups in order to determine the strength of statistical inferences [220]. No corrections were made to the ANOVA group main effect values to attempt to control experiment-wise error rates for the reasons outlined by Feise [75] (see Section 4.2.4). In the case of the follow-up simple main effect tests, a Bonferroni correction was applied (see

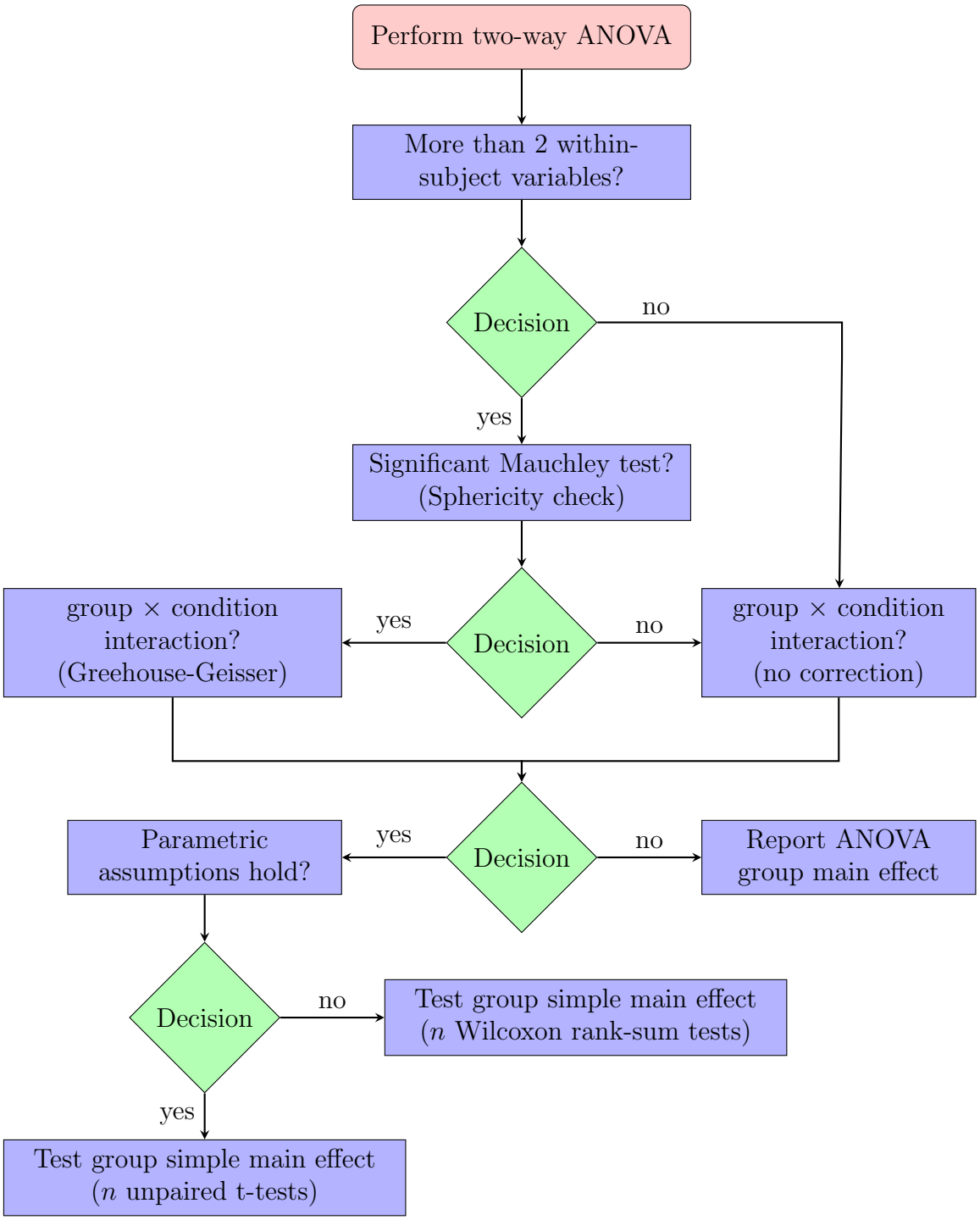

Figure 6.7 – Statistical process decision making flow chart. The number of tests used to assess the simple main effect of group depends on the number of conditions n for a given independant variable. See Section 6.2.11 for more details. Source: Figure 8.2 (modified and adapted) in [151].

Section 3.7.1) based on the total number of planned comparisons ($n = 4$ in the case of the STPs and dynamic stability and $n = 3$ for the fluency measures). This approach controls Type I error rates, without being too restrictive (considering all pairwise comparisons would be overly conservative) and allows for greater confidence in the reported significant differences. The correction procedure can lead to situations in which a significant interaction does not produce any significant simple group effects. In these cases, trends are reported. Instead of adjusting the α level, reported p-values were multiplied by n and assessed against the standard $\alpha = 0.05$ level.

All tests were performed at the $\alpha = 0.05$ level, unless otherwise stated. ANOVA procedures and Mauchley's test were implemented in SPSS (v21, IBM Corp., Armonk, USA). All other statistical analyses were performed in Matlab (v2012b, The Mathworks Inc., Natick, USA). Bar graphs show means and confidence intervals.

6.3 Results

6.3.1 Spatio-temporal parameters

All STPs required the Greenhouse-Geisser correction to the group × condition interaction p-value based on a significant Mauchley's test ($p < 0.001$).

The temporal parameters of stride velocity and stance time revealed no significant group × condition interactions ($p = 0.233$ and $p = 0.377$, respectively). A significant group main effect revealed that the CP group consistently reduced their stride velocity across all conditions, compared to their TD peers ($p < 0.001$) (Fig. 6.8 a). For stance time, the follow-up main effect for group was also non-significant ($p = 0.130$), suggesting that this metric was unaffected by the explored factors (Fig. 6.8 b).

Significant group × condition interactions were found for the spatial parameters of stride length ($p = 0.002$) and stride width ($p < 0.001$). For stride length, subsequent

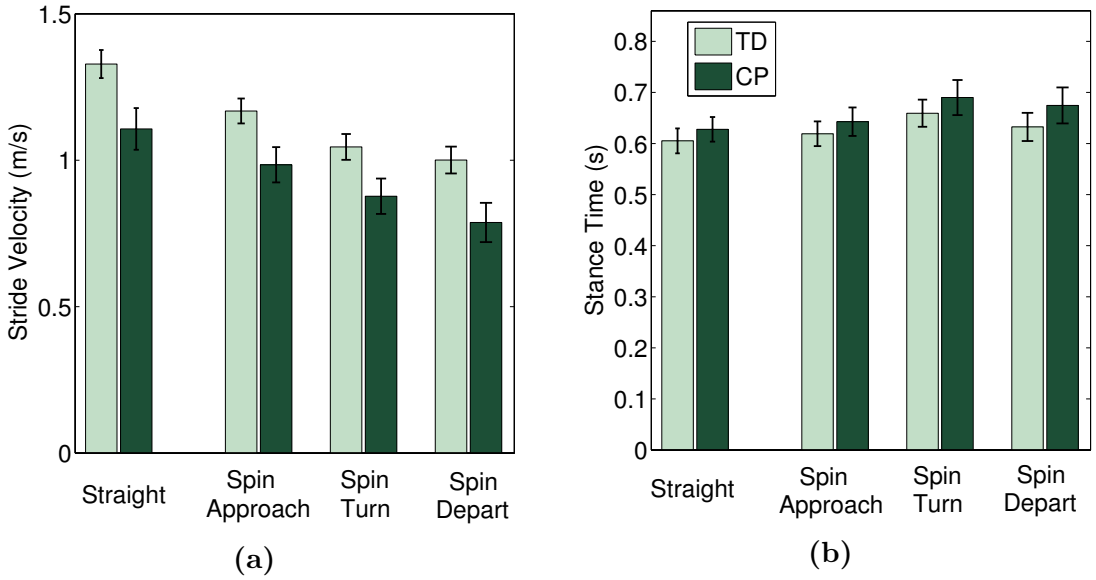

Figure 6.8 – Temporal parameters of (a) stride velocity and (b) stance time across group and condition.

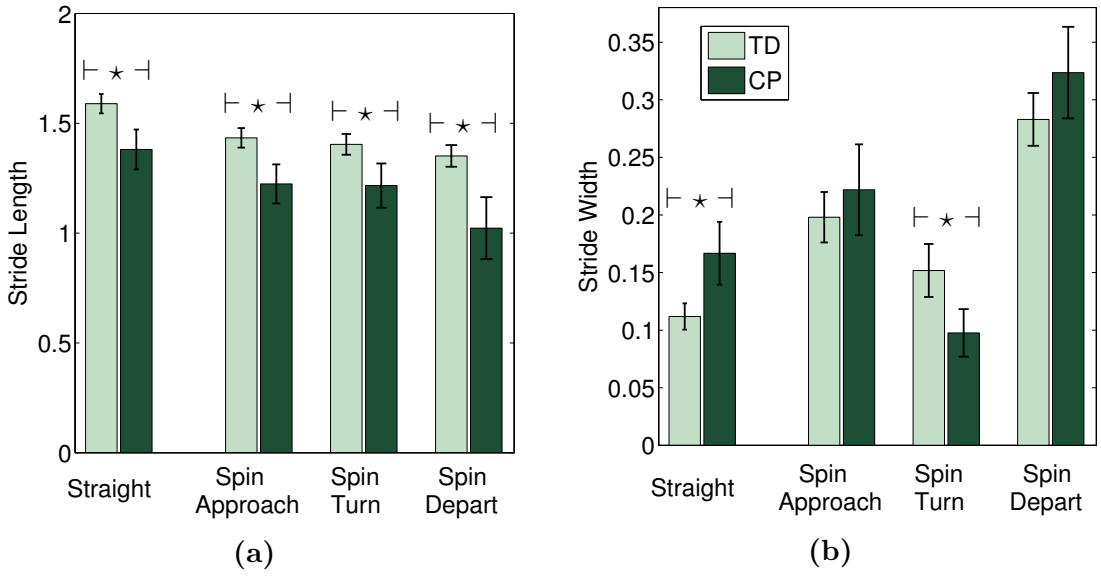

Figure 6.9 – Spatial parameters of (a) stride length and (b) stride width across group and condition. Significant group simple main effects ($\star$) shown.

testing of the simple main effect of group showed significant differences across all paired comparisons ($p \leqslant 0.001$). Effect sizes for the straight and spin approach conditions were similar ($d = 1.17$ and $d = 1.19$, respectively), but smaller for the turn ($d = 0.91$) and larger for the depart ($\Delta = 2.02$) phases (Fig. 6.9 a). For stride

width, simple main effect tests for group revealed an increase during straight walking ($p = 0.001$ and $\Delta = 1.46$), but decreased during the spin turn phase ($p = 0.003$ and $\Delta = 0.71$) for the CP group compared to the TD group (Fig. 6.9 b).

6.3.2 Dynamic stability measures

For the two-way ANOVAs of dynamic stability (MOS_{MIN} and MOS_{AV}) and related measures (COM_{MIN} and COM_{AV}), homogeneity of variance was not assumed via Mauchley's test ($p \leqslant 0.045$), leading to interpretation of Greenhouse-Geisser corrected group $\times$ condition interaction p-values.

For MOS_{MIN}, a significant group $\times$ condition interaction was identified ($p = 0.040$); however, after Bonferroni correction, no follow-up simple group main effect tests were significant. The depart phase showed a trend toward larger MOS_{MIN} for the CP group (Fig. 6.10 a). For MOS_{AV}, a significant group $\times$ condition interaction ($p = 0.020$) led to identification of decreased MOS_{AV} for the CP children compared to their TD peers during the approach phase of the turn via a simple main effect test ($p = 0.002$ and $d = 0.98$) (Fig. 6.10 b).

Both COM_{MIN} and COM_{AV} showed significant group $\times$ condition interaction effects ($p<0.001$ and $p = 0.002$, respectively). For COM_{MIN}, further analysis revealed that the COM was positioned more medially with respect to the BOS for children with CP compared to their TD peers during the spin turn phase ($p < 0.001$ and $d = 1.39$) (Fig. 6.11 a). For COM_{AV} simple main effect tests revealed a number of differences. During straight walking, the CP group showed a greater medially oriented COM with respect to the BOS ($p = 0.048$ and $\Delta = 1.03$), while during the turn ($p < 0.001$ and $\Delta = 1.56$) and depart ($p = 0.044$ and $\Delta = 1.56$) phases the COM was shifted less laterally, compared to the TD group (Fig. 6.11 b).

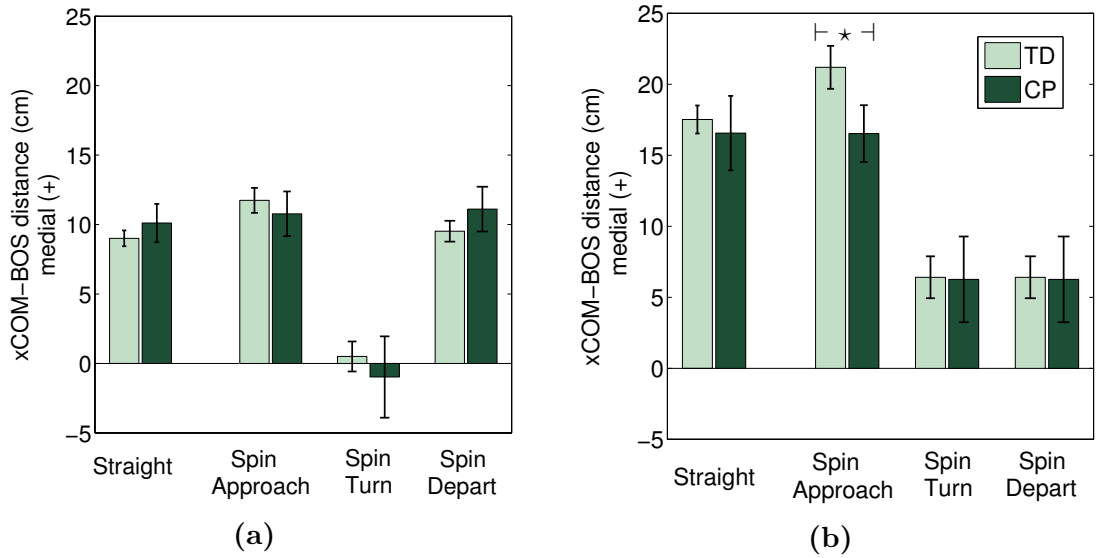

Figure 6.10 – Extrapolated centre of mass to base of support (xCOM-BOS) medio-lateral (a) minimum (MOS_{MIN}) and (b) average (MOS_{AV}) distance across group and condition. Significant group simple main effects ($\star$) shown.

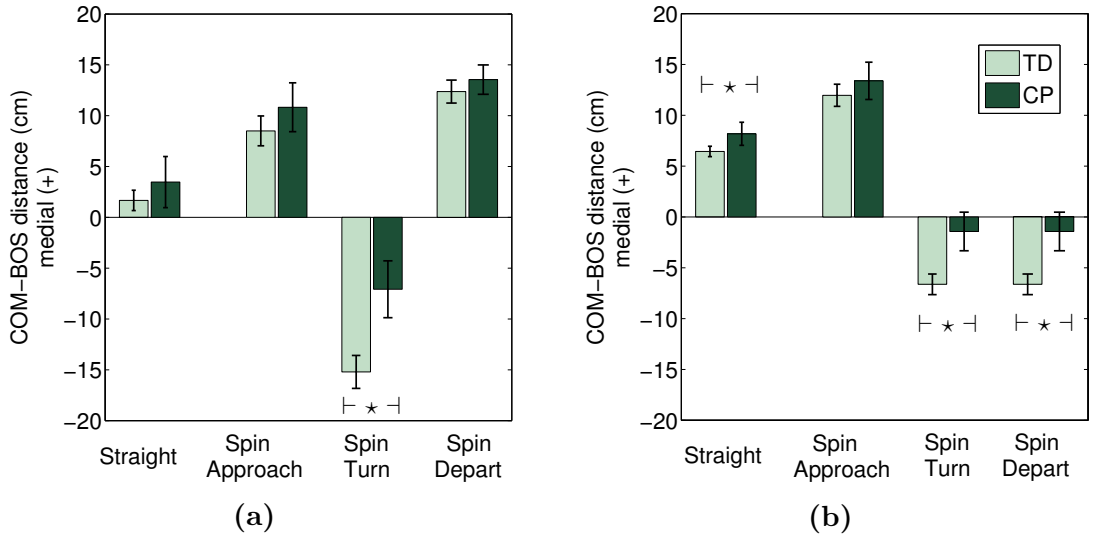

Figure 6.11 – Center of mass to base of support (COM-BOS) medio-lateral (a) minimum (COM_{MIN}) and (b) average (COM_{AV}) distance across group and condition. Significant group simple main effects ($\star$) shown.

6.3.3 Fluency measures

Both fluency measures required a Greenhouse-Geisser correction to the identified group $\times$ condition interaction p-values based on a significant Mauchley's test ($p = 0.031$ and $p = 0.001$ for θ_{TURN} and V_{DROP}, respectively).

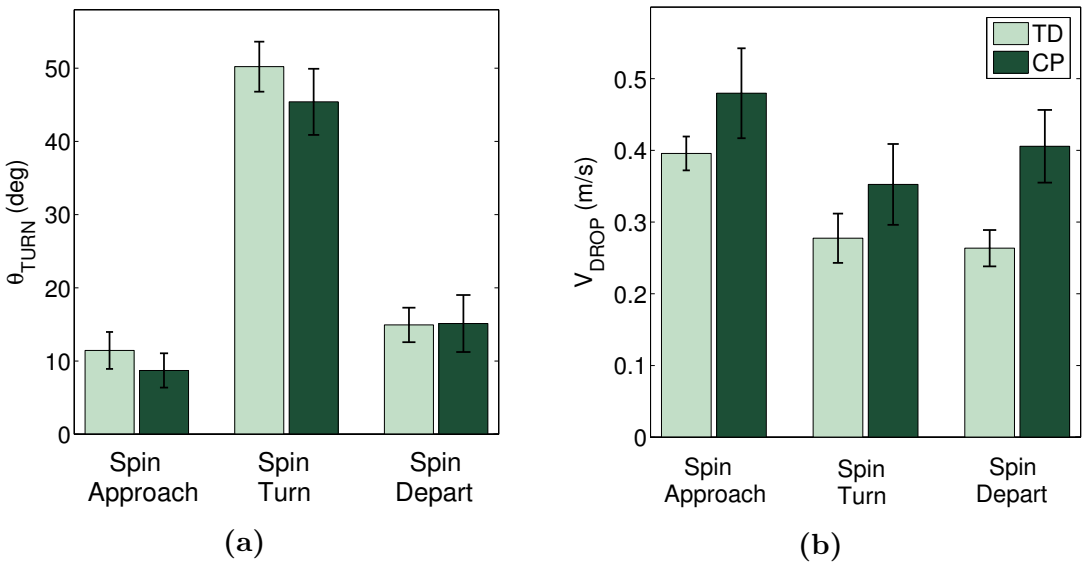

Figure 6.12 – Fluency measures of (a) turn angle (θ_{TURN}) and (b) velocity drop (V_{DROP}) across group and condition.

For θ_{TURN}, a non-significant two-way interaction ($p = 0.407$) was obtained, but a follow-up significant group main effect ($p = 0.008$) revealed a reduction in the CP group, regardless of turn phase (Fig. 6.12 a). For V_{DROP}, the interaction was also not significant ($p = 0.083$). Group main effect revealed an overall increase in V_{DROP} for the CP group, regardless of condition ($p < 0.001$) (Fig. 6.12 b).

6.3.4 Joint kinematics

Group-level analysis

Starting with the discrete events, no significant group × condition interactions were obtained ($p \geqslant 0.164$). Follow-up main effect tests for group were significant for 4 out of 8 kinematic measures (Fig. 6.13). Regardless of condition, HipIntRot ($p = 0.009$), KneeFS ($p < 0.001$), and KneeTS ($p = 0.014$) were found to be significantly increased for the CP group. AnkleFS changed polarity ($p = 0.017$), i.e. the TD group made contact with a slightly dorsiflexed ankle, while the CP group began the gait cycle with a plantarflexed ankle, again regardless of condition.

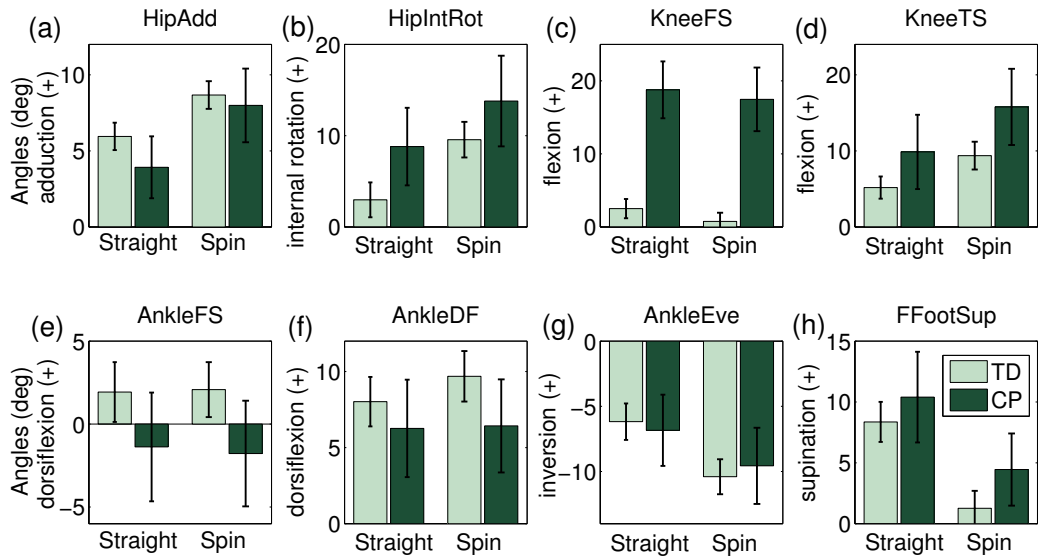

Figure 6.13 – Discrete kinematic events of (a) HipAdd, (b) HipIntRot, (c) KneeFS, (d) KneeTS, (e) AnkleFS, (f) AnkleDF, (g) AnkleEve, and (h) FFootSup across group and condition. See Section 6.2.9 and Fig. 6.5 for event description.

For the relative discrete events, only the δKneeTS group $\times$ condition interaction was significant ($p = 0.046$), suggesting that the CP group adapted differently to the turning condition than their TD peers. Follow-up simple main effect tests showed that although the CP group was unable to extend their knee as fully as the TD group during both straight ($p = 0.004$) and turning ($p = 0.020$) conditions, the difference across groups was larger for the straight condition ($\Delta = 1.82$ vs $\Delta = 1.49$ for the straight and turning conditions, respectively). Main group effect tests for the δHipAdd, δHipIntRot, δKneeFS, δAnkleFS, δFFootSup showed increased difference from the TD mean value regardless of condition for the CP group ($p < 0.030$).

For the TVS metrics, all group $\times$ condition interactions were found to be non-significant ($p \geqslant 0.438$); however, follow-up main effect tests showed significant increase in all measures for the CP group ($p < 0.014$) (Fig. 6.14).

For the overall TPS, group $\times$ condition interactions was non-significant ($p = 0.313$); however, the follow-up main effect test showed a significant increase in RMS difference for the CP group, regardless of condition ($p < 0.001$) (Fig. 6.15).

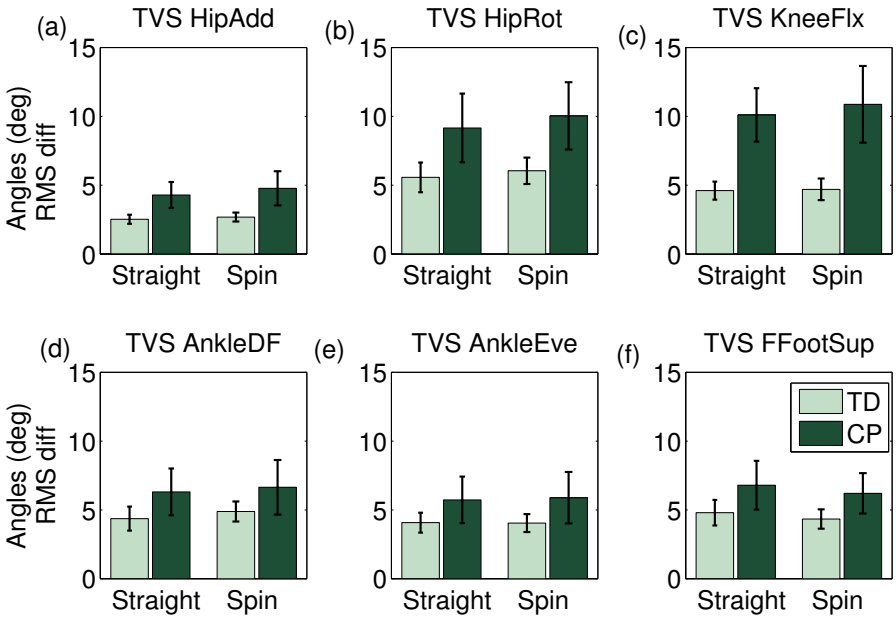

Figure 6.14 – Turning Variable Score (TVS) based on the root mean squared difference (RMS diff) for (a) HipAdd, (b) HipRot, (c) KneeFlx, (d) AnkleDF, (e) AnkleEve, and (f) FFootSup kinematics during ipsilateral turn stance phase across group and condition. See Section 6.2.9 for event description.

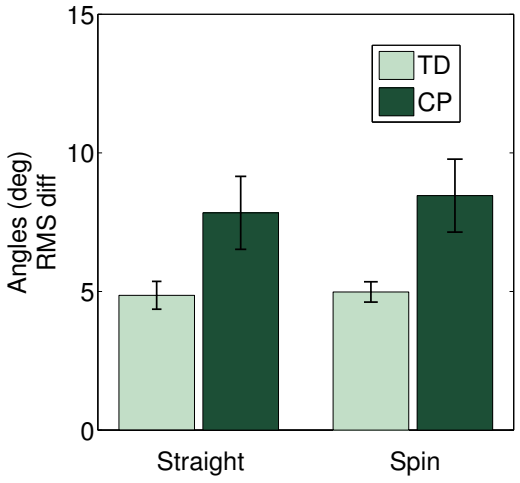

Figure 6.15 – Turning Profile Score based on root mean square difference (RMS diff) average of Turning Variable Scores across group and condition.

Subject-level analysis

Subject-specific analyses of discrete kinematic events revealed that more children in the CP group exhibited abnormal kinematic patterns for KneeFS, KneeTS, AnkleDF, AnkleEve, and FFootSup during turning than during straight walking based on the

Table 6.5 – Frequency distribution of abnormal discrete events for children with CP

Condition	Hip Add	Hip IntRot	Knee FS	Knee TS	Ankle FS	Ankle DF	Ankle Eve	FFoot Sup
Straight	17	19	20	18	19	18	16	18
Spin	17	19	**22**	**20**	17	**20**	**19**	**20**

Bold font where more children with CP were outside the TD range for turning. See Section 6.2.9 and Fig. 6.5 for event description.

range of normative data from the TD group (Table 6.5). For KneeFS, no child with CP was identified as being within the confidence interval range of the TD group for turning, but for straight walking 2 subjects (C1314A and N0258B) were not detected as having abnormal kinematics. In terminal stance (KneeTS), analysis of the straight walking data resulted in 4 children with CP (C1270A, C1313A, C1318A, and N0258B) appearing to have normal kinematics. Of these, only N0258B was not flagged as having abnormal kinematics during turning. None of the 4 children in the CP group (C0716D, C831D, C1215B, and C1499A) with AnkleDF within the TD confidence interval range for straight walking remained within the normative range for turning gait. Similarly, the children with normal kinematics for AnkleEve (C0635E, C0831D, C1090C, C1171B, C1215B) and FFootSup (C1171B, C1215B, C1270A, N0258B) were all identified as having gait deviations via turning gait analysis.

Analysis of relative events showed that deviation from normative data was increased in turning compared to straight walking in a number of children with CP (Fig. 6.16). The greatest increase was seen for δHipIntRot where 16 children with CP showed increased difference from normative data during turning. For δKneeFS, δKneeTS, and δAnkleFS, 13 children had a larger deviation during turning, while 12 were identified from δAnkleDF data. Finally, 10 children had increased difference from the normative data during turning for δHipAdd, δAnkleEve, and δFFootSup.

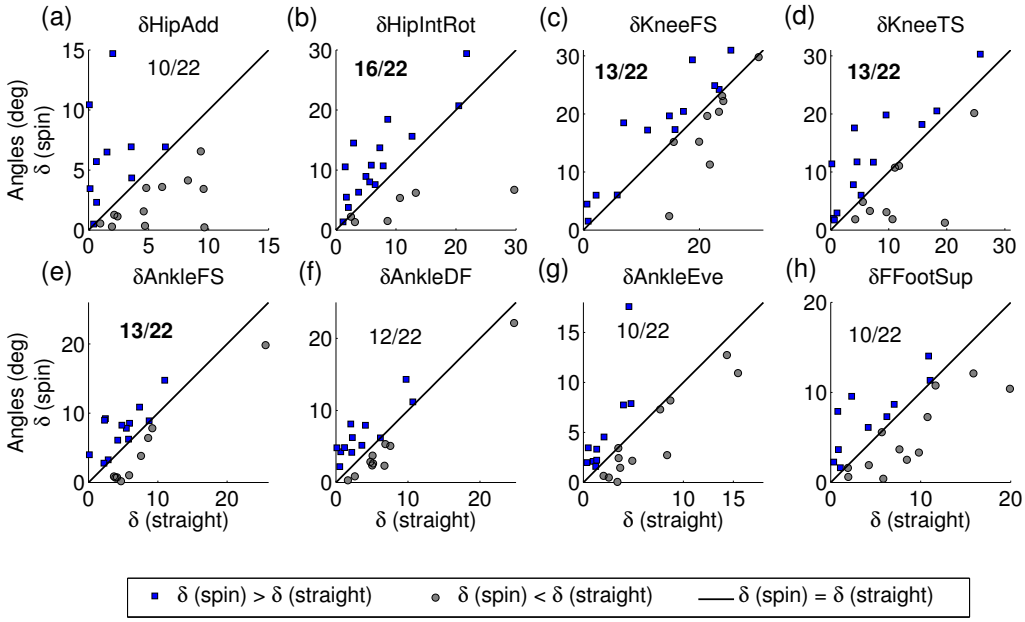

Figure 6.16 – Relative discrete kinematic events of (a) δHipAdd, (b) δHipIntRot, (c) δKneeFS, (d) δKneeTS, (e) δAnkleFS, (f) δAnkleDF, (g) δAnkleEve, and (h) δFFootSup across condition for each child with CP. Bold font for proportions where most children with CP increased difference from TD group for turning. See Section 6.2.9 for event description.

Table 6.6 – Frequency distribution of abnormal kinematic Turning Variable Scores and Turning Profile Score for children with CP

Condition	TVS HipAdd	TVS HipRot	TVS KneeFlx	TVS AnkleDF	TVS AnkleEve	TVS FFootSup	TPS
Straight	21	15	21	17	14	18	19
Spin	21	**17**	**22**	17	**18**	15	**20**

Bold font for Turning Variable Scores (TVS) and Turning Profile Score (TPS) where most children with CP were outside the TD range for turning. See Section 6.2.9 for event description.

For TVS, detection of abnormal gait patterns was improved in a number of cases. More children were identified as having abnormal kinematics during turning for TVS HipRot, TVS KneeFlx, and TVS AnkleEve (Table 6.6). For TVS HipRot, C0831D, C0842E, C1090C, C1215B, C1314A, C1318A, and N0258B were within the normal range for straight walking. Of these children, only N0258B also revealed a normal gait

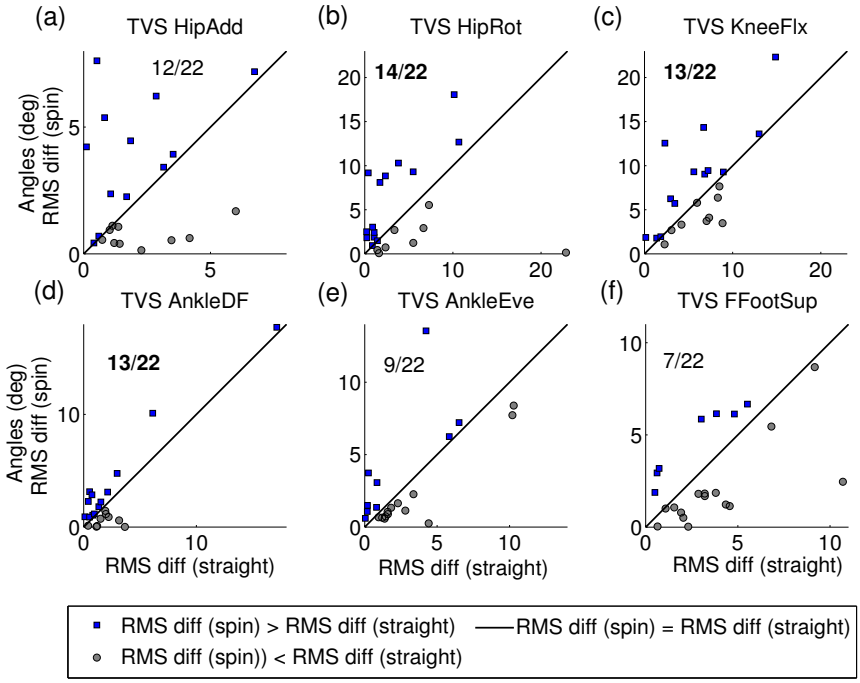

Figure 6.17 – Kinematic Turning Variable Score (TVS) for (a) HipAdd, (b) HipRot, (c) KneeFlx, (d) AnkleDF, (e) AnkleEve, and (f) FFootSup across condition for each child with CP. Bold font for proportions where most children with CP increased difference from TD group for turning. See Section 6.2.9 for event description.

pattern during turning gait. For TVS KneeFlx, C1314A was detected to have abnormal kinematics during turning, but not during straight walking. For TVS AnkleEve, many children (C0635E, C0716D, C0831D, C1171B, C1215B, C1313A, C1314A, and C1393A) showed normal kinematics during straight walking, with only C0635E and C1215B still considered to possess normal kinematics during turning.

The RMS difference during turning was increased for many subjects in each TVS parameter (Fig. 6.17). For TVS HipRot, 14 children showed increased difference from the normative data for turning, while for TVS KneeFlx and TVS AnkleDF, there were 13. For TVS HipAdd, TVS AnkleEve, and TVS FFootSup, 12, 9, and 7 children, respectively, showed greater variation from the norm during turning.

Analysis of the overall TPS metric showed that C0831D, C1314A, and C1423A were considered to have normal kinematics during straight walking. All showed abnormal

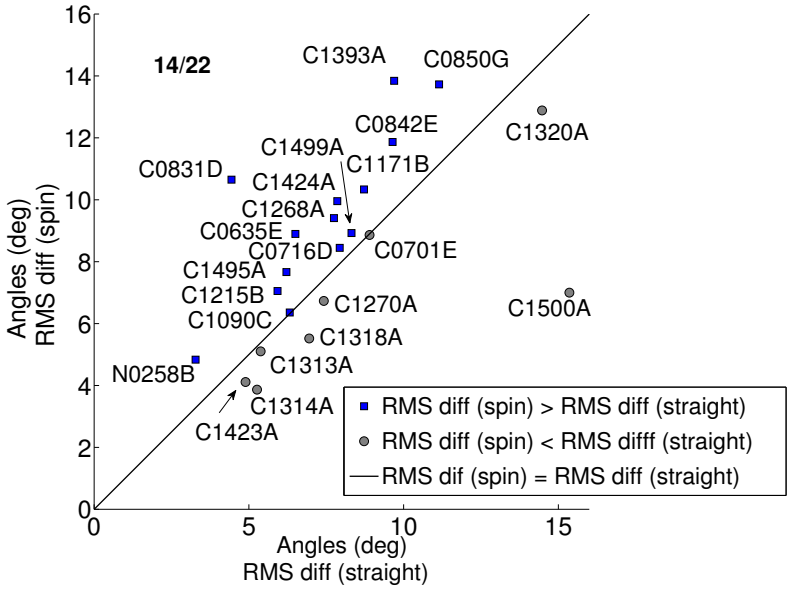

Figure 6.18 – Kinematic Turning Profile Score during straight and turning conditions for each child with CP. Bold font for proportion where most children with CP increased difference from TD group for turning. Subject codes also shown.

kinematics during turning gait (Table 6.6). Moreover, the difference from the normative data was increased for the turning condition in 14/22 subjects (Fig. 6.18).

6.4 Discussion

This study investigated kinematic measures during turning gait in children with CP. There were few overall group × condition differences across metrics, possibly due to the heterogeneity of the CP group. Subject specific analyses showed that for a number of metrics turning gait was a better discriminant of pathology than the standard straight walking protocol.

6.4.1 Spatio-temporal parameters

All STPs for straight walking in TD children were similar to normative data [146]. With regard to STP adaptations during turning in children with CP, not all hypotheses could be verified. The hypothesis for stride velocity could not be completely

confirmed. Although it was found that children with CP decreased their speed compared to the TD controls, they did so in a consistent fashion across both straight and turning gait conditions. Thus, the analysis of stride velocity during turning did not provide further insight, compared to the analysis of straight walking. For stance time, contrary to the stated hypothesis, no changes were seen across conditions or group. It appears that stance time is not a relevant parameter for the analysis of turning gait. Possibly, this metric may not be sensitive enough to capture changes related to stability issues during turning in children with CP. As hypothesized, the manner in which stride length and stride width were modulated across conditions and group was found to be different (significant group $\times$ condition interactions). The CP group reduced their stride length during all conditions; however, the reduction was most amplified during the depart phase (Fig. 6.9 a), suggesting that children with CP might experience difficulty transitioning back towards the straight walking gait pattern towards the end of the turning manoeuvre, possibly due to balance deficits or an excessive decrease in speed. Stride width results show that children with CP tend to approach the turn with a wider support base only to reduce their stride width during the turn, compared to their TD peers (Fig. 6.9 b). This strategy might improve stability in the early phase of the turn, but may lead to a risk of tripping as the feet are brought closer together as the turn progresses.

6.4.2 Dynamic stability

The MOS_{MIN} values during straight walking for the TD group were similar to those reported by others [17, 85], regardless of cohort age differences (adults vs children) and the choice of markers used to define the lateral BOS of the foot. For straight walking, stability has been shown to be compromised in CP children via the Foot Placement Estimator [31]; however, here MOS values were unable to detect any significant differences. Increased COM-BOS medio-lateral distance, in agreement with the work of

Hsue et al. [117]), and other kinematic changes resulted in the CP group exhibiting similar dynamic stability values to their TD peers for straight walking.

During turning, different strategies appear to have been implemented. For the approach phase, the CP group maintained a smaller MOS_{AV} than their TD peers, despite a larger COM-BOS distance (COM_{MIN}). This suggests that TD children take advantage of velocity to prepare for turning, while children with CP are more reliant on body orientation. After this initial manoeuvre, children with CP do not lean as far laterally as their TD peers. Possibly the early medial lean technique is implemented to avoid having to lean further laterally in the later phases of the turn, decreasing risk of falls. In the study of Romkes et al. [186], the COM remained within the BOS throughout the turn for most children with CP (9/13); however, turn style was not reported and details of specific gait deviations were not provided. Despite changes in COM position, both groups showed similar MOS in the final turning stages.

Also of interest is the large variability in MOS_{MIN} during the turn phase for children with CP. Likely, a variety of foot placements were implemented based on specific gait and balance limitations. Finally, although changes in MOS within turn phases was not statistically analysed (condition effect), the turn phase appears to be the most unstable portion of the turn.

Investigation of muscle and external force contributors to COM acceleration may provide further clues about how stability is maintained during turning gait.

6.4.3 Fluency

The use of θ_{TURN} and V_{DROP} to assess turning ability is novel, however, the latter measure has been used previously to quantify fluency in sit-to-walk tasks [133, 148]. Contrary to the stated hypotheses, θ_{TURN} decreased and V_{DROP} increased in a similar fashion, respectively, regardless of turn phase, in children with CP compared to

their TD peers (Fig. 6.12). Nonetheless, analysis of overall group differences in these metrics suggests that although children with CP were still able to successfully perform turning manoeuvres, their ability to rotate the body over the stance limb and maintain momentum was compromised. It is well known that walking at lower than optimal speeds results in increased energy expenditure [179]; however, it is likely that the CP group adopted this strategy regardless to maintain stability and avoid falls. Future work to identify specific deficiencies that lead to decreased turning fluency in children with CP is warranted.

6.4.4 Joint kinematics

The straight walking kinematics for the TD group were consistent with available normative data [194]. As hypothesized, both discrete and continuous parameters were able to discern differences across groups during turning that were masked in straight walking. For the discrete parameters, two approaches were taken. In the first, a dichotomous "in" or "out" state was ascribed to each event for a given child and condition based on whether the event value lay within or outside the TD normative range, respectively. In the second (δe analysis), the distance (in degrees) between a subject's event and the normative data determined whether a child's gait pattern was more dissimilar to the normative data during turning or straight walking. The two approaches appear to provide relevant information that could be used in clinical gait assessment. The parameters chosen were based on clinical observation [214] and past turning studies [68]; however, it is possible that other points of interest along the gait cycle might be explored. To remedy this situation, the continuous events (TVS and TPS) based on the RMS difference between subject and normative data over the entire stance phase were computed. These measures synthesize information from time dependant curve data into a set of values (TVS) or a single score (TPS) from which it is possible to quantify turning ability. As in the case of the discrete

events, it is possible to explore other joints during different parts of the turning cycle as well as to investigate the contralateral limb.

Several kinematic components investigated were able to distinguish children with CP from their TD peers. The kinematic adaptations seen in the CP group may have been implemented in order to reduce fall risk and ensure successful turning within existing biomechanical constraints. Therefore, attempting to normalize kinematic parameters towards TD values may not be warranted, rather monitoring of changes pre and post-intervention may be more appropriate. Future studies might explore why some children with CP stray further from the average data during turning, while others are more dissimilar to their TD peers only during straight walking.

6.4.5 Clinical applications

This study shows that for many children in the CP group turning gait has the ability to better discern and quantify gait deviations than straight walking. In cases where gait deviations are substantial, straight walking analysis often provides sufficient data to inform decision making; however, in children with milder gait deviations, as in the present cohort, turning analysis may be of added benefit. For example, if straight walking analysis reveals only minor differences compared to normative data, despite a child's reported difficulty in daily locomotor activities, turning protocols may be considered. Moreover, it may be that functional scores such as the GMFCS are more closely related to turning gait metrics as the task more closely approximates real-life situations. Including turning gait in clinical gait analysis sessions may therefore lead to the identification of abnormal patterns masked by traditional analysis and may better inform treatment options. Turning analysis could also be used to improve the assessment of treatment outcomes.

While measures such as stride length, stride width, MOS, and joint kinematic parameters were able to discriminate across group and condition, it is recommended that the choice of metric for turning gait assessment be based in part on the specific pathologies present in the child under investigation. From that perspective, all variables described in this study, while not possessing the ability to discern amplified or different adaptation in the entire cohort, could be used to guide treatment options, monitor progression in gait ability during pre and post-operative gait assessments, and provide better indication of treatment outcomes.

6.4.6 Limitations and other considerations

Four main limitations require further consideration. First, the children with CP in this study presented with mild gait deviations and consequently significant differences across groups and conditions were relatively small. Possibly, larger differences may be found in children with more severe involvement. Second, the gait classification algorithm identified 18 children with CP with different gait patterns for each limb (asymmetrical). These side differences may result in unique adaptations during left and right side turning gait manoeuvres; yet, sides were combined for analysis and a single representative trial was selected. The additional factor "side" was not investigated in order to avoid a complex three-way ANOVA design (effect of side would have to be identified via a three-way side $\times$ group $\times$ condition interaction) from which it would be difficult to extract significance given the sample size (and associated power). Thus, the current analysis may result in misleading findings for subjects with important asymmetries in their gait pattern. For example, for subject C1500A, a fourteen year old boy with a non-classified (left) and jump (right) gait pattern (Table 6.1), increased TPS difference from his TD peers was found in straight walking (right limb ipsilateral), but not during turning (left limb ipsilateral) (Fig. 6.18). These differences

are driven more by pathology (right side more affected with a large hip internal rotation angle) than by specific adaptations across conditions. For this child, as well as in other populations such as children with hemiplegic CP, the side factor should not be ignored. Therefore, it is recommended that the choice to investigate side differences could be determined based on clinical examination. Future work to identify specific muscular deficiencies and/or skeletal malalignment that lead to the adaptations described in this study is certainly warranted. Third, only the spin turn strategy was investigated as most children from both groups preferred to turn in this style. Analysis of step turn manoeuvres may reveal additional, or even contrary, information, but was not included. Using the normative kinematic data of Chapter 4, a similar analysis could be conducted for a child with CP unable to perform spin turns. Evolution from a step to spin turn strategy on its own may be a sign of improved mobility. Finally, fluency was only measured using one of the three measures (hesitation) proposed by Kerr et al. [133]. Coordination and smoothness may also provide a more complete picture of fluency, but may be difficult to implement in turning gait.

6.4.7 Conclusion

This study investigated kinematic variables across straight walking and turning conditions in children with CP and their TD peers, providing clinicians and researchers with relevant tools for the assessment of turning gait in this population. The exploration of other metrics, such as joint kinetics, could also provide further insights into the turning mechanisms used by children with CP and aid in clinical assessment.

Chapter 7

Turning Gait in Children with Cerebral Palsy

Part II Kinetics

The analysis of kinematic quantities during turning gait in children with cerebral palsy (CP) of Chapter 6 suggests that, for a number of kinematic parameters, children with CP adapt to turning in a unique way, compared to their typically developing (TD) peers; however, the causes of these changes remain unexplored. As kinematics are driven by net joint torques and external forces acting on the body, these quantities are investigated in the present chapter. Analyses performed are similar to those for the kinematics study of Chapter 6.

7.1 Introduction

Turning gait induces kinematic changes compared to straight walking that are driven by differences in joint kinetic and external force profiles in TD children (Chapter 4 and 5) as well as in healthy adults [88, 104, 219, 226, 251]. Moreover, children with CP reveal unique kinematic adaptations compared to their TD peers (Chapter 6), suggesting that kinetic changes might also be modified in unique ways. Possibly, the existence of pathological muscle activation patterns in children with CP may lead to even greater differences across tasks for kinetic quantities than for kinematics.

In Chapter 5, analyses focus on ground reaction forces (GRFs), free vertical torque (T_Z), joint moments, and joint power. These same parameters are explored herein. As with the kinematic analyses of Chapter 6, a combination of discrete and continuous methods in which the unique waveforms of each child with CP can be accounted may be relevant. For the GRF components, impulse over the entire stance phase can be computed [88]. This allows for an estimation of the overall effect of the GRF in accelerating the body centre of mass towards the new walking direction and can therefore reveal differences in turning technique. For T_Z, based on the TD analysis, the maximum value may reveal turning adaptations in the CP group. Finally, for the joint moments and power, as with the joint kinematic analyses of Section 6.2.9, both discrete events and continuous analyses resulting in summary scores, have merit. For the aforementioned kinetic quantities to be clinically relevant, it is imperative to show that changes during turning for children with CP result in better differentiation with respect to their TD peers than straight walking.

Therefore, the aims of this chapter were to determine if children with CP modify kinetic quantities in unique ways compared to both their TD peers and straight walking. Based on the kinematic changes observed in Chapter 6 and the results of studies in other populations it was hypothesized that for children with CP (1) GRF

impulse would be decreased in the medio-lateral and antero-posterior direction, (2) maximum T_Z would be decreased, and (3) joint kinetic quantities would show greater deviations in both discrete and continuous measures during turning gait compared to their TD peers and straight walking.

Knowledge of the kinetic quantities responsible for the kinematic changes observed during turning tasks can provide further insight into control mechanisms of gait and may lead to improved management of gait disorders in children with CP.

7.2 Methods

7.2.1 Ethical considerations

All procedures were approved by the local ethics committee and all children provided informed assent/consent for inclusion in the study (see Section 3.1).

7.2.2 Patient group

All twenty-two children with CP included in the kinematic analysis of Chapter 6 were considered for this investigation. Of these, four were excluded due to missing or incomplete force plate data (C0701E, C1215B, C1268A, and C1318A). Kinetic data were available for all eighteen remaining subjects during straight walking, but only for thirteen during the approach phase and fourteen during the turn phase of spin turns (Table 7.1). Subject-specific anthropometrics along with relevant clinical information can be found in Table 6.1, while group summaries are presented in Table 7.2.

7.2.3 Control group

Fifty-four TD children from the database were considered for this study. As in the kinetic study of Chapter 5, six were excluded due to marker occlusions or missing force

Table 7.1 – List of children with CP included in the kinetic analysis

Subject	Straight	Spin Approach	Spin Turn
C0635E	✓		✓
C0716D	✓	✓	
C0831D	✓	✓	
C0842E	✓		✓
C0850G	✓	✓	✓
C1090C	✓	✓	✓
C1171B	✓	✓	✓
C1270A	✓		
C1313A	✓	✓	
C1314A	✓	✓	✓
C1320A	✓	✓	✓
C1393A	✓	✓	✓
C1423A	✓		✓
C1424A	✓	✓	✓
C1495A	✓		✓
C1499A	✓	✓	✓
C1500A	✓	✓	✓
N0258B	✓	✓	✓

plate data (see Table 3.1 for the list of subjects analysed). The remaining unmatched TD group ($n = 48$) was significantly younger than the CP group ($p = 0.001$, unpaired t-test). Exclusion of those younger than seven and one randomly selected eight year old resulted in a TD control group matched for age, mass, height, and leg-length ($p \geqslant 0.057$), but non-normally distributed on these variables (Table 7.2).

7.2.4 Data collection and processing

The data were collected and processed as described in Sections 6.2.4 and 5.2.4, respectively. For the reasons outlined in Section 6.2.5, kinetic step turn data were not analysed. Due to the limitations of the experimental set-up, data for turning trials are only available during the approach and turn phase.

Table 7.2 – Summary of subject anthropometric data

Group	n	Age (years)	Weight (kg)	Height (cm)	Leg-length (cm)	Sex
TD Straight	41	11.3 (10.5–12.1)	42.5 (13.4)	151.3 (15.0)	80.4 (8.3)	18F, 23M
TD Spin (A)	34	11.5 (10.7–12.3)	43.1 (14.2)	152.3 (14.6)	80.8 (8.1)	15F, 19M
TD Spin (T)	32	11.2 (10.3–12.0)	41.8 (13.6)	150.2 (14.3)	79.7 (8.0)	13F, 19M
CP Straight	18	12.7 (11.4–14.1)	42.9 (13.8)	151.4 (16.8)	80.1 (9.3)	6F, 12M
CP Spin (A)	13	12.5 (11.0–13.9)	41.3 (13.0)	152.9 (15.6)	81.1 (8.8)	5F, 8M
CP Spin (T)	14	12.6 (11.2–14.1)	43.7 (14.2)	149.1 (16.6)	78.5 (9.3)	5F, 9M

Mean (standard deviation) or median (95% confidence interval based on binomial distribution [86, pp. 26–31]) for normally or non-normally distributed anthropometrics, respectively, in the TD and CP groups for straight walking along with the spin approach (A) and turn (T) phase. Sample size (n) and sex (female (F) and male (M)) shown.

7.2.5 Ground reaction force impulse

The impulse generated by a component of the GRF over a time interval [0, t] is defined as [100, p. 258]:

$$\mathbf{J} = \int_0^t \boldsymbol{GRF} dt \tag{7.1}$$

Given the discrete nature of the data collected, the definite integral in Eq. 7.1 was estimated via the trapezoidal rule using the function *trapz* in Matlab (v2012b, The Mathworks Inc., Natick, USA). Impulse was computed during the approach and turn phase for each GRF component. Impulse components are expressed in the turning coordinate system, as each was computed from the transformed GRF components (see Section 5.2.4). For the antero-posterior GRF, negative (J_{AP}^{-}) and positive (J_{AP}^{+}) impulses, associated with the posteriorly and anteriorly directed force, respectively, were computed. For the medio-lateral GRF, the total impulse (J_{ML}^{T}), representative of the net impulse in the medio-lateral direction, was evaluated. Finally, for the vertical GRF, the total positive impulse (J_{V}^{+}) was obtained. The GRF term in Eq. 7.1 was time normalized to 100% of the stance phase (%SP) and amplitude normalized by subject mass, leading to impulse with units of ($N \cdot \%SP/kg$).

7.2.6 Free vertical torque

T_Z was computed via Eq. 3.6.4 as described in Section 3.6.4. Maximum T_Z values near opposite foot-strike during the approach and turn phase were extracted.

7.2.7 Joint kinetics

As with the joint kinematic analysis of Section 6.2.9, joint kinetics were analysed for the ipsilateral limb using both discrete and continuous approaches.

For the discrete analysis, eight events (e) were identified (Fig. 7.1). Based on clinical experience [214], maximum (max) ankle plantarflexor moment (AnklePF), max ankle power (AnkleP) and max knee valgus moment (KneeVal) were extracted. Moreover, max knee external rotator moment in stance (KneeRot), max hip abductor moment in stance (HipAbdSt), max hip abductor moment during swing approach (HipAbdSwA), max hip abductor moment during swing depart (HipAbdSwD), and max hip internal rotator moment during swing depart (HipRot) were evaluated based on known differences across conditions in the TD group (see Section 5.3.3). As with the kinematic analysis of Section 6.2.9, relative events (δe) were computed via Eq. 6.2.9 to take into account differences in the directionality of changes across children with CP.

For the continuous analysis, a kinetic Turning Variable Score (kTVS) was computed for the ankle power as well as knee valgus, knee rotator, hip abductor, and hip rotator moment curves using Eq. 6.2.9. A kinetic Turning Profile Score (kTPS) was then computed via Eq. 6.17; however, the ankle power kTVS was not included to avoid averaging metrics with different units. For turning, kTVS and kTPS were evaluated during the turn stance phase only.

These joint kinetic metrics (e, δe, kTVS, and kTPS) were statistically analysed across groups (see Section 7.2.8), but also compared for individual subjects to account for

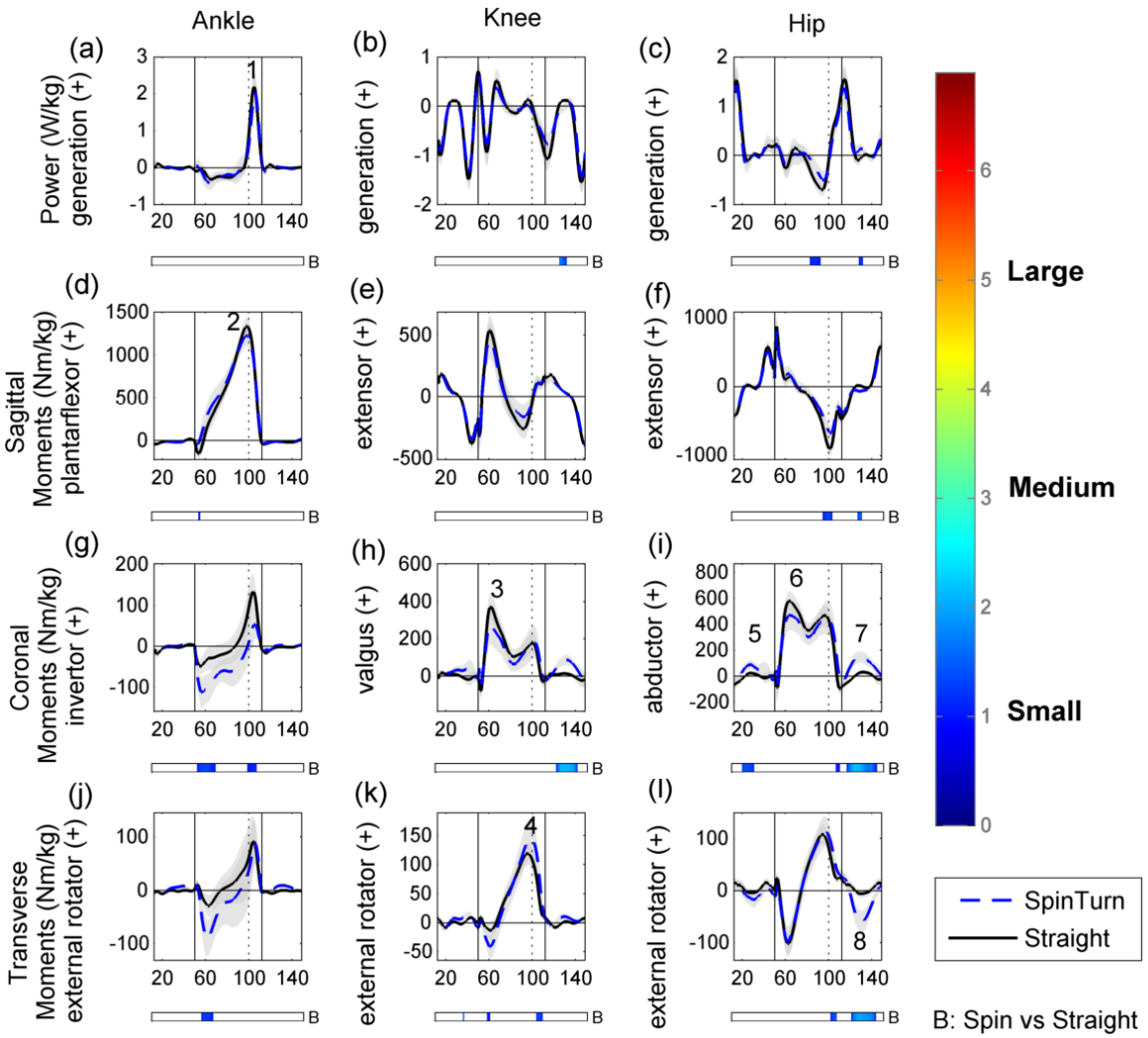

Figure 7.1 – Ipsilateral hip, knee, and hindfoot with respect to tibia (HF/TB) kinetics from the TD group for straight and spin conditions. Location of events: AnkleP (1), AnklePF (2), KneeVal (3), KneeRot (4), HipAbdSwA (5), HipAbdSt (6), HipAbdSwD (7), and HipRot (8) also shown.

different adaptations based on specific gait pathology in children with CP. For each event e, kTVS, and kTPS, the total number of children from the CP group outside the 95% confidence interval was recorded for each condition. It was assumed that these children demonstrated abnormal kinetic patterns. Also, the total number of children in the CP group with δe, kTVS, and kTPS larger during turning than straight walking was also recorded. A diagrammatic representation of these two analyses is shown for a kinematic parameter in Fig. 6.6.

7.2.8 Statistical analysis

Main statistical tests

For all kinetic variables, a mixed analysis of variance (ANOVA) with between-subject factor group (two levels: CP and TD) was conducted. For J^{-}_{AP}, J^{+}_{AP}, J^{T}_{ML}, J^{+}_{V}, and T_Z, the between-subject factor comprised two levels (straight and spin approach phase or straight and spin turn phase for the contralateral or ipsilateral limb, respectively). For e, δe, kTVS, and kTPS the between-subject factor also had two levels (straight and spin). Thus, for all dependant variables 2×2 ANOVAs were performed. All tests conducted were based on the flowchart of Section 6.2.11 (Fig. 6.7).

Assumptions and other considerations

Choice of a parametric (unpaired t-test) or non-parametric (Wilcoxon rank-sum test) approach was based on evaluation of assumptions in Section 6.2.11. A Bonferroni correction was applied by multiplying the group simple main effect p-values by the number of planned comparisons (two). Standardized effect size, Cohen's d (d) under parametric assumptions and Glass's delta (Δ) otherwise were computed (see Section 3.8.2). All tests were performed at the $\alpha = 0.05$ level, unless otherwise stated. All ANOVAs were implemented in SPSS (v21, IBM Corp., Armonk, USA), while other statistical analyses were performed in Matlab (v2012b, The Mathworks Inc., Natick, USA). Bar graphs show means and confidence intervals.

7.3 Results

7.3.1 Ground reaction force impulse

There were many significant findings across group and condition for the contralateral and ipsilateral impulse values during the approach and turn phase, respectively.

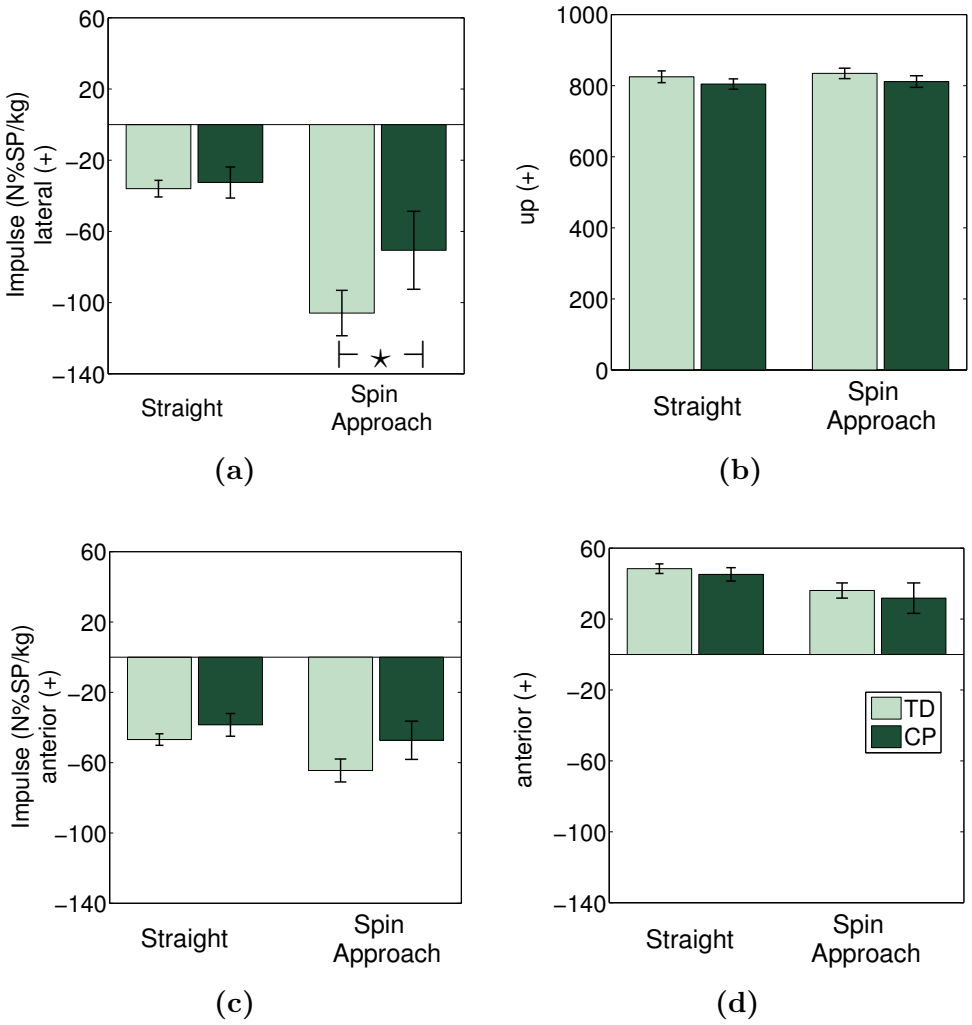

Figure 7.2 – Contralateral impulse over the stance phase (SP) for (a) medial-lateral, (b) vertical, (c) anterior (braking), and (d) posterior (propulsive) ground reaction force across group and condition. Significant group simple main effect ($\star$) shown.

For the contralateral limb, J^T_{ML} showed a significant group $\times$ condition interaction ($p = 0.002$). Group simple main effect tests showed that the CP group decreased J^T_{ML} medially only during the approach phase of turning, compared to their TD peers ($p = 0.010$ and $d = 0.96$) (Fig. 7.2 a). In the antero-posterior direction, no significant interaction effects were found (Fig. 7.2 c and d); however, J^-_{AP} analysis revealed that the CP group decreased their braking impulse regardless of condition compared to the TD group ($p = 0.020$). In the vertical direction, no significant interaction or group main effects were obtained (Fig. 7.2 b).

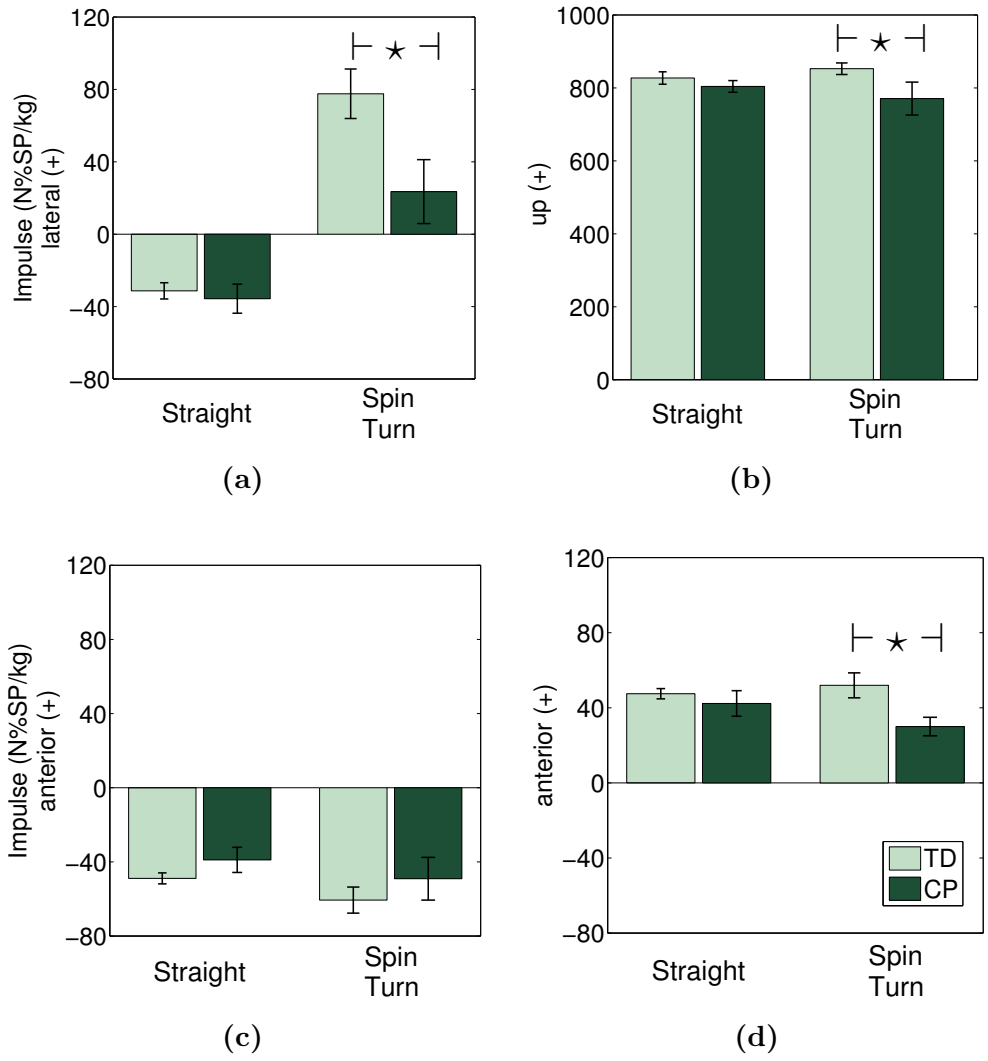

Figure 7.3 – Ipsilateral impulse over the stance phase (SP) for (a) medial-lateral, (b) vertical, (c) anterior (braking), and (d) posterior (propulsive) ground reaction force across group and condition. Significant group simple main effect ($\star$) shown.

For the ipsilateral limb, J^T_{ML} revealed a group $\times$ condition interaction ($p < 0.001$). Follow-up tests showed that J^T_{ML} was significantly reduced for the CP group during the spin turn phase compared to the TD group ($p < 0.001$, $d = 1.56$) (Fig. 7.3 a). In the antero-posterior direction, after a non-significant interaction result, J^-_{AP} was found to be consistently reduced for the CP group, regardless of condition ($p = 0.002$) (Fig. 7.3 c). For J^+_{AP} a significant group $\times$ condition interaction was obtained ($p = 0.010$). Follow-up group simple main effect tests showed that the CP group generated a smaller propulsive impulse than the TD group during the turn phase ($p = 0.001$,

$\Delta = 1.19$) (Fig. 7.3 d). Finally, J_V^+ revealed a significant group $\times$ condition interaction ($p = 0.005$), leading to a follow-up test highlighting that J_V^+ was decreased for the CP group during the turn phase ($p \leqslant 0.001$ and $d = 1.28$) (Fig. 7.3 b).

7.3.2 Free vertical torque

Non-significant group $\times$ condition interactions were obtained for T_Z of the contralateral and ipsilateral limb; however, significant group main effect tests showed that the CP group consistently reduced maximum T_Z compared to their TD peers ($p = 0.002$ and $p = 0.001$ for the contralateral and ipsilateral sides, respectively) (Fig. 7.4).

7.3.3 Joint kinetics

Group-level analysis

Evaluation of group-level discrete events revealed numerous differences. For KneeVal and HipAbdSwA, significant group $\times$ condition interactions were found ($p = 0.001$ and $p = 0.024$, respectively). Evaluation of paired differences showed that KneeVal was significantly larger for the TD group during straight walking ($p = 0.001$ and $d = 1.38$) (Fig. 7.5 c). For HipAbdSwA, simple main effect tests did not lead to significant differences after Bonferroni correction, but suggested a trend towards higher straight walking maximum hip abductor moment for the CP group (Fig. 7.5 e). For AnkleP, AnklePF, KneeRot, and HipAbdSwD, a lack of group $\times$ condition interaction led to the observation of significant group main effects. AnkleP, AnklePF, and KneeRot decreased ($p < 0.001$, 0.017, and 0.001, respectively), while HipAbdSwD increased ($p < 0.001$) for the CP group, compared to their TD peers, regardless of condition (Fig. 7.5 a, b, d, and g).

The relative discrete events showed significant group $\times$ condition interactions for δKneeRot ($p = 0.015$) and δHipRot ($p = 0.008$). For δKneeRot, the CP group was

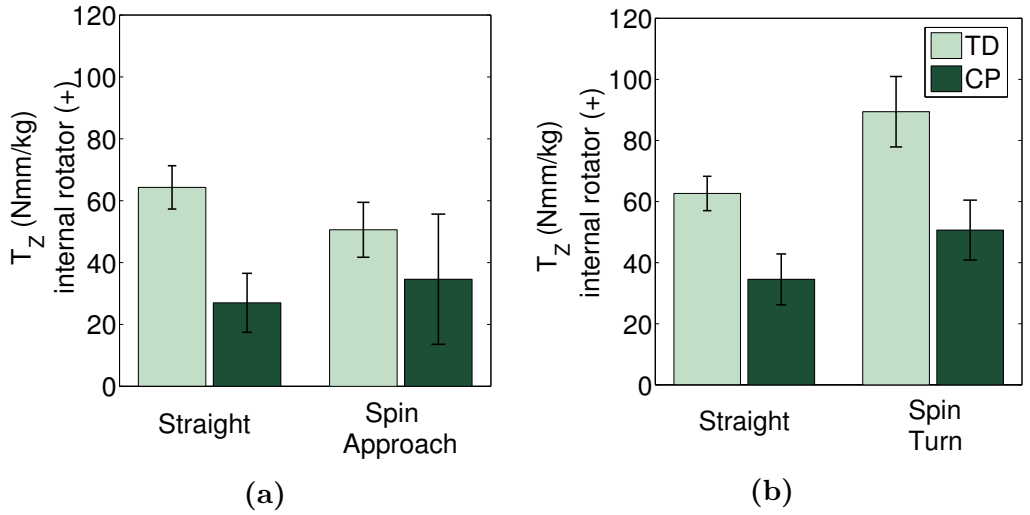

Figure 7.4 – Free vertical torque (T_Z) for the (a) contralateral and (b) ipsilateral limb.

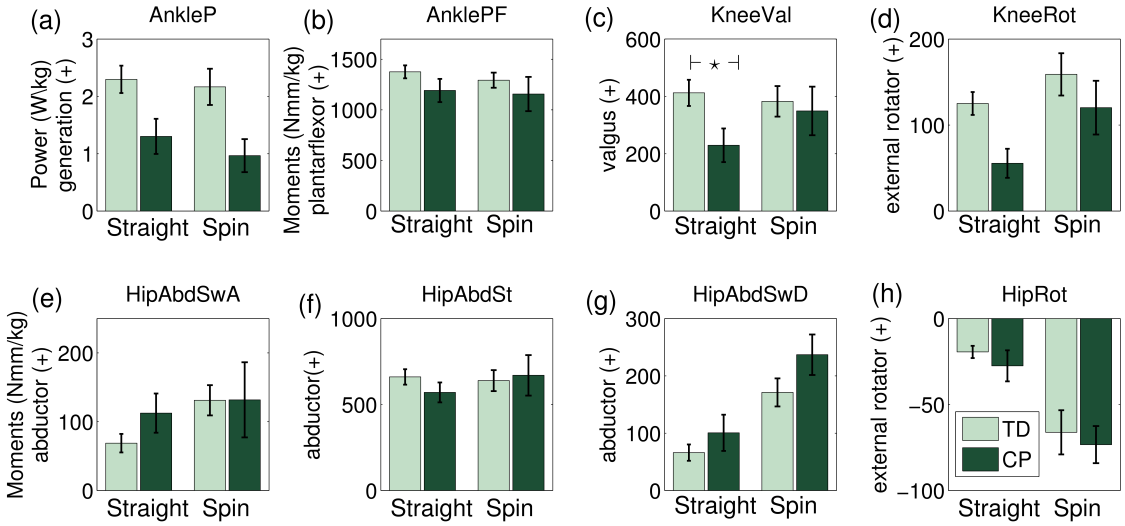

Figure 7.5 – Discrete kinetic events of (a) AnkleP, (b) AnklePF, (c) KneeVal, (d) KneeRot, (e) HipAbdSwA, (f) HipAbdSt, (g) HipAbdSwD, and (h) HipRot across group and condition. Significant group simple main effect ($\star$) shown. See Section 7.2.7 and Fig. 7.1 for event description.

found to differ from their TD peers only during straight walking ($p < 0.001$ and $\Delta = 1.61$). For δHipRot, simple main effects did not reveal any significant differences after Bonferroni correction; however, a trend for greater difference from TD subjects was seen for spin turns. Group main effects for δAnkleP, δAnklePF, and δHipAbdSwD ($p = 0.001$, 0.007, and 0.034, respectively) revealed that the CP group data differed more with respect to the normative data than their TD peers.

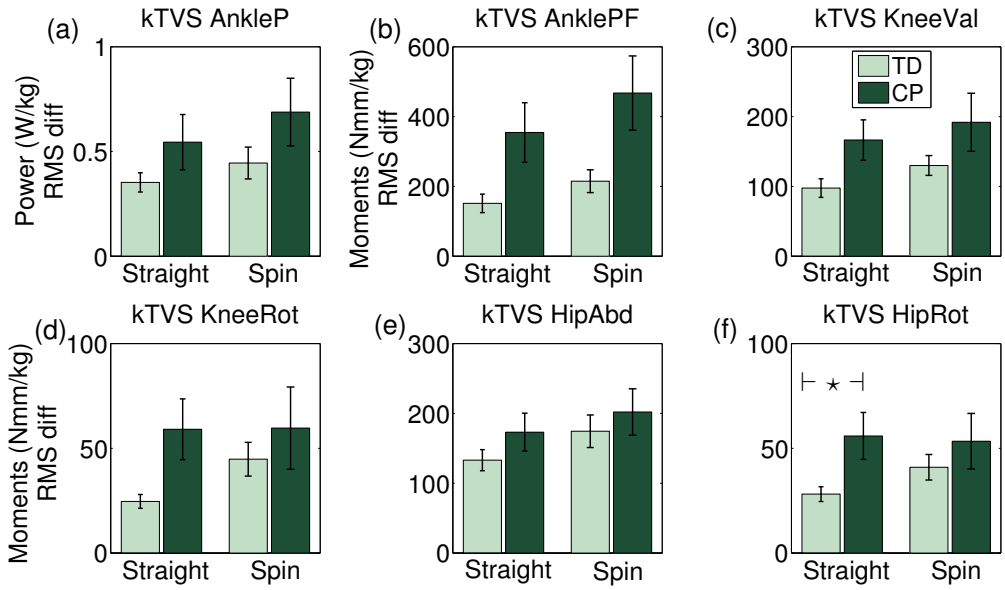

Figure 7.6 – Kinetic Turning Variable Score (kTVS) based on the root mean squared difference (RMS diff) for (a) AnkleP, (b) AnklePF, (c) KneeVal, (d) KneeRot, (e) HipAbd, and (f) HipRot moments during the turn stance phase for the ipsilateral limb across group and condition. Significant group simple main effect ($\star$) shown. See Section 7.2.7 for event description.

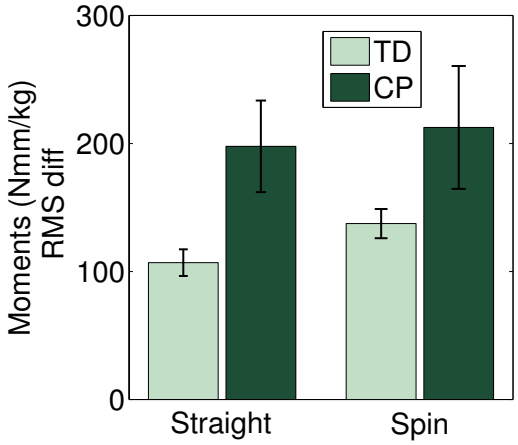

Figure 7.7 – Kinetic Turning Profile Score based on root mean square difference (RMS diff) average of kinetic Turning Variable Scores (moments) across group and condition.

The kTVS analysis resulted in significant group $\times$ condition interaction for kTVS HipRot only ($p = 0.005$) (Fig. 7.6 f). Follow-up group simple main effect test found that kTVS HipRot was greater for the CP group only during straight walking ($p < 0.001$ and $\Delta = 2.47$). A trend towards greater differences in the CP group was found for turning, but it was assessed as non-significant after Bonferonni correction. For the

Table 7.3 – Frequency distribution of abnormal discrete events for children with CP

Condition	Ankle P	Ankle PF	Knee Val	Knee Rot	Hip AbdSwA	Hip AbdSt	Hip AbdSwD	Hip Rot
Straight	16/18	14/18	16/18	17/18	11/18	12/18	13/18	15/18
Spin	11/14	10/14	10/14	7/14	**9/14**	9/14	7/14	6/14

Bold font where proportionately more children with CP were outside the TD range for turning. See Section 7.2.7 and Fig. 7.1 for event description.

remaining variables, group main effect revealed increased difference for the CP group compared to their TD peers ($p \leqslant 0.001$ for kTVS AnkleP, kTVS AnklePF, kTVS KneeVal and kTVS KneeRot; $p = 0.042$ for kTVS HipAbd) (Fig. 7.6 a–e).

For kTPS, no significant group $\times$ condition interaction was found; however, a group main effect test revealed that kTPS was increased for the CP group regardless of condition, compared to their TD peers ($p < 0.001$) (Fig. 7.7).

Subject-level analysis

The subject-level analysis of discrete kinetic events revealed that only HipAbdSwA identified proportionately more children with CP as having abnormal kinetics during turning than during straight walking (Table 7.3). Straight walking analysis suggested that 7 children had normal kinetics (C0716D, C0831D, C1090C, C1313A, C1314A, C1423A, and C1500A), of these only C1500A had normal kinetics for turning.

Analysis of relative events revealed that deviations from normative data increased for the majority of subjects during turning compared to straight walking (Fig. 7.8). The δHipAbdSwA parameter showed the largest increase with 11/14 subjects more different from normative data during turning than during straight walking (Fig. 7.8 e). For δAnkleP, the proportion was 9/14, while for δAnklePF, δKneeRot, δHipAbdSwD, and δHipRot it was 8/14 (Fig. 7.8 a, b, d, g, and h, respectively). It was only possible

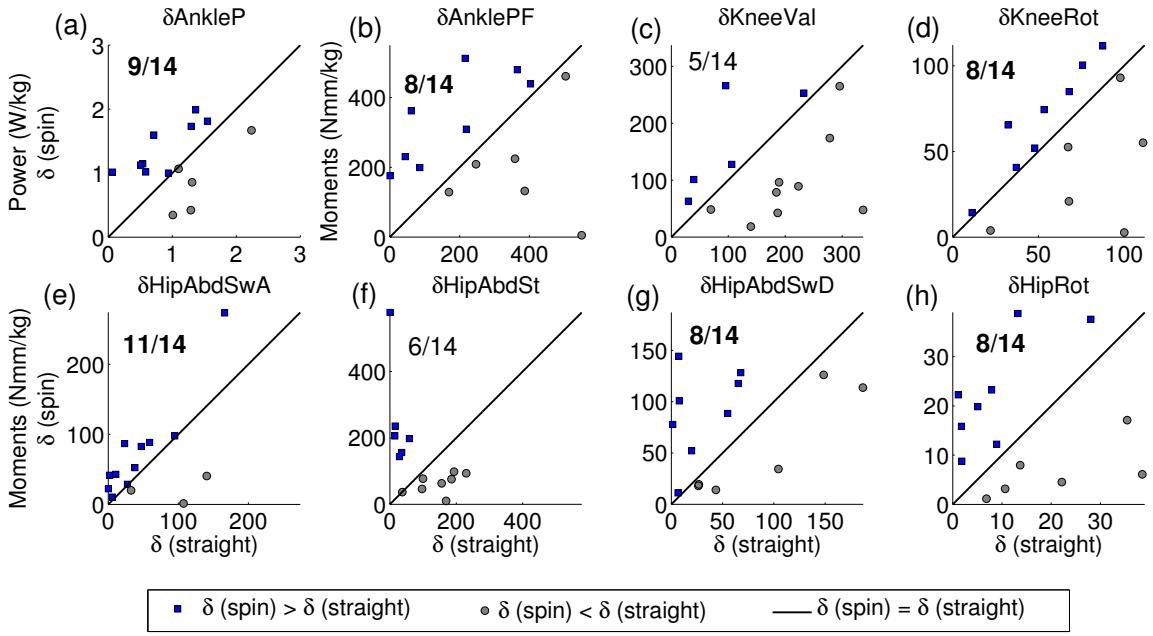

Figure 7.8 – Relative discrete kinetic events of (a) δAnkleP, (b) δAnklePF, (c) δKneeVal, (d) δKneeRot, (e) δHipAbdSwAS, (f) δHipAbdSt, (g) δHipAbdSwD, and (h) δHipRot across condition for each child with CP. Bold font for proportions where most children with CP increased difference from TD group for turning. See Section 7.2.7 for event description.

Table 7.4 – Frequency distribution of abnormal kinetic Turning Variable Scores and kinetic Turning Profile Score for children with CP

Condition	kTVS AnkleP	kTVS AnklePF	kTVS KneeVal	kTVS KneeRot	kTVS HipAbd	kTVS HipRot	kTPS
Straight	18/18	15/18	14/18	17/18	15/18	17/18	15/18
Spin	7/14	9/14	9/14	10/14	9/14	9/14	10/14

See Section 7.2.7 for event description.

to perform relative event analysis on the $n = 14$ children for which kinetic data were available for straight walking and the spin turn phase trials.

All kTVS parameters failed to identify as many children with CP as having abnormal kinematics in turning than for straight walking (Table 7.4). For many parameters difference from the TD data was increased for turning (Fig. 7.9). For kTVS HipAbd, 12/14 children with CP showed greater difference from their TD peers in turning than

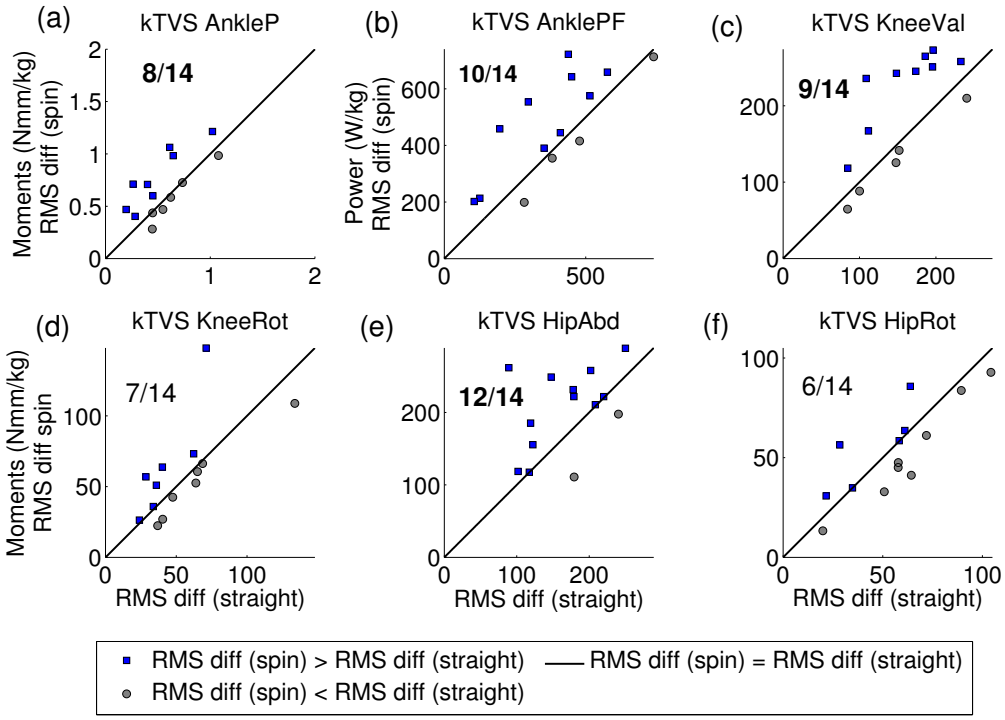

Figure 7.9 – Kinetic Turning Variable Score (kTVS) for (a) AnkleP, (b) AnklePF, (c) KneeVal, (d) KneeRot, (f) HipAbd, and (g) HipRot across condition for each child with CP. Bold font for proportions where most children with CP increased difference from TD group for turning. See Section 7.2.7 for event description.

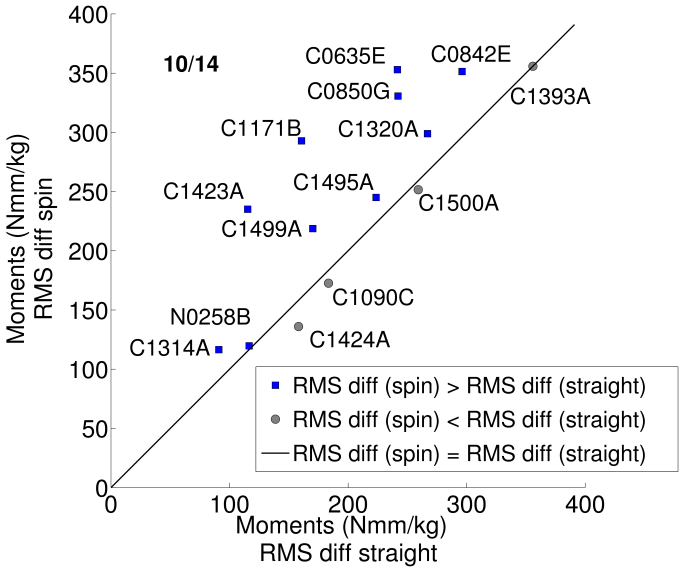

Figure 7.10 – Kinetic Turning Profile Score during straight and turning conditions for each child with CP. Bold font for proportion where most children with CP increased difference from TD group for turning. Subject codes also shown.

during straight walking (Fig. 7.9 e). For kTVS AnklePF, kTVS KneeVal, and kTVS AnkleP, proportions were 10/14, 9/14, and 8/14, respectively (Fig. 7.9 a–c).

Finally, for kTPS fewer children with CP were found to be outside the normative confidence interval during turning (10/14) than during straight walking (15/18) (Table 7.4). Nonetheless, the relative difference from the normative data was increased in 10/14 subjects (Fig. 7.10).

7.4 Discussion

This chapter reveals that a number of kinetic variables can be used to identify unique turning gait adaptations in children with CP. These kinetic quantities drive the joint kinematic changes observed in Chapter 6 and can therefore provide valuable insight into how children with CP achieve reorientation of the body during turning tasks. As with the kinematics, many kinetic variables were able to identify pathology during turning that was masked in straight walking analysis. These measures therefore can be of value in cases where children show only mild deviations during straight walking, despite complaints of real-world gait difficulties.

7.4.1 Ground reaction force impulse

The magnitude of the horizontal impulse quantities (J^{+}_{AP}, J^{-}_{AP}, and J^{T}_{ML}) during straight walking in the TD group are similar to those presented by Glaister et al. [88]. For 90° turning, previous studies have only presented impulse data for the step turn strategy [88, 219]. Consistent with the mechanics of the step turn, in which the outside foot is planted and the turn occurs in the opposite direction, results during the turn phase in the study of Glaister et al. [88] show larger J_{ML} values than presented here; however, J_{AP} quantities remain similar. For step turns, the approach and depart steps are taken with the inside limb and may be similar to a "mild" spin turn (see

Section 6.2.5). In agreement with this concept, the current J^T_{ML} results for the turn phase (inside limb) are oriented in the same direction (laterally), but larger than those for the approach of the step turn (inside limb) of Glaister et al. [88].

As hypothesized, unique adaptations during turning gait in children with CP were revealed by the analysis of impulse. During the approach phase, J^T_{ML} was reduced for the children with CP, while J^T_{ML}, J^+_{AP}, and J^+_V were all decreased for the turn phase, compared to their TD peers. In classical mechanics, impulse is related to a change in momentum via the impulse-linear momentum theorem [100, pp.258–259]. This relationship has been shown to hold during a number of locomotor tasks, including 90° turning [123]. Therefore, it appears that children with CP turn without changing their momentum as much as their TD peers. In contrast, results for the velocity drop (V_{DROP}) parameter from Chapter 6 suggest a greater change in overall momentum during turning for the CP group. Presumably, J^T_{ML} which was computed from the GRF in the body-based reference frame, represents a more accurate measure of momentum change in the medio-lateral direction than V_{DROP}. Future studies might focus further on the impulse-momentum relationship during turning gait. Finally, the reduction in J^+_V and J^+_{AP} during the turn phase may be related to decreased lower-limb muscle strength and overall velocity during turning in children with CP.

All impulse values remained similar across groups for straight walking, but showed unique changes during turning, suggesting that this metric may be clinically relevant in the management of gait for children with CP.

7.4.2 Free vertical torque

The hypothesis regarding T_Z could only be partially verified. While it was found that children with CP reduced maximum T_Z during turning compared to their TD peers, the decrease was similar in straight walking (significant group main effect). Therefore,

the use of maximum T_Z may not be clinically relevant in the analysis of turning gait in children with CP, at least during pre-planned turns. Possibly, unanticipated or quicker turns are required to elicit a different response across groups.

7.4.3 Joint kinetics

As hypothesized, both discrete and continuous measures were able to identify unique adaptations to turning gait in children with CP; however, both faired better in the subject-level analyses than the group based investigations.

Discrete parameter analysis of the entire CP group only revealed a single group × condition interaction of limited interest (leading to a group simple main effect of decreased knee valgus moment during straight walking only). Similarly, continuous approaches using summary scores (kTVS and kTPS) were only able to discern one group × condition interaction effect, leading again only to differences to the TD group during straight walking (increased hip rotation in the CP group). Subject-level analyses showed that for most discrete parameters (6/8), turning gait data were further from the norm than straight walking data for the majority of children with CP. For the continuous measures, 4/6 kTVS parameters and the overall kTPS showed that the majority of children with CP had a greater deviation from the norm during turning than during straight walking.

Each approach described in this chapter has the potential to identify joint kinetic pathology in children with CP. Choice of method to implement should depend on the group under investigation and particular study goals.

7.4.4 Clinical applications

As with the kinematic analysis of Chapter 6, the study of kinetic parameters during turning gait can be used to better differentiate children with CP from their TD peers.

Impulse can provide an overall estimation of the ability of children with CP to alter their momentum during turning, while joint kinetics (both discrete and continuous) may allow for specific deficiencies to be identified. Choice of which measures to investigate should be made on a case-by-case basis.

While clinical interpretation of the results for each child with CP is outside the scope of this thesis, two general findings based on the summary scores are worth highlighting. First, the overall TPS from Chapter 6 and kTPS here, do not show consistent trends across subjects: children with CP that are more dissimilar to their TD peers during turning with regard to kinematic variables, may not be with respect to kinetic variables, underlining the importance of both categories of metrics for gait analysis. Second, there appears to be no clustering of subjects based on Gross Motor Classification Scale (GMFCS) or gait pattern. Although larger cohorts may be required to fully explore trends, the present results suggest that adaptations are unpredictable based on subject characteristics, strengthening the case for analysis of turning gait in a clinical setting.

7.4.5 Limitations and other considerations

In addition to the limitations listed for the kinematic analysis (see Section 6.4.6), this study presents further specific limitations. First, the analysis was limited to the approach and turn phase of the turning cycle. Additional information from the depart step was not available. Future studies could add an obliquely positioned force plate or start trials perpendicular to the gait walkway to capture this information. Second, also related to the force plate positioning, in some cases, different subjects were analysed for the approach and turn phase of turning and for straight walking (Table. 7.1). Therefore, differences (or lack thereof) may be related both to condition and specific subjects investigated. Nonetheless, the alternative of analysing subjects

for which complete data were available would have been overly restrictive (only ten subjects). Finally, only ipsilateral limb joint kinetic parameters were investigated. Analysis of the contralateral side might also reveal interesting adaptations and could be explored in future studies depending on research goals.

7.4.6 Conclusion

This study investigated kinetic quantities during turning gait and revealed that a number of unique changes are manifest in children with CP. Kinetic parameters are responsible for joint kinematic changes and may therefore provide researchers and clinicians with a better understanding of turning gait. A more in-depth understanding of the underlying mechanisms of turning gait may be available through simulation based musculo-skeletal modelling.

Chapter 8

Musculoskeletal Modelling of Turning Gait

THIS chapter presents the results of a musculo-skeletal modelling study of turning gait in typically developing (TD) children undertaken in collaboration with the Human Movement Biomechanics Research Group of Dr. Ilse Jonkers at the Katholieke Universiteit Leuven. The feasibility of developing simulations for children with cerebral palsy (CP) during turning is also explored via a case study. As the methods implemented in this project are substantially different from the main investigations of this thesis, in depth literature review and methods sections are included. A manuscript version of this chapter (TD analysis only) was submitted to the *Journal of Biomechanics* in March 2015; however, results for the child with CP were not included.

8.1 Introduction

Turning is achieved via controlled movement of the whole body centre of mass (COM) towards the new walking direction [47, 171, 250]. Although different turning strategies have been described in the literature, the results of Section 6.2.5 suggest that for pre-planned 90° turns, the spin strategy, in which the body rotates about the inside, or ipsilateral (Ipsi) limb with respect to the turning direction, is preferred by both TD children and children with CP. The spin turn develops over three phases. First, during the approach phase, the contralateral (Contra) limb initiates the turn. Next, in the turn phase, the majority of body rotation occurs about the Ipsi limb. Finally, during the depart phase the Contra limb continues the rotation required to resume straight gait in the new walking direction (see Section 2.6). Each phase reveals unique joint kinematic and joint kinetic adaptations, both between groups and across conditions (see Chapters 4–7).

The medio-lateral redirection of the COM during turning type tasks is achieved via precisely timed muscle activations. Past studies have reported changes in amplitude or timing of muscle activation patterns [48, 105, 115]. Of these, the work of Hase and Stein [105] has provided the most comprehensive analysis of spin turn muscle activations, albeit during changes in body orientation of 180°. Hase and Stein [105] presented a plausible interpretation of how muscles contribute to the task of turning based on surface electromyographic (sEMG) muscle activation data; however, they were unable to identify the relative contributions of each muscle to COM acceleration. Previous studies have highlighted that muscle induced segment acceleration is difficult to quantify based on muscle activations or net joint moments alone, especially for biarticular muscles, since a muscle can accelerate segments which it does not span [254, 255]. Simulation using muscle actuated dynamic models can quantify the contributors to segment acceleration [255] and can reveal the mechanisms used

to control COM movement. Using this method, it was determined that during the stance phase of straight walking, the hip abductors and ankle plantarflexors are important contributors to COM acceleration away from and towards the stance limb, respectively [124, 167]. These control strategies remain unexplored for turning in both TD children and children with CP. Moreover, the use of simulations has been shown to benefit the management of gait in children with CP [139].

Therefore, the aims of this study were to quantify the contribution of muscles, gravity, and velocity-related forces (Coriolis and centrifugal) to COM medio-lateral acceleration during 90° pre-planned spin turns and in straight walking for TD children and to demonstrate applicability to clinical practice via a case study of a child with CP. For both straight walking and spin turns, the Contra and Ipsi step, corresponding to the approach and turn phase for spin turns, were analysed (Fig. 8.1 a). It was hypothesized that during the approach phase (1) Contra hip abductors would increase contribution to acceleration towards the Ipsi side (towards the turn centre) and (2) Contra ankle plantarflexors would also show contribution towards the ipsilateral side, instead of towards the Contra side (away from the turn centre), compared to straight walking. For the turn phase, it was hypothesized that (3), the contribution of the Ipsi hip abductors to acceleration to the Contra side (away from the turn centre) would decrease and (4) the Ipsi ankle plantarflexors would further induce acceleration towards the Ipsi side (towards the turn centre), compared to straight walking.

Better knowledge of real-world tasks such as turning augments the understanding of gait. Moreover, the use of turning tasks and gait simulations in clinical settings has the potential to lead to improvements in the management and treatment of gait deviations in populations with restricted gait ability such as children with CP.

8.2 Methods

8.2.1 Ethical considerations

All procedures were approved by the local ethics committee and all children provided informed assent/consent for inclusion in the study (see Section 3.1).

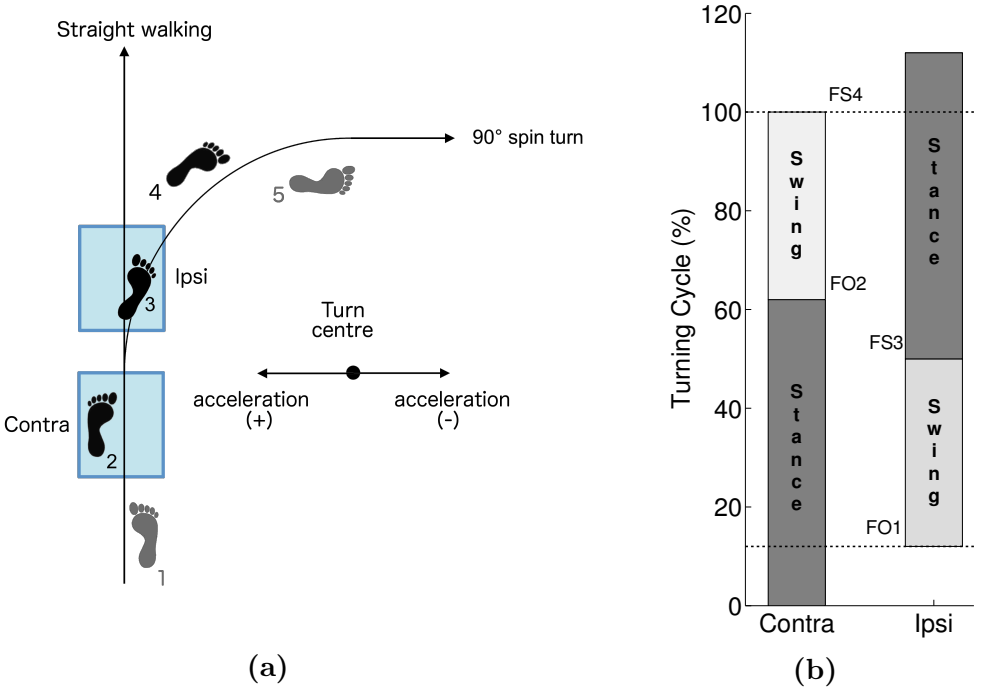

Figure 8.1 – Diagrammatic representation of (a) foot placements during a 90° spin turn to the right and (b) foot-strike (FS) and foot-off (FO) events as a percentage of the turning cycle (162% of the gait cycle). Data partitioned between dotted horizontal lines from FO1 (12%) to FS4 (100%) for simulations. The approach and turn phase correspond to stance phase 2 and 3 for the contralateral (Contra) and ipsilateral (Ipsi) limb, respectively. Acceleration towards the Ipsi side, i.e. towards the turn centre for spin turns, negative, while acceleration toward the Contra side i.e. away from the turn centre, positive. Depart phase (step 4) as well as initial (step 1) and terminal (step 5) steps, not analysed.

8.2.2 Subjects

Fifty-four TD children from the database were considered for this study. Forty-three subjects were excluded due to missing force plate and/or sEMG data, required to

drive and validate simulations, respectively (see Table 3.1 for the list of subjects analysed). Thus, data from eleven TD subjects (11.2 ± 2.9 years, 151.2 ± 17.7 cm, 42.2 ± 10.8 kg, 5 girls and 6 boys) were retained for analysis.

The case study involves a fourteen year-old boy with mild CP (C1500A) presenting with deterioration in walking distance and complaints of right knee pain and right leg muscle fatigue. The automatic gait classification algorithm of Sangeux et al. [188] revealed an unclassified (left) and jump (right) knee pattern (Table 6.1). Clinical examination found fixed knee flexion and ankle equinus contracture on the right, a left flexible planovalgus foot with a midfoot break, and a leg-length discrepancy (right side shorter). During straight walking, he exhibited right-sided pelvic retraction (pelvis rotated to the right), as well as reduced peak hip extension, adduction, and internal rotation. The clinical team recommended correction of the right knee and ankle contractures, barring any structural problems at the hip, and possible release of the adductors, followed by a post-operative gait assessment. Turning analyses were conducted on a right spin turn trial.

8.2.3 Data collection and initial processing

The data collection processing steps are described in Sections 3.3.3 and 3.4, respectively. Also, as described in Section 3.3.1, the sEMG electrodes were placed over the rectus femoris, semitendinosus, lateral gastrocnemius, and tibialis anterior. For four subjects, muscle activity from the gluteus medius was also collected. Data were imported into Matlab (v2012b, The Mathworks Inc., Natick, USA) where the raw sEMG data were smoothed using a 4th order zero-lag band-pass (10–500 Hz) Butterworth filter and further processed to obtain the root mean square (RMS) average of the signal (over a 50 ms moving average window) as in Jansen et al. [124]. The sEMG data were then amplitude normalized to 100% of the signal (% dynamic maximum).

In order to validate the simulation results (joint kinematics, joint kinetics, and muscle activations), visual comparisons between experimental and simulated data were conducted. For turning, both the Ipsi and Contra limb data, normalized over all available time frames (12–100%) of the gait cycle were verified, while for straight walking, data from the two sides were merged, assuming symmetry, to obtain a complete gait cycle normalized to 100% (see Appendix A.2).

Experimental data were collected over a series of steps; however, data for simulation were only available from foot-off of the Ipsi limb (foot-off 1) to foot-strike of the Contra limb (foot-strike 4), between which ground reaction forces were measured (Fig. 8.1). Assuming that single-limb support begins at approximately 12% of the gait cycle [173, p. 12], data were normalized over the remaining 88%. Trials were then divided into approach and turn phases. The approach phase begins in single limb support of the Contra limb (foot-off 1) and ends at foot-off 2. The turn phase begins in single-limb support of the Ipsi limb (foot-off 2), but ends at Contra foot-strike (foot-strike 4). All normalization procedures were conducted after developing simulations in the non-normalized time domain.

8.2.4 Center of mass acceleration during turning

Analysis of the COM acceleration, in the non-rotated global coordinate system, using the twice differentiated position of the COM computed by the Plug-in Gait (PiG) modeller [128] during straight walking and turning gait was conducted using the Bootstrap approach of Section 3.8.3. Significant differences were found in all three directions (antero-posterior, vertical, and medio-lateral); however, changes in the medio-lateral direction showed the largest effect-sizes (Fig. 8.2). Given these findings, analyses in this chapter focus on the medio-lateral direction.

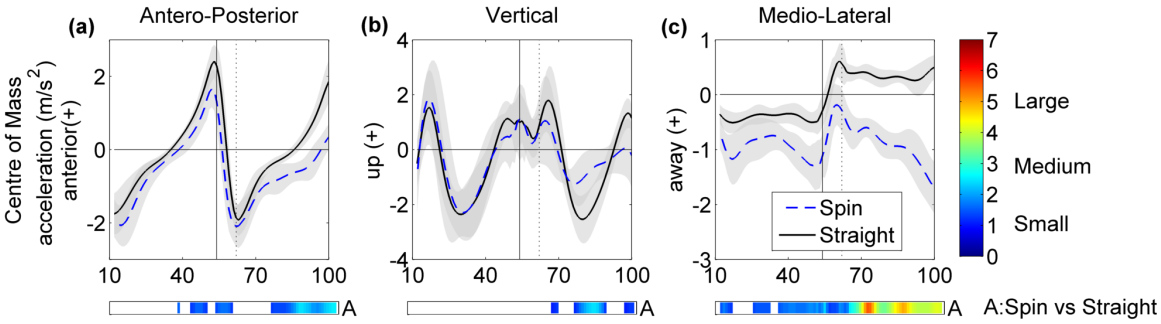

Figure 8.2 – Centre of mass acceleration for spin and straight conditions with corresponding Bootstrap confidence bands (CBs) from 12–100% of the turning cycle. Solid vertical lines indicate ipsilateral foot-strike and dotted vertical lines, contralateral foot-off. Colourbars show areas where mean difference CBs reveal significant differences with intensity representing effect size from small (blue) to large (red). As in the analyses of Chapters 4 and 5, zones of significant difference with changes of less than 5% of maximum CB width not shown.

8.2.5 Gait2392: a lower-limb musculoskeletal model

Simple models such as the inverted-pendulum model [38] and standard gait models, such as the PiG [128], have been implemented throughout this thesis to estimate dynamic stability (Section 6.2.7) as well as joint kinematics and kinetics (Chapters 4–7), respectively. Unfortunately, these models are unable to determine the contribution of individual muscles, ligaments, tendons, and other structures to net joint moments. This limitation occurs because the inverse dynamics solution is mathematically indeterminate [229]. In order to solve for the contribution of individual muscles to joint moments and to better understand their role in the movement of the COM, detailed information about muscle parameters and assumptions about how muscles function must be included in the model.

Musculoskeletal models estimate muscle properties and have been used to gain further knowledge about the role of muscles in gait [57, 126, 127, 144, 145, 175] as well as to plan and predict surgical outcomes [26, 79, 139, 181]. The development of an open-source graphical interface platform (OpenSim) by Delp et al. [56] has popularized musculoskeletal modelling of gait in the last decade. The OpenSim platform contains

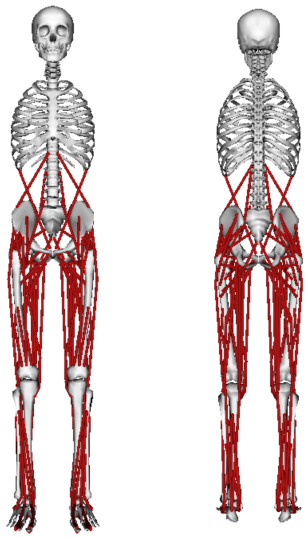

Figure 8.3 – The Gait2392 model with 92 actuators representing 76 muscles.

a number of predefined models that can be customized by the user. For walking studies, the Gait2392 is widely used [52, 124, 145] and is implemented herein.

General model characteristics

Gait2392 comprises the upper body of the Anderson and Pandy model [8] and the lower-limb model of Delp et al. [57] with a knee model developed by Yamaguchi and Zajac [252] (Fig. 8.3). It is a three-dimensional, twenty-three degree-of-freedom (DOF) model with ninety-two actuators representing seventy-six muscles.

Segment parameters

The shape of the lower-limb bones in the Gait2392 model were determined by digitizing bone surface data from a single cadeveric subject [57]. The original model of Delp et al. [57] comprised a pelvis, femur, patella, tibia, talus, calcaneus, and toe segments; however, the patella was later removed by Ajay Seth during the implementation of the model in the OpenSim framework [158, Gait2392 and 2354 Models]. A single rigid segment defining the upper-body (torso) was added from the Ander-

son and Pandy model [8]. Mass and inertial body segment parameters for the talus, calcaneus, and toes were derived using a mathematical model of a foot of known volume and density (1.1 g/cm^3) [158, Gait2392 and 2354 Models], while those of the remaining segments were experimentally obtained from anthropometric data of five healthy young adult subjects (26 ± 3 years, 177 ± 3 cm, and 70.1 ± 7.8 kg) [8]. Parameters were scaled to the dimensions of a 1.8 m and 75.2 kg subject in the OpenSim implementation [158, Gait2392 and 2354 Models].

Muscle geometry

The paths for each of the eighty-six lower-limb muscle actuators were determined from the anatomical landmarks obtained via the lower-limb bone shapes. In earlier work by Brand [25], muscle paths were simply defined as straight lines between an origin and insertion point based on cadaver specimens in the anatomical position. Delp et al. [57] allowed for additional bending points ("via" and "wrapping" points) in some muscles to avoid muscles passing through bones and other muscles during movement. The number of bending points change for each muscle as a function of joint angle. In the Gait2392 model, the three gluteus maximus actuators still cross through other structures when the hip is forced into large flexion angles [158, Gait2392 and 2354 Models], possibly leading to incorrect muscle dynamics in these movements. The origin and insertion points for the six trunk muscles were shown schematically in Anderson and Pandy [8], but details of how these points were chosen were not reported. Based on the muscle paths and bone geometry, moment arms and musculo-tendon lengths are then computed [57].

Model joints

The back, hip, knee, ankle, subtalar, and metatarsalphalangeal (MTP) joints allow movement between model segments. The back is modelled as a three DOF ball-and-

socket joint positioned near the third lumbar vertebrae based on experimental data from the doctoral thesis of Anderson [7]. The hip is also defined as a three DOF ball-and-socket joint, while the ankle, subtalar, and MTP joints are one DOF revolute (hinge) joints. The knee has a single flexion-extension DOF, but allows the contact point between the tibia and femur to vary based on angle [252]. The pelvis segment is given six DOF to allow the model to rotate and move freely within a three-dimensional space. Together, all account for the twenty-three DOF of the Gait2392 model.

Musculo-tendon actuators

Muscle force depends on both musculo-tendon length and velocity [240, pp. 210–222]. In order to estimate this relationship, Delp et al. [57] created individual models for each muscle actuator using as a starting point an existing generic Hill-type muscle model [253]. The generic model was customized using estimated muscle parameters (maximum isometric force, optimal muscle fibre length, pennation angle, tendon slack length, and physiological cross-sectional area) to compute the force-length relationship for each actuator. In the original paper, muscle properties were validated by comparing experimental maximum joint torques to those computed via the summation of each actuator moment for a given joint. Excellent agreement was reported for all joints in the model in Delp's doctoral thesis [55]. In the manuscript, an example is given for the ankle joint in which the experimental plantarflexor moment and the summed contributions of soleus, gastronemius and "other" plantarflexors (presumably flexor digitorum longus, flexor hallucis londus, tibialis posterior, and the peronei also included in the model) show good agreement [57]. Nonetheless, in the implementation of the Gait2392 model for OpenSim, Anderson increased the muscle strengths [158, Gait2392 and 2354 Models]) as the original strengths of Delp et al. [57] appeared weak in comparison to later results based on living subjects [8, 34].

8.2.6 Development of dynamic simulations

Dynamic simulations were performed in OpenSim (v3.1, Stanford, USA) by running a dedicated workflow [56]. This workflow consisted of scaling, inverse kinematics (IK), inverse dynamics (ID), residual reduction algorithm (RRA), and static optimization (SO) procedures. Additionally, since the goal of this part of the thesis was to identify and quantify the muscle and passive dynamic contributors to COM acceleration, an induced acceleration analysis (IAA) was also performed. These steps, along with the preliminary set-up procedure are now described.

Preparation for dynamic simulations

In OpenSim, there are no tools to import experimental data; however, two well known Matlab (The Mathworks Inc., Natick, USA) routines exist that can generate the required OpenSim files from *c3d* data [70, 143]. Of these, the Litchwark toolbox [143] was chosen as it is quick, provides useful graphical feedback of subject motion, and relies on the powerful BTK-toolkit [15] to deal with *c3d* file reading. Prior to running the Litchwark toolbox, start and end events for the motion, between which the ground reaction forces (GRFs) are known, were identified in the Vicon Nexus software environment (v1.8.4, Vicon Motion Systems Ltd., Oxford, UK). These events correspond to the first foot-off (FO1) and the fourth foot-strike (FS4) of Fig. 8.1 b.

Subject scaling

In the scaling step, the generic model is proportionally scaled to the dimensions of the current subject by comparing the distance between pairs of virtual markers on the model and experimental markers captured during a static trial. The user has full control on the choice of markers to be used to scale each segment (along with their weightings) and can apply proportional scaling in each dimension. Once the scale

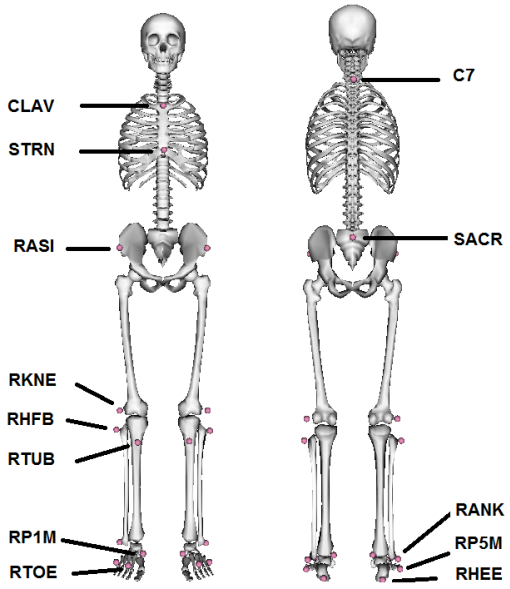

Figure 8.4 – Virtual markers for the Gait2392 model. Scaling performed using CLAV as well as left (L) and right (R) ASI, KNE, HFB, ANK, HEE, and TOE. Remaining markers used for kinematic tracking.

Table 8.1 – Marker pairs for scaling of body segments

Segment	Marker pairs
Torso	LASI–CLAV, RASI–CLAV
Pelvis	LASI–RASI
Right/Left Femur	RASI–RKNE, LASI–LKNE
Right/Left Tibia	RHFB–RANK, LHFB–LANK
Right/Left Foot	RHEE–RTOE, LHEE–LTOE

All markers weighed equally for scaling purposes. See Fig. 8.4 for marker positions.

factor for each segment is determined, both the segment and muscle properties are scaled [56]. Here, only markers (all weighted equally) were used to scale the segments of the generic model (Fig. 8.4 and Table 8.1).

The generic model does not contain markers: the user must add virtual markers to the model skeleton based on the marker set of the experimental data. Therefore, as part of the evaluation of the scaling procedure, the error between model and experimental markers needs to be checked. Moreover, in line with the OpenSim best

practices document [158], it is important to verify that sagittal plane hip and ankle angles remain small, assuming that the subject was able to maintain a neutral posture during the static pose. There is an an offset between pelvic tilt values computed by the Gait2392 and PiG attributable to differences in the pelvic local coordinate system. Here, the angle between the global vertical axes and the vector formed by the SACR and the midpoint between the two anterior superior iliac spine markers (RASI and LASI) (see Fig. 8.4) was added to the Gait2392 pelvic and hip sagittal plane angle values to allow comparison across models [158, Gait2392 and 2354 Models].

Inverse kinematics

Once the generic model is scaled to the dimensions of the subject, the software can simulate the subject motion by determining the positions of each segment that best matches the experimental markers. This is done by minimizing a weighted squared error function for the m markers and a joints chosen by the user [56]:

$$err = \sum_{i=1}^{m} w_i(x_i - \hat{x}_i)^2 + \sum_{j=1}^{a} w_j(\theta_j - \hat{\theta}_j)^2 \tag{8.1}$$

where x_i is the ith experimental marker three-dimensional position

$\hat{x}_i$ is the ith model marker three-dimensional position

θ_j is the jth experimental joint angle

$\hat{\theta}_j$ is jth model joint angle

w_i is the ith marker weighting factor

w_j is the jth joint angle weighting factor

Here, only markers were used to simulate motion (all w_j terms in Eq. 8.1 set to 0). Markers of easily identifiable landmarks with little skin motion artefact were weighted twice as heavily as others (absolute weighting coefficients are not as important as the relative weightings between markers [158, Best Practices]) (Table 8.2).

Table 8.2 – Inverse kinematics markers and weightings

Segment	Marker	Weighting (w_i)
Torso	C7	10
	STRN	10
	CLAV	10
Pelvis	LASI, RASI	20
	SACR	20
Right / Left Femur	RKNE, LKNE	10
Right / Left Tibia	RHFB, LHFB	20
	RTUB, LTUB	10
	RANK, LANK	10
Right / Left Foot	RHEE, LHEE	10
	RP1M, LP1M	10
	RP5M, LP5M	10
	RTOE, LTOE	10

See Fig. 8.4 marker positions.

Inverse dynamics

OpenSim computes joint kinetics during the ID process allowing the user to validate simulated joint moments with experimental data.

Using the generalized position (q), velocity ($\dot{q}$), and acceleration ($\ddot{q}$) notation, representing the minimum set of quantities required to describe the system's DOF [254], the equation of motion which includes the contribution of muscle (F_m), gravity (F_g), Coriolis and centrifugal (F_v), and ground reaction (F_{grf}) forces is given as:

$$[M]\ddot{q} = F_g + F_v + F_{grf} + [R]F_m \tag{8.2}$$

where $[M]$ is the system mass matrix

$[R]$ is a matrix of moment arms

Note that, anthropometric quantities, relative segment mass, and joint centre locations used to compute joint kinetic quantities in OpenSim and by the PiG modeller differ, making comparisons across methods difficult.

Residual reduction

The estimation of kinetic quantities via inverse dynamic analysis is prone to errors from a number of sources, including the estimation of body segment parameters, joint centre locations, and skin motion artefact [182]. These errors lead to dynamic inconsistencies between measured and computed quantities for both forces and moments [135]. In other words, Newton's and Euler's second laws of motion are broken. In order to remedy the situation, residual forces (F_{res}) and moments (M_{res}) can be added to the motion equations summed over each segment s:

$$\mathbf{F}_{ext} = \sum_{i=1}^{s} m_i \cdot \mathbf{a_i} - \mathbf{F}_{res} \tag{8.3}$$

$$\mathbf{M}_{ext} = \sum_{i=1}^{s} \boldsymbol{I_i} \cdot \boldsymbol{\alpha_i} + \boldsymbol{\omega_i} \times (\boldsymbol{I_i} \cdot \boldsymbol{\omega_i}) - \mathbf{M}_{res} \tag{8.4}$$

where $\mathbf{F}_{ext}$ are the external forces acting on the body

$\mathbf{M}_{ext}$ are the external moments acting on the body

m_i is the mass of the ith segment

$\mathbf{a_i}$ is the linear acceleration of the ith segment

$\boldsymbol{I_i}$ is the inertia tensor of the ith segment

$\boldsymbol{\omega_i}$ is the angular velocity of the ith segment

$\boldsymbol{\alpha_i}$ is the angular acceleration of the ith segment

Although there are numerous algorithms to reduce residuals [56, 135, 227], the RRA method of Delp et al. [56] was chosen for the present investigation.

In the RRA, small perturbations to kinematics and body segment parameters are made in an attempt to reduce the residuals. The algorithm then suggests modifications to the torso COM position, the overall body mass, and the segment trajectories. These changes were manually applied to the scaled subject model before running the

SO procedure to compute muscle activations. The RRA results were evaluated as "good", "okay", or "bad" based on the OpenSim documentation [158].

Static optimization

The human muscular system is said to be redundant: for most joints, the body has many more muscles than DOF. Nonetheless, for non-novel tasks, individuals without musculo-skeletal pathology produce similar motions (kinematics) via similar muscle activation patterns. In the context of gait, muscle activation patterns have shown consistency across TD children walking at a given speed [194]. This suggests that the central nervous system selects muscle activation patterns based on some unknown function(s) subject to physical constraints [39].

Mathematically, attempting to solve for individual muscle forces (or moments) in a redundant system results in an underdetermined problem, i.e. the number of unknowns exceeds the number of available equations [49]. This type of problem can be solved using optimization theory [39]. Although, there are advanced methods based on dynamic (time-dependant) optimization, here the focus remains on SO as both approaches produce similar results for gait [9].

In general, the optimization process attempts to minimize an objective (performance) function U for a set of variables x_n:

$$\text{minimize } U(x_1,\ x_2,\ \ldots,\ x_n) \tag{8.5}$$

Subject to equality and inequality constraints:

$$\phi_k(x_1,\ x_2,\ \ldots,\ x_n) = 0 \tag{8.6}$$

$$\psi_i(x_1,\ x_2,\ \ldots,\ x_n) \geqslant 0 \tag{8.7}$$

where ϕ_k, is the kth equality constraint

ψ_i is the ith inequality constraint

Performance functions are usually chosen on the basis that the central nervous system aims to minimize some physiologically relevant variable during the performance of a given task [39]. In OpenSim, the performance function aims to minimize the square of the muscle activations (a_m), at each time frame t, based on the early work of Crowninshield and Brand [49]:

$$U(t) = \sum_{m=1}^{n} (a_m(t))^2 \tag{8.8}$$

The exponent in Eq. 8.8 can be set to any integer, but here the default squared function was used. The user also has the choice of two equality constraints [9]:

$$\sum_{m=1}^{n} (a_m(t) \cdot F_m^0) \cdot r_{mj(t)} = M_j(t) \tag{8.9}$$

$$\sum_{m=1}^{n} [a_m(t) \cdot f(F_m^0, l_m, v_m)] \cdot r_{mj(t)} = M_j(t) \tag{8.10}$$

where F_m^0 is the maximum isometric force of the mth muscle

r_{mj} is the moment arm of the mth muscle at the jth joint

M_j is the jth joint moment

l_m is the length of the mth muscle

v_m is the shortening velocity of the mth muscle

In the work of Anderson and Pandy [9], Eq. 8.9 and 8.10 are described as the non-physiological and physiological constraints, respectively. The physiological constraint attempts to model the force-length-velocity relationship of muscle force generation [9] and was used here. Anderson and Pandy found only small differences in muscle activations between the two constraint possibilities [9].

The optimization problem defined by Eqs. 8.8 and 8.10 is handled by an interior point optimizer (Ipopt) algorithm [234]. This algorithm was designed to solve large-scale, non-linear optimization problems and is thus ideally suited to the problem of determining muscle activations.

Validation of computed muscle activations against experimental results remains a challenge. A study investigating cat locomotion showed that optimization results did not agree well with direct measurement of surgically removed muscles; however, the authors suggested that refinement of the models could improve agreement [108]. As such approaches are not feasible in human studies, simulated activations are usually compared against sEMG patterns. The work of Heintz et al. [106] showed that, via preliminary measurement of maximum voluntary contractions, it was possible to use the EMG-to-force processing method of Bogey et al. [22] to assess the validity of SO derived muscle activations. These authors reported good correlations between the two methods of muscle activation estimation, with the ankle plantarflexor and dorsiflexor muscles showing better agreement than the knee extensors and flexors [106]. Regardless, the most popular approach, and the one taken here, is to qualitatively assess the agreement between normalized SO and sEMG patterns [9, 101, 124, 216].

Induced acceleration analysis

The muscle activations derived from SO quantitatively describe the force production of each muscle throughout the motion of interest. Without further processing, it remains unknown what the role of these forces are with respect to controlling movement [255]. An IAA can be used to quantify each contributor, such as muscle force or gravity, to the acceleration of a given segment or of the COM.

In 1989, Zajac and Gordon [254] stressed that muscles that act to accelerate a joint that it spans can also accelerate other body segments. Although, this was previously known, their work has been influential in the development of IAA. Early attempts to relate muscle force to segment accelerations were made using dynamic models actuated by net joint torques [132, 183]. These models shed some light on the control mechanisms of gait, but it remained difficult to interpret exact muscle function, especially for biarticular muscles [255]. The first IAA using a muscle actuated dynamic

model was conducted by Neptune et al. [159]. Their process can be best summarized by starting with Eq. 8.2 solved for the acceleration term:

$$\ddot{q} = [M]^{-1} \cdot \Big(F_g + F_v + F_{grf} + [R]F_m \Big) \tag{8.11}$$

The left hand side of Eq. 8.11 is the total acceleration of the system made up of its gravitational ($\ddot{q}_g$), velocity ($\ddot{q}_v$), GRF ($\ddot{q}_{grf}$), and muscular ($\ddot{q}_m$) contributors:

$$\ddot{q} = \ddot{q}_g + \ddot{q}_v + \ddot{q}_{grf} + \ddot{q}_m \tag{8.12}$$

Given the linear relationship between force and acceleration, the contribution to $\ddot{q}$ of a particular component (gravitational, velocity, GRF, or muscular) can be obtained by setting all other forces in Eq. 8.11 to zero. For example, the contribution to acceleration by muscles can be obtained as:

$$\ddot{q_m} = [M]^{-1} \cdot [R]F_m \tag{8.13}$$

This approach was taken to solve for the contribution of joint moments by Riley et al. [183]; however, the direct use of Eq. 8.13 is problematic because F_m is not independent of F_{grf}, i.e. the application of F_m changes F_{grf} [255]. Rather, Eq. 8.13 should be rewritten to include the contribution of F_m to F_{grf} (F^m_{grf}):

$$\ddot{q_m} = [M]^{-1} \cdot \Big([R]F_m + F^m_{grf} \Big) \tag{8.14}$$

In Eq. 8.14, both $\ddot{q_m}$ and F^m_{grf} are unknown. This problem can be solved through two main methods [158, User's Guide]. First, via a perturbation analysis, in which the effect of a small increase in F_m (e.g. 1 N) on F_{grf} is determined. Assuming linearity, F^m_{grf} is found by multiplying the change in F_{grf} by F_m [144, 145, 159]. The second approach is the kinematic constraint method, currently implemented in OpenSim [158,

User's Guide]. In this method, F_{grf} in Eq. 8.11 is replaced by a constraint matrix C mapping constraint forces λ to a system of generalized forces [102]:

$$[M]\ddot{q} = F_g + F_v + [C]\lambda + [R]F_m \tag{8.15}$$

There are three possible kinematic constraint models implemented in OpenSim [158, User's Guide]; however, it is the "RollingOnSurface" setting, recently shown to outperform "point" or "weld" constraints [103], that was chosen. With respect to the point of ground contact, this constraint disallows floor penetration, horizontal velocity, and vertical twist [102].

8.2.7 Statistical analysis

Muscles with similar functions were grouped as in Jansen et al. [124] (Table 8.3). To ensure that no contributor to COM medio-lateral acceleration was overlooked, the per cent (%) variance of the total COM medial-lateral acceleration signal over the time interval t explained by each single muscle, muscle group, gravity or velocity component m was computed:

$$V_m = \frac{var(C)}{\sum_{i=1}^{m} var(C)} \tag{8.16}$$

where C is a $t \times m$ matrix of induced acceleration components

$var(C)$ is a $1 \times m$ row vector of variances

The V_m values $(1 \times m)$ were sorted by decreasing order of explained variance and the first n components, representing 95% of the overall COM acceleration, were retained (Table 8.4). Of these, only those explaining at least 5% of the variance were considered to be major contributors and statistically analysed. A scree plot for the approach phase of straight walking is presented for demonstration purposes (Fig. 8.5).

Table 8.3 – Muscle groups and associated abbreviations

Abbreviation	Description
ADD	Adductor longus, brevis, and magnus (3 actuators)
DF	Tibialis anterior, extensor digitorum, and extensor hallucis
ERSPN	Erector spinae
GAS	Gastrocnemius (medial and lateral)
GMAX	Gluteus maximus (anterior, medial, and posterior actuators)
GMED	Gluteus medius (anterior, medial, and posterior actuators)
GMIN	Gluteus minimus (anterior, medial, and posterior actuators)
HAMS	Semimembranosus, semitendinosus, bicep femoris long head
ILIPSO	Iliacus and psoas
SOL	Soleus
VAS	Vastus intermedius, medialis, and lateralis

Table 8.4 – Top contributors to the center of mass medio-lateral acceleration

	Approach phase		Turn phase	
variance (%)	Straight	Spin	Straight	Spin
$[40, 100]$		Contra GMED		Ipsi GAS
$[30, 40[$			Ipsi VAS	
$[20, 30[$	Contra GMED	Contra SOL	Ipsi GAS	Ipsi SOL
$[10, 20[$	Contra GAS Contra SOL	Gravity	Ipsi SOL Ipsi GMED	
$[5, 10[$	Contra VAS Ipsi GMED Gravity	Contra ILIPSO		Gravity
$[0, 5[$	Velocity Contra ILIPSO Ipsi HAMS Contra DF Ipsi VAS Contra GMIN	Contra GAS Contra ERSPN Contra GMAX Velocity force Ipsi HAMS Ipsi GMED Contra VAS Contra GMIN	Gravity Ipsi DF Ipsi ILIPSO Contra ADD Ipsi GMAX	Contra ERSPN

Components accounting for 95% of the variance in the total medio-lateral center of mass acceleration by decreasing order. Ipsilateral (Ipsi) and contralateral (Contra) muscles shown. See Table 8.3 for muscle abbreviations.

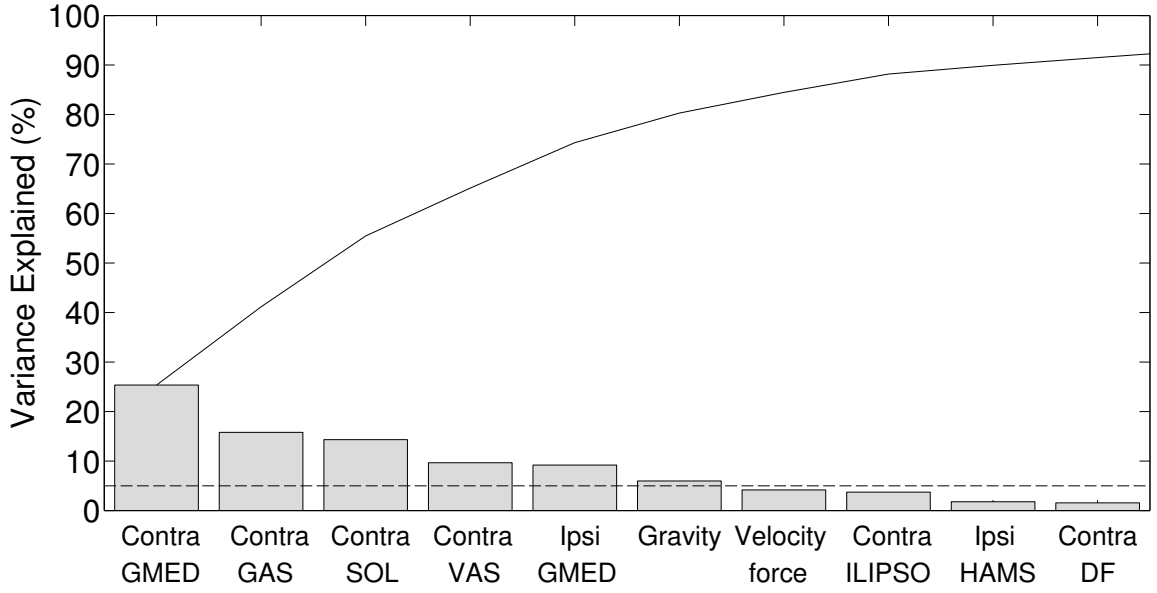

Figure 8.5 – Components accounting for 95% of the total medio-lateral centre of mass acceleration in the approach phase for straight walking. The dashed horizontal line represents the 5% cut-off under which components were not considered to be major contributors. Ipsilateral (Ipsi) and contralateral (Contra) muscles shown. See Table 8.3 for muscle abbreviations.

The average accelerations of the COM (sum of all contributors) and each major contributor were statistically analysed across straight walking and spin turns for the approach and turn phases. Parametric assumptions, choice of statistical tests (paired t-test or Wilcoxon signed-rank test), and effect size formulae (Cohen's d (d) or Glass's delta (Δ)) were chosen according to criteria from Section 4.2.4. Significance level set at $\alpha = 0.05$. Error variances were non-homogeneous for Ipsi GMED (approach) and for total COM, Ipsi SOL, and Ipsi GAS during the turn phase.

8.3 Validation

Verification of the outputs of the dynamic simulation steps of Section 8.2.6 helps provide confidence in the simulation results. It is difficult to truly validate a given simulation; however, for subject scaling and RRA, OpenSim provides ranges of acceptable error, while for the IK, ID, SO, and IAA steps, visual comparison of experimentally

measured quantities with those from the dynamic simulations is often considered sufficient [158, Best Practices]. These verifications were conducted based on ensembled data for all subjects for straight and turning gait simulations of this study.

8.3.1 Subject scaling

The error between the experimental and model (virtual) markers was evaluated. The maximum and RMS errors were found to be larger than recommended (3.5 vs 2.0 cm and 1.4 vs 1.0 cm, respectively), mainly due to the larger error in the STRN and C7 upper-body trunk markers. Static posture of the model was checked via joint kinematics. On average, hip and ankle sagittal plane angles were within bounds (< 10.0 and $< 5.0°$, respectively).

8.3.2 Inverse kinematics

The IK procedure was verified by comparing simulation results against experimental joint kinematics computed by the PiG modeller [128]. Good agreement was found for both straight (Fig. 8.6) and turning gait (Figs. 8.7 and 8.8) conditions.

8.3.3 Inverse dynamics

Despite differences in model parameters, good agreement was found between the simulated and experimental joint moments during straight (Fig. 8.9) and turning gait (Figs. 8.10 and 8.11) conditions.

8.3.4 Residual reduction

The RRA resulted in an overall F_{res} maximum and RMS average of 16.7 (okay) and 3.5 N (good), respectively as well as M_{res} maximum and RMS average of 33.2 (good)

and 0.94 Nm (good), respectively. Translational (position) RMS errors were of 1.3 cm (good), while rotational (joint angle) RMS errors were negligible (good).

8.3.5 Static optimization

Overall, good agreement was found between SO and sEMG data for straight walking (Fig. 8.12) and turning gait (Fig. 8.13). Best agreement occurred with gastronemius and semitendinosus. For the tibialis anterior, the patterns were similar, but the peak caused by dorsiflexion of the ankle in early swing identified in the sEMG data was not as evident in the SO results for straight walking. At the knee, the combined SO activation patterns of rectus femoris and vastus medialis account for the variability in the sEMG signal. Finally, for the gluteus medius, disagreement between sEMG and SO results were obtained. Although electrode placement may have played a role, the experimental results were in good agreement with published normative data [242], suggesting that rather the SO results were less accurate. Nonetheless, the SO activations were considered to be acceptable, given that it is the differences across conditions that are of interest in this investigation, not the absolute values.

8.3.6 Induced acceleration analysis

Validation of the IAA was conducted by comparing the sum of each contributor to the COM acceleration against the overall COM acceleration (superposition) [158, User's Guide]. The COM position of experimental data (computed by the PiG modeller [231]) and the scaled model were twice differentiated to obtain acceleration data. Comparison of IAA results with both COM acceleration estimations showed good agreement for straight (Fig. 8.14) and turning gait (Fig. 8.15) conditions.

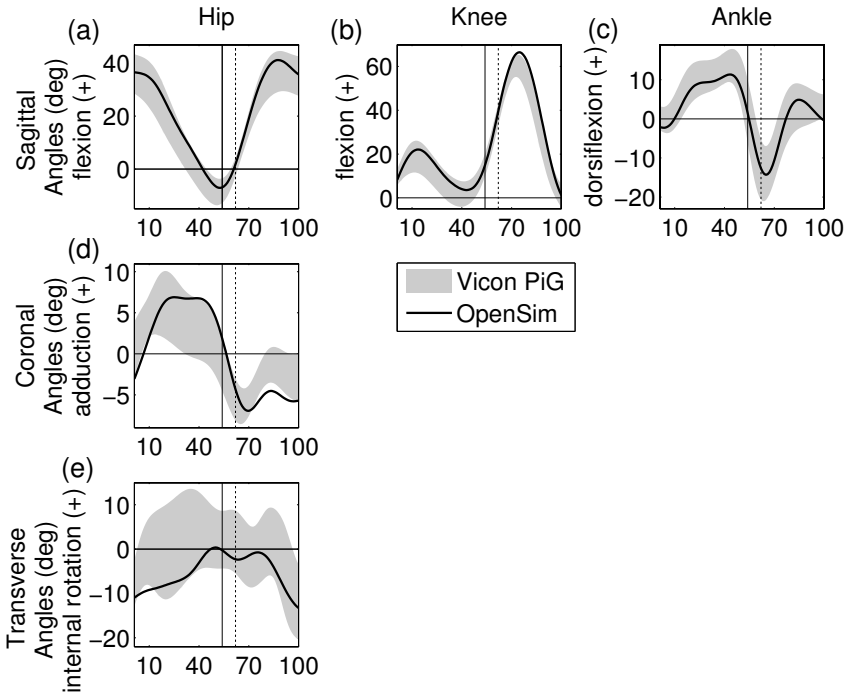

Figure 8.6 – Kinematics for straight walking (0–100% of the gait cycle). Solid (ipsilateral foot-strike) and dotted (contralateral foot-off) vertical lines as well as mean simulated (OpenSim) and standard deviation of Plug-in Gait (Vicon PiG) data shown.

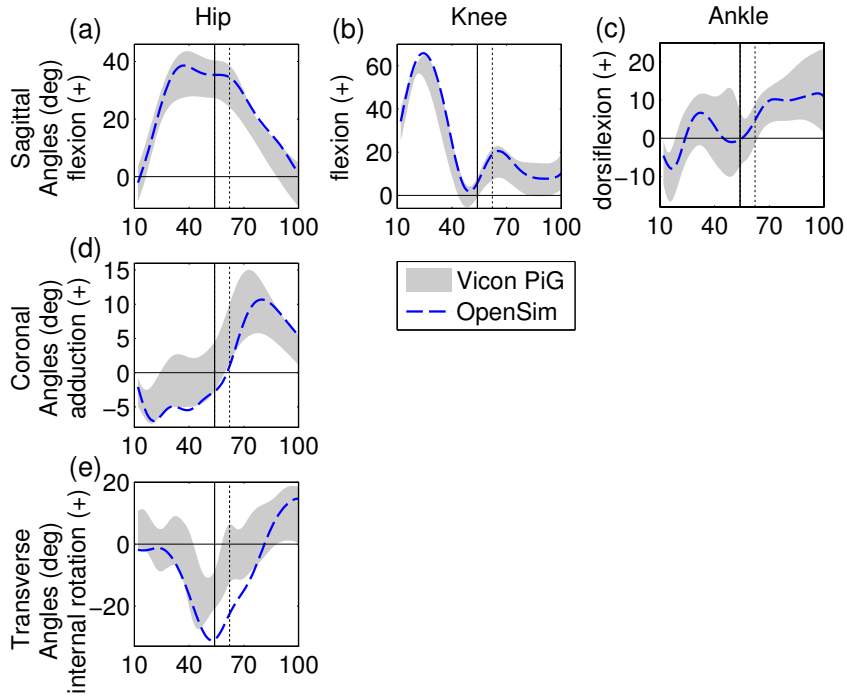

Figure 8.7 – Ipsilateral kinematics for spin turns (12–100% of the gait cycle). Solid (ipsilateral foot-strike) and dotted (contralateral foot-off) vertical lines as well as mean simulated (OpenSim) and standard deviation of Plug-in Gait (Vicon PiG) data shown.

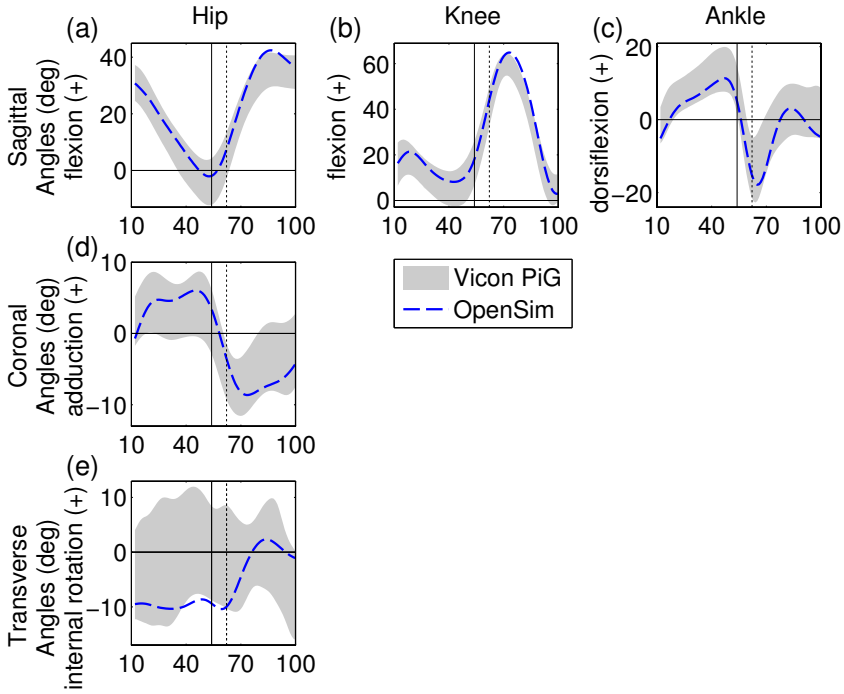

Figure 8.8 – Contralateral kinematics for spin turns (12–100% of the gait cycle). Solid (ipsilateral foot-strike) and dotted (contralateral foot-off) vertical lines as well as mean simulated (OpenSim) and standard deviation of Plug-in Gait (Vicon PiG) data shown.

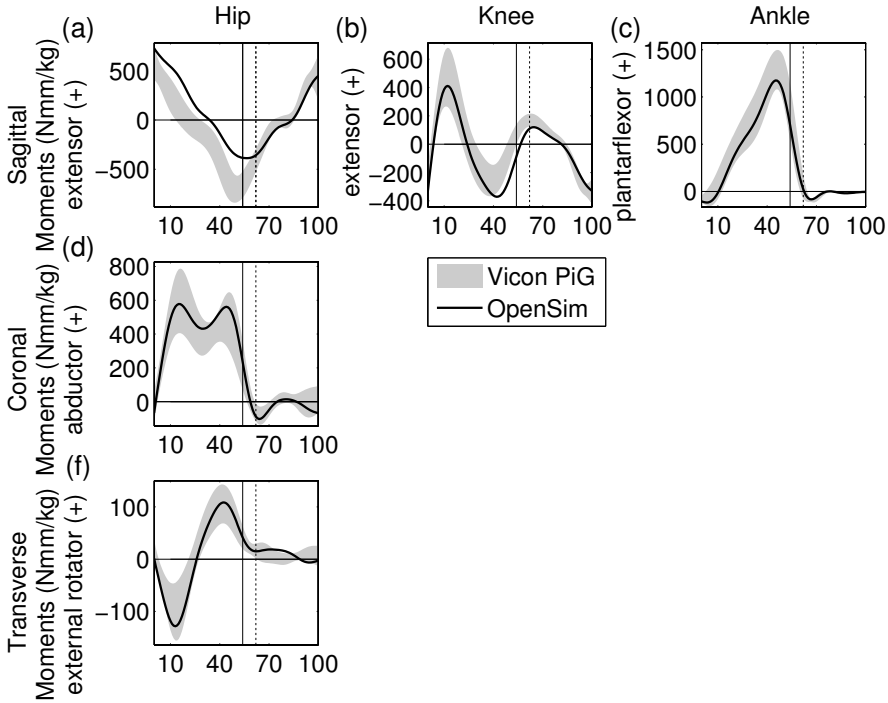

Figure 8.9 – Moments for straight walking (0–100% of the gait cycle). Solid (ipsilateral foot-strike) and dotted (contralateral foot-off) vertical lines as well as mean simulated (OpenSim) and standard deviation of Plug-in Gait (Vicon PiG) data shown.

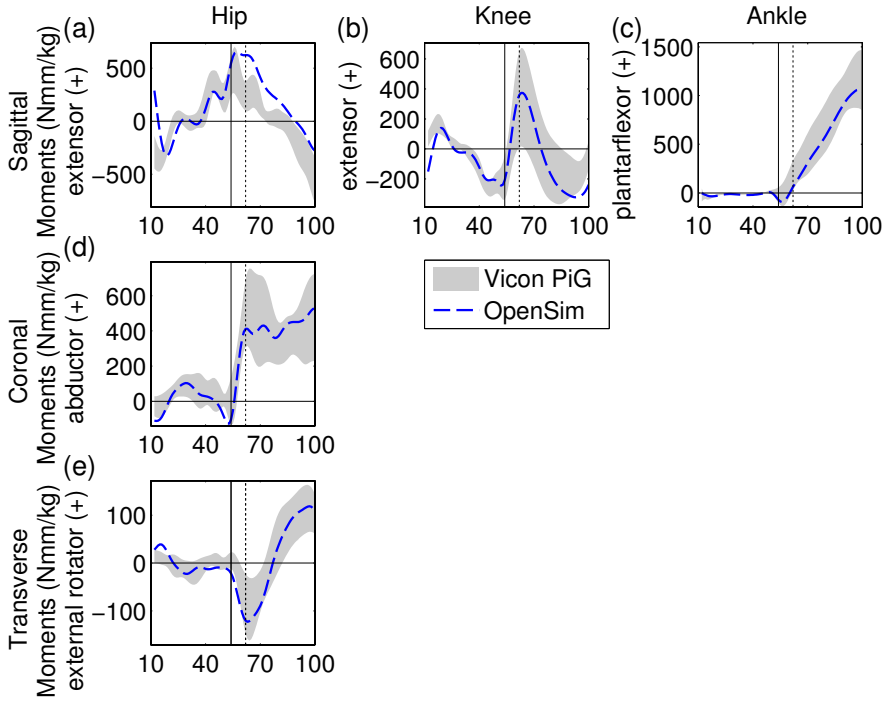

Figure 8.10 – Ipsilateral moments for spin turns (12–100% of the gait cycle). Solid (ipsilateral foot-strike) and dotted (contralateral foot-off) vertical lines as well as mean simulated (OpenSim) and standard deviation of Plug-in Gait (Vicon PiG) data shown.

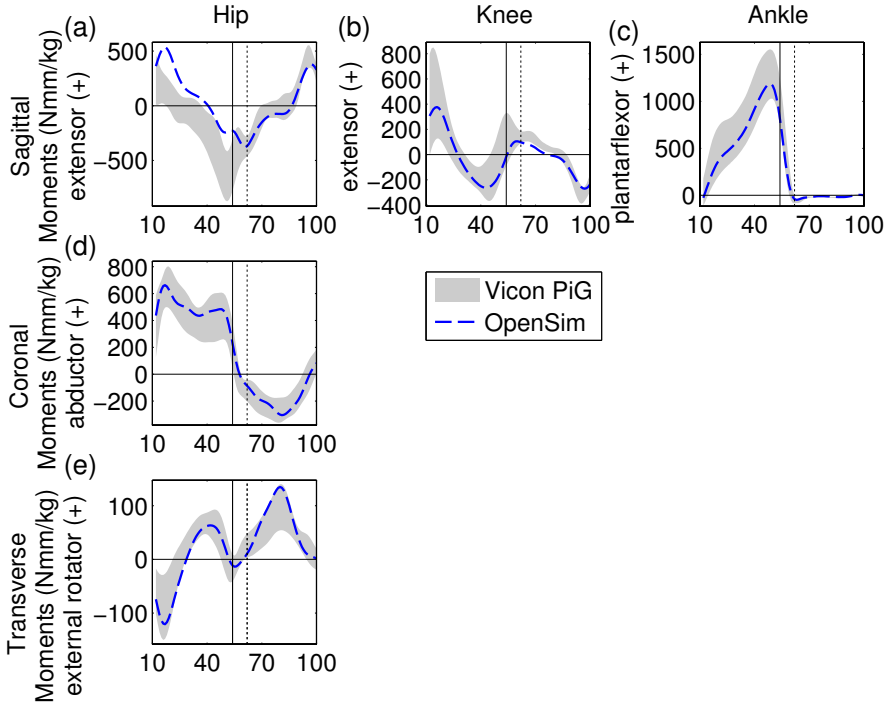

Figure 8.11 – Contralateral moments for spin turns (12–100% of the gait cycle). Solid (ipsilateral foot-strike) and dotted (contralateral foot-off) vertical lines as well as mean simulated (OpenSim) and standard deviation of Plug-in Gait (Vicon PiG) data shown.

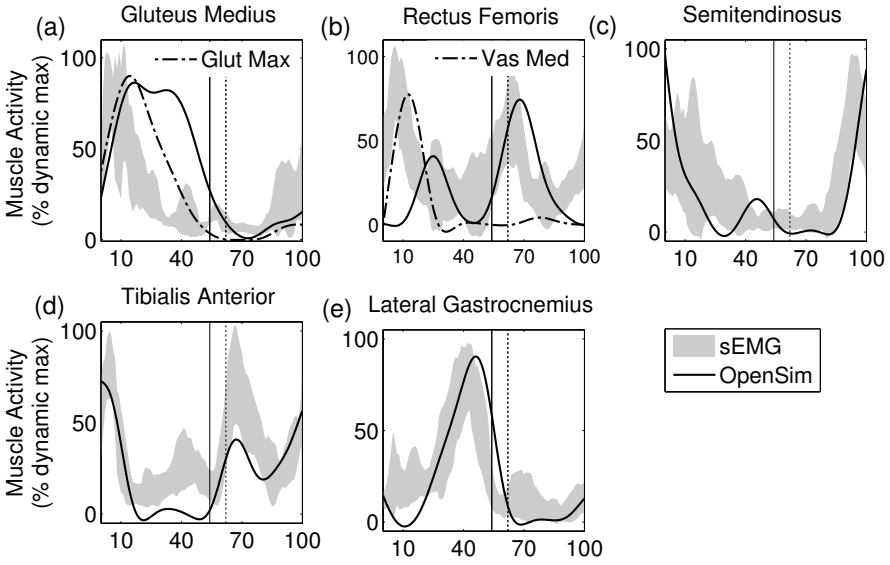

Figure 8.12 – Muscle activity for straight walking (0–100% of the gait cycle). Solid (ipsilateral foot-strike) and dotted (contralateral foot-off) vertical lines as well as mean simulated (OpenSim) and standard deviation of surface electromyographic (sEMG) data shown. For (a) and (b) gluteus maximus (Glut Max) and vastus medialis (Vas Med) activity from OpenSim, respectively, also shown.

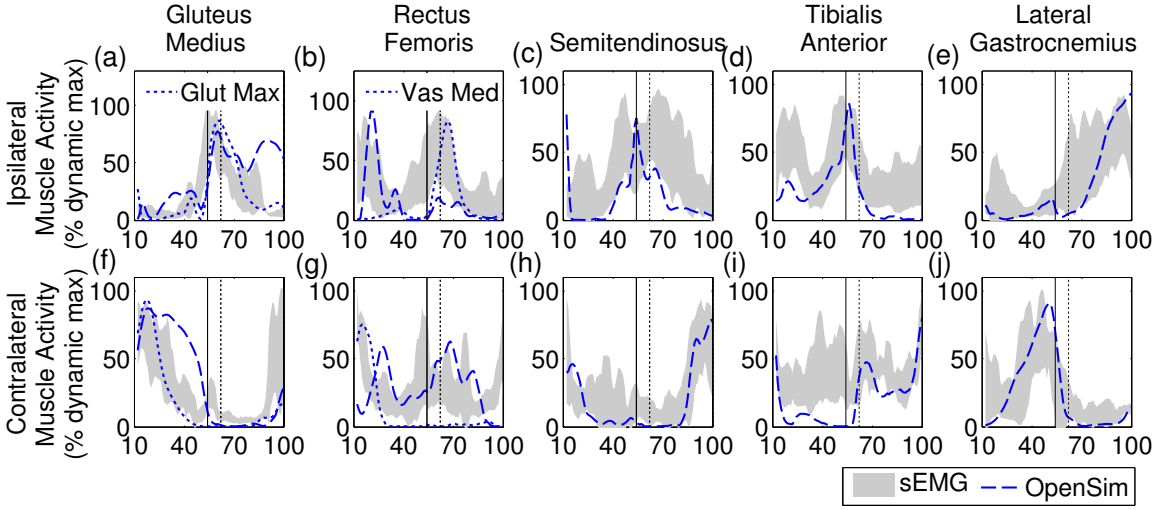

Figure 8.13 – Ipsilateral and contralateral muscle activity for spin turn (12–100% of the gait cycle). Solid (ipsilateral foot-strike) and dotted (contralateral foot-off) vertical lines as well as mean simulated (OpenSim) and standard deviation of surface electromyographic (sEMG) data shown. For (a) and (b) gluteus maximus (Glut Max) and vastus medialis (Vas Med) activity from OpenSim, respectively, also shown.

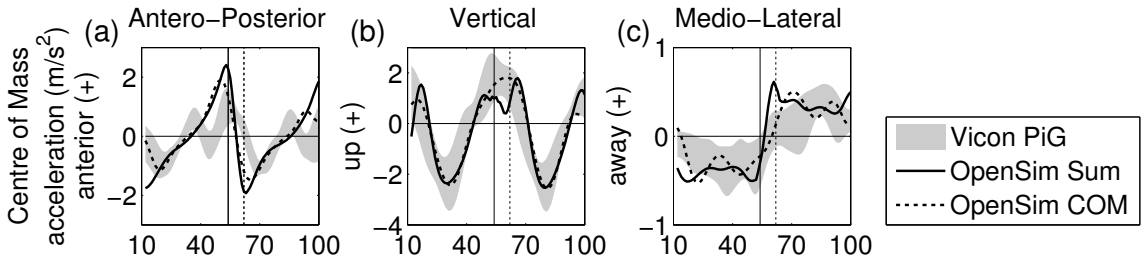

Figure 8.14 – Centre of mass (COM) acceleration for straight walking (12–100% of the gait cycle). Solid (ipsilateral foot-strike) and dotted (contralateral foot-off) vertical lines as well as mean sum of all muscle accelerations (OpenSim Sum), second derivative of COM position from simulations (OpenSim COM), and standard deviation of second derivative of Plug-in Gait model COM position (Vicon PiG) shown.

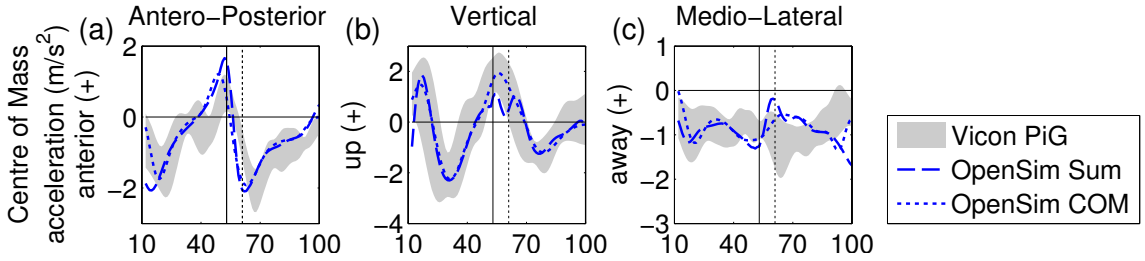

Figure 8.15 – Centre of mass (COM) acceleration for spin turns (12–100% of the gait cycle). Solid (ipsilateral foot-strike) and dotted (contralateral foot-off) vertical lines as well mean sum of all muscle accelerations (OpenSim Sum), second derivative of COM position from simulations (OpenSim COM), and standard deviation of second derivative of Plug-in Gait model COM position (Vicon PiG) shown.

8.4 Results

8.4.1 Centre of mass acceleration

The main contributors to COM acceleration during straight walking and turning accurately reproduced the total COM acceleration signal (Fig. 8.16). During the approach phase, the medio-lateral COM acceleration towards the Ipsi side (towards the turn centre) was increased during turning (-0.93 m/s^2) compared to straight walking (-0.34 m/s^2) ($p < 0.001$ and $d = 2.29$) (Fig. 8.17 a). During the turn phase, the COM continued to be accelerated towards the Ipsi side for spin turns (-0.88 m/s^2), but shifted towards the Contra side (away from the turn centre) for straight walking (0.36 m/s^2) ($p < 0.001$ and $\Delta = 8.60$) (Fig. 8.17 b).

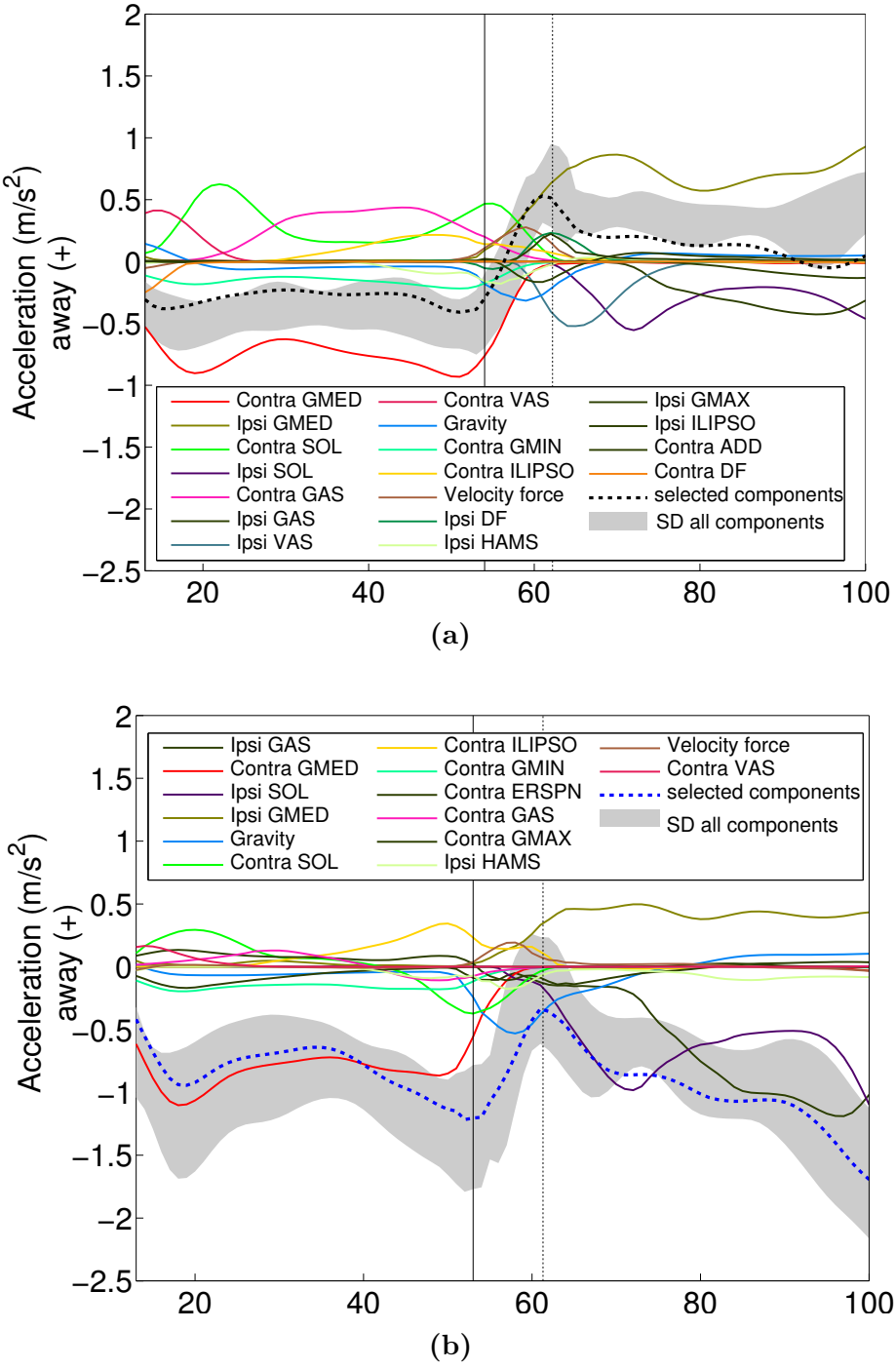

Figure 8.16 – Main contributors to medio-lateral COM acceleration (12–100% of the gait cycle) for (a) straight and (b) spin turns with solid and dashed vertical lines at ipsilateral (Ipsi) foot-strike and contralateral (Contra) foot-off, respectively. Standard deviation (SD) of all components as well as summed acceleration from selected components also shown. See Table 8.3 for muscle abbreviations.

8.4.2 Contributors to centre of mass acceleration

For the approach phase of straight walking and turning, 10 muscles, gravity, and velocity-related forces accounted for 95% of the overall variability in the COM medio-lateral acceleration pattern (Table 8.4). For straight walking, the main contributors were Contra GMED (25.3%), Contra GAS (15.7%), Contra SOL (14.3%), Contra VAS (9.6%), Ipsi GMED (9.1%), and gravity (5.9%).

For the approach phase of spin turns, it was Contra GMED (40.0%), Contra SOL (21.5%), gravity (12.4%), and Contra ILIPSO (6.3%) that were most important. Contributions to COM acceleration towards the Contra side (away from the turn centre) were reduced during spin turns for Contra GAS (0.23 vs 0.02 m/s^2, $p < 0.001$, and $d = 2.40$), Contra SOL (0.29 vs 0.01 m/s^2, $p < 0.001$, and $d = 2.16$), and Contra VAS (0.06 vs 0.03 m/s^2, $p = 0.002$, and $d = 1.02$), while contribution towards the Ipsi side (towards the turn centre) was increased for gravity (-0.07 vs -0.12 m/s^2, $p < 0.001$, and $d = 1.64$), compared to straight walking (Fig. 8.17 a).

For the turn phase, both conditions showed that a reduced number of components were required to account for 95% of the variability in the medio-lateral COM acceleration signal (Table 8.4). For straight walking, 8 muscles and gravity were required, with Ipsi VAS (31.7%), Ipsi GAS (23.3%), Ipsi SOL (16.0%), and Ipsi GMED (9.6%) identified as the main contributors. For turning, only 3 muscles and gravity accounted for most of the variability. Of these, Ipsi GAS (65.2%), Ipsi SOL (20.4%), and gravity (7.3%) each accounted for at least 5% of the variance. Contribution to COM acceleration towards the Contra side (away from the turn centre) was reduced during spin turns for Ipsi GMED (0.73 vs 0.43 m/s^2, $p < 0.001$, and $d = 2.36$), while acceleration towards the Ipsi side (towards the turn centre) was increased for Ipsi GAS (-0.23 vs -0.68 m/s^2, $p < 0.001$, and $\Delta = 4.51$) and Ipsi SOL (-0.30 vs -0.66 m/s^2, $p = 0.013$, and $\Delta = 6.00$), compared to straight walking (Fig. 8.17 b).

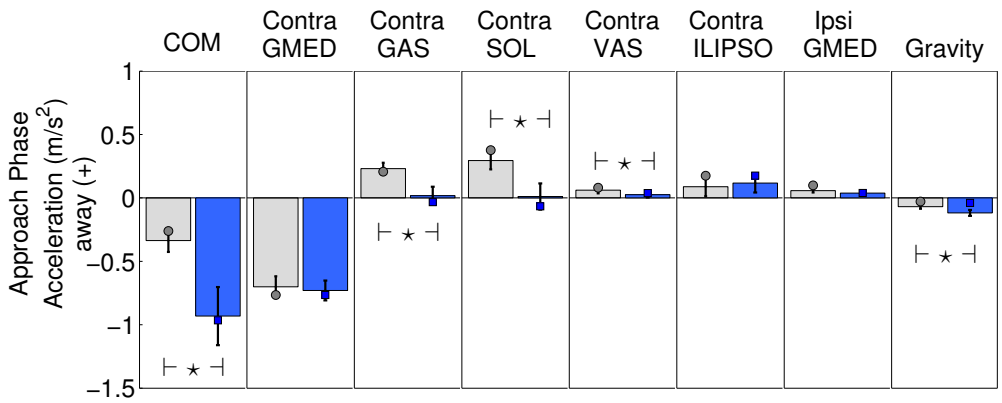

(a)

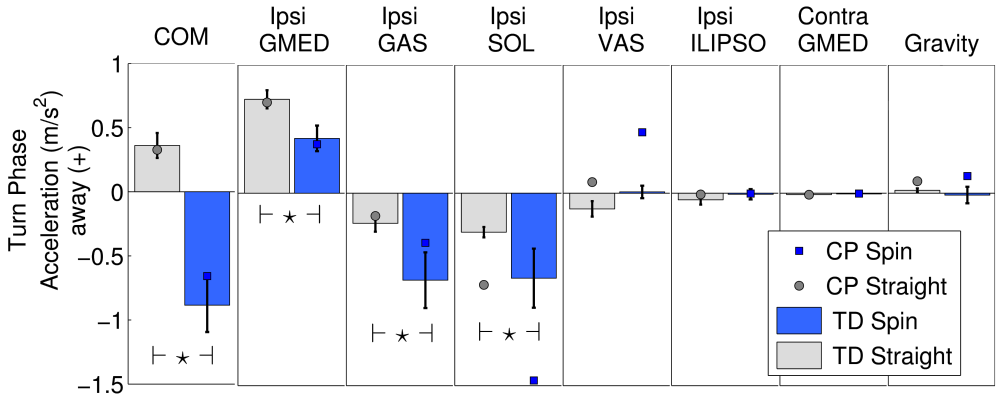

(b)

Figure 8.17 – Average medio-lateral acceleration of the centre of mass (COM) and contributions from major muscle groups and gravity across condition for the (a) approach and (b) depart phase. During the approach, the contralateral (Contra) and the ipsilateral (Ipsi) limbs are in stance and swing, respectively. During the turn, Ipsi and Contra limbs are in stance and swing, respectively. Significant difference between conditions ($\star$) as well as data for one child with CP also shown. Ipsi ILIPSO and Contra GMED not major contributors during the turn phase, but shown for completion. See Table 8.3 for muscle abbreviations.

8.4.3 Case study

The child with CP showed similar overall medio-lateral COM acceleration and similar contributions from the main muscles and gravity compared to his TD peers during the approach phase (all differences $\leqslant 0.09$ m/s^2) (Fig. 8.17 a). During the turn phase, differences were more pronounced (Fig. 8.17 b). He was unable to accelerate his COM towards the turn centre as much as his TD peers (-0.66 vs -0.88 m/s^2). This overall

decrease arose from an Ipsi VAS that tended to accelerate the COM away from the turn centre (0.48 m/s^2) and a decrease in Ipsi GAS contribution towards the turn centre (-0.39 vs -0.68 m/s^2) despite a large increase in Ipsi SOL contribution towards the turn centre (-1.46 vs -0.66 m/s^2), compared to his TD peers. Differences from the mean TD data were larger during the turn than during straight walking for the overall COM (0.23 vs 0.03 m/s^2), Ipsi GAS (0.29 vs 0.06 m/s^2), Ipsi SOL (0.80 vs 0.41 m/s^2), Ipsi VAS (0.47 vs 0.21 m/s^2), and gravity (0.15 vs 0.07 m/s^2).

8.5 Discussion

The purpose of this study was to determine the role of muscles, gravity and velocity-related forces in the control and redirection of the COM during turning. A dynamic simulation of gait and an induced acceleration analysis revealed that TD children mainly modulate hip abductor (GMED) and ankle plantarflexor (SOL and GAS) contributions to control medio-lateral COM acceleration during turning gait. Significant changes in COM acceleration contribution during the approach and turn phase are summarized diagrammatically (Figs. 8.18 a and b, respectively).

(a) **(b)**

Figure 8.18 – Diagrammatic representation of significant increases (red) and decreases (blue) to muscle medio-lateral centre of mass acceleration contributions during the (a) approach and (b) turn phase of spin turns, compared to straight walking.

8.5.1 Control of centre of mass acceleration

The results for the overall COM medio-lateral acceleration during straight walking are comparable to previous studies. For straight walking, the medio-lateral COM position presents a sinusoidal pattern that oscillates at the stride frequency rate and is directed towards the stance limb [122]. This motion results in an acceleration pattern that tends to pull the COM back towards the body midline with each step [124, 167]. In terms of the reference system of this study (Fig. 8.1), first towards the Ipsi side (towards the turn centre) and then towards the Contra side (away from the turn centre) over the gait cycle (Fig. 8.16). Contributors to medio-lateral COM acceleration presented here agree with previous investigators: hip abductors and ankle plantarflexors contribute to and oppose the COM acceleration, respectively [124, 167].

For turning, two hypotheses were proposed for each phase of the movement. For the approach phase, it was posited that Contra hip abductors would increase contribution towards the Ipsi side (towards the turn centre) while Contra ankle plantarflexors would switch from an opposing (towards the Contra side or away from the turn centre) to a supporting (towards the Ipsi side/turn centre) acceleration contribution, compared to straight walking. These hypotheses were not confirmed. Instead, Contra GMED contributions remained similar to straight walking, resulting in an increased acceleration of the COM towards the turn centre only via a reduction of Contra GAS and Contra SOL contribution to acceleration away from the turn. In other words, turning appears to be initiated only by a reduction in muscle contribution, possibly representing a more efficient use of muscles than the paradigm proposed. For the turn phase, the hypotheses were confirmed: Ipsi GMED contribution to acceleration towards the Contra side (away from the turn) was reduced, while Ipsi GAS and Ipsi SOL acceleration contributions towards the Ipsi side/turn centre were increased, compared to straight walking. The Ipsi GMED contribution to acceleration away

from the turn centre may be sustained to avoid a large increase in hip adduction angle and maintain pelvis stability during turning [105], regardless of its opposition to the task criteria of accelerating the COM towards the turn centre. The increased contribution of Ipsi GAS and Ipsi SOL may also have helped to reaccelerate the COM in the forward direction after the reduction in gait speed that occurs during turning (see Chapter 4); however, similar ankle push-off power generation across tasks would suggest that this may not be the case (see Chapter 5).

Previous turning gait studies with a focus on COM kinematics have mainly been descriptive. In the early work of Patla et al. [171], redirection of the COM position was attributed to changes in foot placement and trunk motion, but how subjects modulated muscle activity to achieve these new postures remained unclear. Later, Xu et al. [250] found that the COM to centre of pressure distance was modulated in an anticipatory fashion as a way to"initiate the disequilibrium necessary to produce the turn". Here, using an induced acceleration analysis, not only were anticipatory effects noted (change in overall COM acceleration during the approach phase), but the muscles responsible could also be identified and their contributions quantified.

8.5.2 Clinical applications

Recent work has revealed that the path of the COM could discriminate between children with CP and their TD peers [186] and that tangential COM velocity was decreased in Parkinsonian patients compared to age matched healthy controls [19]. These studies suggest that further knowledge about COM control during turning via simulation might be of clinical relevance. Thus far simulation studies in clinical populations have been limited to straight walking protocols [10, 216, 217].

Here, a dynamic simulation was performed to compare the contributors to COM acceleration during straight walking and a right spin turn for one child with CP presenting

with fixed knee flexion and ankle equinus contractures on the right side. In agreement with the third hypothesis, amplified deviations from normative patterns during turning compared to straight walking seem to be related to existing musculo-skeletal abnormalities. Ipsi VAS and Ipsi SOL showed over contribution to acceleration away from and towards the turn centre, respectively. It appears that the increased Ipsi SOL contribution was necessary to overcome the detrimental contribution of Ipsi VAS. Possibly, increased activity of the major knee extensors to accommodate a more flexed gait pattern had an unintended consequence of hindering turn progression. Note that automatically chosen representative trial for this subject in the kinematic and kinetic studies of Chapters 6 and 7, respectively, was a left spin turn.

The current analysis has the potential to supplement traditional evaluation, most notably in cases in which recommendations for surgery based on straight walking may be unclear. Further work in a larger group of children with CP is necessary to determine if turning adaptations can be well predicted based on known gait deviations.

8.5.3 Limitations and other considerations

The results suggest that the majority of the medio-lateral acceleration required to turn occurs during the approach phase (total COM acceleration of -0.93 and -0.88 m/s^2 for the approach and turn phase, respectively) (Fig. 8.17); however, it is likely that additional acceleration is gained during Ipsi pre-swing via the ankle plantarflexor push-off power generation burst. Unfortunately, it was not possible to record this information given the experimental set-up. The use of force plates positioned along the turning path or methods in which force plate data can be simulated [78] might allow for investigation of the complete turning cycle, including the depart step. Another limitation may relate to the preference of implementing a SO algorithm over a dynamic optimization approach, but given agreement between the experimental

and simulated muscle activations and previous studies suggesting only minimal improvement using dynamic optimization [9], results appear reliable. The rolling constraint of the foot-ground contact model used in the induced acceleration analysis does not allow for twisting of the foot about the global vertical axis [103]. Nonetheless, the rolling constraint was favoured since in Section 5.3.2 peak torques during spin turns, although increased, were of a similar order of magnitude to those experienced during straight walking (78.9 vs 56.0 Nmm/kg) and other models (point and weld constraint) have been shown to less adequately reproduce experimental GRFs leading to possible misleading acceleration contributions [103]. Moreover, analyses of the antero-posterior and vertical COM acceleration were not conducted. Visualization of the overall COM accelerations in these planes showed only minor differences across conditions (Fig. 8.2) suggesting that they are secondary to the more important medio-lateral changes described herein.

For the case study, use of more realistic muscle properties and skeletal anatomy in the dynamic model as well as constrained muscle activations [217] may have improved the reliability of findings. Here, it was simply shown that simulation of turning gait in children with CP is feasible and may provide useful information for clinical management of gait in this population. Further investigations are certainly warranted.

Chapter 9

Conclusions

The main aims of this thesis were to quantify the biomechanical adaptations of 90° turning gait in typically developing (TD) children and to determine if the implementation of this task in clinical gait analysis could benefit the management of gait in children with cerebral palsy (CP). The analyses showed that kinematic, kinetic, and muscular contribution differences exist between turning gait and straight walking in TD children and that for some of these metrics, deviations become more pronounced during turning gait than in straight walking for children with CP.

Novel or untraditional approaches implemented to obtain the above results should be highlighted. First, the use of the Bootstrap method to estimate variability and conduct statistical analysis, allowing for difference to be obtained over the entire turning cycle, represents a substantial improvement over standard discrete time point approaches and is rather rare in biomechanics. Second, identifying turning strategies via pelvis movement is novel and likely more reliable than simple visual assessment and more robust than existing approaches. Finally, to the knowledge of the author, this is the first study to compare both 90° turning strategies over the three turning phases in any population as well as the only study to quantify the contributors to centre of mass (COM) acceleration during 90° spin turns via simulation.

9.1 Turning Gait in Typically Developing Children

The results of Chapters 4 and 5 suggest that TD children turn in a similar manner to healthy adults: they progress through the turn in three distinct phases (approach, turn, and depart) [88] and adopt the two main strategies (step and spin) [105].

Turning gait is characterized by a decrease in gait speed and stride length as well as an increase in stance time, compared to straight walking. For spin turns, the inside hip, with respect to turn centre, increases adduction and internal rotation while the ankle everts and the forefoot reduces supination during the turn phase. At this time, the outside hip adductor and external rotator moments increase. The simulation study of Chapter 8 reveals that the outside ankle plantarflexor muscle contribution to COM acceleration away from the turn centre is reduced during the approach phase allowing the turn to be initiated. Afterwards, contributions to acceleration away from the turn centre by inside limb hip abductor decreases while contribution towards the turn centre by the ankle plantarflexors increase, further accelerating the COM towards the new walking direction. For step turns, mirror-like kinematic and kinetic adaptations occur as the main turn phase is performed about the outside leg. The outside hip increases hip abduction and external rotation while the ankle and forefoot increase inversion and supination, respectively. Moreover, the inside hip reveals increased abductor and internal rotator moments. These adaptations can be regarded as strategy dependent; however, taking the non-traditional view of considering the step turn as two smaller spin turns (approach and depart phase) separated by rotation about the outside limb (turn phase) reveals that each limb performs a similar function on a step-by-step basis. It is plausible that some of the changes in muscle contributions revealed by the simulation study in spin turns might also apply to step turns. Nevertheless, as stability issues may underpin choice of strategy [225], unique muscular contributions to COM acceleration are expected across turn styles.

9.2 Turning Gait in Children with Cerebral Palsy

The analyses of turning gait in children with CP of Chapters 6 and 7 focus on the spin turn strategy as step turns were found to be a less popular choice in the current cohort. Of the quantities analysed, stride width, margin of stability, and ground reaction force impulse were best able to distinguish overall spin turn differences across groups. In the more relevant context of analysing turning gait for a specific child with CP, quantifying the relative change in a given metric compared to normative data, using either discrete events or curve data, appears to be most informative.

For the joint kinematics, amplified differences during spin turns were identified in most children with CP for maximum hip internal rotation, knee sagittal plane angle at foot-strike and terminal stance, and ankle sagittal angle at foot-strike. Analysis of the analogous gait curves as well as the overall curves via the Turning Profile Score also revealed differences for most children with CP. For the joint kinetics, maximum ankle plantarflexor moment and power, knee rotator moment, hip abductor moment during swing approach and depart, as well as hip rotator moment during swing depart were more different for most children with CP during spin turns compared to straight walking and their TD peers. The analogous continuous measures all showed larger differences during turning for most children with CP, except for hip rotation. The continuous knee valgus angle also identified most children with CP as having more abnormal gait during turning.

9.3 Clinical Recommendations

The results of this thesis suggest that for many parameters turning gait may be more sensitive to gait deviations than straight walking for children with CP. Clinical gait analysis of turning gait in this population should focus on measures which change

disproportionately or are greatly amplified across conditions compared to TD children. Although these metrics may vary based on the specific gait abnormalities present in a given child with CP, the quantities identified herein may serve as a general starting point for analysis. It is not recommended that turning gait replace straight walking analysis, but rather, that it may be used additionally when straight walking reveals only small differences in gait parameters (rendering clinical decision-making difficult), despite a child's reported difficulty during community or home based walking.

9.4 Future Directions

The main categories of gait metrics explored in this thesis could be used to further analyse turning gait. Of these, spatio-temporal parameters (STPs) are convenient since they can be collected using a number of different technologies and show relatively large differences across conditions. Future studies investigating how STPs change with turn angle and gait speed could reveal the full spectrum of changes required to modulate between straight walking and various turning gaits. Also, although this thesis focuses on lower-limb and intra-foot kinematics, knowledge of upper-body movements, coordination, and sequencing of changes, may provide further insights into the mechanics of turning gait. Furthermore, due to the limitations of the experimental set-up, it was not possible to analyse joint kinetics over the entire turning cycle, leaving some kinetic adaptations unexplored. Future studies should also strive to develop new metrics that could quantify turning ability, allowing researchers and clinicians to identify people at risk of falls, guide treatment decisions, and gauge improvements after interventions. Moreover, determining if turning gait measures relate better to motor function scores than straight walking metrics would benefit clinical practice. Finally, simulation of turning gait and other tasks in clinical gait analysis is a promising field that warrants further investigation.

Appendix A

Derivations and Further Notes

A.1 Dynamic Stability

The second order non-homogeneous linear differential equation presented in Section 6.2.7 (Eq. 6.7) is solved here:

$$\ddot{x} - \omega_0^2 x = -\omega_0^2 p_x \tag{A.1}$$

First, the corresponding homogeneous equation must be solved:

$$\ddot{x} - \omega_0^2 x = 0 \tag{A.2}$$

Based on the form of Eq. A.2, the following solutions can be attempted:

$$x_1 = \cosh(\omega_0 t) \tag{A.3}$$

$$x_2 = \sinh(\omega_0 t) \tag{A.4}$$

$$\text{where } \cosh = \frac{1}{2}(e^t + e^{-t}) \text{ and } \sinh = \frac{1}{2}(e^t - e^{-t})$$

Eq. A.2 is correctly solved by x_1 and its second derivative $\ddot{x_1} = \omega_0^2 \cosh(\omega_0 t)$:

$$\omega_0^2 \cosh(\omega_0 t) - \omega_0^2 \cosh(\omega_0 t) = 0 \tag{A.5}$$

Similarly, it can be shown that x_2 also provides a correct solution. As both x_1 and x_2 are solutions to Eq. A.2 and neither is a constant multiple of the other, then the

complementary solution is [140, Theorem 15.4]:

$$x_c = A\cosh(\omega_0 t) + B\sinh(\omega_0 t) = 0 \tag{A.6}$$

The particular solution can be found using the method of undetermined coefficients. Based on the form of Eq. A.1 a constant solution is attempted:

$$x_p = C \tag{A.7}$$

Substituting x_p and its second derivative (0) into Eq. A.1 solves for C:

$$0 - \omega_0^2 C = -\omega_o^2 p_x \tag{A.8}$$

$$C = p_x \tag{A.9}$$

The general solution can then be expressed as [140, Theorem 15.6]:

$$x = x_c + x_p \tag{A.10}$$

$$x = A\cosh(\omega_0 t) + B\sinh(\omega_0 t) + p_x \tag{A.11}$$

Finally, coefficients A and B can be determined from the boundary conditions. The first boundary condition $x(0) = x_0$ provides a solution for A:

$$x(0) = A\cosh(0) + B\sinh(0) + p_x = x_0 \tag{A.12}$$

$$A + p_x = x_0 \tag{A.13}$$

$$A = x_0 - p_x \tag{A.14}$$

B is solved via the second boundary condition $\dot{x}(0) = v_0 x$ in a similar way:

$$\dot{x}(0) = A\sinh(\omega_0 t) + \omega_0 B\cosh(\omega_0 t) = v_0 x \tag{A.15}$$

$$A\sinh(0) + \omega_0 B\cosh(\omega_0 t) = v_0 x \tag{A.16}$$

$$B\omega_0 = v_0 x \tag{A.17}$$

$$B = \frac{v_0 x}{\omega_0} \tag{A.18}$$

Plugging in the values for A and B gives the correct solution (Eq. 6.8):

$$x(t) = p_x + (x_0 - p_x)\cosh(\omega_0 t) + \frac{v_{0x}}{\omega_0}\sinh(\omega_0 t) \tag{A.19}$$

A.2 Graphing of a Full Gait Cycle

Data for the simulation study of Chapter 8 were analysed over a partial gait cycle, given the limitations of the experimental set-up. Therefore, as described in Section 8.2.3, in order to represent a complete gait cycle for straight walking, portions from each limb were merged together. The second part of the gait cycle (13–100%) was obtained from the limb in contact with the first force plate, while the first portion (0–12%) was extracted from the limb striking the 2nd force plate. This resulted in a complete gait cycle with a discontinuity at the merger point. Visualization of the frequency spectrum for the sagittal plane knee angle for a random trial (Fig. A.1 a) suggested that a filter with a cut-off frequency of 5 Hz would smooth out the discontinuity artefact. Application of a fourth-order zero-lag Butterworth filter with the chosen cut-off frequency resulted in a smooth merger point with little degradation of the original signal (Fig. A.1 b).

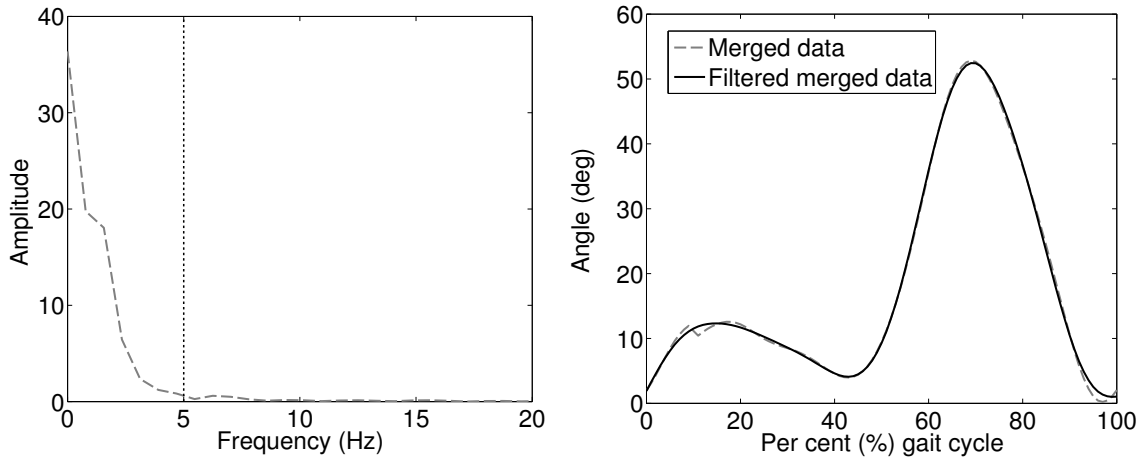

Figure A.1 – Demonstration of the merging of sides for graphing of straight walking simulation over a full gait cycle (0–100%) via the sagittal knee angle graph (a) frequency spectrum of signal with dotted vertical line showing chosen cut-off frequency (5 Hz) and (b) original and filtered merged data.

Bibliography

[1] Abbas G., Taylor M.J., Diss C., and Mostofi S.B. The biomechanical differences in turning gait with and without ankle brace. In *Proc. of the British Orthopaedic Association conference*. Liverpool, UK. Sep 16–19th, 2008.

[2] Adams J.M. and Perry J. *Gait analysis: Clinical decision making*, chapter 10. In Rose J. and Gamble J.G., editors, Human Walking. 3rd edition. Lippincott Williams & Wilkins, Philadelphia, USA, 2006.

[3] Akram S.B., Frank J.S., and Chenouri S. Turning behavior in healthy older adults: Is there a preference for step versus spin turns? *Gait Posture*, 31(1):23–6, 2010.

[4] Akram S.B., Frank J.S., and Fraser J. Effect of walking velocity on segment coordination during pre-planned turns in healthy older adults. *Gait Posture*, 32(2):211–4, 2010.

[5] Alaqtash M., Sarkodie-Gyan T., Yu H.Y., Fuentes O., Brower R., and Abdelgawad A. Automatic classification of pathological gait patterns using ground reaction forces and machine learning algorithms. In *Proc. of the 33rd IEEE Eng Med Biol Soc conference*. Boston, USA. Aug 30–Sep 3rd. 2011.

[6] Almosnino S., Kajaks T., and Costigan P.A. The free moment in walking and its change with foot rotation angle. *Sports Med Arthrosc Rehabil Ther Technol*, 1(1):19, 2009.

[7] Anderson F.C. *A dynamic optimization solution for a complete cycle of normal gait: An analysis of muscle functon and joint contact force.* Ph.D. Thesis, University of Texas at Austin, 1999.

[8] Anderson F.C. and Pandy M.G. A dynamic optimization solution for vertical jumping in three dimensions. *Comput Methods Biomech Biomed Engin*, 2(3):201–31, 1999.

[9] Anderson F.C. and Pandy M.G. Static and dynamic optimization solutions for gait are practically equivalent. *J Biomech*, 34(2):153–61, 2001.

[10] Arnold A.S., Liu M.Q., Schwartz M.H., Ounpuu S., and Delp S.L. The role of estimating muscle-tendon lengths and velocities of the hamstrings in the evaluation and treatment of crouch gait. *Gait Posture*, 23(3):273–81, 2006.

[11] Ayalon M., Ben-Sira D., Hutzler Y., and Gilad T. Reliability of isokinetic strength measurements of the knee in children with cerebral palsy. *Dev Med Child Neurol*, 42(6):398–402, 2000.

[12] Bacon-Shone V. and Bacon-Shone J. Gait of normal Hong Kong Chinese children: The Bootstrap approach. *Hong Kong Physiother J*, 18(1):21–5, 2000.

[13] Baker R., Finney L., and Orr J. A new approach to determine the hip rotation profile from clinical gait analysis data. *Hum Mov Sci*, 18(5):655–67, 1999.

[14] Baker R., McGinley J.L., Schwartz M.H., Beynon S., Rozumalski A., Graham H.K., and Tirosh O. The Gait Profile Score and Movement Analysis Profile. *Gait Posture*, 30(3):265–9, 2009.

[15] Barre A. and Armand S. Biomechanical toolkit: Open-source framework to visualize and process biomechanical data. *Comput Meth Prog Bio*, 114(1):80–7, 2014.

[16] Becher J.G. Pediatric rehabilitation in children with cerebral palsy: General management, classification of motor disorders. *J Prosthet Orthot*, 14(4):143–9, 2002.

[17] Beltran E.J., Dingwell J.B., and Wilken J.M. Margins of stability in young adults with traumatic transtibial amputation walking in destabilizing environments. *J Biomech*, 47(5):1138–43, 2014.

[18] Berg K.O., Wood-Dauphinee S.L., Williams J.I., and Maki B. Measuring balance in the elderly: Validation of an instrument. *Can J Public Health*, 83 Suppl 2:S7–11, 1992.

[19] Bhatt H., Pieruccini-Faria F., and Almeida Q.J. Dynamics of turning sharpness influences freezing of gait in Parkinson's disease. *Parkinsonism Relat Disord*, 19(2):181–5, 2013.

[20] Bickel O.J. and Freedman D.A. Asymptotic normality and the Bootstrap in stratified sampling. *Ann Stat*, 12(2):470–82, 1984.

[21] Boakes J.L. and Rab G.T. *Muscle activity during walking*, chapter 6. In Rose J. and Gamble J.G., editors, Human Walking. 3rd edition. Lippincott Williams & Wilkins, Philadelphia, USA, 2006.

[22] Bogey R.A., Perry J., and Gitter A.J. An EMG-to-force processing approach for determining ankle muscle forces during normal human gait. *IEEE Trans Neural Syst Rehabil Eng*, 13(3):302–10, 2005.

[23] Boyce W.F., Gowland C., Hardy S., Rosenbaum P.L., Lane M., Plews N., Goldsmith C., and Russell D.J. Development of a quality-of-movement measure for children with cerebral-palsy. *Phys Ther*, 71(11):820–32, 1991.

[24] Bracha H.S., Seitz D.J., Otemaa J., and Glick S.D. Rotational movement (circling) in normal humans: Sex difference and relationship to hand, foot and eye preference. *Brain Res*, 411(2):231–5, 1987.

[25] Brand R.A., Crowninshield R.D., Wittstock C.E., Pedersen D.R., Clark C.R., and van Krieken F.M. A model of lower extremity muscular anatomy. *J Biomech Eng*, 104(4):304–10, 1982.

[26] Brand R.A. and Pedersen D.R. Computer modeling of surgery and a consideration of the mechanical effects of proximal femoral osteotomies. In Welch R.W., editor, The Hip. C.V. Mosby, St. Louis, USA. 1984.

[27] Brégou-Bourgeois A., Mariani B., Aminian K., Zambelli P.Y., and Newman C.J. Spatio-temporal gait analysis in children with cerebral palsy using, foot-worn inertial sensors. *Gait Posture*, 39(1):436–42, 2014.

[28] Bruening D.A., Cooney K.M., and Buczek F.L. Analysis of a kinetic multi-segment foot model part II: Kinetics and clinical implications. *Gait Posture*, 35(4):535–40, 2012.

[29] Bruening D.A. and Ridge S.T. Automated event detection algorithms in pathological gait. *Gait Posture*, 39(1):472–7, 2014.

[30] Bruijn S.M., Meijer O.G., Beek P.J., and van Dieen J.H. Assessing the stability of human locomotion: A review of current measures. *J R Soc Interface*, 10(83):1–23, 2013.

[31] Bruijn S.M., Millard M., van Gestel L., Meyns P., Jonkers I., and Desloovere K. Gait stability in children with cerebral palsy. *Res Dev Disabil*, 34(5):1689–99, 2013.

[32] Caderby T., Yiou E., Peyrot N., Begon M., and Dalleau G. Influence of gait speed on the control of mediolateral dynamic stability during gait initiation. *J Biomech*, 47(2):417–23, 2014.

[33] Cao C., Ashton-Miller J.A., Schultz A.B., and Alexander N.B. Abilities to turn suddenly while walking: Effects of age, gender, and available response time. *J Gerontol A Biol Sci Med Sci*, 52(2):M88–93, 1997.

[34] Carhart M.R. *Biomechanical analysis of compensatory stepping: Implications for paraplegics standing Via FNS*. Ph.D. Thesis, Arizona State University, 2000.

[35] Carpenter J. and Bithell J. Bootstrap confidence intervals: When, which, what? A practical guide for medical statisticians. *Stat Med*, 19(9):1141–64, 2000.

[36] Carriero A., Zavatsky A.B., Stebbins J., Theologis T., and Shefelbine S.J. Determination of gait patterns in children with spastic diplegic cerebral palsy using principal components. *Gait Posture*, 29(1):71–5, 2009.

[37] Carson M.C., Harrington M.E., Thompson N., O'Connor J.J., and Theologis T. Kinematic analysis of a multi-segment foot model for research and clinical applications: A repeatability analysis. *J Biomech*, 34(10):1299–307, 2001.

[38] Cavagna G.A., Thys H., and Zamboni A. The sources of external work in level walking and running. *J Physiol*, 262(3):639–57, 1976.

[39] Challis J.H. Producing physiologically realistic individual muscle force estimations by imposing constraints when using optimization techniques. *Med Eng Phys*, 19(3):253–61, 1997.

[40] Chang W.N., Lipton J.S., Tsirikos A.I., and Miller F. Kinesiological surface electromyography in normal children: Range of normal activity and pattern analysis. *J Electromyogr Kinesiol*, 17(4):437–45, 2007.

[41] Chao E.Y.S. Justification of triaxial goniometer for the measurement of joint rotation. *J Biomech*, 13(12):989–1006, 1980.

[42] Chau T., Young S., and Redekop S. Managing variability in the summary and comparison of gait data. *J Neuroeng Rehabil*, 2:22, 2005.

[43] Chen I.H., Yang Y.R., Chan R.C., and Wang R.Y. Turning-based treadmill training improves turning performance and gait symmetry after stroke. *Neurorehabil Neural Repair*, 28(1):45–55, 2014.

[44] Chernick M.R. *Bootstrap methods: A guide for practitioners and researchers*. Wiley, Hoboken, USA, 2nd edition, 2008.

[45] Chow J.W. Transverse plane moments and ranges of motion of the lower extremity during walking and turning in unilateral total knee replacement individuals. In *Proc. of the 21st International Society of Biomechanics conference*. Taipei, Taiwan. Jul 1–5th, 2007.

[46] Cohen J. *Statistical power analysis for the behavioral sciences*. L. Erlbaum Associates, Hillsdale, USA, 2nd edition, 1988.

[47] Courtine G. and Schieppati M. Human walking along a curved path. I. Body trajectory, segment orientation and the effect of vision. *Eur J Neurosci*, 18(1):177–90, 2003.

[48] Courtine G. and Schieppati M. Human walking along a curved path. II. Gait features and EMG patterns. *Eur J Neurosci*, 18(1):191–205, 2003.

[49] Crowninshield R.D. and Brand R.A. A physiologically based criterion of muscle force prediction in locomotion. *J Biomech*, 14(11):793–801, 1981.

[50] Cumming R.G. and Klineberg R.J. Fall frequency and characteristics and the risk of hip fractures. *J Am Geriatr Soc*, 42(7):774–8, 1994.

[51] Curtis D.J., Bencke J., Stebbins J., and Stansfield B. Intra-rater repeatability of the Oxford Foot Model in healthy children in different stages of the foot roll over process during gait. *Gait Posture*, 30(1):118–21, 2009.

[52] Damiano D.L., Arnold A.S., Steele K.M., and Delp S.L. Can strength training predictably improve gait kinematics? A pilot study on the effects of hip and knee extensor strengthening on lower-extremity alignment in cerebral palsy. *Phys Ther*, 90(2):269–79, 2010.

[53] Davis R.B. and Kaufman K.R. *Kinetics of human walking*, chapter 4. In Rose J. and Gamble J.G., editors, Human Walking. 3rd edition. Lippincott Williams & Wilkins, Philadelphia, USA, 2006.

[54] Davis R.B., Ounpuu S., Tyburski D., and Gage J.R. A gait analysis data-collection and reduction technique. *Hum Mov Sci*, 10(5):575–87, 1991.

[55] Delp S.L. *A computer-graphics system to analyze and design musculoskeletal reconstructions of the lower limb*. Ph.D. Thesis, Stanford University, 1990.

[56] Delp S.L., Anderson F.C., Arnold A.S., Loan P., Habib A., John C.T., Guendelman E., and Thelen D.G. OpenSim: Open-source software to create and analyze dynamic simulations of movement. *IEEE Trans Biomed Eng*, 54(11):1940–50, 2007.

[57] Delp S.L., Loan J.P., Hoy M.G., Zajac F.E., Topp E.L., and Rosen J.M. An interactive graphics-based model of the lower extremity to study orthopaedic surgical procedures. *IEEE Trans Biomed Eng*, 37(8):757–67, 1990.

[58] Desailly E., Daniel Y., Sardain P., and Lacouture P. Foot contact event detection using kinematic data in cerebral palsy children and normal adults gait. *Gait Posture*, 29(1):76–80, 2009.

[59] Desailly E., Khouri N., Sardain P., Yepremian D., and Lacouture P. Rectus femoris transfer and musculo-skeletal modeling: Effect of surgical treatment on gait and on rectus femoris kinematics. *Gait Posture*, 34(4):519–23, 2011.

[60] Deschamps K., Staes F., Roosen P., Nobels F., Desloovere K., Bruyninckx H., and Matricali G.A. Body of evidence supporting the clinical use of 3D multisegment foot models: A systematic review. *Gait Posture*, 33(3):338–49, 2011.

[61] Desloovere K., Wong P., Swings L., Callewaert B., Vandenneucker H., and Leardini A. Range of motion and repeatability of knee kinematics for 11 clinically relevant motor tasks. *Gait Posture*, 32(4):597–602, 2010.

[62] Dite W. Development of a clinical measure of turning for older adults. *Am J Phys Med Rehabil*, 81(11):857–66, 2002.

[63] Dixon P.C., Böhm H., and Döderlein L. Ankle and midfoot kinetics during normal gait: A multi-segment approach. *J Biomech*, 45(6):1011–6, 2012.

[64] Dixon P.C., Bowtell M.V., and Stebbins J. The use of regression and normalisation for the comparison of spatio-temporal gait data in children. *Gait Posture*, 40(4):521–5, 2014.

[65] Dixon P.C., Loh J.J., Michaud-Paquette Y., and Pearsall D.J. The Zoosystem: An open-source movement analysis Matlab toolbox. In *Proc. of the 23rd European Society for Movement Analysis in Adults and Children conference*. Rome, Italy. Sep 29–Oct 4th.

[66] Dixon P.C. and Pearsall D.J. Gait dynamics on a cross-slope walking surface. *J App Biomech*, 26(1):17–25, 2010.

[67] Dixon P.C., Stebbins J., Theologis T., and Zavatsky A.B. Kinetics of turning gait in typically developing children. In *Proc. of the 24th International Society of Biomechanics conference*. Natal, Brazil. Aug 4–9th, 2013.

[68] Dixon P.C., Stebbins J., Theologis T., and Zavatsky A.B. Spatio-temporal parameters and lower-limb kinematics of turning gait in typically developing children. *Gait Posture*, 38(4):870–5, 2013.

[69] Dixon P.C., Stebbins J., Theologis T., and Zavatsky A.B. Ground reaction forces and lower-limb joint kinetics of turning gait in typically developing children. *J Biomech*, 47(15):3726–33, 2014.

[70] Dorn T.W. Gait Extract Toolbox for Matlab, v1.71, 2008.

[71] Duhamel A., Bourriez J.L., Devos P., Krystkowiak P., Destee A., Derambure P., and Defebvre L. Statistical tools for clinical gait analysis. *Gait Posture*, 20(2):204–12, 2004.

[72] Efron B. Bootstrap methods: Another look at the Jackknife. *Ann Stat*, 7(1):1–26, 1979.

[73] Efron B. The length heuristic for simultaneous hypothesis tests. *Biometrika*, 84(1):143–57, 1997.

[74] Eng J.J. and Winter D.A. Kinetic-analysis of the lower-limbs during walking: What information can be gained from a 3-Dimensional model. *J Biomech*, 28(6):753–8, 1995.

[75] Feise R.J. Do multiple outcome measures require p-value adjustment? *BMC Med Res Methodol*, 2:8, 2002.

[76] Filho M.C., Yoshida R., Carvalho Wda S., Stein H.E., and Novo N.F. Are the recommendations from three-dimensional gait analysis associated with better postoperative outcomes in patients with cerebral palsy? *Gait Posture*, 28(2):316–22, 2008.

[77] Fischer O. Der Gang des Menschen (German). *Abhandlungen der Mathematisch-Physischen Classe der Königlich Sächsischen Gesellschaft der Wissenschaften*, 24(1):1–163, 1899.

[78] Fluit R., Andersen M.S., Kolk S., Verdonschot N., and Koopman H.F. Prediction of ground reaction forces and moments during various activities of daily living. *J Biomech*, 47(10):2321–9, 2014.

[79] Fox M.D. and Delp S.L. Contributions of muscles and passive dynamics to swing initiation over a range of walking speeds. *J Biomech*, 43(8):1450–5, 2010.

[80] Franzen E., Paquette C., Gurfinkel V.S., Cordo P.J., Nutt J.G., and Horak F.B. Reduced performance in balance, walking and turning tasks is associated with increased neck tone in Parkinson's disease. *Exp Neurol*, 219(2):430–8, 2009.

[81] Fuller J.R., Adkin A.L., and Vallis L.A. Strategies used by older adults to change travel direction. *Gait Posture*, 25(3):393–400, 2007.

[82] Gage J.R. Role of gait analysis in the treatment of cerebral-palsy. *J Pediatr Orthoped*, 14(6):701–2, 1994.

[83] Gan S.M., Tung L.C., Tang Y.H., and Wang C.H. Psychometric properties of functional balance assessment in children with cerebral palsy. *Neurorehabil Neural Repair*, 22(6):745–53, 2008.

[84] Gard S.A. and Childress D.S. What determines the vertical displacement of the body during normal walking. *J Prosthet Orthot*, 13(3):64–7, 2001.

[85] Gates D.H., Scott S.J., Wilken J.M., and Dingwell J.B. Frontal plane dynamic margins of stability in individuals with and without transtibial amputation walking on a loose rock surface. *Gait Posture*, 38(4):570–5, 2013.

[86] Gibbons J.D. *Nonparametric statistics*. SAGE Publications, Thousand Oaks, USA, 1993.

[87] Glaister B.C., Bernatz G.C., Klute G.K., and Orendurff M.S. Video task analysis of turning during activities of daily living. *Gait Posture*, 25(2):289–94, 2007.

[88] Glaister B.C., Orendurff M.S., Schoen J.A., Bernatz G.C., and Klute G.K. Ground reaction forces and impulses during a transient turning maneuver. *J Biomech*, 41(14):3090–3, 2008.

[89] Glaister B.C., Orendurff M.S., Schoen J.A., and Klute G.K. Rotating horizontal ground reaction forces to the body path of progression. *J Biomech*, 40(15):3527–32, 2007.

[90] Glaister B.C., Schoen J.A., Orendurff M.S., and Klute G.K. Mechanical behavior of the human ankle in the transverse plane while turning. *IEEE Trans Neural Syst Rehabil Eng*, 15(4):552–9, 2007.

[91] Glass G.V., McGraw B., and Smith M.L. *Meta-analysis in social research*. SAGE Publications, Thousand Oaks, USA, 1981.

[92] Glick S.D. and Cox R.D. Nocturnal rotation in normal rats: Correlation with amphetamine-induced rotation and effects of nigrostriatal lesions. *Brain Res*, 150(1):149–61, 1978.

[93] Glick S.D., Weaver L.M., and Meibach R.C. Amphetamine-induced rotation in normal cats. *Brain Res*, 208(1):227–9, 1981.

[94] Grasso R., Prevost P., Ivanenko Y.P., and Berthoz A. Eye-head coordination for the steering of locomotion in humans: An anticipatory synergy. *Neurosci Lett*, 253(2):115–8, 1998.

[95] Green L.B. and Hurvitz E.A. Cerebral palsy. *Phys Med Rehabil Clin N Am*, 18(4):859–82, 2007.

[96] Groen B.E., Geurts M., Nienhuis B., and Duysens J. Sensitivity of the OLGA and VCM models to erroneous marker placement: Effects on 3D-gait kinematics. *Gait Posture*, 35(3):517–21, 2012.

[97] Grood E.S. and Suntay W.J. A joint coordinate system for the clinical description of three-dimensional motions: Application to the knee. *J Biomech Eng*, 105(2):136–44, 1983.

[98] Guglielmetti S., Nardone A., De Nunzio A.M., Godi M., and Schieppati M. Walking along circular trajectories in Parkinson's disease. *Mov Disord*, 24(4):598–604, 2009.

[99] Hak L., van Dieen J.H., van der Wurff P., Prins M.R., Mert A., Beek P.J., and Houdijk H. Walking in an unstable environment: Strategies used by transtibial amputees to prevent falling during gait. *Arch. Phys. Med.*, 94(11):2186–93, 2013.

[100] Halliday D., Resnick R., and Walker J. *Fundamentals of physics*. John Wiley & Sons, New York, USA, 4th edition, 1993.

[101] Hamner S.R. and Delp S.L. Muscle contributions to fore-aft and vertical body mass center accelerations over a range of running speeds. *J Biomech*, 46(4):780–7, 2013.

[102] Hamner S.R., Seth A., and Delp S.L. Muscle contributions to propulsion and support during running. *J Biomech*, 43(14):2709–16, 2010.

[103] Hamner S.R., Seth A., Steele K.M., and Delp S.L. A rolling constraint reproduces ground reaction forces and moments in dynamic simulations of walking, running, and crouch gait. *J Biomech*, 46(10):1772–6, 2013.

[104] Hasan S.S., Edmondstone M.A., Limbird T.J., Shiavi R.G., and Peterson S.W. Reaction force patterns of injured and uninjured knees during walking and pivoting. *J Electromyogr Kinesiol*, 1(3):218–28, 1991.

[105] Hase K. and Stein R.B. Turning strategies during human walking. *J Neurophysiol*, 81(6):2914–22, 1999.

[106] Heintz S. and Gutierrez-Farewik E.M. Static optimization of muscle forces during gait in comparison to EMG-to-force processing approach. *Gait Posture*, 26(2):279–88, 2007.

[107] Hensinger R.N. *Standards in paediatric orthopaedics.* Raven Press, New York, USA, 1986.

[108] Herzog W. and Leonard T.R. Validation of optimization models that estimate the forces exerted by synergistic muscles. *J Biomech*, 24 Suppl 1:31–9, 1991.

[109] Heyrman L., Feys H., Molenaers G., Jaspers E., Monari D., Meyns P., and Desloovere K. Three-dimensional head and trunk movement characteristics during gait in children with spastic diplegia. *Gait Posture*, 38(4):770–6, 2013.

[110] Hof A.L. Scaling gait data to body size. *Gait Posture*, 4(3):222–3, 1996.

[111] Hof A.L. The 'extrapolated center of mass' concept suggests a simple control of balance in walking. *Hum Mov Sci*, 27(1):112–25, 2008.

[112] Hof A.L., Gazendam M.G.J., and Sinke W.E. The condition for dynamic stability. *J Biomech*, 38(1):1–8, 2005.

[113] Hollands K.L., Pelton T., Wimperis A., Whitham D., Jowett S., Sackley C., Alan W., and van Vliet P. Visual cue training to improve walking and turning after stroke: A study protocol for a multi-centre, single blind randomised pilot trial. *Trials*, 14(1):276, 2013.

[114] Houck J.R., Duncan A., and De Haven K.E. Comparison of frontal plane trunk kinematics and hip and knee moments during anticipated and unanticipated walking and side step cutting tasks. *Gait Posture*, 24(3):314–22, 2006.

[115] Houck J.R., Wilding G.E., Gupta R., De Haven K.E., and Maloney M. Analysis of EMG patterns of control subjects and subjects with ACL deficiency during an unanticipated walking cut task. *Gait Posture*, 25(4):628–38, 2007.

[116] Hreljac A. and Marshall R.N. Algorithms to determine event timing during normal walking using kinematic data. *J Biomech*, 33(6):783–6, 2000.

[117] Hsue B.J., Miller F., and Su F.C. The dynamic balance of the children with cerebral palsy and typical developing during gait. Part I: Spatial relationship between COM and COP trajectories. *Gait Posture*, 29(3):465–70, 2009.

[118] Hsue B.J., Miller F., and Su F.C. The dynamic balance of the children with cerebral palsy and typical developing during gait Part II: Instantaneous velocity and acceleration of COM and COP and their relationship. *Gait Posture*, 29(3):471–6, 2009.

[119] Huxham F., Baker R., Morris M.E., and Iansek R. Footstep adjustments used to turn during walking in Parkinson's disease. *Mov Disord*, 23(6):817–23, 2008.

[120] Huxham F., Gong J., Baker R., Morris M., and Iansek R. Defining spatial parameters for non-linear walking. *Gait Posture*, 23(2):159–63, 2006.

[121] Imai T., Moore S.T., Raphan T., and Cohen B. Interaction of the body, head, and eyes during walking and turning. *Exp Brain Res*, 136(1):1–18, 2001.

[122] Inman V.T., Ralston H.J., and Todd F. *Human locomotion*, chapter 1. In Rose J. and Gamble J.G., editors, Human Walking. 3rd edition. Lippincott Williams & Wilkins, Philadelphia, USA, 2006.

[123] Ishimura K. and Sakurai S. Degree of agreement between impulse and magnitude of momentum change for different types of movements. *Gait Posture*, 37(3):467–9, 2013.

[124] Jansen K., De Groote F., Duysens J., and Jonkers I. How gravity and muscle action control mediolateral center of mass excursion during slow walking: A simulation study. *Gait Posture*, 39(1):91–7, 2014.

[125] Jenkyn T.R., Shultz R., Giffin J.R., and Birmingham T.B. A comparison of subtalar joint motion during anticipated medial cutting turns and level walking using a multi-segment foot model. *Gait Posture*, 31(2):153–8, 2010.

[126] John C.T., Seth A., Schwartz M.H., and Delp S.L. Contributions of muscles to mediolateral ground reaction force over a range of walking speeds. *J Biomech*, 45(14):2438–43, 2012.

[127] Jonkers I., Stewart C., and Spaepen A. The study of muscle action during single support and swing phase of gait: Clinical relevance of forward simulation techniques. *Gait Posture*, 17(2):97–105, 2003.

[128] Kadaba M.P., Ramakrishnan H.K., and Wootten M.E. Measurement of lower extremity kinematics during level walking. *J Orthop Res*, 8(3):383–92, 1990.

[129] Kadaba M.P., Ramakrishnan H.K., Wootten M.E., Gainey J., Gorton G., and Cochran G.V. Repeatability of kinematic, kinetic, and electromyographic data in normal adult gait. *J Orthop Res*, 7(6):849–60, 1989.

[130] Kaufman K.R. and Sutherland D.H. *Kinematics of normal human walking*, chapter 3. In Rose J. and Gamble J.G., editors, Human Walking. 3rd edition. Lippincott Williams & Wilkins, Philadelphia, USA, 2006.

[131] Kavanagh J.J., Morrison S., and Barrett R.S. Coordination of head and trunk accelerations during walking. *Eur J Appl Physiol*, 94(4):468–75, 2005.

[132] Kepple T.M., Siegel K.L., and Stanhope S.J. Relative contributions of the lower extremity joint moments to forward progression and support during gait. *Gait Posture*, 6(1):1–8, 1997.

[133] Kerr A., Pomeroy V.P., Rowe P.J., Dall P., and Rafferty D. Measuring movement fluency during the sit-to-walk task. *Gait Posture*, 37(4):598–602, 2013.

[134] Kirkwood B. and Stern J. *Essential medical statistics*. Blackwell Publishing, Oxford, UK, 2nd edition, 2003.

[135] Kuo A.D. A least-squares estimation approach to improving the precision of inverse dynamics computations. *J Biomech Eng*, 120(1):148–59, 1998.

[136] Kwon Y.H. Theory, 1998. http://www.kwon3d.com. Accessed, Aug 22nd, 2014.

[137] Lam T. and Luttmann K. Turning capacity in ambulatory individuals post-stroke. *Am J Phys Med Rehabil*, 88(11):873–83, 2009.

[138] Lamontagne A., Paquette C., and Fung J. Stroke affects the coordination of gaze and posture during preplanned turns while walking. *Neurorehabil Neural Repair*, 21(1):62–7, 2007.

[139] Laracca E., Stewart C., Postans N., and Roberts A. The effects of surgical lengthening of hamstring muscles in children with cerebral palsy—the consequences of pre-operative muscle length measurement. *Gait Posture*, 39(3):847–51, 2014.

[140] Larson R., Hostetler R.P., and Edwards B.H. *Calculus of a single variable: Early transcendental functions*. Houghton Mifflin Company, 3rd edition, 2002.

[141] Lenhoff M.W., Santner T.J., Otis J.C., Peterson M.G., Williams B.J., and Backus S.I. Bootstrap prediction and confidence bands: A superior statistical method for analysis of gait data. *Gait Posture*, 9(1):10–7, 1999.

[142] Lewis J.L. and Lew W.D. Note on description of articulating joint motion. *J Biomech*, 10(10):675–8, 1977.

[143] Lichtwark G. Matlab OpenSim PipelineTools v2, 2011.

[144] Liu M.Q., Anderson F.C., Pandy M.G., and Delp S.L. Muscles that support the body also modulate forward progression during walking. *J Biomech*, 39(14):2623–30, 2006.

[145] Liu M.Q., Anderson F.C., Schwartz M.H., and Delp S.L. Muscle contributions to support and progression over a range of walking speeds. *J Biomech*, 41(15):3243–52, 2008.

[146] Lythgo N., Wilson C., and Galea M. Basic gait and symmetry measures for primary school-aged children and young adults whilst walking barefoot and with shoes. *Gait Posture*, 30(4):502–6, 2009.

[147] MacWilliams B.A., Cowley M., and Nicholson D.E. Foot kinematics and kinetics during adolescent gait. *Gait Posture*, 17(3):214–24, 2003.

[148] Malouin F., McFadyen B., Dion L., and Richards C.L. A fluidity scale for evaluating the motor strategy of the rise-to-walk task after stroke. *Clin Rehabil*, 17(6):674–84, 2003.

[149] Marey E.J. Etudes pratiques sur la marche de l'homme: Expériences faites à la station physiologique du Parc des Princes (French). *La Nature: Revue des sciences et de leurs applications aux arts et à l'industrie, 119–23*, 1885.

[150] Mari S., Serrao M., Casali C., Conte C., Ranavolo A., Padua L., Draicchio F., Iavicoli S., Monami S., Sandrini G., and Pierelli F. Turning strategies in patients with cerebellar ataxia. *Exp Brain Res*, 222(1-2):65–75, 2012.

[151] Maxwell S.E. and Delaney H.D. *Designing experiments and analyzing data: A model comparison perspective*. Wadsworth Publishing, Belmont, USA, 1989.

[152] McManus V., Guillem P., Surman G., and Cans C. SCPE work, standardization and definition–an overview of the activities of SCPE: A collaboration of European CP registers. *Zhongguo Dang Dai Er Ke Za Zhi*, 8(4):261–5, 2006.

[153] Mersmann F., Bohm S., Bierbaum S., Dietrich R., and Arampatzis A. Young and old adults prioritize dynamic stability control following gait perturbations when performing a concurrent cognitive task. *Gait Posture*, 37(3):373–7, 2013.

[154] Milandri G. *Turning gait: Characterisation for use in clinial gait analysis.* M.Sc. Thesis, University of Oxford, 2011.

[155] Milner C.E., Davis I.S., and Hamill J. Free moment as a predictor of tibial stress fracture in distance runners. *J Biomech*, 39(15):2819–25, 2006.

[156] Mohr C., Landis T., Bracha H.S., and Brugger P. Opposite turning behavior in right-handers and non-right-handers suggests a link between handedness and cerebral dopamine asymmetries. *Behav Neurosci*, 117(6):1448–52, 2003.

[157] Motulsky H. and Christopoulos A. *Fitting models to biological data using linear and nonlinear regression. A practical guide to curve fitting.* Oxford University Press, New York, USA, 2004.

[158] National Centre for Simulation in Rehabilitation Research. OpenSim support site, 2014. http://opensim.stanford.edu/support/. Accessed, Dec 15th, 2014.

[159] Neptune R.R., Kautz S.A., and Zajac F.E. Contributions of the individual ankle plantar flexors to support, forward progression and swing initiation during walking. *J Biomech*, 34(11):1387–98, 2001.

[160] Noonan K.J., Halliday S., Browne R., O'Brien S., Kayes K., and Feinberg J. Interobserver variability of gait analysis in patients with cerebral palsy. *J Pediatr Orthoped*, 23(3):279–87, 2003.

[161] Norlin R., Odenrick P., and Sandlund B. Development of gait in the normal child. *J Pediatr Orthop*, 1(3):261–6, 1981.

[162] O'Byrne J.M., Jenkinson A., and O'Brien T.M. Quantitative analysis and classification of gait patterns in cerebral palsy using a three-dimensional motion analyzer. *Journal of Child Neurology*, 13(3):101–8, 1998.

[163] O'Connor C.M., Thorpe S.K., O'Malley M.J., and Vaughan C.L. Automatic detection of gait events using kinematic data. *Gait Posture*, 25(3):469–74, 2007.

[164] Olshen R., Biden E., Wyatt M., and Sutherland D. Gait analysis and the Bootstrap. *Ann Stat*, 17(4):1419–40, 1989.

[165] Orendurff M.S., Segal A.D., Berge J.S., Flick K.C., Spanier D., and Klute G.K. The kinematics and kinetics of turning: Limb asymmetries associated with walking a circular path. *Gait Posture*, 23(1):106–11, 2006.

[166] Palisano R., Rosenbaum P., Walter S., Russell D., Wood E., and Galuppi B. Development and reliability of a system to classify gross motor function in children with cerebral palsy. *Dev Med Child Neurol*, 39(4):214–23, 1997.

[167] Pandy M.G., Lin Y.C., and Kim H.J. Muscle coordination of mediolateral balance in normal walking. *J Biomech*, 43(11):2055–64, 2010.

[168] Paquette M.R., Fuller J.R., Adkin A.L., and Vallis L.A. Age-related modifications in steering behaviour: Effects of base-of-support constraints at the turn point. *Exp Brain Res*, 190(1):1–9, 2008.

[169] Pataky T.C. One-dimensional statistical parametric mapping in Python. *Comput Method Biomec*, 15(3):295–301, 2012.

[170] Pataky T.C., Vanrenterghem J., and Robinson M.A. Zero- vs. one-dimensional, parametric vs. non-parametric, and confidence interval vs. hypothesis testing procedures in one-dimensional biomechanical trajectory analysis. *J Biomech*, In Press. DOI: http://dx.doi.org/10.1016/j.jbiomech.2015.02.051.

[171] Patla A.E., Adkin A., and Ballard T. Online steering: Coordination and control of body center of mass, head and body reorientation. *Exp Brain Res*, 129(4):629–34, 1999.

[172] Patla A.E., Prentice S.D., Robinson C., and Neufeld J. Visual control of locomotion: Strategies for changing direction and for going over obstacles. *J Exp Psychol Hum Percept Perform*, 17(3):603–34, 1991.

[173] Perry J. and Burnfield J.M. *Gait analysis: Normal and pathological function*. Slack Publishing, Thorofare, USA, 2nd edition, 2010.

[174] Peterson M.G.E., Murray-Weir M., Root L., Lenhoff M., Daly L., and Wagner C. Bootstrapping gait data from people with cerebral palsy. In *Proc. of the 13th IEEE Comp Med Sy conference*. Houston, USA. Jun 23–24th, 2000.

[175] Piazza S.J. and Delp S.L. The influence of muscles on knee flexion during the swing phase of gait. *J Biomech*, 29(6):723–33, 1996.

[176] Pierrynowski M.R. and Galea V. Enhancing the ability of gait analyses to differentiate between groups: Scaling gait data to body size. *Gait Posture*, 13(3):193–201, 2001.

[177] Podsiadlo D. and Richardson S. The timed "Up & Go": A test of basic functional mobility for frail elderly persons. *J Am Geriatr Soc*, 39(2):142–8, 1991.

[178] Prosser L.A., Lauer R.T., VanSant A.F., Barbe M.F., and Lee S.C.K. Variability and symmetry of gait in early walkers with and without bilateral cerebral palsy. *Gait Posture*, 31(4):522–6, 2010.

[179] Ralston H.J. Energy-speed relation and optimal speed during level walking. *Int Z Angew Physiol*, 17(4):277–83, 1958.

[180] Ramsay J. and Silverman B. *Functional data analysis*. Springer, New York, USA, 1997.

[181] Reinbolt J.A., Fox M.D., Schwartz M.H., and Delp S.L. Predicting outcomes of rectus femoris transfer surgery. *Gait Posture*, 30(1):100–5, 2009.

[182] Riemer R., Hsiao-Wecksler E.T., and Zhang X. Uncertainties in inverse dynamics solutions: A comprehensive analysis and an application to gait. *Gait Posture*, 27(4):578–88, 2008.

[183] Riley P.O. and Kerrigan D.C. Kinetics of stiff-legged gait: Induced acceleration analysis. *IEEE Trans Rehabil Eng*, 7(4):420–6, 1999.

[184] Rodda J.M., Graham H.K., Carson L., Galea M.P., and Wolfe R. Sagittal gait patterns in spastic diplegia. *J Bone Joint Surg Br*, 86(2):251–8, 2004.

[185] Røislien J., Skare O., Gustavsen M., Broch N.L., Rennie L., and Opheim A. Simultaneous estimation of effects of gender, age and walking speed on kinematic gait data. *Gait Posture*, 30(4):441–5, 2009.

[186] Romkes J. Patients with diplegic cerebral palsy walking along a curved path. In *Proc. of the 21st European Society for Movement Analysis in Adults and Children conference*. Stockholm, Sweden. Sep 12–15th, 2012.

[187] Saleh M. and Murdoch G. In defense of gait analysis. Observation and measurement in gait assessment. *J Bone Joint Surg Br*, 67(2):237–41, 1985.

[188] Sangeux M., Rodda J.M., and Graham H.K. Automatic classification of sagittal gait pattern: The plantar flexion-knee extension couple index and scatter plot. In *Proc. of the 19th Gait and Clinical Movement Analysis Society conference*. Delaware, USA. Jun 24–27th.

[189] Saunders J.B., Inman V.T., and Eberhart H.D. The major determinants in normal and pathological gait. *J Bone Joint Surg Am*, 35-A(3):543–58, 1953.

[190] Schaafsma J.D., Balash Y., Gurevich T., Bartels A.L., Hausdorff J.M., and Giladi N. Characterization of freezing of gait subtypes and the response of each to levodopa in Parkinson's disease. *Eur J Neurol*, 10(4):391–8, 2003.

[191] Schache A.G., Baker R., and Lamoreux L.W. Defining the knee joint flexion-extension axis for purposes of quantitative gait analysis: An evaluation of methods. *Gait Posture*, 24(1):100–9, 2006.

[192] Schache A.G., Baker R., and Vaughan C.L. Differences in lower limb transverse plane joint moments during gait when expressed in two alternative reference frames. *J Biomech*, 40(1):9–19, 2007.

[193] Schneiberg S., McKinley P., Gisel E., Sveistrup H., and Levin M.F. Reliability of kinematic measures of functional reaching in children with cerebral palsy. *Developmental Medicine and Child Neurology*, 52(7):e167–73, 2010.

[194] Schwartz M.H., Rozumalski A., and Trost J.P. The effect of walking speed on the gait of typically developing children. *J Biomech*, 41(8):1639–50, 2008.

[195] Schwartz M.H., Trost J.P., and Wervey R.A. Measurement and management of errors in quantitative gait data. *Gait Posture*, 20(2):196–203, 2004.

[196] Schweizer K., Cattin P.C., Brunner R., Müller B., Huber C., and Romkes J. Automatic selection of a representative trial from multiple measurements using principle component analysis. *J Biomech*, 45(13):2306–9, 2012.

[197] Scott S.H. and Winter D.A. Talocrural and talocalcaneal joint kinematics and kinetics during the stance phase of walking. *J Biomech*, 24(8):743–52, 1991.

[198] Scott S.H. and Winter D.A. Biomechanical model of the human foot: Kinematics and kinetics during the stance phase of walking. *J Biomech*, 26(9):1091–1104, 1993.

[199] Sedgman R., Goldie P., and Iansek R. Development of a measure of turning during walking. In *Proc. of the 1st Advancing rehabilitation conference*. Melbourne, Australia. Nov. 2–4th, 1994.

[200] Segal A.D., Orendurff M.S., Czerniecki J.M., Schoen J., and Klute G.K. Comparison of transtibial amputee and non-amputee biomechanics during a common turning task. *Gait Posture*, 33(1):41–7, 2011.

[201] Segal A.D., Orendurff M.S., Czerniecki J.M., Shofer J.B., and Klute G.K. Local dynamic stability in turning and straight-line gait. *J Biomech*, 41(7):1486–93, 2008.

[202] Segal A.D., Orendurff M.S., Czerniecki J.M., Shofer J.B., and Klute G.K. Local dynamic stability of amputees wearing a torsion adapter compared to a rigid adapter during straight-line and turning gait. *J Biomech*, 43(14):2798–803, 2010.

[203] Simpson K.J. and Jiang P. Foot landing position during gait influences ground reaction forces. *Clin Biomech (Bristol, Avon)*, 14(6):396–402, 1999.

[204] Singh K. On the asymptotic accuracy of Efron's Bootstrap. *Ann Stat*, 9(6):1187–95, 1981.

[205] Singh K. and Xie M. *Bootstrap: A statistical method*. 2010. In Peterson, P., Baker, E., and McGaw, B., editors, International Encyclopedia of Education, vol. 7. Elsevier, Oxford, UK, 2010.

[206] Skrba Z., O'Mullane B., Greene B.R., Scanaill C.N., Fan C.W., Quigley A., and Nixon P. Objective real-time assessment of walking and turning in elderly adults. In *Proc. of the 31st IEEE Eng Med Biol Soc conference*. Minneapolis, USA. Sep. 2–6th, 2009.

[207] Spildooren J., Vercruysse S., Desloovere K., Vandenberghe W., Kerckhofs E., and Nieuwboer A. Freezing of gait in Parkinson's disease: The impact of dual-tasking and turning. *Mov Disord*, 25(15):2563–70, 2010.

[208] Spildooren J., Vercruysse S., Meyns P., Vandenbossche J., Heremans E., Desloovere K., Vandenberghe W., and Nieuwboer A. Turning and unilateral cueing in Parkinson's disease patients with and without freezing of gait. *Neuroscience*, 207:298–306, 2012.

[209] Sreenivasa M.N., Frissen I., Souman J.L., and Ernst M.O. Walking along curved paths of different angles: The relationship between head and trunk turning. *Exp Brain Res*, 191(3):313–20, 2008.

[210] Stack E., Jupp K., and Ashburn A. Developing methods to evaluate how people with Parkinson's disease turn 180 degrees: An activity frequently associated with falls. *Disabil Rehabil*, 26(8):478–84, 2004.

[211] Stansfield B.W., Hillman S.J., Hazlewood M.E., and Robb J.E. Regression analysis of gait parameters with speed in normal children walking at self-selected speeds. *Gait Posture*, 23(3):288–94, 2006.

[212] Stebbins J. Oxford Foot Model training day. Oxford, UK. Jul 3rd, 2008.

[213] Stebbins J., Harrington M., Thompson N., Zavatsky A.B., and Theologis T. Repeatability of a model for measuring multi-segment foot kinematics in children. *Gait Posture*, 23(4):401–10, 2006.

[214] Stebbins J., Harrington M., Thompson N., Zavatsky A.B., and Theologis T. Gait compensations caused by foot deformity in cerebral palsy. *Gait Posture*, 32(2):226–30, 2010.

[215] Stebbins J. and Theologis T. Relationship between motion of the hallux and the foot in cerebral palsy. In *Proc. of the 21st European Society for Movement Analysis in Adults and Children conference*. Vienna, Austria. Sep 15–17th, 2011.

[216] Steele K.M., Seth A., Hicks J.L., Schwartz M.H., and Delp S.L. Muscle contributions to vertical and fore-aft accelerations are altered in subjects with crouch gait. *Gait Posture*, 38(1):86–91, 2013.

[217] Steele K.M., Seth A., Hicks J.L., Schwartz M.S., and Delp S.L. Muscle contributions to support and progression during single-limb stance in crouch gait. *J Biomech*, 43(11):2099–105, 2010.

[218] Stokes V.P., Andersson C., and Forssberg H. Rotational and translational movement features of the pelvis and thorax during adult human locomotion. *J Biomech*, 22(1):43–50, 1989.

[219] Strike S.C. and Taylor M.J. The temporal-spatial and ground reaction impulses of turning gait: Is turning symmetrical? *Gait Posture*, 29(4):597–602, 2009.

[220] Sullivan G.M. and Feinn R. Using effect size—or why the p value is not enough. *J Grad Med Educ*, 4(3):279–82, 2012.

[221] Sutherland D. The development of mature gait. *Gait Posture*, 6(2):163–70, 1997.

[222] Sutherland D., Olshen R., and Biden E. *The development of mature walking*. Mac Keith Press, London, UK, 1988.

[223] Sutherland D.H. The evolution of clinical gait analysis. Part II Kinematics. *Gait Posture*, 16(2):159–79, 2002.

[224] Sutherland D.H. and Davids J.R. Common gait abnormalities of the knee in cerebral palsy. *Clin Orthop Relat Res*, (288):139–47, 1993.

[225] Taylor M.J. *Three-dimensional biomechanical analysis of turning gait in both able-bodied and trans-tibial amputee populations*. Ph.D. Thesis, Roehampton University, 2006.

[226] Taylor M.J., Dabnichki P., and Strike S.C. A three-dimensional biomechanical comparison between turning strategies during the stance phase of walking. *Hum Mov Sci*, 24(4):558–73, 2005.

[227] Thelen D.G. and Anderson F.C. Using computed muscle control to generate forward dynamic simulations of human walking from experimental data. *J Biomech*, 39(6):1107–15, 2006.

[228] Tinetti M.E. Performance-oriented assessment of mobility problems in elderly patients. *J Am Geriatr Soc*, 34(2):119–26, 1986.

[229] Vaughan C.L., Davis B.L., and O'Connor J.C. *Dynamics of human gait*. Kiboho Publishers, Cape Town, South Africa, 2nd edition, 1999.

[230] Ventura J.D., Segal A.D., Klute G.K., and Neptune R.R. Compensatory mechanisms of transtibial amputees during circular turning. *Gait Posture*, 34(3):307–12, 2011.

[231] Vicon . Plug-in Gait manual v1. http://www.irc-web.co.jp. Accessed, Aug 22nd 2014.

[232] Vielledent S., Kerlirzin Y., Dalbera S., and Berthoz A. Relationship between velocity and curvature of a human locomotor trajectory. *Neurosci Lett*, 305(1):65–9, 2001.

[233] Visser J.E., Voermans N.C., Oude Nijhuis L.B., van der Eijk M., Nijk R., Munneke M., and Bloem B.R. Quantification of trunk rotations during turning and walking in Parkinson's disease. *Clin Neurophysiol*, 118(7):1602–6, 2007.

[234] Wächter A. and Biegler L.T. On the implementation of a primal-dual interior point filter line search algorithm for large-scale nonlinear programming. *Math. Program.*, 106(1):25–57, 2006.

[235] Waite J.C., Beard D.J., Dodd C.A.F., Murray D.W., and Gill H.S. In vivo kinematics of the ACL-deficient limb during running and cutting. *Knee Surg Sport Tr A*, 13(5):377–84, 2005.

[236] Watts H.G. Gait laboratory analysis for preoperative decision-making in spastic cerebral-palsy: Is it all its cracked up to be? *J Pediatr Orthoped*, 14(6):703–4, 1994.

[237] Weber W. and Weber E.F. *Mechanik der menschlichen Gehwerkzeuge: Eine anatomisch-physiologische Untersuchung* (German). Dietrich, Leipig, Germany, 1836.

[238] White R., Agouris I., Selbie R.D., and Kirkpatrick M. The variability of force platform data in normal and cerebral palsy gait. *Clin Biomech*, 14(3):185–92, 1999.

[239] Wiley M.E. and Damiano D.L. Lower-extremity strength profiles in spastic cerebral palsy. *Dev Med Child Neurol*, 40(2):100–7, 1998.

[240] Winter D.A. *Biomechanics and motor control of human movement*. John Wiley and Sons, New York, USA, 2nd edition, 1990.

[241] Winter D.A. Human balance and posture control during standing and walking. *Gait Posture*, 3(4):193–214, 1995.

[242] Winter D.A. and Yack H.J. EMG profiles during normal human walking: Stride-to-stride and inter-subject variability. *Electroencephalogr Clin Neurophysiol*, 67(5):402–11, 1987.

[243] Wolf S.L., Catlin P.A., Gage K., Gurucharri K., Robertson R., and Stephen K. Establishing the reliability and validity of measurements of walking time using the Emory Functional Ambulation Profile. *Phys Ther*, 79(12):1122–33, 1999.

[244] Woltring H.J. A FORTRAN package for generalized, cross-validatory spline smoothing and differentiation. *Adv Eng Softw UK*, 8(2):10413, 1986.

[245] Wren T.A.L., Gorton G.E., Ounpuu S., and Tucker C.A. Efficacy of clinical gait analysis: A systematic review. *Gait Posture*, 34(2):149–53, 2011.

[246] Wren T.A.L., Lening C., Rethlefsen S.A., and Kay R.M. Impact of gait analysis on correction of excessive hip internal rotation in ambulatory children with cerebral palsy: A randomized controlled trial. *Dev Med Child Neurol*, 55(10):919–25, 2013.

[247] Wren T.A.L., Otsuka N.Y., Bowen R.E., Scaduto A.A., Chan L.S., Dennis S.W., Rethlefsen S.A., Healy B.S., Hara R., Sheng M., and Kay R.M. Outcomes of lower extremity orthopedic surgery in ambulatory children with cerebral palsy with and without gait analysis: Results of a randomized controlled trial. *Gait Posture*, 38(2):236–41, 2013.

[248] Wren T.A.L., Rethlefsen S.A., Healy B.S., Do K.P., Dennis S.W., and Kay R.M. Reliability and validity of visual assessments of gait using a modified physician rating scale for crouch and foot contact. *J Pediatr Orthoped*, 25(5):646–50, 2005.

[249] Wright C.J., Arnold B.L., Coffey T.G., and Pidcoe P.E. Repeatability of the modified Oxford Foot Model during gait in healthy adults. *Gait Posture*, 33:108–12, 2010.

[250] Xu D., Carlton L.G., and Rosengren K.S. Anticipatory postural adjustments for altering direction during walking. *J Mot Behav*, 36(3):316–26, 2004.

[251] Xu D., Chow J.W., and Wang Y.T. Effects of turn angle and pivot foot on lower extremity kinetics during walk and turn actions. *J Appl Biomech*, 22(1):74–9, 2006.

[252] Yamaguchi G.T. and Zajac F.E. A planar model of the knee joint to characterize the knee extensor mechanism. *J Biomech*, 22(1):1–10, 1989.

[253] Zajac F.E. Muscle and tendon: Properties, models, scaling, and application to biomechanics and motor control. *Crit Rev Biomed Eng*, 17(4):359–411, 1989.

[254] Zajac F.E. and Gordon M.E. Determining muscle's force and action in multi-articular movement. *Exerc Sport Sci Rev*, 17:187–230, 1989.

[255] Zajac F.E., Neptune R.R., and Kautz S.A. Biomechanics and muscle coordination of human walking. part II: Lessons from dynamical simulations and clinical implications. *Gait Posture*, 17(1):1–17, 2003.

[256] Zeni J.A., Jr., Richards J.G., and Higginson J.S. Two simple methods for determining gait events during treadmill and overground walking using kinematic data. *Gait Posture*, 27(4):710–4, 2008.

[257] Zhang B.L., Zhang Y.C., and Begg R.K. Gait classification in children with cerebral palsy by Bayesian approach. *Pattern Recogn*, 42(4):581–86, 2009.